



HAL
open science

Dynamics of cancer cells in the tumor core and role of the extracellular matrix in invasion

Ralitza Staneva

► **To cite this version:**

Ralitza Staneva. Dynamics of cancer cells in the tumor core and role of the extracellular matrix in invasion. Cellular Biology. Université Sorbonne Paris Cité, 2018. English. NNT : 2018USPCB123 . tel-02517626

HAL Id: tel-02517626

<https://theses.hal.science/tel-02517626>

Submitted on 24 Mar 2020

HAL is a multi-disciplinary open access archive for the deposit and dissemination of scientific research documents, whether they are published or not. The documents may come from teaching and research institutions in France or abroad, or from public or private research centers.

L'archive ouverte pluridisciplinaire **HAL**, est destinée au dépôt et à la diffusion de documents scientifiques de niveau recherche, publiés ou non, émanant des établissements d'enseignement et de recherche français ou étrangers, des laboratoires publics ou privés.

Université Paris Descartes

Ecole doctorale Frontières du Vivant (ED 474)

Institut Curie, UMR 144

Dynamique des cellules cancéreuses dans le cœur tumoral et rôle de la matrice extracellulaire dans l'invasion métastatique

Dynamics of cancer cells in the tumor core and role of the extracellular matrix in invasion

Présentée par Ralitza Staneva

Thèse de doctorat de Biologie Cellulaire

Dirigée par Danijela Matić Vignjević

Présentée et soutenue publiquement le 21 novembre 2018

Devant un jury composé de :

Dr. Catherine Monnot	Rapporteur
Prof. Giorgio Scita	Rapporteur
Dr. Isabelle Bonnet	Examineur
Dr. Pablo Vargas	Examineur
Prof. Françoise Brochard-Wyart	Examineur
Dr. Danijela Matić Vignjević	Directeur de thèse

Abbreviations

AFM	Atomic force microscopy
AOM	Azoxymethane
APC	Adenomatous polyposis coli
BM	Basement membrane
CAF	Carcinoma-associated fibroblast
DMH	Dimethylhydrazine
DSS	Dextran sulfate sodium
ECM	Extracellular matrix
EMT	Epithelial-to-mesenchymal transition
ER	Estrogen receptor
FACIT	Fibril-associated collagen
FAK	Focal adhesion kinase
FAP	Familial adenomatous polyposis
FGF	Fibroblast growth factor
FN	Fibronectin
GAG	Glycosaminoglycan
GSK-3 β	Glycogen synthase kinase-3 β
HGF	Hepatocyte growth factor
HNPCC	Hereditary nonpolyposis colorectal cancers
LOH	Loss of heterozygosity
LOX	Lysyl oxidase
MAPK	Mitogen-activated protein kinase

MMP	Matrix metalloprotease
NICD	Notch intracellular domain
PDGF- β	Platelet-derived growth factor β
PG	Proteoglycan
SHG	Second harmonic generation
SLRP	Small leucine-rich proteoglycan
TAM	Tumor-associated macrophages
TCF4	Transcription factor 4
TGF- β	Transforming growth factor β
TNF- α	Tumor necrosis factor- α
VEGF	Vascular endothelial growth factor
α -SMA	α -smooth muscle actin

Table of contents

Chapter 1 - Introduction and objectives	11
Part 1 - Colorectal cancer and murine models	13
I. Intestinal homeostasis - a model system for cell migration and tumorigenesis	13
II. Colorectal cancer	17
a. Genetic alterations in CRC initiation and progression.....	17
b. CRC progression and staging.....	20
III. Mouse models of intestinal cancer.....	21
a. Genetic mouse models of CRC	21
b. Carcinogen-induced mouse models	31
c. Transplantation models of CRC.....	31
Part 2 - The Cancer Microenvironment	33
I. Local invasion and metastasis in cancer progression.....	33
II. The cancer microenvironment.....	35
a. Functions of the ECM	35
b. The cellular fraction of the tumor microenvironment	36
i. Immune cells can be friends or enemies of cancer cells	36
ii. Carcinoma-associated fibroblasts as professional matrix secreting and remodeling cells.....	37
iii. Endothelial cells, pericytes and orchestration of neoangiogenesis in tumors.....	38
c. The protein fraction of the tumor microenvironment.....	41
III. Composition of the cancer ECM	41
a. Collagens are the major proteins of the extracellular matrix.....	41
b. Synthesis and assembly of collagen I, the archetypal fibrillar collagen.....	45
c. Glycosaminoglycans and proteoglycans occupy large amounts of space and form hydrated gels.....	47

d.	Elastic fibers provide tissues their elasticity.....	49
e.	Glycoproteins confer additional functions to ECMs	51
IV.	The basement membrane, a specialized type of ECM supporting epithelia ...	53
a.	Composition of the basement membrane.....	54
b.	Assembly of the basement membrane.....	57
V.	The tumor microenvironment is continuously remodeled in tumor progression	58
	Part 3 - Cancer cell migration through the tumor microenvironment.....	59
I.	Single cell migration.....	59
a.	Cell migration on 2D substrates.	59
b.	Cell migration in 3D environments	61
II.	Collective migration	65
III.	Extracellular determinants of cell migration.....	68
a.	ECM density and pore size.....	68
b.	Stiffness.....	68
c.	Fiber architecture and orientation	69
	Part 4 - Physics of cancer	71
I.	The ECM can resist different forms of physical challenges.....	71
a.	Type I collagen resists tensile forces/ stretch	71
b.	The polysaccharide hydrogel resists compressive forces	74
c.	Elastic fibers have the ability to stretch and recoil	74
II.	The physical properties of the ECM are altered in cancer.....	76
a.	Cancer tissues are stiffer than their normal counterparts.....	76
b.	The ECM is in large part responsible for the stiffening of cancer tissues ...	78
c.	Tumor tissues experience compressive stresses	81
III.	Jamming transition in cancer	83

Chapter 2 - Results	89
Part 1. Migration of cancer cells in tumors	91
Part 2. Role of matric stiffening in invasion	113
Part 3. Invasion of the basement membrane by cancer tumoroids	133
Part 4. Intravital imaging of cancer cells in intestinal tumors	143
Chapter 3 - Conclusion and Discussion	147
Chapter 4 - Materials and Methods	159
Chapter 5 - Bibliography	181
Chapter 6 - Annexes	203

Abstract

Carcinoma development is a multistep process, in which accumulation of genetic alterations promotes the sustained proliferation and altered differentiation of epithelial cells. Cancer progression is accompanied by two crucial events: stiffening of the cancer tissue and acquisition of a migratory phenotype by cancer cells. Using 3D *in vitro* models, we address the role and timing of matrix stiffening on cancer cell invasion. Using imaging of mouse tumor tissue explants, we describe the migration properties in deep regions of the tumor core. Indeed, most solid tumors, including colorectal cancer, are composed of a central differentiated core region and an invasive front forming the interface between tumor and stromal tissue. Although most studies have focused on cancer cell migration in the invasive front, cancer cells from the tumor core can also potentially metastasize. To address cell motility in the tumor core, we developed a methodology to image tumor explants from spontaneously-forming tumors in real time using long-term two-photon microscopy. We found that cancer cells in the tumor core are remarkably dynamic and exhibit correlated migration patterns, giving rise to local "currents" and large-scale tissue dynamics. Collagen structures in the tumor core appear to influence the direction of these local currents. Although cells exhibit stop-and-start migration with intermittent pauses, pausing does not appear to be required during division. We thus show that cancer cells in the tumor core are not stationary as previously thought, and exhibit coordinated migration. In order to address the question of the importance of tissue rigidity in the chronology of tumor invasion, we have developed a biomimetic *in vitro* assay of collagen invasion. Using low concentrations of the sugar threose, we can stiffen 3D collagen matrices and control the stiffening in time with no direct effect on residing cells. We demonstrate that depending on the timing of its stiffening, the collagen matrix can either inhibit or promote cancer cell invasion: at an early stage stiff matrices encapsulate the tumor and prevent cancer cell invasion, while matrix stiffening after the onset of invasion promotes cancer cell migration. Our study suggests that adding a temporal dimension in *in vitro* models to analyze biological processes in 4D is necessary to fully capture their complexity.

CHAPTER 1

INTRODUCTION AND OBJECTIVES

Foreword

The lab of Danijela Matić Vignjević is interested in cell migration in homeostasis and cancer, using the mouse intestine as a model. In line with this, the goal of my PhD is to understand how cancer cells migrate in the core of spontaneously developing intestinal tumors in mice, and to determine the role of extracellular matrix stiffening in cancer cell invasion. Therefore, I will first introduce the intestinal homeostasis, then I will describe the perturbations of this homeostasis that are found in colon cancer in patients. I will pursue with mouse models that have been generate to better understand the disease. Because I was interested in the effect of alterations in the cancer stroma in invasion, I will describe the cancer microenvironment and the principles of cell migration in this microenvironment, before describing the physical properties that accompany neoplastic development.

PART 1 - COLORECTAL CANCER AND MURINE MODELS

I. Intestinal homeostasis - a model system for cell migration and tumorigenesis

The gastrointestinal tract is composed of two anatomically and functionally distinct parts, the small and large intestine (Radtke, Clevers and Riccio, 2006). The small intestine is further subdivided in duodenum, jejunum and ileum in the antero-posterior axis, whereas the large intestine is composed by colon and rectum. Both small and large intestine are lined by a single-layered columnar epithelium folded in a repetitive structure. The epithelium of the small intestine is organized in self renewing crypt-villus units. The crypts form epithelial invaginations within the connective tissue and contain the intestinal stem cells, Paneth cells, as well as transit amplifying cells. The intestinal stem cells are endowed with self-renewing and multipotent capacity that allows them to sustain the intestinal epithelial homeostasis. Intestinal stem cells give rise to transit amplifying cells which migrate up the crypt-villus axis and differentiate into specialized intestinal cell types, namely absorptive enterocytes, enteroendocrine cells, mucus-secreting Goblet cells, Tuft cells, microfold (M) cells and Paneth cells (Clevers, 2013; Barker, 2014). Upon crypt exit, the intestinal epithelium forms villi, finger-like protrusions in the intestinal lumen, that dramatically increase the absorptive surface of the intestine (Radtke, Clevers and Riccio, 2006). Unlike the intestine, the colonic epithelium at the crypt exits forms a flat surface devoid of villi, reflecting the functional differences between small and large intestine.

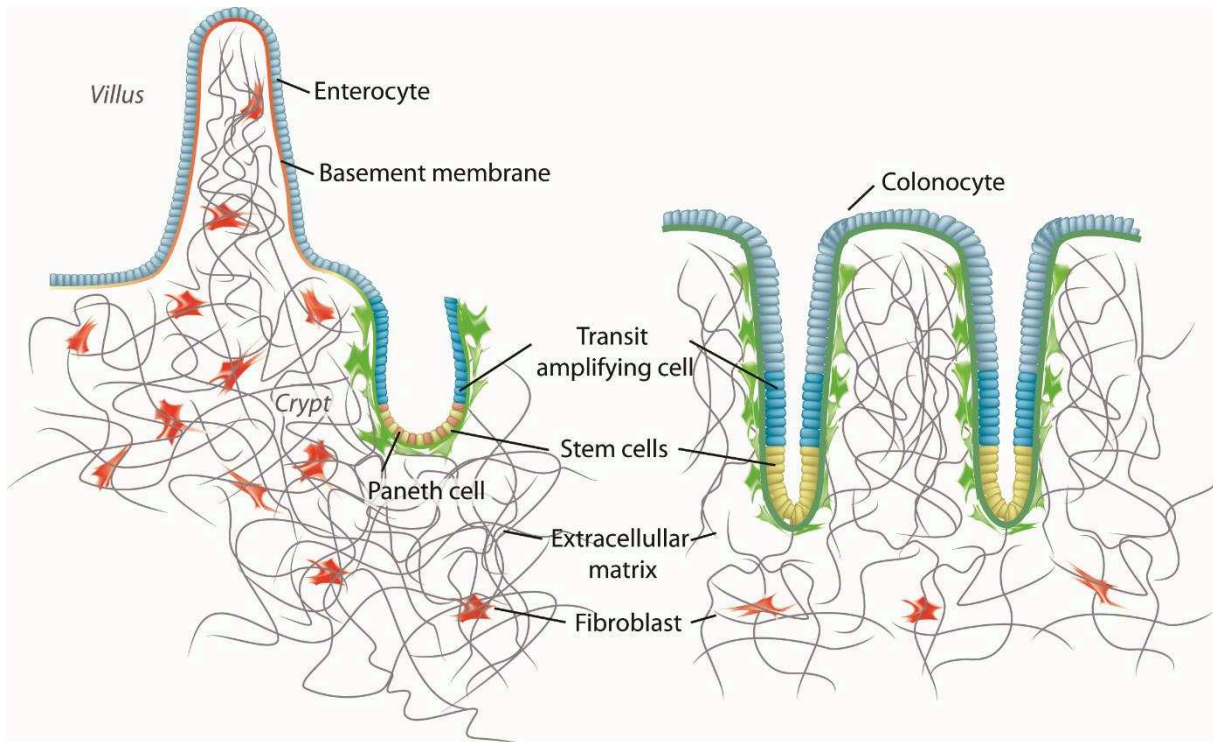


Figure 1. Schematic representation of the gut and colon.

The basal surface of the intestinal epithelium is lined by a basement membrane (BM), a thin and dense sheet of specialized extracellular matrix (ECM). The BM is composed of interconnected networks of laminin and collagen IV, stabilized by glycoproteins such as nidogen, and heparan sulfate proteoglycans such as perlecan and agrin (Glentis, Gurchenkov and Vignjevic, 2014). The BM provides structural and adhesive support to the epithelium, maintains cell polarity and separates epithelium from the stromal compartment underneath, leading to a compartmentalization of the intestinal tissue (Li and Thompson, 2003; Glentis, Gurchenkov and Vignjevic, 2014).

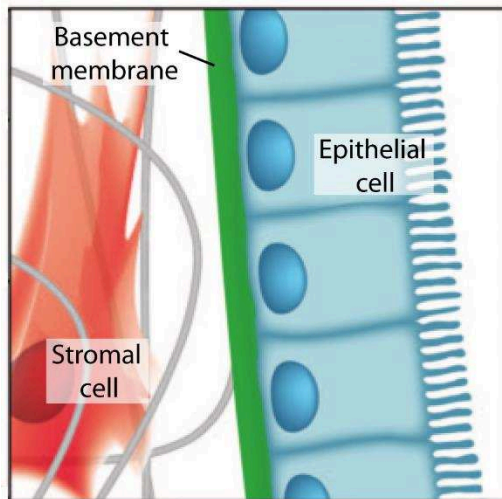


Figure 2. The Basement membrane organizes epithelial tissues.

The basement membrane (green) separates two functionally distinct compartments: the epithelial compartment (blue), and the stromal compartment, rich in stromal cells, such as fibroblasts, and in extracellular matrix components (gray). Modified from Glentis, Gurchenkov and Vignjevic, 2014

The stroma compartment underneath the BM is mainly composed of type I collagen fibers interpenetrated by nerves and blood and lymphatic vessels (Gracz and Magness, 2014). Various cell types populate the stroma of the gut: immune cells, pericytes, endothelial cells and fibroblasts. I will further describe the roles of the BM and underlying stroma in the gut physiology and tumorigenesis in Chapter 3 of the Introduction.

Interestingly, the intestine is one of the fastest self-renewing tissues, as the average life span of an epithelial cell is less than 7 days in human and 3-4 days in mice. In the mouse, around 300 cells are produced in each crypt per day (Marshman, Booth and Potten, 2002), while this high generation of cells is continuously compensated by cell loss at the tip of the villus. Thus the intestinal homeostasis is maintained by a balance between cell proliferation in the crypt, cell migration and differentiation in the villus and cell extrusion and death on the top of the villus (Barker, 2014). This delicate balance can be perturbed by oncogenic insults that arise in the intestine and ultimately lead to tumor formation. Several signaling pathways orchestrate the delicate balance between cell proliferation and differentiation in homeostatic conditions, among which the Wnt is a master regulator of cell fate in the intestine. Deregulated Wnt signaling is a primary driver of colon cancer and physiological Wnt signaling is a driver of crypt proliferation (Clevers, 2013). Indeed, Wnt signaling has an essential role in the regenerative capacity of the adult epithelium, since cell proliferation and crypt integrity were lost after embryonic ablation of the major intestinal Wnt effector protein, transcription factor 4 (TCF4) (Korinek *et al.*, 1998). β -catenin is the major effector of the Wnt pathway. There are two pools of β -catenin in the cells, one at the cell membrane, and the other intracellular, in the cytoplasm or in the

nucleus. At the membrane, β -catenin binds E-Cadherin and stabilizes adherent junctions. In the absence of Wnt signal, the cytoplasmic pool of β -catenin is continuously targeted for degradation by a multi-protein complex comprising the tumor suppressor APC (adenomatous polyposis coli), the scaffold protein Axin and Glycogen Synthase Kinase-3 β (GSK-3 β). Upon binding to APC/Axin2/GSK-3 β complex, β -catenin is phosphorylated by GSK-3 β , ubiquitinated and degraded by the proteasome. Wnt ligands are only present in the crypt compartment where they bind to their receptors on the intestinal stem cells. Upon binding of Wnt to the heterodimeric receptor complex Frizzled/LRP, the degradation machinery is inactivated, β -catenin is stabilized and enters the nucleus where it binds the co-activators LEF/TCF and activates target genes, such as *c-myc*, *c-jun* and *cyclinD1*, that promote proliferation. Even though precisely tuned, the fine balance of the Wnt pathway regulation can be altered and provide an oncogenic soil for neoplastic development.

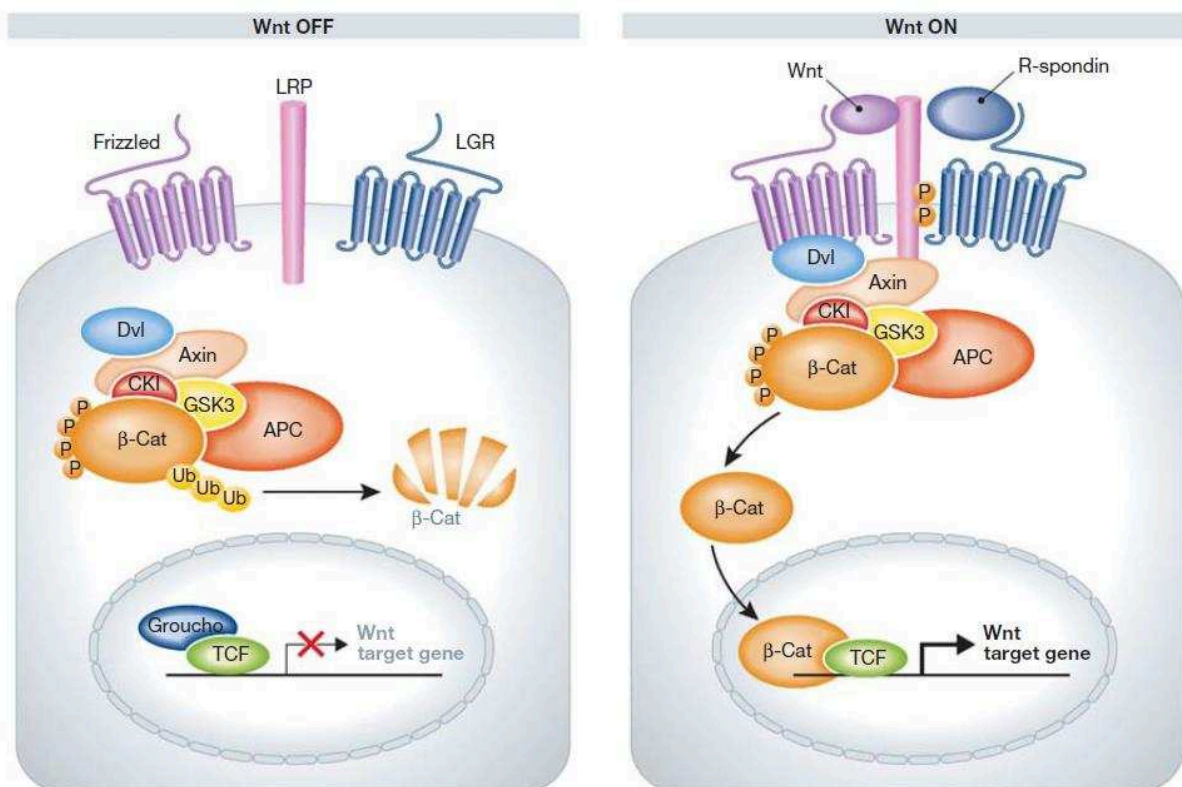


Figure 3. The Wnt pathway. In the absence of Wnt signal, β -catenin is continuously targeted by the APC/Axin/GSK-3 β complex for degradation by the proteasome. Upon binding of Wnt to Frizzled, the degradation machinery is inactivated, β -catenin is stabilized and enters the nucleus where it binds the co-activators LEF/TCF and activates target genes. From Schwijers and Clevers, 2012.

II. Colorectal cancer

Colorectal cancer is the third most common cancer worldwide with 9.7% of the total number of cancers diagnosed (Ferlay *et al.*, 2015). Overall, 1.36 million new cases were diagnosed in 2012 worldwide (Ferlay *et al.*, 2015). In men, it ranks third after lung cancer and prostate cancer, with 10% of cancer cases. In women, it ranks second after breast cancer with 9.2 % of cases (Ferlay *et al.*, 2015). Colorectal cancer ranks fourth in terms of deaths in men and women, with 8.5% of cancer-associated deaths (Ferlay *et al.*, 2015), among which metastasis is the major cause of cancer-associated mortality (Valastyan and Weinberg, 2011). Twenty-five percent of patients already have metastasis at colorectal cancer diagnosis, and an additional 25-35% will develop metastases during disease progression (Van Cutsem *et al.*, 2006). Interestingly, colorectal cancer survival is highly linked with the stage at which cancer is diagnosed, with a better survival upon early diagnosis. Indeed, when diagnosed at the localized carcinoma *in situ* stage, 5-year survival rate is 90 %, whereas survival drops to 70% for regionally invasive tumors and to 10% when distant metastases are found (Ries *et al.*, 2007; Hagggar, Boushey and Ph, 2009).

a. Genetic alterations in CRC initiation and progression

90% of CRC cases are sporadic whereas 10% are linked with an inherited predisposition to colon cancer development, with two main syndromes: familial adenomatous polyposis (FAP) and hereditary nonpolyposis colorectal cancers (HNPCC). Interestingly, mutations that mediate colon carcinogenesis have been discovered through genetic studies of hereditary cancer predisposition syndromes such FAP and HNPCC (Taketo and Edelmann, 2009). In this respect, the first direct connection between the Wnt pathway and human disease came in the early 1990s, when the APC gene was discovered in the hereditary FAP syndrome (Kinzler *et al.*, 1991; Nishisho *et al.*, 1991). Rapidly, the large cytoplasmic APC protein was found to interact with β -catenin (Rubinfeld *et al.*, 1993; Su, Vogelstein and Kinzler, 1993). In the absence of functional APC, which acts as a brake on β -catenin, Wnt signaling is constitutively and inappropriately activated. Thus a direct consequence of *Apc* mutation is the accumulation of β -catenin in the nuclei of intestinal stem cells where it induces upregulated proliferation.

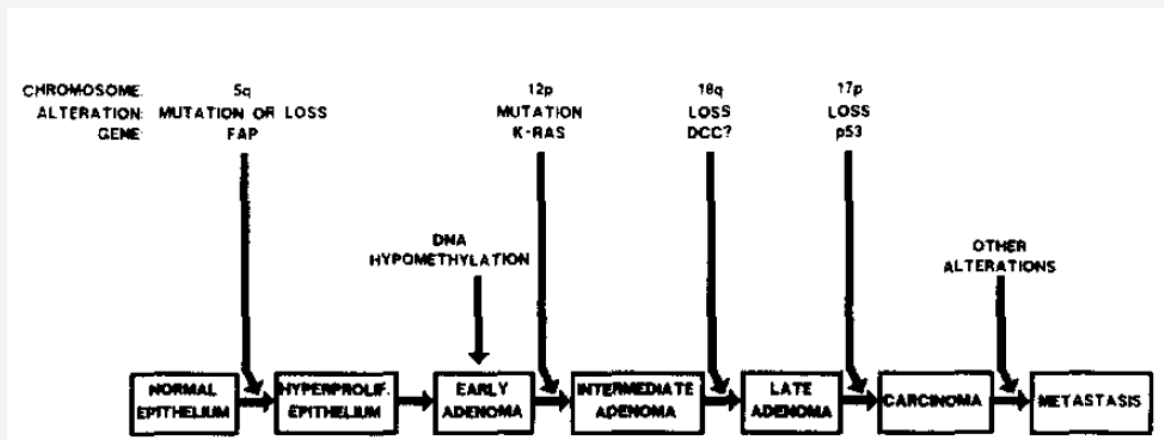
In FAP, germline mutations in APC leads to polyposis, an inherited cancer predisposition syndrome in which more than 100 polyps can develop in the colon. In FAP patients carrying the germline mutations in APC, the probability of colorectal cancer development by the age of 40 years is almost 100%. In sporadic or familial colorectal cancer, colon tumors evolve from small polyps to malignant and invasive tumors. Interestingly, APC mutations appear as an early event in colon carcinogenesis (Kinzler and Vogelstein, 1998). In a small subgroup of tumors with wild-type APC, stabilizing mutations on serine/threonine residues of β -catenin that render the protein resistant to the β -catenin degradation complex activate Wnt signaling (Morin *et al.*, 1997; Markowitz and Bertagnoli, 2010). In 50-80% of sporadic colorectal cancers, loss of the second APC allele (loss of heterozygosity, LOH) occurs specifically in intestinal cells and drives the formation of polyps.

Oncogenic mutations of Ras proteins occur in 50% of colorectal cancers (Janssen *et al.*, 2002), among which K-ras is most frequently mutated. Mutations in K-ras lock the protein in its active form and mediate its tumorigenic activity via the activation on MAPK (Mitogen-activated protein kinase) cascade that controls cell proliferation and apoptosis.

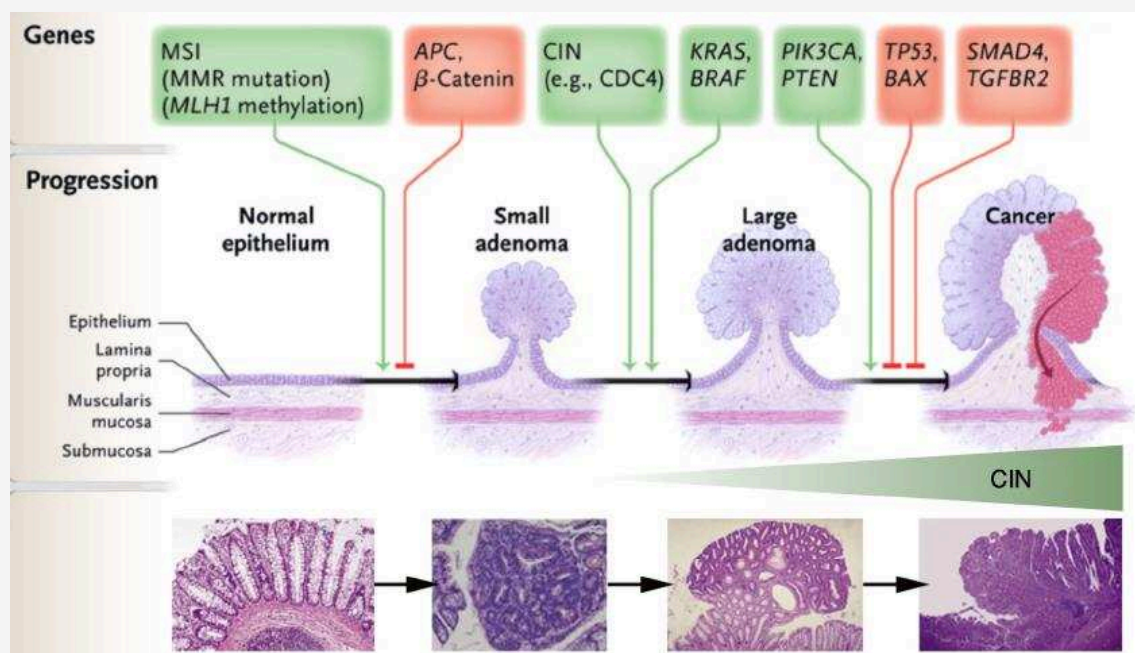
In most colorectal tumors, the two p53 alleles are inactivated, usually by a combination of a missense mutation that inactivates the transcriptional activity of p53 and a 17p chromosomal deletion that eliminates the second p53 allele (Baker *et al.*, 1990). Wild-type p53 mediates cell-cycle arrest and via a cell-death checkpoint, thus mutated p53 leads to an escape of apoptosis of aberrant cells. p53 gene mutations are relatively rare in adenomas and the loss of p53 allele often coincides with the transition of large adenomas into invasive carcinomas (Bert Vogelstein *et al.*, 1981; Fearon and Vogelstein, 1990; Baker *et al.*, 1990). The inactivation of transforming growth factor β (TGF- β) signaling occurs in about one third of colorectal cancers, with mutations occurring either in TGF- β receptor 2 kinase domain or, more commonly, in downstream TGF- β effectors such as SMAD transcription factors, leading to deregulated cell proliferation.

Box 1. A route to the first colorectal carcinogenesis models.

Back in 1990, Fearon and Vogelstein set the bases of understanding of colorectal carcinogenesis. Their model proposes a sequential acquisition of specific genetic alterations involving oncogenes, such as *ras*, and tumor suppressor genes. They propose that a mutation in chromosome 5q is an initial and driving event in intestinal carcinogenesis. Rapidly, this mutation has been discovered to occur in the APC gene (Kinzler et al., 1991; Nishisho et al., 1991), that has been then shown to interact with β -catenin (Rubinfeld *et al.*, 1993; Su, Vogelstein and Kinzler, 1993). Therefore, activation of the Wnt/ β -catenin pathway, most commonly through inactivating mutations in APC, occurs early on in CRC and initiates the formation of benign polyps. Progression to later adenoma and carcinoma requires activating mutations in the EGF receptor pathway, through mutations in K-ras, and inactivating mutations in the p53 tumor suppressor.



More recently, additional pathways implicated in colorectal cancer progression have been identified, among which chromosome instability (CIN), microsatellite instability (MSI), or aberrant mismatch repair (MMR). A renewed view of the sequential colorectal carcinogenesis is provided by Markowitz and colleagues.



(Adapted from Markowitz and Bertagnoli, 2010)

More recently, additional pathways implicated in colorectal cancer progression have been identified, among which chromosome instability, aberrant DNA methylation in promoter-associated CpG islands (Markowitz and Bertagnolli, 2010), or DNA repair defects. In particular, inactivation of genes required for repair of base–base mismatches in DNA can be inherited, as in hereditary nonpolyposis colon cancer (HNPCC), or acquired, as in tumors with methylation-associated silencing of a gene that encodes a DNA mismatch-repair protein. Patients with HNPCC experience increased rates of replication errors at short repeat sequences, termed microsatellite instability (MSI), in their genomic DNA (Taketo and Edelmann, 2009). Those germline defects in mismatch-repair genes confer a lifetime risk of colorectal cancer of about 80%, with cancers evident by the age of 45 years.

b. CRC progression and staging.

Colorectal cancer progresses from early adenoma to invasive adenocarcinoma. Twenty-five percent of patients present with metastasis at colorectal cancer diagnosis, and an additional 25-35% will develop metastases during disease progression (Van Cutsem *et al.*, 2006). The staging of colorectal cancer describes how deep the tumor has penetrated into the colon tissue or to other organs such as lymph nodes or distant organs (Cunningham *et al.*, 2010). The TNM (tumor – lymph node – metastasis) classification answers the following diagnosis criteria:

T: Has the tumor grown into the wall of the colon? If so how many layers?

N: Has the tumor spread to lymph nodes? If so, where and how many?

M: Has the tumor metastasized to distant locations? If so, where and how much?

It is crucial to carefully assess the stage of colorectal cancer at diagnosis, because this will determine the cancer treatment (Cunningham *et al.*, 2010).

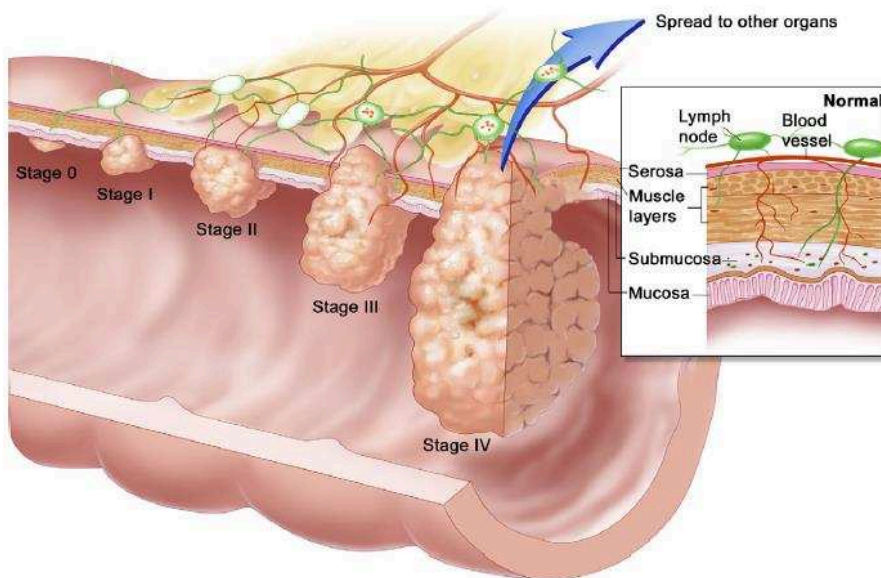


Figure 4: Colorectal cancer stages. As colorectal cancer progresses from the carcinoma in situ stage to the metastatic stage, cancer cells sequentially invade through the different layers of the colon.

III. Mouse models of intestinal cancer

Numerous mouse models have been developed in order to mimic the molecular pathways behind CRC. They have provided a better understanding of the CRC carcinogenesis, but in some aspects fail to fully recapitulate the human pathophysiology. Three main CRC mouse models have been developed, either genetically engineered, chemically induced, or transplantation-induced, that differ on the methodology used to generate the colorectal tumors.

a. Genetic mouse models of CRC

There are several mouse models that harbor mutations in genes involved in the human disease.

Apc mutant mice. Historically, the first genetic mouse models of intestinal carcinogenesis harbor mutations in the *Apc* gene. The first mouse mutant in the *Apc* gene was identified in a colony of mice following random mutagenesis (Moser, Pitot and Dove, 1990). This mutant was called *Min*, for Multiple Intestinal Neoplasia, and carries a truncation mutation at codon 850 of the *Apc* gene (Su *et al.*, 1992), hence referred to as *Apc^{Min}*. Heterozygote *Apc^{Min}* mice on a C57BL/6 background typically develop approximately 30 polyps in the small intestine. Using gene knockout technology in

embryonic stem cells, several *Apc* mutations have been constructed, with different codon truncations of the *Apc* gene, such as *Apc*^{Δ716} and *Apc*^{1638N} (Fodde *et al.*, 1994; Oshima *et al.*, 1995). Similar to *Apc*^{Min} mice, both knockout mutants develop polyps mainly in the small intestine. However, the polyp numbers are very different, with 300 polyps in *Apc*^{Δ716}, and only 3 in *Apc*^{1638N}. Despite the numerous polyps developing in the small intestine of the *Apc*^{Δ716} and *Apc*^{Min} mice, only a few polyps are formed in the colon. With an additional mutation in the *Cdx2* gene in *Apc*^{Δ716} mice, the compound mutant strain can develop numerous polyps in the distal colon (Aoki *et al.*, 2003), mimicking the localization of polyps found in human patients. Using *Apc*^{Δ716} mice, it was shown that polyp formation is initiated by loss of heterozygosity (LOH) at the *Apc* locus in the cells of the proliferative crypt zone, followed by formation of an outpocket in the intestine (Oshima *et al.*, 1995, 1997).

TGF-β pathway mutations. Mutations in the TGF-β pathways occur in one third of human colorectal cancer. Thus, to mimic those mutations, mice mutant for downstream effectors of TGF-β, such as PTEN and Smad3, have been generated (Zhu *et al.*, 1998; He *et al.*, 2007). Interestingly, combination of *Apc* mutations with TGF-β pathway mutations can modify the tumor progression phenotypes of *Apc* mice and give new insights in colorectal pathophysiology. Indeed, while all *Apc* mutant mice develop adenomatous polyps, they do not progress into invasive or metastatic adenocarcinomas at any significant frequencies. For example, introduction of Smad4 mutation into the *Apc*^{Δ716} polyposis mice results in locally invasive malignant adenocarcinomas (Takaku *et al.*, 1998). The intestinal polyps in these mice progress rapidly into very invasive adenocarcinomas, however these adenocarcinomas do not metastasize during the life span of the mice.

HNPCC mouse models. Patients with hereditary HNPCC carry heterozygous mutations in one of the DNA mismatch repair (MMR) genes, with a majority of cases associated with mutations in Mlh1, Msh2, and Msh6 (Peltomäki, 2003; Vasen and Boland, 2005; Rustgi, 2007). Therefore, mouse models bearing alterations in the Mlh1, Msh2 and Msh6 genes have been developed. However, there are phenotypic differences between MMR knockout mice and patients with HNPCC. For example, homozygous Msh2, Msh6, and Mlh1

knockout mice develop gastrointestinal cancers, but unlike patients with HNPCC, most mice die prematurely due to aggressive lymphomas (Taketo and Edelmann, 2009). The combination of Mlh1 and Apc^{1638N} mutant mice dramatically increased the number and invasiveness of intestinal tumors, consequently decreasing mice survival (Edelmann *et al.*, 1999).

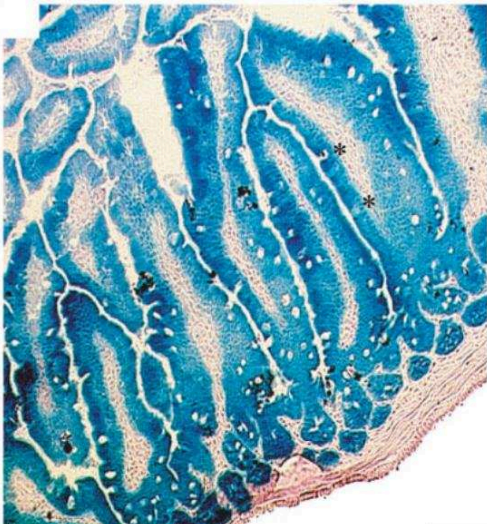
Interestingly, the genetic mouse models of intestinal carcinogenesis described above are constitutive, which means that the genetic alterations occur early on and are present throughout all stages of development, which can give rise to embryonic lethality. In order to circumvent these difficulties, nowadays conditional mouse models are mostly used, based on recombinase-mediated gene disruption. They allow to control the timing of expression or knockout of a given gene (using inducible systems) and to restrict its expression to desired tissues (using tissue specific promoters). β -catenin, Ras and NICD/p53 mutant mice are the main conditional colorectal cancer models.

β -catenin mutant mice. Because APC forms a complex with other proteins that mediate the Wnt signaling pathway, mouse models have been used to determine whether mutations in other components of the complex can also induce polyp formation. As mentioned above, stabilizing mutations might occur in β -catenin, in a subpopulation of human colon tumors that do not carry APC mutations. Therefore, conditional mutations that stabilize β -catenin have been expressed in the mice intestinal epithelium. Stabilized β -catenin was expressed under the calbindin promoter, that is expressed in the differentiated enterocytes (Colnot *et al.*, 1998). In that case, mice developed only a few polyps in the small intestine (Romagnolo *et al.*, 1999). In contrast, 700 to 3000 polyps were formed in the small intestine of mice in which a stabilized floxed β -catenin was induced by the expression of a Cre recombinase under the cytokeratin 19 promoter, or fatty acid binding protein gene promoter (Harada *et al.*, 1999). Interestingly, cytokeratin 19 and fatty acid binding protein are expressed in transit amplifying cells, therefore the increased development of polyps in these mice confirms the role of Wnt signaling in polyp formation and suggests that polyps are more probably initiated from the transient amplifying cells, rather than from differentiated enterocyte cells.

Box 2. The villin promoter, a revolution in intestinal carcinogenesis.

To induce tissue-specific expression of genes in the intestine, several promoters can be used to drive Cre recombinase expression. The promoter of the intestinal protein villin is currently the best one to restrict gene expression to the intestine, from stem cells of the crypt to differentiated enterocytes (El Marjou et al., 2004). Villin, an actin-binding protein, is expressed in the entire intestinal epithelium and kidney, but in no other tissues. To temporally control the expression of gene, the Cre recombinase can be modified by the fusion with the mutated ligand-binding domain of estrogen receptor (ER). CreER^{T2} protein is expressed in the tissue of interest and is localized in the cytoplasm. Upon injection of tamoxifen, a selective estrogen receptor ligand, tamoxifen binds to the ER part of the chimeric CreER^{T2}, that allows translocation of the Cre into the nucleus, where it can recombine its loxP-flanked DNA substrate (Feil, Valtcheva and Feil, 2009).

Cre-mediated expression of the reporter gene β -galactosidase takes place in the visceral endoderm (an extraembryonic tissue) and in the developing gut starting from E10.5 (El Marjou et al., 2004).



Cre-mediated expression of the reporter gene β -galactosidase takes place homogeneously throughout the crypt-villus axis of vil-Cre/Rosa26R mice. The mesenchymal cells are negative.

Scale bar, 50 μ m

Adapted from El Marjou et al., 2004.

Ras mutant mice. Because Ras oncogenes are mutated in about 50% of human colorectal cancers, transgenic mouse models with mutated Ras have been generated. Janssen and colleagues have generated a mouse that expresses K-ras^{V12G}, the most frequent oncogenic mutation found in human tumors (Janssen *et al.*, 2002). In order to specifically target this mutation in the gut, K-ras^{V12G} was put under control of the murine villin promoter, that is active in epithelial cells of the large and small intestine. More than 80% of the transgenic animals displayed intestinal lesions, ranging from aberrant crypt foci to invasive adenocarcinomas. Expression of K-ras^{V12G} caused activation of the MAP kinase cascade, and the tumors were frequently characterized by deregulated cellular proliferation. The

average number of tumors in the small intestine was 2.5 per animal, with lesions localized mainly in the duodenum (46%), jejunum (44%), and rarely in colon (7%). These tumors recapitulated all stages of tumor progression as well as a part of the genetic alterations found in human colorectal cancer. Indeed, secondary mutations were found to spontaneously occur, among which mutations in the p53 tumor suppressor. Interestingly, spontaneous p53 mutations are very rare in the case of Apc-induced intestinal lesions in mice, and they have never been detected in either the *Apc^{1638N}* nor in the *Apc^{Min}* mouse model. This seems to indicate that inactivation of the p53 tumor suppressor cooperates with K-ras in the progression of colorectal tumors. Unexpectedly, no evidence of inactivating mutations in Apc were found in the K-ras^{V12G} mouse, indicating that the pathway to intestinal cancer is not necessarily a single road centered around Apc.

NICD/p53 mouse. Colorectal carcinogenesis doesn't necessarily follow the classic Apc – K-ras – p53 route, and other regulators of the process have recently been described. The Notch signaling pathway is important for the maintenance of cell proliferation and the prevention of cell differentiation in the crypt (Fre *et al.*, 2005; Van Es *et al.*, 2005). I will describe this model in more details because I used it in my PhD.

Notch pathway in cancer: Notch signaling regulates cell fate choices and pattern formation during the development of most tissues, as well as in the continual homeostatic renewal of tissues such as the intestinal epithelium (Artavanis-Tsakonas, Rand and Lake, 1999; Fre *et al.*, 2005). In human and mice, Notch signaling pathway consists of Notch ligands (Jagged1, Jagged2, Delta-like ligand1, -3 and -4), Notch receptors (Notch 1–4) and several downstream target genes such as p21 and Hes-1 (Artavanis-Tsakonas, Rand and Lake, 1999). Notch protein is a single-pass transmembrane receptor that requires proteolytic cleavage to function (Artavanis-Tsakonas, Rand and Lake, 1999; Bray, 2006). It provides the simplest and most direct signaling pathway known from a cell-surface receptor to the nucleus. When activated by the binding of Jagged or Delta-like ligands expressed by a neighboring cell, the Notch receptor is cleaved by ADAM (A Disintegrin And Metalloprotease) and subsequently by the γ -secretase complex within the transmembrane domain. This proteolytic processing causes release of the Notch

intracellular domain (NICD) from the membrane and translocation of the NICD into the nucleus. Nuclear NICD interacts with the DNA-binding CSL (for CBF-1, Su(H), Lag-1) and stimulates expression of Notch target genes, resulting in enhanced proliferation (myc, Ccnd1) survival (Bcl-2, NF- κ B) and suppression of secretory cell differentiation (Hes1) (Bray, 2006).

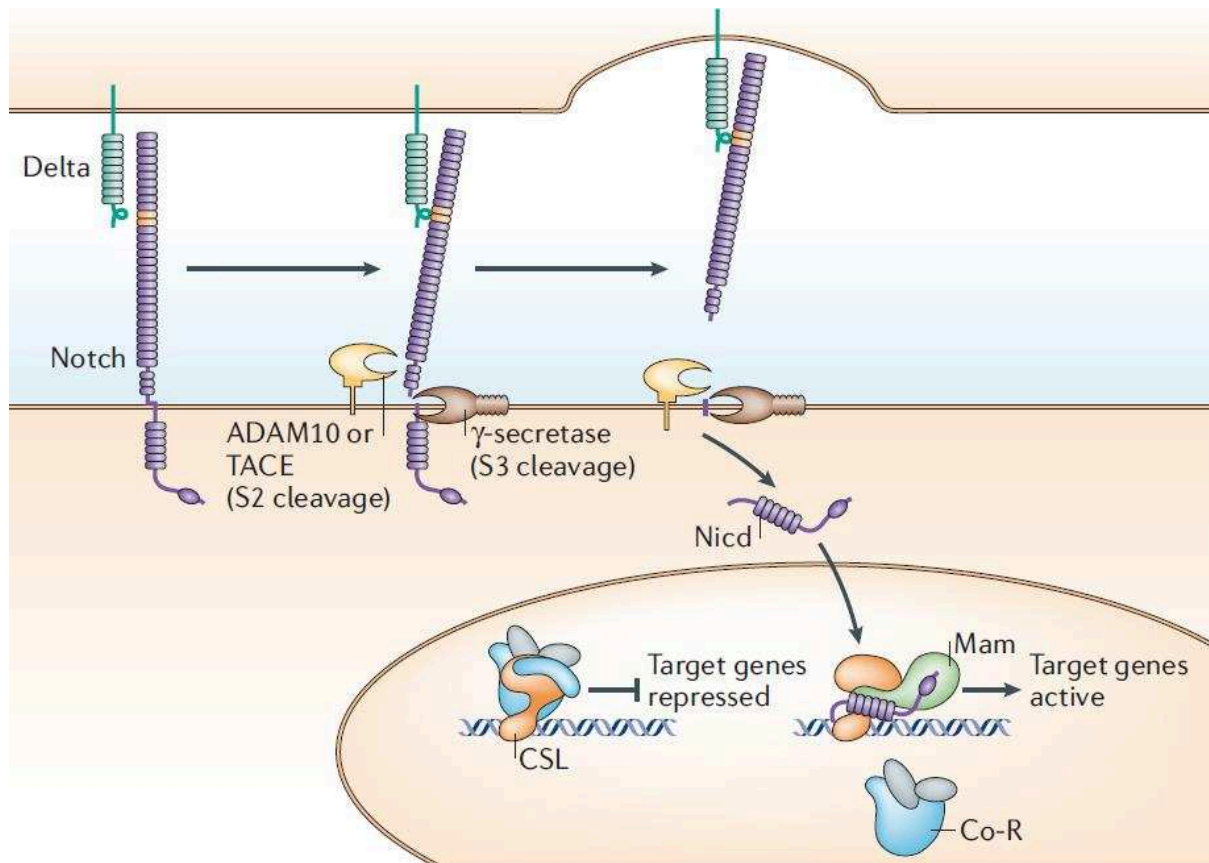


Figure 5. Notch signaling pathway. Upon binding to Delta (green), cytoplasmic tail of Notch (purple) is cleaved by ADAM and γ -secretase to generate NICD (Notch Intracellular Domain), which enters the nucleus and interacts with CSL complex (orange). The co-activator Mastermind (Mam, green) and other transcription factors (see also FIG. 4) are recruited to the CSL complex, whereas co-repressors (Co-R, blue and grey) are released. Notch target gene are thus activated. From Bray, 2006

Notch was first identified in 1919 by geneticist Thomas Hunt Morgan. Morgan named the gene after the notches that appeared in the wings of *Drosophila melanogaster* lacking a gene copy (Garber, 2007). In 1937, Donald Poulson showed that *Drosophila melanogaster* embryos lacking Notch fail to develop mesoderm and endoderm, and that they display an overproduction of neural tissue at the expense of epidermal tissue (Poulson, 1937). This observation established the role of Notch in determining cell fate. The role of Notch signaling in cancer was not recognized until 1991 when Notch1 was suspected to be related to the development of T-cell acute leukemia (Ellisen *et al.*, 1991). Aberrantly activated Notch signaling has been observed during the carcinogenesis of many human cancers, such as pancreatic, breast, prostate, liver, lung, ovarian, renal and colon cancer, and leukemia (Weng *et al.*, 2004; Qiao and Wong, 2009). In colon cancer, Notch ligands are produced by stromal cell types, notably tumor endothelial cells (Lu *et al.*, 2013).

Using the Notch signaling pathway, the laboratory of Sylvie Robine at Institut Curie has generated a mouse model of aggressive intestinal carcinoma that metastasize to the lymph nodes, peritoneum and liver (Chanrion *et al.*, 2014). This is one of the rare cancer models of intestinal tumors that progresses to the metastatic stage, and therefore it mimics more closely the human pathology. In this model, the formation of invasive carcinoma is driven by the expression of a conditionally activated Notch1 receptor (NICD) and the deletion of the p53 tumor suppressor in the digestive epithelium (pVillin-Cre-ERT2; LSL-NICD-nGFP; p53^{F/F} mice, thereafter referred to as NICD/p53 mice) (Chanrion *et al.*, 2014). The intestinal epithelial cells express a nuclear GFP, which allows tracking cancer cells over time, and is therefore a precious tool for following cell dynamics over time.

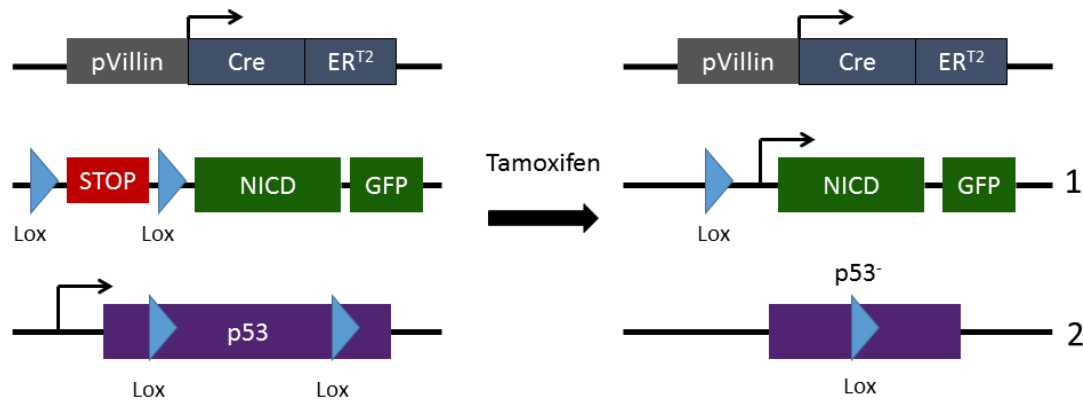


Figure 6. Genetic construct of the NICD/p53 mouse. Upon tamoxifen injection, CreER^{T2} drives the excision of: 1) a STOP codon upstream of NICD and nGFP, and 2) the p53 tumor suppressor.

In the NICD/p53 mouse model, one third of animals develops tumors 5 months post tamoxifen induction, which are staged as adenoma (42%) or adenocarcinoma (58%). The tumors are predominantly located in the jejunum, ileum and rarely in the colon (Chanrion *et al.*, 2014). Tumors are classified as moderately or poorly differentiated (59.3% of total tumors) with complete invasion of the intestinal wall. Regarding distant metastasis, one fourth of mice present lymph node infiltration and 10% have liver metastases, proving the capacity of NICD/p53 tumor cells to disseminate. Half of the animals develop peritoneal carcinosis, with cancer cells infiltrating several tissues, including liver, spleen, diaphragm, mesentery and the abdominal wall. Importantly, liver, lymph node and peritoneum are common implantation environments for metastases in advanced colorectal cancer in humans, demonstrating that the NICD/p53 tumor model efficiently mimics the metastatic spreading of the human disease.

In primary NICD/p53 tumors cancer cells are present in foci. The tumor core is composed of large cohesive clusters expressing E-cadherin (Chanrion *et al.*, 2014). The invasive front is composed of smaller clusters, and of single GFP-positive cancer cells in contact with stromal collagen fibers. These single cells express Epithelial-to-Mesenchymal (EMT) transcription factors, such as Zeb1, and have lost E-cadherin expression (Chanrion *et al.*, 2014). Whether cancer cells gain the ability to migrate only when they reach the invasive front; or whether they are intrinsically motile is unclear.

One of the goals of my PhD is to characterize cancer cell migration pattern in deep core regions of these NICD/p53 tumors.

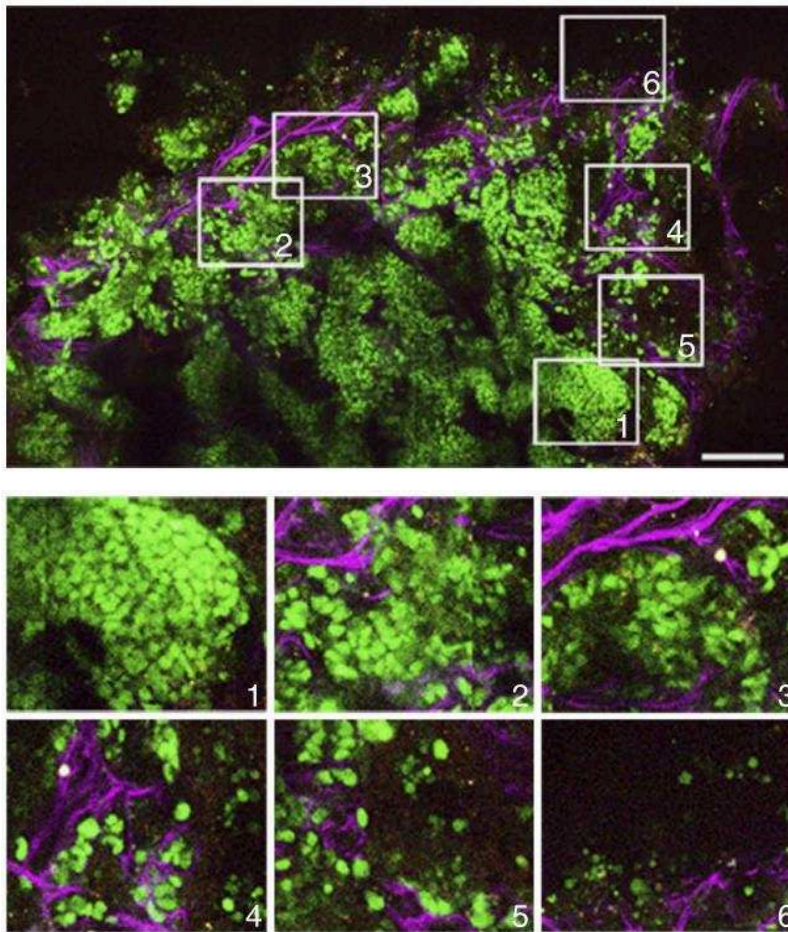


Figure 7. Organization of NICD/p53 tumors. NICD/p53 tumors present large central regions of cancer cell clusters (tumor core, insets 1-3), with peripheral single cancer cells invading the stroma (invasive front, insets 4-6). Nuclear GFP (green) and collagen (SHG, magenta). From Chanrion *et al.*, 2014

NICD/p53 mice display single cells that have undergone EMT (Chanrion *et al.*, 2014). In order to understand the interactions between the Notch signaling pathway and p53 in promoting the EMT phenotype, Chanrion and colleagues have built a signaling map based on existing literature. According to this map, a set of key EMT transcription factors (Snail, Slug, Zeb1, Zeb2, Twist1) are under control of several upstream mechanisms: they are directly induced at the transcriptional level by the activated form of Notch (Maier *et al.*, 2010), but are downregulated at the translational level by several miRNAs (mir200, mir34, mir203 and mir192) that are under transcriptional control of p53 family genes (Knouf *et al.*, 2012).

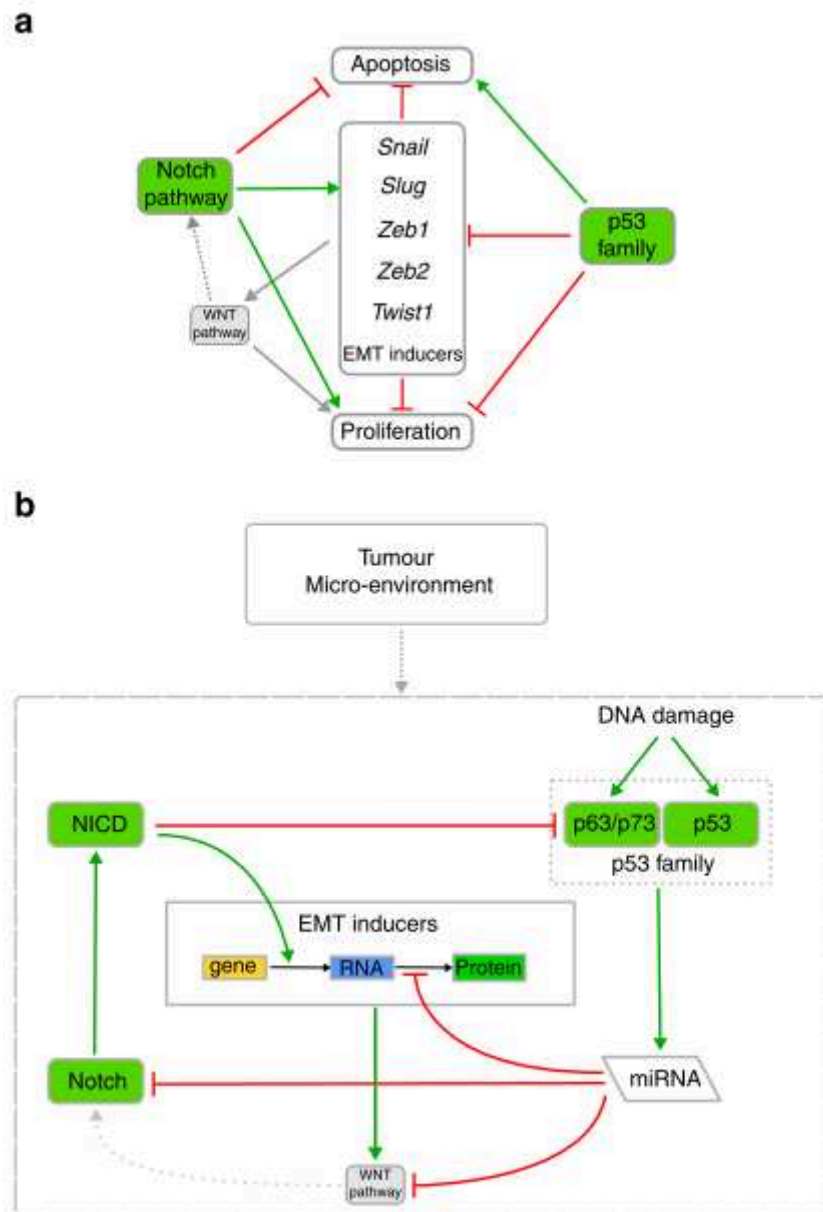


Figure 8. Hypothesis on Notch-p53 interplay. Green and grey arrows depict an activating effect, red arrows indicate an inhibiting effect and dotted line indicates an indirect effect. a) Schematic view of three signaling pathways (Wnt, Notch and p53) and the effect on apoptosis, proliferation and EMT induction. b) Schematic view at a molecular level showing the involvement of Notch and Wnt pathways, p53 family and microRNAs in activating EMT inducers. The p53 family members (p53, p63 and p73) can be activated by DNA damage and can induce transcription of miRNAs. These miRNAs target mRNAs coding for β -catenin (Wnt pathway), Notch and the EMT inducers (Snail, Twist, Slug, Zeb1 and Zeb2). Those EMT inducers activate the Wnt pathway that, in turn, activates the Notch pathway, resulting in the activation of Notch (NICD). NICD activates the gene expression of EMT inducers, but can also inhibit transcription of p63 and p73, but not p53. Various signals from tumor microenvironment as extracellular matrix (ECM) components, inflammatory and growth factors, or hormones can sensitize the activation of EMT program. From Chanrion *et al.*, 2014

b. Carcinogen-induced mouse models

Most cases of CRC arise sporadically, and environmental factors, such as exposure to low dose carcinogens, enhances the risk of tumor incidence. Carcinogens are molecules that directly provoke DNA damage or alter cellular processes important for the maintenance of homeostasis. Common examples of carcinogens of the intestine are smoke, radiation, or alcohol in high doses. Dimethylhydrazine (DMH) and its metabolite azoxymethane (AOM) are powerful carcinogen widely used to induce intestinal carcinogenesis in mice. Combination of carcinogens and pro-inflammatory treatments drastically accelerates tumor growth in mice, decreasing by three folds the time required for tumor apparition. That is why AOM injections are often combined with dextran sulfate sodium (DSS) treatments. DSS is a potent inducer of inflammation and particularly applicable when the focus of the study is on tumor progression driven by colitis, as in ulcerative colitis or Crohn disease. Mice treated with AOM/DSS develop tumors in the colon that range from adenoma to invasive carcinoma (Tanaka *et al.*, 2003; Suzuki *et al.*, 2004). Because AOM induces random mutations in the genome, the tumors are not defined genetically and progress at different speeds between animals. However, this model has the advantage to cause tumors in the colon, contrary to most genetic mouse models.

c. Transplantation models of CRC

Because metastasis is responsible for most colon cancer mortality, it is important to use mouse models of intestinal cancer metastasis. Apart from the NICD/53 model, no genetic mouse model takes intestinal tumors to their most advanced, metastatic stage. Even in NICD/p53 mice, metastasis is a rather rare event (25% of mice) and takes more than one year to develop. In order to accelerate the study of colorectal metastasis in mice, it is possible to use transplantation (xenograft) models. These models have been important tools for evaluating a variety of therapeutic compounds, especially before genetic mouse models were available. In these studies, human colon cancer cell lines or tissue pieces were transplanted into immunocompromised mice, such as nude mice or NOD-SCID mice. The site of injection of the cancer cells such as the choice of an immunocompromised mouse strain are important parameters in transplantation studies. Subcutaneous injection of the human colon cancer cell line HT29 in SCID mice gave rise to primary subcutaneous tumors and lung metastases (Mitchell, Horny and Schumacher, 1997). Subcutaneous

injection has the advantage to be easy to perform, but the skin microenvironment dramatically differs from the colonic one. In order to solve this issue, orthotopic implantation of colon cancer cell can be performed, in the mouse caecum, as a model of the colon, or directly in the colon (Bettenworth *et al.*, 2016). For example, implantation of LS174T human colon cancer cells into the cecum resulted in primary tumors in the caecum with metastasis to mesenteric lymph nodes and the liver, mimicking human metastatic sites. Recently, due to the advances made in miniaturizing endoscopy tools, it has become possible to perform colonoscopy imaging of the mouse colon (Becker, Fantini and Neurath, 2007). Colonoscopy-guided injection of tumor cells in the colon allows for the engraftment of truly orthotopic tumors. Moreover, after engraftment, tumor progression can be regularly monitored using colonoscopy, which makes colorectal tumor surveillance much easier than before.

PART 2 - THE CANCER MICROENVIRONMENT

I. Local invasion and metastasis in cancer progression

Carcinoma development is a multistep process, in which accumulation of genetic and epigenetic alterations promotes the sustained proliferation and altered differentiation of epithelial cells. Metastasis is a critical step in cancer progression and the major cause of cancer-associated mortality (Valastyan and Weinberg, 2011). The metastatic colonization of distant organs requires the completion of a complex series of biological events. Before local invasion occurs, a tumor arising in an epithelial tissue – a carcinoma in situ – is confined in the boundaries of the basement membrane. The basement membrane is a dense and rigid matrix mainly composed of type IV collagen and laminin, which lines and organizes all epithelia, separating them from the surrounding stromal compartment (Yurchenco, 2011; Glentis, Gurchenkov and Vignjevic, 2014). During the initial steps of cancer invasion, cancer cells breach the basement membrane and migrate through the neighboring stroma composed of extracellular matrix (ECM), and different cell types, among which fibroblasts and immune cells (Chambers, Groom and MacDonald, 2002). Once having reached the blood vessels, cancer cells intravasate in the lumen and flow through the vasculature before arresting at distant organs. There, they extravasate and migrate into the stroma of distant tissues, where they have to survive and proliferate to give rise to clinically detectable macrometastases (Valastyan and Weinberg, 2011).

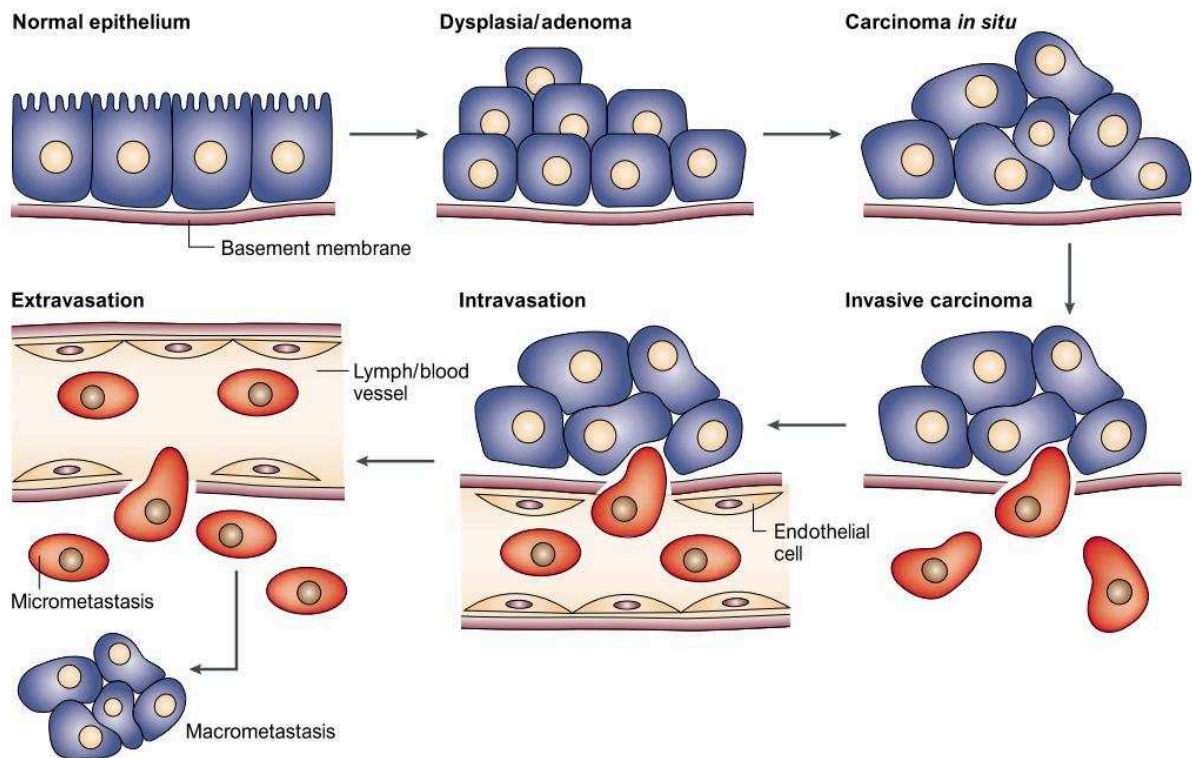


Figure 9. The metastatic cascade. As carcinoma progresses, cancer cells acquire migration capabilities and escape the primary tumors to seed distant metastases. Adapted from Thiery, 2002

Invasive cancer cells are not alone in their journey. They continuously interpret signals from their microenvironment or stroma. In addition to genetic changes in the cancer cells, the tumor microenvironment also becomes altered (Egeblad, Rasch and Weaver, 2010). Interestingly, a “normal” microenvironment can have the ability to revert cancer cells to a “normal” phenotype (Bissell and Hines, 2011) suggesting that the tumor microenvironment plays an active role in tumor progression. Thus, the tumor stroma enhances the malignant traits of carcinoma cells (such as an increased migration) by physical and chemical cues. Tumor cells and stroma share bidirectional interactions (Valastyan and Weinberg, 2011).

II. The cancer microenvironment

a. Functions of the ECM

Cell anchorage and cell-matrix adhesion. The ECM provides the substrate on which cells adhere. Adhesion of a cell to different ECM components mediates intracellular signaling which is crucial for tissue homeostasis and cancer progression. I will address in more details cell receptors of the ECM and their roles in cancer cell migration in Chapter 3.

Source of biochemical signals for cells. The ECM acts as a reservoir for soluble growth factors and regulates their distribution, activation, and presentation to cells (Hynes, 2009; Rozario and DeSimone, 2010; Sarrazin, Lamanna and Esko, 2011). It is often proposed that growth factors can be released from the ECM by proteolytic cleavage of the ECM. This places the ECM in the role of localized reservoir for growth factors that will be released from the solid phase to function as traditional, soluble ligands. However, some growth factors actually bind to their signaling receptors with the heparan sulfate glycosaminoglycan as a cofactor, acting as solid-phase ligands (Hynes, 2009). For example, the binding of FGF to its receptor (FGFR) depends on a heparan sulfate chain binding simultaneously (Mohammadi, Olsen and Goetz, 2005). There are also a number of examples of growth factors binding to ECM proteins themselves, without the involvement of glycosaminoglycans, supporting the notion that the presentation of growth factor signals by ECM proteins is an important part of ECM function. For example, fibronectin binds hepatocyte growth factor (HGF) and form complexes of Met (the HGF receptor) and integrins (the ECM receptors), leading to enhanced cell migration (Rahman *et al.*, 2005).

Source of mechanical signals for cells. The physical properties of the ECM refer to its rigidity, porosity, spatial arrangement and fiber orientation. The ECM provides protection for cells thanks to its resistance to stretch and compression (Alberts *et al.*, 2014). In addition to physical protection of cells, the ECM also instructs cell behaviors by its

biomechanical properties that regulate cells adhesion, migration, differentiation and survival. I will present in more details which physical properties of the ECM regulate cell behaviors in Chapter 4.

b. The cellular fraction of the tumor microenvironment

Tumors are complex tissues composed of multiple distinct cell types that participate in heterotypic interactions with one another. During tumor progression, there is an increase in the number of stromal cells in the tumor microenvironment. The most abundant non-neoplastic cells in the tumor microenvironment are immune cells, carcinoma-associated fibroblasts (CAFs), endothelial cells and pericytes (Joyce and Pollard, 2009).

i. Immune cells can be friends or enemies of cancer cells

Immune cells in cancerous tissues belong to the innate immunity, including macrophages, neutrophils, mast cells, myeloid-derived suppressor cells, dendritic cells and natural killer (NK) cells, and to the adaptive immunity, such as T and B cells lymphocytes. The immune cells which infiltrate tumors have dual roles, that antagonize or enhance tumor development and progression (Hanahan and Weinberg, 2011), depending on the tumor type, on the immune cells in presence and on the cross-talk between both. Virtually every neoplastic lesion contains immune cells present at densities ranging from subtle infiltrations to gross inflammations (Hanahan and Weinberg, 2011). Such immune responses are thought to reflect an attempt by the immune system to eradicate tumors, and indeed, there is increasing evidence for anti-tumoral responses of immune cells (Hanahan and Weinberg, 2011). As cancer cells acquire a high number of mutations and alterations they express tumor-specific antigens that can be recognized as non-self and thereby activate the immune system, eventually leading to the killing of cancer cells (Janssen *et al.*, 2017).

However, by 2000, there was evidence that the tumor-associated inflammatory response had also the unanticipated, paradoxical effect of enhancing tumorigenesis and cancer progression. The infiltrating immune system can supply key molecules to the tumor microenvironment, including growth factors that sustain proliferation, survival factors that limit cell death, proangiogenic factors and ECM-modifying enzymes that facilitate,

invasion, angiogenesis and metastasis (DeNardo, Andreu and Coussens, 2010; Grivennikov, Greten and Karin, 2010; Qian and Pollard, 2010). As an example, immune cells (excluding NK cells) produce tumor-promoting cytokines, including IL-6, IL-8, IL-1 β , tumor necrosis factor- α (TNF- α), which increase NF- κ B and STAT3 signaling in nearby malignant cells (Joyce and Pollard, 2009). Tumor-associated macrophages (TAM) are recruited to the tumor microenvironment where they are educated by microenvironmental cues. Educated TAMs produce paracrine factors promoting neo-angiogenesis, immunosuppression, local inflammation, cell migration, invasion and intravasation (Pollard, 2004).

ii. Carcinoma-associated fibroblasts as professional matrix secreting and remodeling cells

In the body, fibroblasts are the main generators of ECMs scaffolds that other cells are immersed in. Carcinoma-associated fibroblasts (CAFs) represent fibroblasts present in an activated state in tumors, where they assemble ECM and secrete it, to a greater extent than normal fibroblasts (Kalluri and Zeisberg, 2006). A hallmark of CAFs is the expression of α -smooth muscle actin (α SMA), which contributes to their contractility (Hinz *et al.*, 2001). CAFs have been shown to substantially contribute to the development of desmoplastic stroma. Various cell types are thought to be a source for the emergence of CAFs, among resident normal fibroblasts, endothelial cells, pericytes, smooth muscle cells, adipocytes and bone marrow-derived progenitors, such as mesenchymal stem cells (Mishra *et al.*, 2008). CAFs secrete growth factors and ECM, and remodel the ECM, thus making the tumor site highly fibrotic (Kalluri and Zeisberg, 2006). CAFs have been shown to stimulate cancer cell invasion through diffusible molecules (De Wever *et al.*, 2004; Orimo *et al.*, 2005), physical remodeling of the ECM (Gaggioli *et al.*, 2007; Goetz *et al.*, 2011; Calvo *et al.*, 2013; Attieh *et al.*, 2017; Glentis *et al.*, 2017) and by direct interaction with cancer cells, leading their invasion into the matrix (Labernadie *et al.*, 2017).

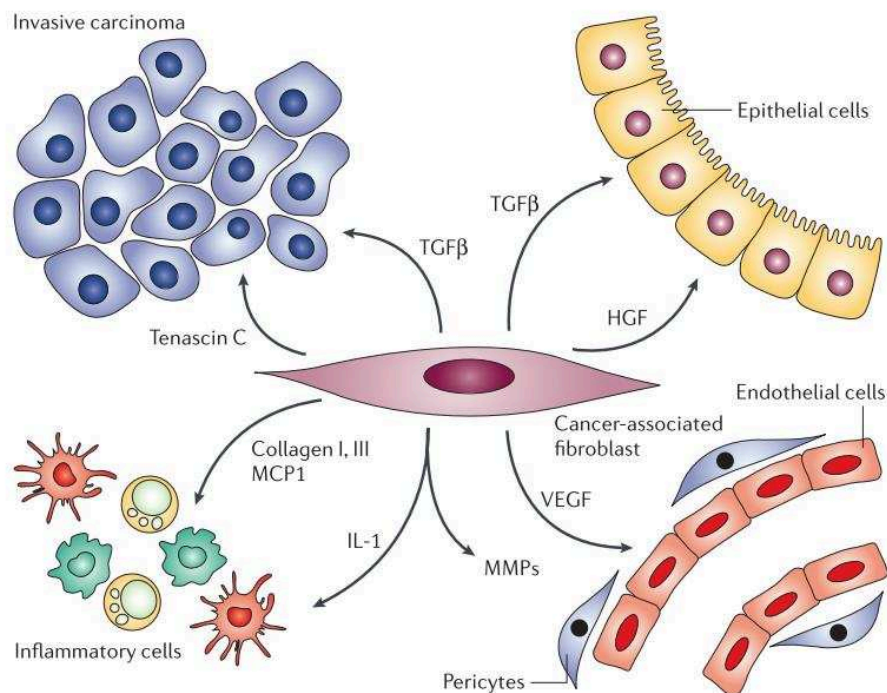


Figure 10. Carcinoma-associated fibroblasts influence the behavior of other cells in the tumor microenvironment. Besides their role in secreting and remodeling the ECM, CAFs also interact with the various cell types in the tumor microenvironment through diffusible molecules. CAFs mediate the inflammatory response by secreting chemokines such as monocyte chemotactic protein 1 (MCP1) and interleukins such as IL-1. Fibroblasts interact with endothelial cells by secreting vascular endothelial growth factor (VEGF). CAFs also provide potentially oncogenic signals such as transforming growth factor- β (TGF- β) and hepatocyte growth factor (HGF) to normal epithelial cells and cancer cells. From Kalluri and Zeisberg, 2006

iii. Endothelial cells, pericytes and orchestration of neoangiogenesis in tumors

Endothelial cells line the interior of blood and lymphatic vessels and they control the passage of materials and the transit of white blood cells into and out of the bloodstream. Veins, arteries, capillaries, and lymphatics all develop from small vessels constructed primarily of endothelial cells and basement membrane, whereas connective tissue and smooth muscle are added later for larger vessels, under the influence of signals from the endothelial cells (Alberts *et al.*, 2014). Endothelial cells are capable to extend and remodel the network of blood vessels, therefore they are key player in the process of neoangiogenesis occurring in tumors. Indeed, during tumor progression, angiogenesis is almost always activated. It causes normally quiescent vasculature to sprout new vessels

that help sustain expanding neoplastic growths (Hanahan and Folkman, 1996). Angiogenesis is a crucial event in tumor development because the presence of blood vessels allows vascular escape of cancer cells and later metastasis (Hanahan and Weinberg, 2011). The best known proangiogenic factor is vascular endothelial growth factor A (VEGF-A), that induces proliferation and migration of endothelial cells (Olsson *et al.*, 2006; Hanahan and Weinberg, 2011). VEGF gene expression can be upregulated both by hypoxia and by oncogene signaling (Carmeliet, 2005). In addition, other proangiogenic signals, such as members of the fibroblast growth factor (FGF) family, have been implicated in sustaining tumor angiogenesis when their expression is upregulated (Baeriswyl and Christofori, 2008).

The blood vessels produced within tumors are typically aberrant: tumor neovasculature is marked by convoluted and excessive vessel branching, enlarged and distorted vessels, erratic blood flow, small hemorrhages, leakiness, and abnormal levels of endothelial cell proliferation and apoptosis (Baluk *et al.*, 2003).

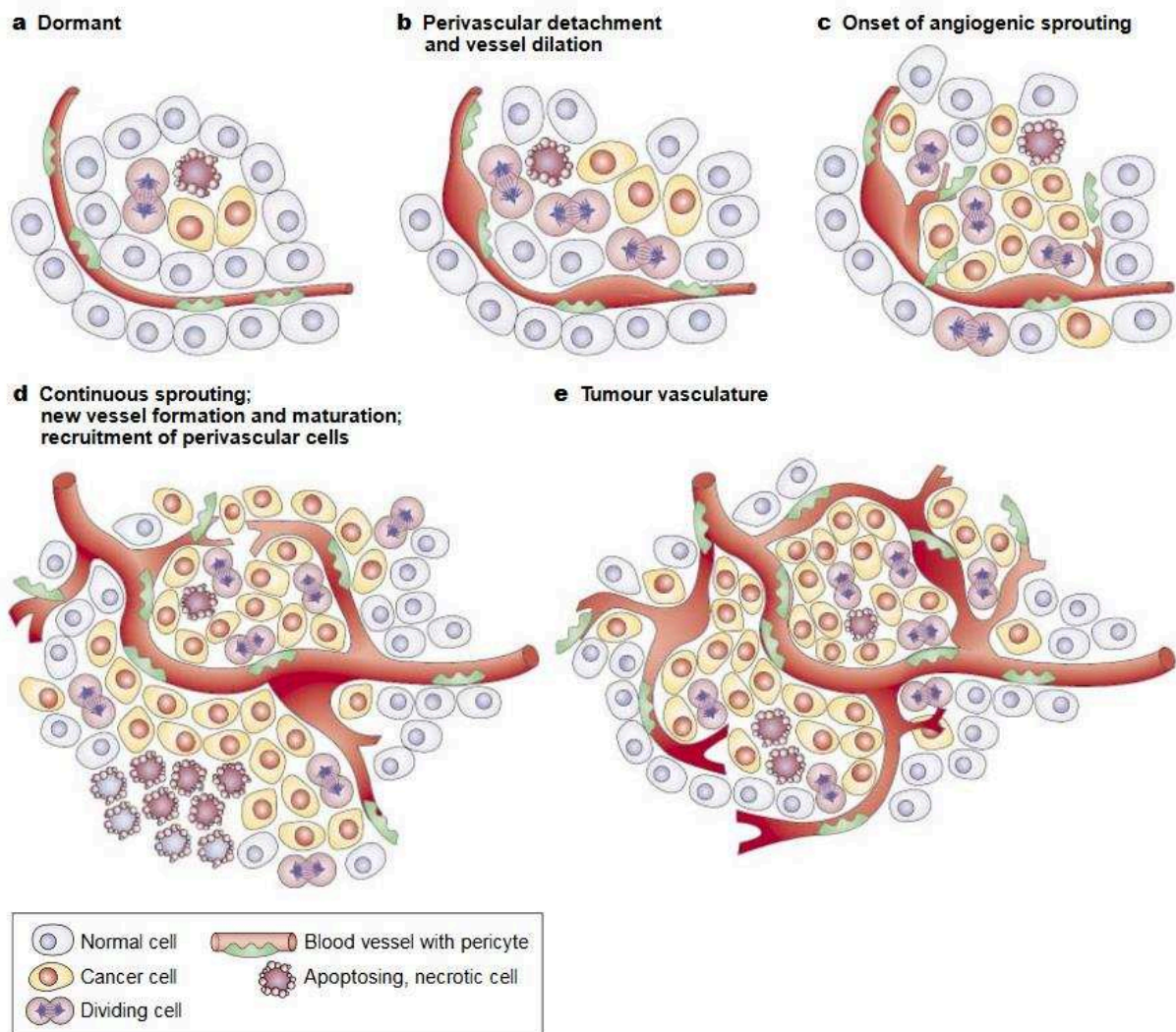


Figure 11. Tumor neoangiogenesis. The initiation of angiogenesis begins with pericyte detachment and vessel dilation (b), followed by angiogenic sprouting (c), new vessel formation and maturation, and the recruitment of perivascular cells (d). Blood-vessel formation will continue as long as the tumor grows (e). From Bergers and Benjamin, 2003

Pericytes are mesenchymal cells, related to vascular smooth muscle cells, that wrap themselves around small vessels. The recruitment of pericytes to blood vessels depends on platelet-derived growth factor β (PDGF- β) secreted by the endothelial cells (Song *et al.*, 2005). Indeed, mice that lack either PDGF-B or PDGFR- β show severe deficits in pericyte coverage of blood vessels, leading to widespread vascular leakage. Pericytes help remodel, stabilize and mature blood vessels thanks to their contractility and multiple cytoplasmic processes (Song *et al.*, 2005). Pericytes govern vessel stability and function

also through a crosstalk with endothelial cells, both cell types influencing each other's mitotic rate, differentiation and growth arrest (Song *et al.*, 2005).

During pathological angiogenesis in tumors, pericytes acquire structural and morphological abnormalities. They are frequently more loosely associated with blood vessels, and reduced in number when compared with normal tissue. This leads to vessels leakage, thus promoting cancer cell dissemination. Genetic ablation of pericytes has been shown to increase metastatic rates in insulinoma and breast cancer (Paiva *et al.*, 2018).

c. The protein fraction of the tumor microenvironment

The extracellular matrix (ECM) is the non-cellular component present within all tissues and it provides essential physical scaffolding for cells, as well as biochemical and biomechanical cues for tissue morphogenesis, differentiation and homeostasis. The importance of the ECM is illustrated by the wide-range of syndromes that arise from genetic abnormalities in ECM proteins (Järveläinen *et al.*, 2009). All ECMs are composed of water, proteins and polysaccharides (Hynes and Naba, 2012). However, the composition and organization of ECMs vary tremendously between tissues (Rozario and DeSimone, 2010; Mecham, 2012). The ECM is not a static and stable scaffold, but is surprisingly dynamic and constantly remodeled by cells. This cell-ECM crosstalk is due to both the biochemical and physical properties of the ECM (Lu, Weaver and Werb, 2012).

III. Composition of the cancer ECM

a. Collagens are the major proteins of the extracellular matrix

Collagens are the most abundant proteins in mammals, where they represent 30% of the total protein mass. Collagens are found in all metazoa and provide structural strength to all forms of ECMs, including the strong fibers of tendons, the matrices of bones and cartilages, the sheets of basement membranes, and the interstitial ECMs, such as the ones of the dermis.

The first evidence that collagen possesses a regular structure at the molecular level was presented in the mid-1930s, when physicists applied X-ray crystallography to elucidate

the organization of biological samples, such as animal tendons, hair and spines (Astbury and Woods, 1934; Wyckoff, Corey and Biscoe, 1935). In a seminal study in 1935, Wyckoff and colleagues have described tendon and hair proteins as examples of the “insoluble [...] group of crystalline protein structures” that possesses typical fiber diffraction patterns visualized by X-ray crystallography (Wyckoff, Corey and Biscoe, 1935).

In 1951, physicists Linus Pauling and Robert Corey described the structure of collagen in which three polypeptide strands are held together in a helical conformation by hydrogen bonds (Pauling and Corey, 1951). More recently, the triple helix as a common structural feature of collagens has been found to range from most of the protein structure (96% for collagen I) to less than 10% (collagen XII) (Ricard-Blum, 2011). This repeating structure forms stable trimeric coiled coils, which can be of varying lengths (Hynes and Naba, 2012).

In 1969 the first collagen protein has been isolated and described in terms of amino acids content by Miller and Matukas (Miller and Matukas, 1969). Since then, a total of 28 members of the collagen superfamily have been described in vertebrates (Ricard-Blum, 2011).

Collagens can be subdivided into subfamilies based on their supramolecular assemblies: collagens forming fibrils, fibril-associated collagens, and network-forming collagens.

Fibrillar collagens provide structural strength to connective tissues. Collagen fibrils are made of collagens II, XI, and IX or of collagens II and III (Wu *et al.*, 2010) in cartilage, and of collagens I and III in skin, and of collagens I and V in cornea (Bruckner, 2010). In the next section, I will describe fibrillar collagen synthesis and assembly using collagen I as an archetypal fibrillar collagen.

Fibril-associated collagens (FACITs) do not aggregate to form fibrils by themselves. They are associated to the surface of collagen fibrils to which they bind in a periodic manner (Ricard-Blum, 2011). For example, collagen IX is covalently linked to the surface of cartilage collagen fibrils mostly composed of collagen II (Olsen, 1997), and collagens XII and XIV are associated to collagen I-containing fibrils in tendons. Moreover, the triple-stranded helical structure of FACITs differs from the one of fibrillary collagens, because it

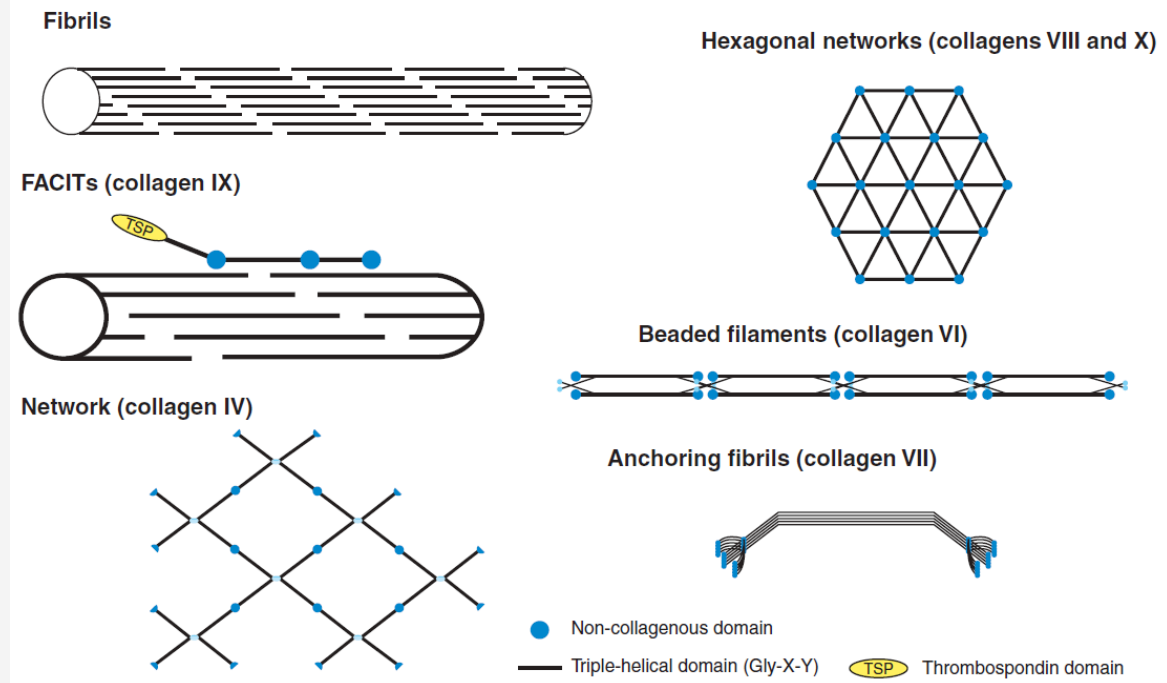
is interrupted by one or two short nonhelical domains, which makes the molecules more flexible than fibrillar collagen molecules. FACITs are thought to be especially important in organizing collagen fibrils. They mediate the interactions of collagen fibrils with one another and with other matrix macromolecules to help determine the organization of the fibrils in the matrix (Ricard-Blum, 2011).

Network-Forming Collagens are another subfamily of collagens. Its most famous member is collagen IV, that forms a network present in the basement membrane that lines epithelia. I will describe its structure and functions in the “basement membrane” section below.

Box 3. The many faces of collagens

The collagen family is composed of large variety of proteins, that differ in size, function, localization and in the nature of macromolecular assemblies they can form.

The supramolecular assemblies adopted by the different collagens help them fulfil their functions. Here are some examples of the myriad of forms adopted by collagens:



From Richard-Bloom, 2011

Different types of collagens adopt different assemblies and are present in various tissues:

Some Types of Collagen and Their Properties				
	Type	Polymerized form	Tissue distribution	Mutant phenotype
Fibril-forming (fibrillar)	I	Fibril	Bone, skin, tendons, ligaments, cornea, internal organs (accounts for 90% of body collagen)	Severe bone defects, fractures (<i>osteogenesis imperfecta</i>)
	II	Fibril	Cartilage, intervertebral disc, notochord, vitreous humor of the eye	Cartilage deficiency, dwarfism (<i>chondrodysplasia</i>)
	III	Fibril	Skin, blood vessels, internal organs	Fragile skin, loose joints, blood vessels prone to rupture (<i>Ehlers-Danlos syndrome</i>)
	V	Fibril (with type I)	As for type I	Fragile skin, loose joints, blood vessels prone to rupture
	XI	Fibril (with type II)	As for type II	Myopia, blindness
Fibril-associated	IX	Lateral association with type II fibrils	Cartilage	Osteoarthritis
Network-forming	IV	Sheetlike network	Basal lamina	Kidney disease (glomerulonephritis), deafness
	VII	Anchoring fibrils	Beneath stratified squamous epithelia	Skin blistering
Transmembrane	XVII	Nonfibrillar	Hemidesmosomes	Skin blistering
Proteoglycan core protein	XVIII	Nonfibrillar	Basal lamina	Myopia, detached retina, hydrocephalus

Note that types I, IV, V, IX, and XI are each composed of two or three types of α chains (distinct, nonoverlapping sets in each case), whereas types II, III, VII, XVII, and XVIII are composed of only one type of α chain each.

From Alberts *et al.*, 2014

b. Synthesis and assembly of collagen I, the archetypal fibrillar collagen.

Type I collagen is the most abundant collagen and the archetypal fibrillar collagen, therefore we will use it as an example for fibrillogenesis. Collagen I has a triple helical structure and assembles into fibrils, having a predominately structural role in tissues.

Collagen polypeptide chains typically display the presence of repeats of the amino-acid triplet Gly-X-Y, where X is frequently proline and Y is frequently hydroxyproline (Alberts *et al.*, 2014). These polypeptide α chains are left-handed polyproline II helices that also called protocollagen strands. In the first steps of collagen fibrillogenesis, three protocollagen strands (two α 1 chains and one α 2 chain) assemble in a right-handed triple helix called procollagen (Mouw, Ou and Weaver, 2014). In the case of fibrillar collagens such as collagen I, the formation of the procollagen triple-helix is initiated from the C-terminus of single protocollagen strands. Procollagen triple helices are stabilized by the presence of glycine as every third residue, and by interchain hydrogen bonds. Procollagen strands are being secreted by the cell in the extracellular space, where the N- and C-terminal propeptides are cleaved, which allows tropocollagen triple helices to self-assemble into microfibrils. In microfibrils, adjacent tropocollagen molecules are displaced from one another by 67 nm, about one-quarter of their length. Microfibrils are then crosslinked by lysyl-oxylase, which allows the formation of robust collagen fibers (Mouw, Ou and Weaver, 2014). During fibrillogenesis, there is a dramatic increase in the size of collagen assemblies. Indeed, a single α helix of protocollagen is 300nm long, whereas the association of numerous collagen fibrils gives rise to fibers that can be up to 1cm long, such as the ones present in tendons. Moreover, the assembly of strong macromolecular structures is essential to enable collagen to support stress in one, two, and three dimensions. I will come back to the physical properties of collagen scaffolds in Chapter 4.

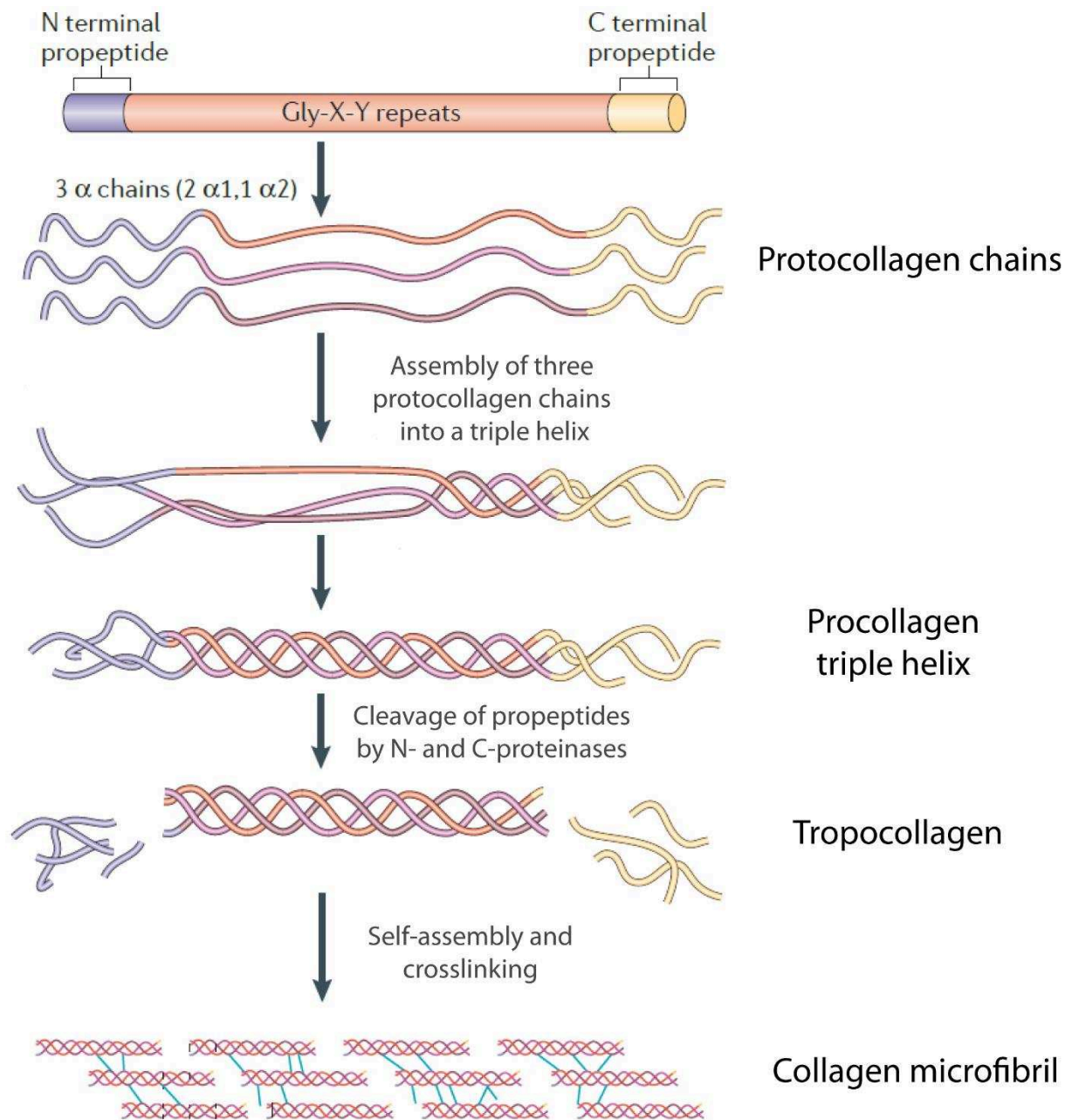


Figure 12. Collagen I assembly. In the first steps of collagen fibrillogenesis, three protocollagen polypeptide chains assemble in a right-handed triple helix called procollagen. After secretion in the extracellular milieu, the N- and C-terminal propeptides are cleaved, which allows tropocollagen triple helices to self-assemble into microfibrils, which are crosslinked by lysyl-oxidase. The association of several microfibrils forms robust collagen fibers (not shown). Adapter from Mouw, Ou and Weaver, 2014

c. Glycosaminoglycans and proteoglycans occupy large amounts of space and form hydrated gels

Glycosaminoglycans (GAGs) are long unbranched polysaccharides consisting of a repeating disaccharide unit (Frantz, Stewart and Weaver, 2010; Alberts *et al.*, 2014). One of the two sugars in the disaccharide is always an amino sugar (N-acetylglucosamine or N-acetylgalactosamine), which in most cases is sulfated. The second sugar is either galactose or uronic acid (glucuronate or iduronate). Based on the difference of repeating disaccharide units comprising GAGs, they can be categorized into four main groups: heparan sulfate, chondroitin sulfate and dermatan sulfate, keratan sulfate, and hyaluronic acid. Because there are sulfate or carboxyl groups on most of their sugars, GAGs are highly negatively charged. This high negative charge leads GAGs to adopt extended conformation because of electrostatic repulsions. This extended conformation of GAGs is facilitated by the fact that the stiffness of polysaccharide chains don't allow much bending. Moreover, the high negative charge allows sequestering of divalent cations such as calcium, causing large amounts of water to be sucked into GAGs by osmosis. GAGs form therefore hydrated gels that possess space-filling and lubrication functions and occupy a large volume relative to their mass (Alberts *et al.*, 2014). The weight of GAGs in connective tissue is usually less than 10% of the weight of proteins, but GAG chains fill most of the extracellular space. Because they are highly hydrated and they adopt extended conformations, GAGs provide the extracellular matrix with additional physical properties not provided by structural proteins alone, such as high resistance to compressive stresses (Frantz, Stewart and Weaver, 2010; Malandrino *et al.*, 2018). GAGs, especially heparan sulfates, also bind many secreted and growth factors into the ECM (Sarrazin, Lamanna and Esko, 2011). For example, binding of FGF to its receptor depends on heparan sulfate as cofactor (Mohammadi, Olsen and Goetz, 2005).

Proteoglycans (PGs) are composed of GAG chains covalently linked to a specific protein core (Frantz, Stewart and Weaver, 2010). Covalent tetrasaccharide bonds allow the link between serine residues on proteins and GAGs (with the exception of hyaluronic acid). PGs have been classified according to their core proteins, localization and GAG composition. The three main families are: small leucine-rich proteoglycans (SLRPs), modular proteoglycans and cell-surface proteoglycans (Schaefer and Schaefer, 2010).

SLRPs, such as decorin, have been involved in multiple signaling pathways including binding to and activation of TGF- β , epidermal growth factor receptor and insulin-like growth factor 1 receptor (Schaefer and Schaefer, 2010). Modular PGs, such as perlecan or testican, can modulate cell proliferation, adhesion and migration (Schaefer and Schaefer, 2010). Cell-surface PGs, such as syndecans, can act as co-receptor facilitating ligand encounters with signaling receptors (Schaefer and Schaefer, 2010).

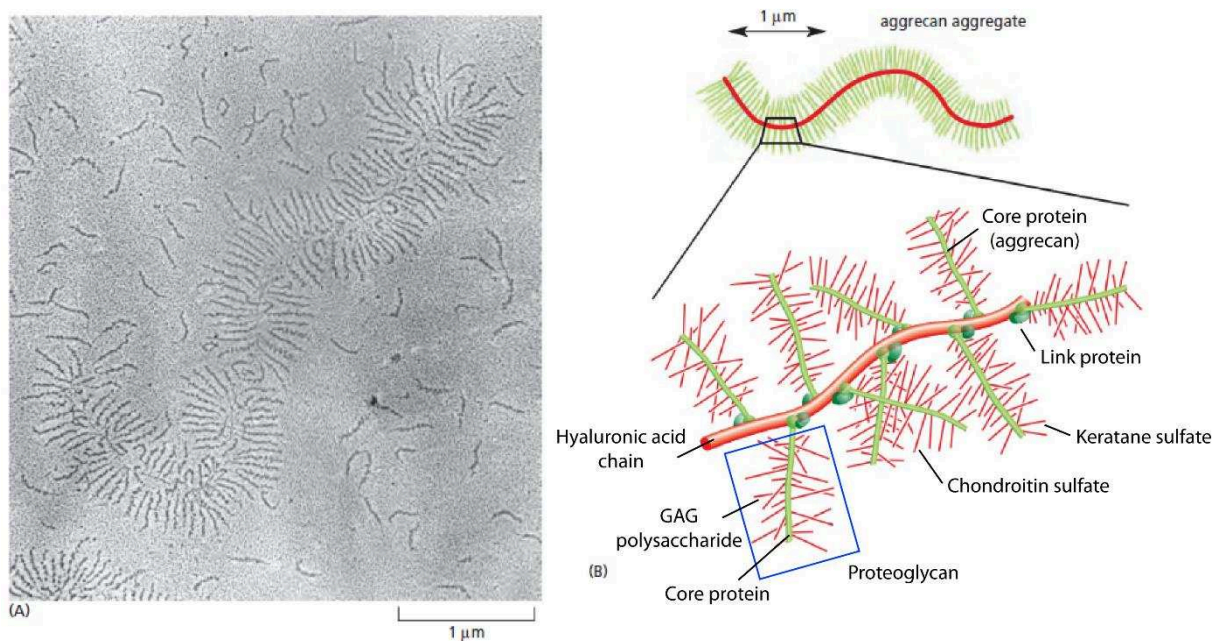


Figure 13. Aggregate of proteoglycans found in conjunctive tissues. (A) An electron micrograph of an aggrecan aggregate revealed by platinum. Many free aggrecan molecules are also visible. (B) A drawing of the giant aggrecan aggregate shown in (A). It consists of about 100 aggrecan proteoglycans bound through the core protein to a single hyaluronic acid chain. A link protein binds both to the core protein of the proteoglycan and to the hyaluronic acid, stabilizing the aggregate. Such a complex occupies a volume equivalent to that of a bacterium. Modified from Alberts *et al.*, 2014

d. Elastic fibers provide tissues their elasticity

A variety of vertebrate connective tissues, such as the ones of blood vessels, lungs and skin, need to be elastic in order to function (Gibson *et al.*, 1986). The network of elastic fibers in the ECM of these tissues gives them the resilience to recoil after transient stretch (Midwood and Schwarzbauer, 2002). I will come back to the physical properties of these special fibers in Chapter 4. Elastic fibers are components of the ECM that are also involved in a number of disease processes such as atherosclerosis, pulmonary deficits, and some cancers (Alberts *et al.*, 2014).

The main component of elastic fibers is elastin, a highly hydrophobic protein which, like collagen, is unusually rich in proline and glycine (Midwood and Schwarzbauer, 2002; Alberts *et al.*, 2014). The biosynthetic precursor of elastin is called tropoelastin and is secreted into the extracellular space and assembled into elastic fibers close to the plasma membrane (Midwood and Schwarzbauer, 2002). After secretion, tropoelastin molecules become highly cross-linked to one another thanks to lysyl-oxylase, generating a large rubber-like network of elastin fibers (Rosenbloom, Abrams and Mecham, 2016). The elastin protein is composed of two types of short segments that alternate along the polypeptide chain: hydrophobic segments, which are responsible for the elastic properties of the molecule; and alanine- and lysine-rich α -helical segments, which are cross-linked to adjacent molecules by covalent bonds on lysine residues. The conformation of elastin molecules in elastic fibers has not been completely elucidated, but it seems that parts of the elastin polypeptide chain adopt a loose “random coil” conformation, and it is the random coil that would allow the network to stretch and recoil like a rubber band (Alberts *et al.*, 2014).

Elastic fibers do not consist solely of elastin. The elastin core is covered with a sheath of microfibrils, each of which has a diameter of about 10 nm (Midwood and Schwarzbauer, 2002). Microfibrilles are composed of a number of distinct glycoproteins, including the large glycoprotein fibrillin, which seem to provide scaffolding to guide elastin deposition. Indeed, microfibrils appear before tropoelastin secretion. They form a scaffold on which elastin is deposited before it is displaced to the periphery of the growing fiber (Midwood and Schwarzbauer, 2002). The assembly of elastic fibers seems to be facilitated by Fibulin 5, that is able to bind both cell surface integrins and tropoelastin proteins (Argraves *et al.*,

2003). In support of that, mice deficient in fibulin 5 have defective assemblages of elastic fibers (Midwood and Schwarzbauer, 2002).

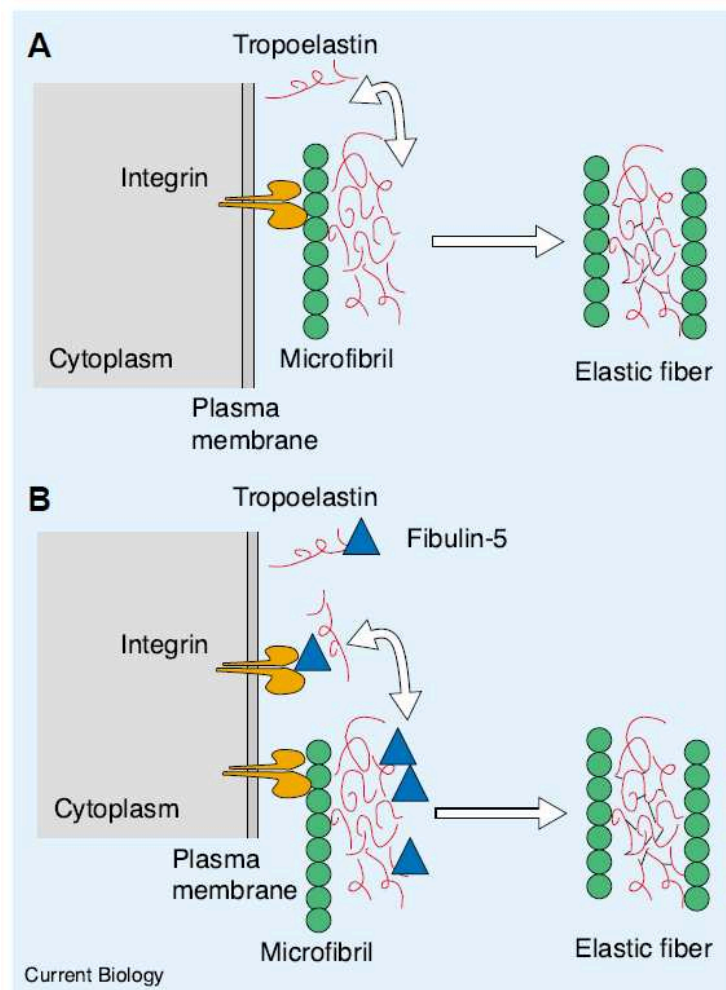


Figure 14. Assembly of elastic fibers. (A) Microfibrils (green) are assembled at the cell surface, where fibrillin interacts with integrin receptors (orange) via RGD sequences. Tropoelastin (red) is secreted from the cell and deposited onto microfibril scaffolds, enabling efficient elastin polymerization. Elastin molecules are joined together by covalent bonds (short black lines) to generate a network. (B) Fibulin-5 may act as a chaperone in elastic fiber assembly. Fibulin-5 binds tropoelastin, as well as integrins (orange). Fibulin-5 may tether elastin to the cell by interacting with. In this way fibulin-5 may regulate elastic fiber assembly by the microfibril machinery. From Midwood and Schwarzbauer, 2002

e. Glycoproteins confer additional functions to ECMs

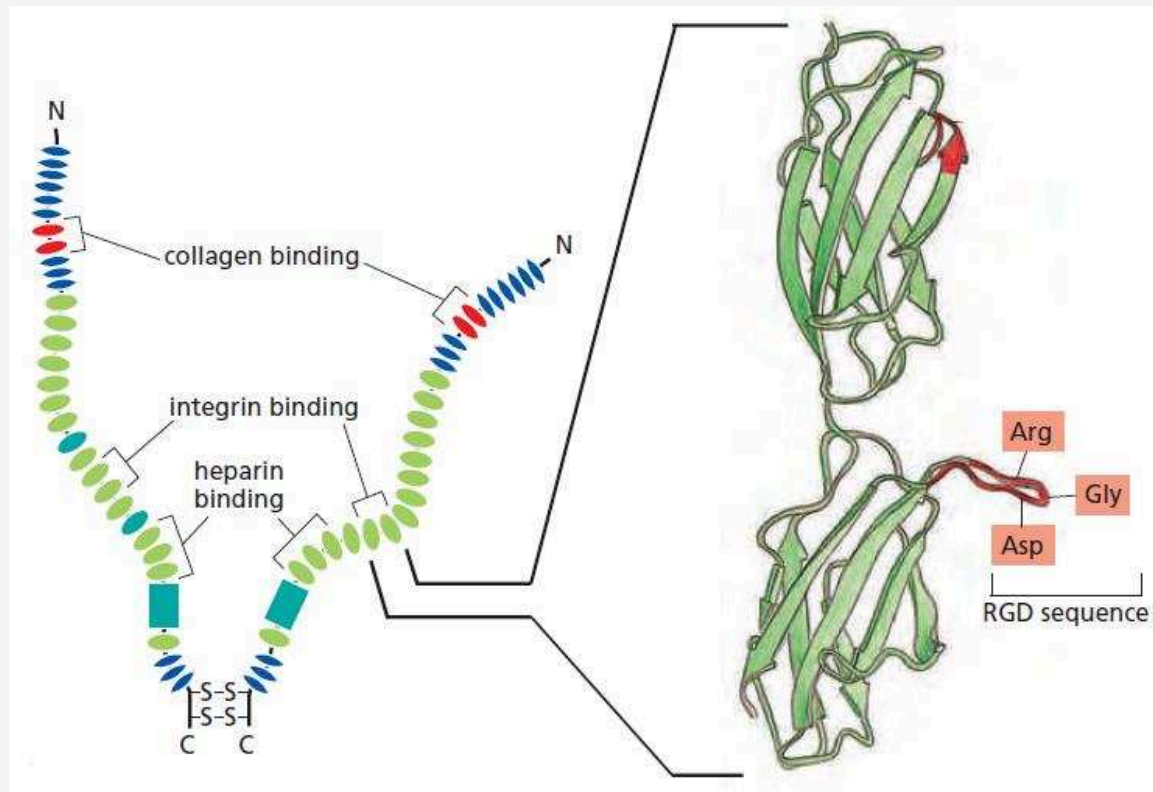
In addition to collagens, glycosaminoglycans and proteoglycans, there are around 200 complex glycoproteins in mammals (Naba *et al.*, 2012) that typically have multiple domains, each with specific binding sites for other matrix macromolecules and for receptors on the surface of cells (Alberts *et al.*, 2014). These proteins therefore contribute to both organizing the matrix assembly and helping cells attach to it. The best-studied ECM glycoproteins are laminin, fibronectin, Tenascin-C and nidogen. I will discuss laminin and nidogen when describing the structure and assembly of the basement membrane.

Fibronectin (FN) is a large and multidomain protein that has the ability to bind simultaneously to cell surface receptors, collagen, proteoglycans and other fibronectin molecules (Schwarzbauer and DeSimone, 2011). Because of these various binding sites, the architecture of FN networks contributes directly to the structure and organization of the wider ECM. By binding to cell surface integrins, FN regulates cell adhesion, migration, and differentiation (Schwarzbauer and DeSimone, 2011).

FN matrix assembly is a cell-mediated process in which secreted FN is converted into a fibrillar network (Pankov and Yamada, 2002). Binding of FN to cells via integrins induces reorganization of the actin cytoskeleton by outside-in signaling, leading to cell-mediated application of tensile forces through focal adhesions (Lemmon, Chen and Romer, 2009; Erickson, 2017). This leads the compact FN molecule to undergo conformational changes that expose cryptic “self-association” sites that promote FN-FN interactions (Pankov and Yamada, 2002; Wierzbicka-Patynowski and Schwarzbauer, 2003). Interactions between FN molecules enable FN fibrils to branch and convert into a dense and stable network (Pankov and Yamada, 2002).

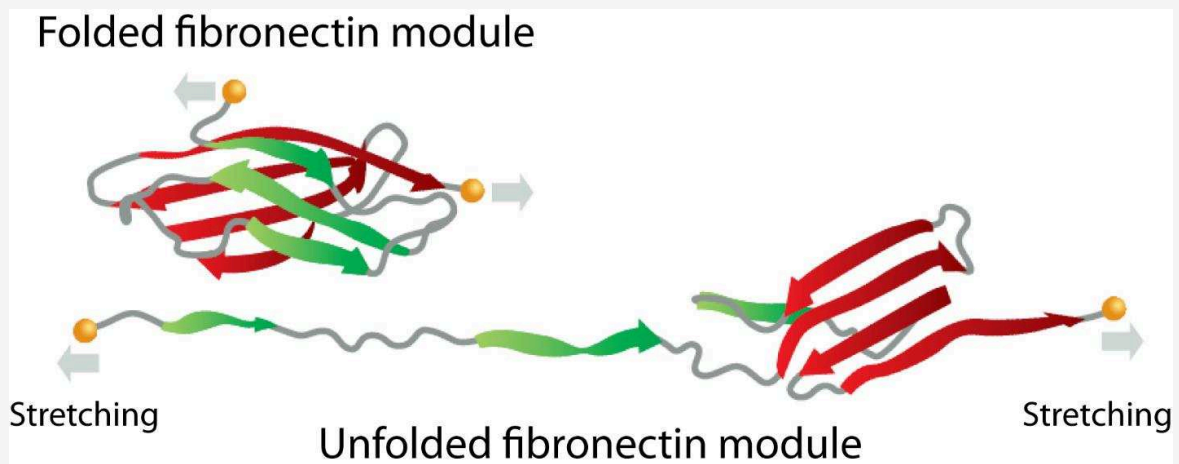
Box 4. Tension sensing by fibronectin

Fibronectin is a versatile extracellular matrix protein in the sense that it possesses binding sites for various ECM components. The two polypeptide chains of FN are similar but generally not identical, being made from the same gene but from differently spliced mRNAs. Each chain is almost 2500 amino acids long and is folded into multiple modules with different structures, that are of 3 types: type I, II, and III. As indicated, some domains are specialized for binding to a particular molecule.



From Alberts *et al.*, 2014

Fibronectin is able to respond to mechanical stress by unfolding. Upon stretch, fibronectin converts force into biochemical signals by exposing cryptic binding sites necessary for protein-protein interactions. It is in particular the FN III1 module that is able to undergo large structural changes upon application of tension (mainly via integrins), as depicted below.



From Viola Vogel and Michael Sheetz, 2006

Tenascin-C is a glycoprotein of connective tissues. It is an hexameric, multimodular ECM protein with several molecular forms that are created through alternative splicing and protein modifications (Midwood *et al.*, 2016). Tenascin-C has many extracellular binding partners, including matrix components, soluble factors and cell surface receptors (Midwood *et al.*, 2016). It is best-known as a modulator of cell adhesion to the ECM owing to its ability to bind to fibronectin, and to alter cell spreading and signaling mediated by fibronectin and integrins (Chiquet-Ehrismann *et al.*, 1986; Midwood *et al.*, 2005). Tenascin-C is incorporated into the ECM in a manner which is dependent upon the presence of heparan sulfate proteoglycans (Giblin and Midwood, 2015). Tenascin-C is widely expressed in embryonic tissues, but restricted in adults to stem cell niches and tendons (Chiquet-Ehrismann *et al.*, 2014) and at sites of active tissue remodeling and inflammation, such as in wound healing and cancer (Giblin and Midwood, 2015).

IV. The basement membrane, a specialized type of ECM supporting epithelia

Basement membranes are thin sheets of ECM at the basal side of every epithelium. They provide structural and adhesive support to cells, coating the basal side of epithelial and endothelial cells and surrounding muscles, adipocytes, and peripheral nerve axons (Glentis, Gurchenkov and Vignjevic, 2014). Many of the genes encoding basement membrane proteins are ancient and emerged about 500 million years ago and they are one of the evolutionary oldest ECM proteins (Ozbek *et al.*, 2010; Hynes, 2012; Fidler *et al.*, 2017). They are found in most metazoan, and one can argue that basement membranes were crucial to the evolution of metazoa (Ozbek *et al.*, 2010; Hynes, 2012). In 1988, Simon-Assman and colleagues addressed the cellular origin of basement membrane components using interspecies tissue recombination (Simon-Assmann *et al.*, 1988). By hybridizing chick mesenchymes with rat endodermal epithelium and using tissue-specific antibodies, they demonstrated that BM components, such as nidogen, laminin and type IV collagen, were successfully deposited only when both epithelial and mesenchymal cell types were associated.

The BM provides structural and adhesive support to the epithelium, maintains cell polarity and separates epithelium from the stromal compartment underneath, leading to a compartmentalization of tissues (Glentis, Gurchenkov and Vignjevic, 2014; Kelley *et al.*, 2014). BMs also serve as a reservoir for growth factors, such as fibroblast growth factor (FGF), transforming growth factor β (TGF- β), vascular endothelial growth factor (VEGF), which play a role in cell survival, migration, and proliferation (Iozzo, Zoeller and Nyström, 2009). Even though BMs represent a physical barrier, they are breached in many physiological or pathological processes, including development, immune response, and tumor invasion.

a. Composition of the basement membrane

Laminin is the most abundant non-collagenous protein in the BM. Laminin is a heterotrimer consisting of α , β , and γ -chains. Laminins are generally composed of a coiled-coil region that is responsible for the assembly of the heterotrimers, a C-terminal LG domain in α chains that is responsible for cell surface adhesion, and an N-terminal LN domain which plays a role in laminin polymerization and network formation (Glentis, Gurchenkov and Vignjevic, 2014). Different combinations of α , β , and γ -chains lead to the generation of 15 different heterotrimers, such as laminin-111 ($\alpha 1\beta 1\gamma 1$) or laminin-211 ($\alpha 2\beta 1\gamma 1$), that have different roles in tissue structure and cell behavior. Chains are joined together via a their coiled-coil domains, from which the N termini of each of the three chains emerge as three arms.

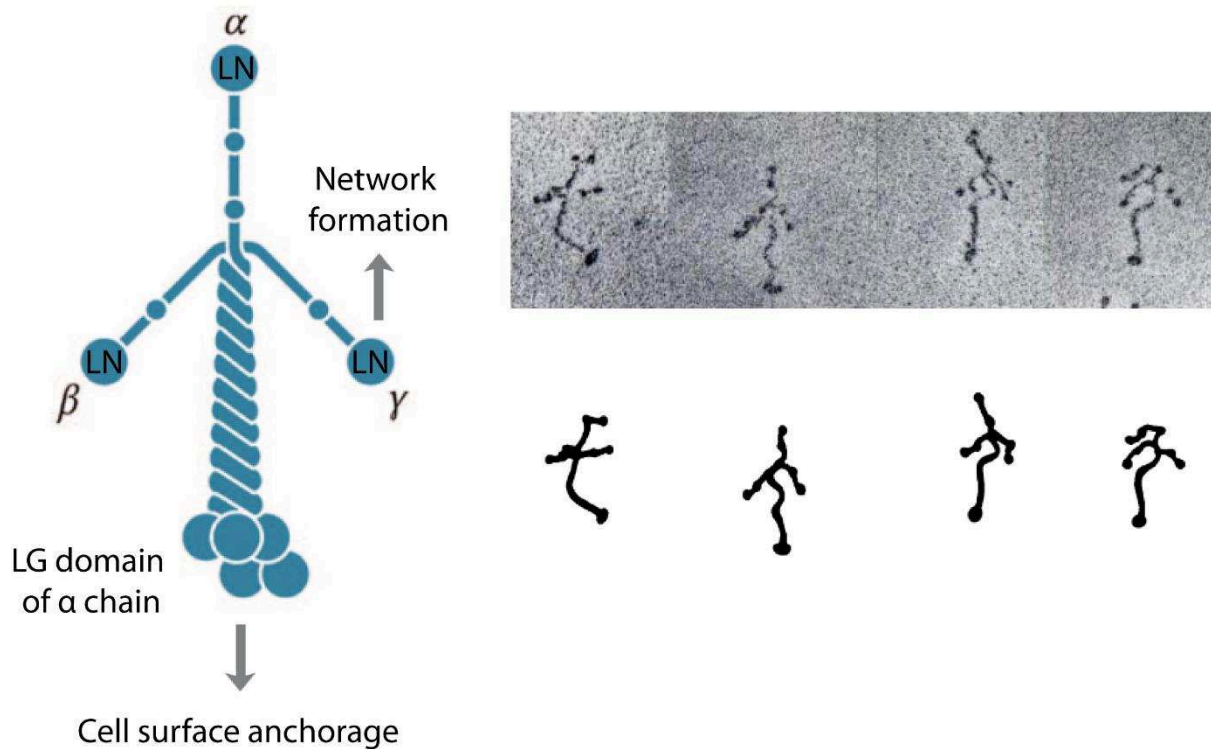


Figure 15. Laminin structure. Left: schematic representation of a laminin heterotrimer with depicted C-terminal LG domain of α chains (for cell surface adhesion), coiled-coil domain (for the assembly of the heterotrimers) and N-terminal LN domain (for laminin network formation). Adapted from Glentis. Right: Electron micrographs of laminin heterotrimers (up) and interpretative drawings (down). From Yurchenco and Schnittky, 1990

Type IV collagen is a non-fibrillar collagen and the most abundant protein in adult human BMs, accounting for more than 50% of the BM protein mass (Halfter *et al.*, 2013). Collagen IV is a heterotrimer of three separately synthesized long protein chains that twist together to form a superhelix; however, they differ from the fibrillar collagens in that the triple-stranded helical structure is interrupted in more than 20 regions, allowing multiple bends (Khoshnoodi, Pedchenko and Hudson, 2008). Collagen IV also differs from fibrillar collagens by its distinct capacity to self-assemble into networks. Indeed, collagen IV molecules interact via their terminal domains to assemble into a flexible network that gives the BM tensile strength. There are six genetically different α -chains ($\alpha 1$ – $\alpha 6$), which can assemble into three different heterotrimers. The most common variant, found in almost all BMs, consists of two $\alpha 1$ subunits and one $\alpha 2$ subunit. Each α chain contains an N-terminal 7S domain that is important for the formation of collagen networks; a collagenous domain that is able to form triple helices; and a C-terminal NC1 domain,

which plays a role in the assembly of the collagen IV dimers (Mouw, Ou and Weaver, 2014).

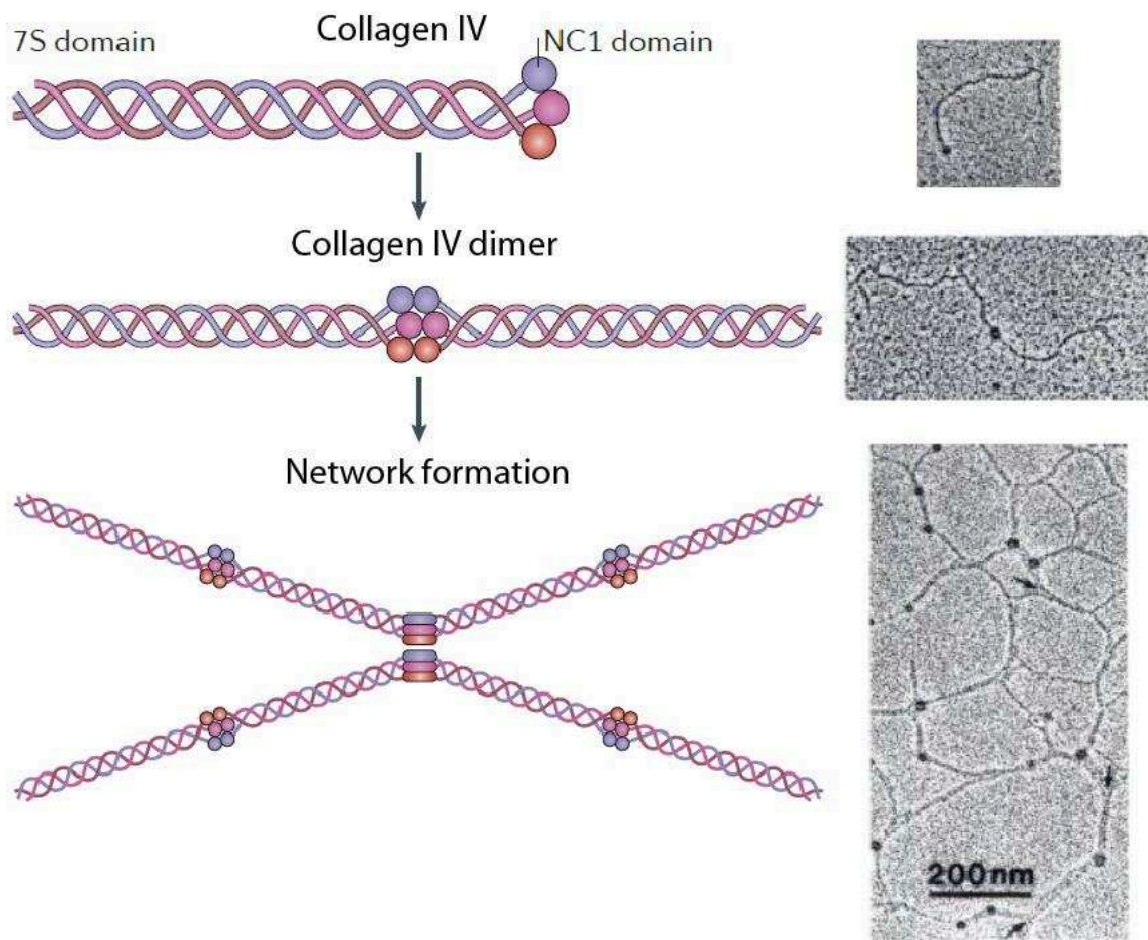


Figure 16. Network formation by collagen IV. Left: collagen IV is characterized by a C-terminal NC1 domain and an N-terminal 7S domain that facilitate the formation of dimers and networks of collagen IV, respectively. Adapted from Mouw and Weaver. Right: electron micrographs of collagen IV molecule (up), dimer (middle) and network (bottom). Adapted from Yurchenco and Schnitty, 1990

b. Assembly of the basement membrane.

Basement membrane assembly is initiated upon laminin secretion by cells. First, the C-terminal LG domains of the α chains of laminin heterotrimers bind to cell surfaces through matrix receptors such as integrins and dystroglycan (Glentis, Gurchenkov and Vignjevic, 2014; Morrissey and Sherwood, 2015). This increase of density of laminin on the cell surface facilitates its polymerization, which is mediated by the α , β , and γ -chains of adjacent laminins (Li and Thompson, 2003; Yurchenco and Wadsworth, 2004). Thus cell surface anchorage of laminin and self-assembly are linked. The polymerized laminin network serves as scaffold for further build-up of basement membrane, including the polymerization of a network of type IV collagen (Poschl *et al.*, 2004). The glycoprotein nidogen and the heparan sulfate proteoglycan perlecan bind both the laminin and collagen networks, and thus help link and stabilize these two lattices (Costell *et al.*, 1999; Glentis, Gurchenkov and Vignjevic, 2014; Morrissey and Sherwood, 2015). Interestingly, these molecules are unable to form basement membranes in the absence of a laminin scaffold (McKee *et al.*, 2007; Glentis, Gurchenkov and Vignjevic, 2014).

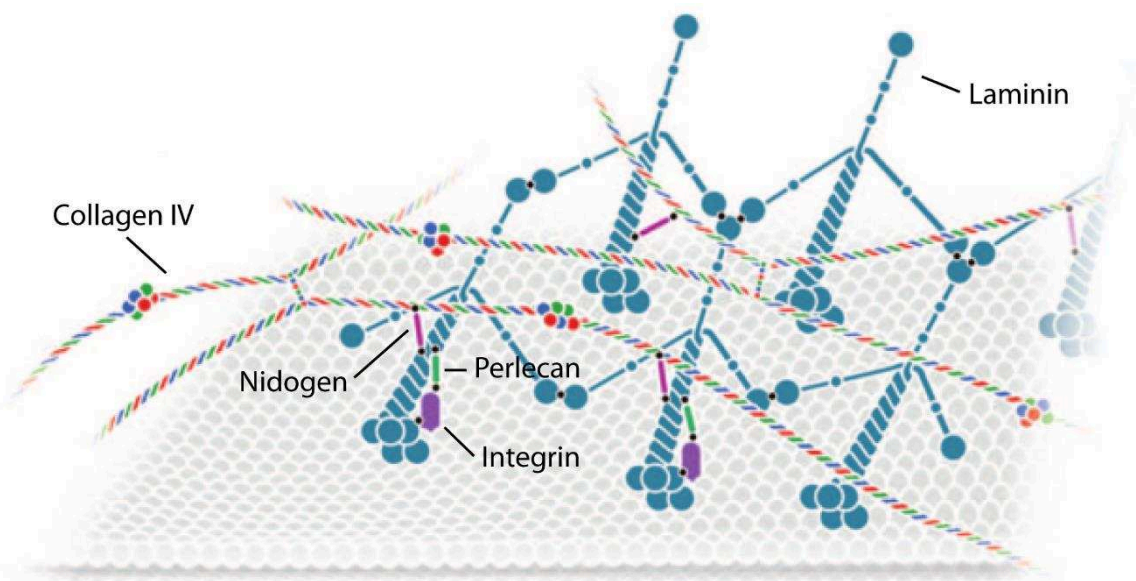


Figure 17. Assembly of the basement membrane. Laminin and collagen IV are secreted in the extracellular milieu. Laminin binds to cell surface receptors, such as integrins, via the LG domain of the α -chain. Intermolecular binding between LN domains of α , β and γ -chains of adjacent laminins results in the formation of a network. Laminin serves as scaffold for the polymerization of a network of collagen IV. Nidogen and perlecan serve as binding bridges between the two networks to form a dense mesh. Adapted from Glentis, Gurchenkov and Vignjevic, 2014

V. The tumor microenvironment is continuously remodeled in tumor progression

The ECM, a highly organized network of crosslinked macromolecules, provides a structural frame for cancer cell migration (Friedl and Wolf, 2010) and its properties are commonly misregulated in cancer. Remodeling of the ECM, in terms of changes in structural organization, fiber alignment, stiffness and molecular composition can promote tumor progression (Friedl and Alexander, 2011).

An essential component of the remodeling of the ECM is proteolytic cleavage of its fibers. This breakdown is also vital but dysregulated in the early steps of local invasion of malignant cells into adjacent tissue. Cancer cells, but also CAFs, are a source of ECM-degrading proteases such as the matrix metalloproteases (MMPs) and other proteases, such as serine proteases, that affect the motility and invasiveness of cancer cells. In cancer, ECM fibers are not only proteolytically cleaved and reorganized, but their synthesis and secretion is also altered. I will come back to the modifications of the ECM in tumor progression in Chapter 3.

PART 3 - CANCER CELL MIGRATION THROUGH THE TUMOR MICROENVIRONMENT

Acquisition of migratory capacity by cells is a key step promoting the metastatic cascade. The first step in metastasis is the migration of cancer cells away from the primary tumor, a process called tumor invasion. Understanding the fundamental principles of cell motility provides therefore valuable insights into cancer metastasis.

I. Single cell migration

a. Cell migration on 2D substrates.

The molecular bases of single cell locomotion have first been described in 2D substrates (King and Parsons, 2011). Cell motility requires an intracellular molecular machinery that allows to fulfill the different sequential steps for migration: 1/ protrusion at the leading edge 2/ adhesion to the substrate 3/contraction of the cell body 4/ retraction of the cell rear and disassembly of adhesion in the rear to allow for cell translocation.

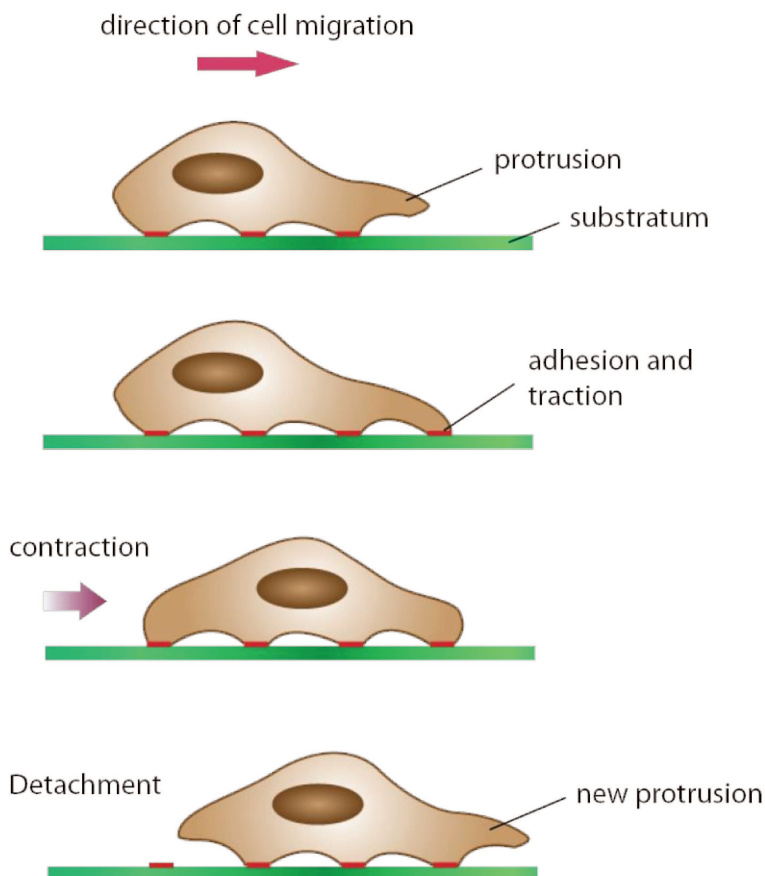


Figure 18. Cell migration on 2D substrates. A cell migrating in 2D must complete a series of steps. First, a protrusion appears at the leading edge and gets anchored to the substratum through cell-ECM adhesions. Then the cell contracts its body and the trailing edge detaches from the substrate, thus allowing for cell translocation.

Protrusion. Back in the 1960's, Abercrombie first described a "locomotory organ" in migrating fibroblasts (Abercrombie, 1961), as a polarized and dynamic cell membrane protrusion. The apparition of a polarized structure in a cell relies on the sensing of gradients of extracellular cues. Cells respond to different extracellular cues that can be chemical (gradients of chemokines or growth factors), physical (stiffness of the substrate), or topological (architecture of the substrate). The asymmetric activation of cell surface receptors promotes the polarization of the cell, which creates morphologically distinct cell front and cell back (King and Parsons, 2011). The cell polarization is accompanied by the relocalization and reorganization of cytoskeletal components such as microtubules and Golgi apparatus in front of the nucleus. A polarized protrusion is born when actin polymerization is sustained in a region that will become the front of the cell. There are two types of actin-rich protrusions: flat, broad and thin called lamellipodia, and finger-like long extensions- filopodia (Faix and Rottner, 2006; Rottner *et al.*, 2017). Lamellipodia contain a network of branched actin filaments and are the main source of force generation for cell locomotion (Pollard and Borisy, 2003; Rottner *et al.*, 2017). Filopodia are composed of a tightly bundled actin filaments and are believed to be a sensory and guidance organelle (Faix and Rottner, 2006). Actin polymerization in these structures is promoted by actin nucleators. The Arp2/3 complex induces the formation of a branched actin organization as the one found in lamellipodia. Filopodial actin filaments are also polymerized by formins such as mDia2. A great diversity of co-factors, that sequester, cap, sever and cross-link actin filaments, accompany the shaping of actin networks.

Attachment. For a cell to advance, a newly extended protrusion needs to adhere the substrate. Nascent adhesions in the front of the cell mature to form focal adhesion, that link the actin cytoskeleton to the ECM (Geiger, Spatz and Bershadsky, 2009; Geiger and Yamada, 2011). Focal adhesions are composed of a large array of proteins with distinct roles: matrix receptors (such as integrins), signaling proteins (such as focal adhesion kinase, FAK), proteins associated to actin (such as talin, vinculin and α -actinin), among which some are force-transducers, and adaptor proteins (such as paxilin). The actin network in lamellipodia and filopodia undergoes rapid retrograde flow due to the membrane resistance to actin polymerization on the leading edge (Gardel *et al.*, 2010). By

linking the actin cytoskeleton to the immobile ECM, focal adhesions modulate the actin retrograde flow and thus act as a “molecular clutch” (Gardel *et al.*, 2010), allowing for transmission of traction to the ECM, while new actin polymerization drives the leading edge forward in a protrusion.

Contraction. Translocation of the cell body follows protrusion and is independent of actin polymerization, but depends on actomyosin bundles contraction thanks to myosin II (Small and Resch, 2005). Stress fibers are actin bundles made of mixed polarity actin filaments and myosin, that attach to focal adhesions; the contraction of stress fibers allows for translocation of the cell body (Gardel *et al.*, 2010).

Retraction. Rear retraction requires the coordinated contraction of the actomyosin cytoskeleton and the disassembly of adhesion in the back of the cell. For an efficient cell migration, cell protrusion and retraction must be tightly coordinated. The tuning of adhesion levels between a cell and its ECM are a key factor, since too much adhesion blocks the cell, whereas too little adhesion doesn't allow force transmission to the ECM. Therefore, for the majority of cell types, the rate of migration is optimal at intermediate levels of adhesion (Gardel *et al.*, 2010). Consequently, the variation of ECM rigidity or density alters cell migration in a biphasic way (Gaudet *et al.*, 2003).

b. Cell migration in 3D environments

Cells have been cultured *in vitro* for over a century (Harrison, 1910; Carrel and Burrows, 1911), providing a key platform for the elucidation of many key cellular processes. Over the last 20 years, advances in the culture of cells in 3D have enabled researchers to model more complex behaviors and tissue functions (Schmeichel and Bissel M., 2003). It has become increasingly acknowledged that for some cell types the switch to the third dimension gives physiologically-relevant insights of cell behaviors. In a seminal study in 1997, Mina Bissell's group showed that antibodies against the β 1-integrin receptor reverted the malignant phenotype of breast cancer cells grown in 3D, however this had never been observed in 2D cultures (Weaver *et al.*, 1997). This study strongly indicates

that changing the way a cell interacts with its environment can drastically alter its behavior. Indeed, a cell in 3D experiences a whole different environment than a cell plated on a planar substrate. In 3D, a cell is in contact with the ECM from all sides, which results in a different distribution of cell-ECM adhesions (Geraldo *et al.*, 2012). The most commonly used 3D environments for cell migration are gels of *in vitro* polymerized collagen fibers. Cells therefore navigate in an environment with a complex architecture of fibers, to which they need to adapt and/or to modify. Because of the discrete nature of collagen fibers, cells can only adhere to specific points in the 3D space and not to a uniform layer as it is in 2D. The physical properties of the substrate are often different, for example stiffness is much lower in 3D than it is on glass, commonly used in 2D migration.

Single cells migrating in 3D use a variety of strategies, depending on cytoskeletal contractility, on the capability to remodel the ECM, and on the strength of cell-matrix adhesions (Friedl *et al.*, 2012). Mesenchymal migration, in which invading cells are elongated, requires high levels of cell-matrix adhesion and proteolysis, whereas amoeboid migration, in which invading cells are rounded, relies on cortical actomyosin contractility (Sanz-Moreno and Marshall, 2010).

Rounded/Amoeboid Migration. Amoeboid migration refers to the movement of rounded cells that lack mature focal adhesions and engage in weak interactions with the substrate (Lämmermann and Sixt, 2009; Friedl and Alexander, 2011). Amoeboid cells migrate with low adhesion to the ECM and high contractility mediated by the actomyosin cytoskeleton. Amoeboid-like motility comes in several variants. The first type is the blebby migration, only seen *in vitro*, in which cells do not adhere or pull on the substrate but rather use a propulsive, Rho-dependent pushing at the cell rear (Paluch *et al.*, 2006; Fackler and Grosse, 2008; Sanz-Moreno and Marshall, 2010; Lorentzen *et al.*, 2011; Poincloux *et al.*, 2011). The second amoeboid type of migration occurs in slightly more elongated cells that display Rac-dependent actin-rich filopodia, are devoid of blebs and move with high velocities (0.4– 5 mm/min) (Clark and Vignjevic, 2015).

Amoeboid cells tend to migrate in the absence of proteolytic ECM degradation by adapting their shape and squeezing through pores in the ECM (Friedl and Wolf, 2003). However, in some cases, amoeboid cells can also display short cellular protrusions associated with

proteolytic activity (Gligorijevic, Bergman and Condeelis, 2014). They move with low velocities (~ 0.1 mm/min) (Clark and Vignjevic, 2015). The origin of amoeboid tumors is often hematopoietic, including leukemias, lymphomas, and small cell lung carcinoma, but amoeboid movements are also detected in other tumor types (Wolf *et al.*, 2003; Madsen and Sahai, 2010).

Mesenchymal migration. Mesenchymal migration is characterized by an elongated ('spindle-shaped') cell body and well developed cell protrusions. Cell-matrix adhesion capabilities of mesenchymal cells are strong and contain multimolecular integrin clusters and proteolytic activity toward the ECM (Wolf *et al.*, 2007). While the protrusions of such cells advance relatively rapidly (~ 0.4 mm/min) (Clark and Vignjevic, 2015), in some cases, the cell rear stays immobile, resulting in relatively slow net translocation (~ 0.2 mm/min) (Clark and Vignjevic, 2015). Tumor cells migrating using mesenchymal type of migration originate from tumors of the connective tissue, including sarcomas. They can also be found in other tumor types after the tumor cells dedifferentiate and lose cell-cell junctions (Brabletz *et al.*, 2001; Friedl and Wolf, 2010; Sanz-Moreno and Marshall, 2010).

		Cell-cell junctions	Tumor type
Individual-cell migration	Single-cell migration		
	Amoeboid	-	Leukemia, lymphoma cell subsets (all tumors)
	Mesenchymal	-	Stromal tumors, epithelial tumors after EMT
	Multicellular streaming		
Multicellular migration	Collective cell migration	Amoeboid (multicellular)	? All tumors developing amoeboid single-cell dissemination
		Mesenchymal (multicellular)	(+) Tumors with mesenchymal invasion; fibroblasts leading tumor cells
		Cluster	++ Moderately differentiated epithelial tumors
		Solid strand	++ Moderately differentiated epithelial tumors with subregions after EMT; basal and squamous cell carcinoma
		Strand (with lumen)	++ Differentiated epithelial tumors; vascular neoplasia
	Strand (protrusive)	++ Moderately differentiated epithelial tumors lacking EMT	

Figure 19. Modes of tumor cell migration. From Friedl and Alexander, 2011.

II. Collective migration

Collective migration refers to the migration of a cohesive group of cells (Friedl and Gilmour, 2009). Collectively migrating cells are physically and functionally connected, through cell–cell junctions and coordination between neighboring cells. Collective migration occurs in a broad range of biological processes, such as morphogenesis, wound healing and pathologies such as cancer. The morphological organization of collectively invading cells can vary considerably. Migration may occur as a directed movement of cells moving individually, in a mode of migration called multicellular streaming. In this case, cells establish weak or transient contacts and independently generate traction force on the matrix (Friedl *et al.*, 2012). Multicellular streaming coordination is most often provided by oriented extracellular matrix structures that align moving cells by contact guidance. Chemokine gradients may as well serve as a guide for multicellular streams, such as in developing organisms (Friedl and Gilmour, 2009). Multicellular streaming has also been observed in orthotopic breast cancer and melanoma models (Roussos *et al.*, 2011).

Alternatively, more cohesive groups of cells maintain cell-cell junctions, that include cadherins, tight junction proteins, adhesion receptors of the immunoglobulin superfamily and gap junctions. These junctions maintain mechanical cohesion of the clusters, multicellular front-back polarity and juxtacrine signaling between neighboring cells (Friedl *et al.*, 2012). Clusters of migrating cells organize their actin cytoskeleton in a “supracellular” structure that coordinates cells and allows mechanical coupling through generation of traction and protrusion force for migration. Collective migration is typically the slowest mode of cancer cell migration (0.01–0.05 mm/min), but faster collective migration (0.2–1 mm/min) has been observed during development *in vivo* (Clark and Vignjevic, 2015).

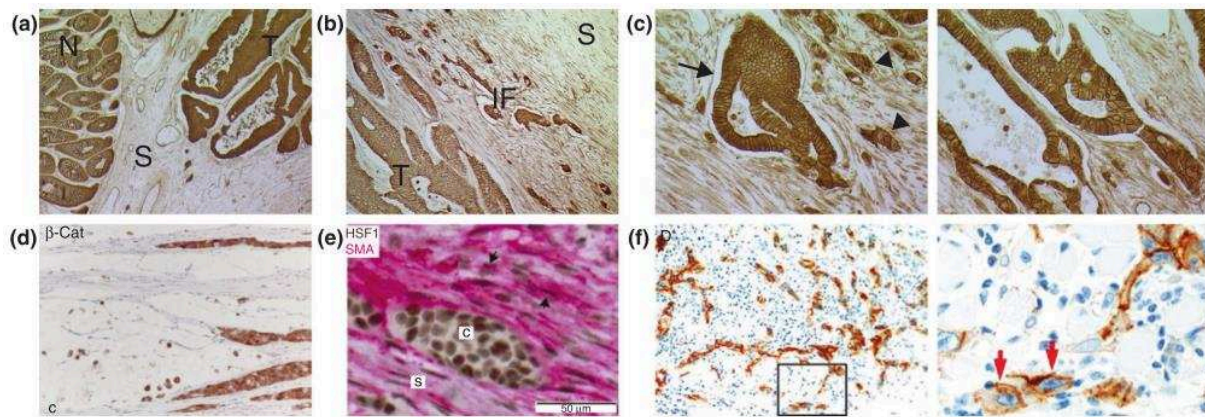


Figure 20. Tumor invasion in human epithelial cancers. (a–c) Colon tissue section from colon cancer patient stained with β -catenin antibody (brown). (a) Difference in epithelial organization between normal glandular tissue (N) and tumorous gland (T) separated by stroma (S). (b) Colon cancer tissue section showing the edge of a tumorous gland (T), the invasive front (IF) and more distal stroma (S), which has not yet been invaded. (c) Invasion phenotypes from colon cancer showing invasive gland structure (left, arrow) and small tumor buds that have separated from the body of the tumor (left, arrowheads) and a cord of connected invasive cells (right). (d) Finger-like strands of invading cancer cells in colon carcinoma. (e) Tissue section from breast cancer patient showing a group of invasive cancer cells (C) surrounded by stroma (S). (f) Tissue section from an oral squamous cell carcinoma displaying thin cords and strands of tumor cells as well as smaller tumor buds at the invasive front. Cells are stained for the nerve growth factor receptor p75NTR (brown) and counterstained with hematoxylin (blue). Right: high-magnification zoom of outlined region in left image. From Clark and Vignjevic, 2015

Size of invading clusters can also dramatically vary, ranging from narrow linear strands of one or two cells in diameter, to broad masses which are multiple cells in diameter and include in their center cells that do not contact the ECM. These are frequently seen in invasive cells of breast, prostate and pancreas cancers (Christiansen and Rajasekaran, 2006). The structure of the front of collectively invading cells can also vary and is often associated with a leading cell with actin-rich protrusions that generate traction on the substrate for forward movement. Interestingly, a stromal cell, such as a fibroblast, can take the lead and guide migration of a cluster of cancer cells (Gaggioli *et al.*, 2007; Labernadie *et al.*, 2017).

It is important to note that migrating groups of cells actively modify the extracellular tissue along their migration path. Leader cells proteolytically clear tracks in the ECM, whereas passage of the cluster can be accompanied by ECM modification such as deposition or realignment (Friedl *et al.*, 2012). This has for example been shown in

collective migration of the colon cancer cell line L-10 on 2D gelatin substrate (Nabeshima, Inoue and Shima, 2000). The anterior protrusive parts of the clusters have shown elevated expression of the matrix-metalloproteases MT1-MMP, and MMP2, that efficiently degrade the ECM (Nabeshima, Inoue and Shima, 2000).

Because I found that cancer cells in the tumor core migrate in a coordinated way, will discuss coordinated migration of large strands of cells more in details in Chapter 4, physics of cancer.

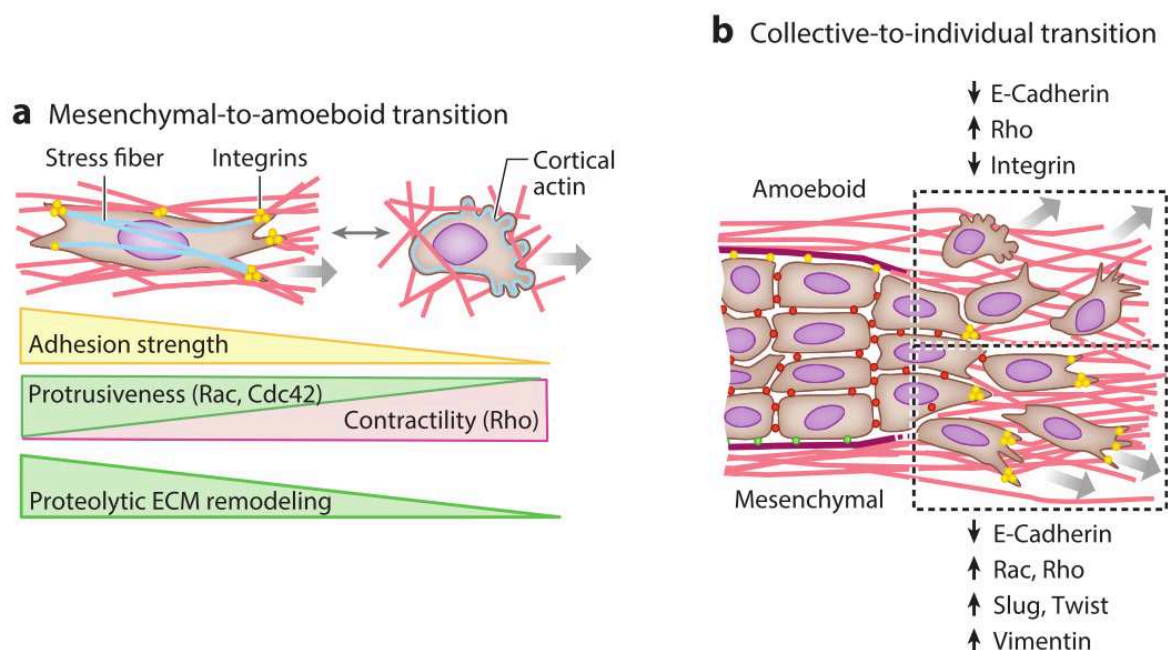


Figure 21. Plasticity between migration modes. Cells can interconvert between migration modes. A. The transition between mesenchymal and amoeboid migration modes is governed by the strength of cell-ECM adhesion, the ability to proteolytically degrade the ECM and the balance between protrusive and contractile behaviors. B. Single cells can detach from collectively migration masses via epithelial-to-mesenchymal transition mediated by upregulation of Slug, Twist and Vimentin and downregulation of E-Cadherin. Modified from te Boekhorst, Preziosi and Friedl, 2016

III. Extracellular determinants of cell migration

Cells that migrate constantly adapt to their extracellular milieu and – very often – modify it. Thus there is bi-directional interaction between cells and their ECM. The ECM provides a structural and molecular frame for migrating cells and therefore impacts (favoring or inhibiting) the mode and efficiency of cell migration.

a. ECM density and pore size

In vivo, extracellular tissues greatly vary in collagen content, fibrillar structure, fiber bundle thickness, and porosity. If the tissue pores largely exceed the cell size, migration rates decrease (Haston, Shields and Wilkinson, 1982; Wolf *et al.*, 2007, 2013; Harley *et al.*, 2008) because cells lose most of their connections to the ECM. Conversely, if pores are too small and way below the cell diameter, cells slow down and eventually may become trapped due to physical hindrance (Haston, Shields and Wilkinson, 1982; Harley *et al.*, 2008). The most rigid compartment of a cell is the nucleus, therefore its deformability (controlled by nuclear lamins A/C) will determine whether a cell can traverse small pore constrictions (Denais *et al.*, 2016; Raab *et al.*, 2016). Besides shape adaptation, cells that can proteolytically cleave ECM fibers counteract physical hindrance by enlarging the pores (Wolf *et al.*, 2007). Thus, the ability of the cell to deform relative to the available space and to remodel tissues through proteolysis determines the mode and efficiency of migration in 3D environments.

b. Stiffness

ECM stiffness (or elasticity), which can be measured as elastic modulus, depends on the collagen content, fiber thickness, and crosslinks between fibers. Stiffness defines the stability and deformability of the tissue scaffold (Shoulders and Raines, 2009). Cells detect matrix stiffness via integrin-mediated adhesions and downstream mechanosensing proteins (Giannone and Sheetz, 2006). Increased substrate stiffness reinforces cell protrusions and focal adhesions by RhoA-mediated actomyosin contraction, leading to the generation of high traction force (Peyton *et al.*, 2008; Ulrich, De Juan Pardo and Kumar, 2009). Conversely, soft matrix does not reinforce focal adhesion formation and

cytoskeletal contractility; it rather supports cell rounding (Ulrich, De Juan Pardo and Kumar, 2009). Consequently, matrix rigidity stimulates directed cell migration, so that cells tend to migrate toward substrate of greater stiffness, a process termed durotaxis (Lo *et al.*, 2000; Li, Guan and Chien, 2005; Isenberg *et al.*, 2009). However, too much stiffness could be deleterious for cells; high adhesion forces can exceed the cell capability to contract and disengage integrins at the rear of the cell, thus a cell becomes stuck. Therefore, for the majority of cell types, the variation of ECM rigidity or density alters cell migration in a biphasic way (Gaudet *et al.*, 2003). One of the goals of my PhD was to determine how collagen rigidity affect cancer cell migration. Therefore, I will further develop the importance of tissue stiffness in Chapter 4.

c. Fiber architecture and orientation

Extracellular matrix comprises a range of architectures, ranging from loose and random to highly aligned structures (Petrie, Doyle and Yamada, 2009; Wolf *et al.*, 2009). In cancerous tissues, work by the lab of Patricia Keely has described three major tumor-associated collagen signatures TACS (Provenzano *et al.*, 2006; Schedin and Keely, 2011). TACS-1 is comprised of curly and anisotropically organized collagen fibers. TACS-2 characterized bundled collagen that surrounds and encapsulates the tumor parallel to the tumor edge. TACS-3 refers to strait collagen bundles oriented parallel to the tumor edge that act like highways for tumor cells to leave the primary tumor and invade the stroma (Conklin and Keely, 2012). Indeed, cancer cell preferentially invade along straightened, aligned collagen fibers that constitute a firm substrate for migration (Conklin and Keely, 2012). Contact guidance along such structures is mediated by mechanosensory integrins that, together with Rho/ROCK-mediated cytoskeletal stiffening, provide directional persistence (Dickinson, Guido and Tranquillo, 1994; Provenzano *et al.*, 2008; Petrie, Doyle and Yamada, 2009). In summary, different ECM environments provide an array of interconnected input parameters that modulate cell adhesion and cytoskeletal organization, and directly impact cell shape, guidance, and mode of migration (Schedin and Keely, 2011).

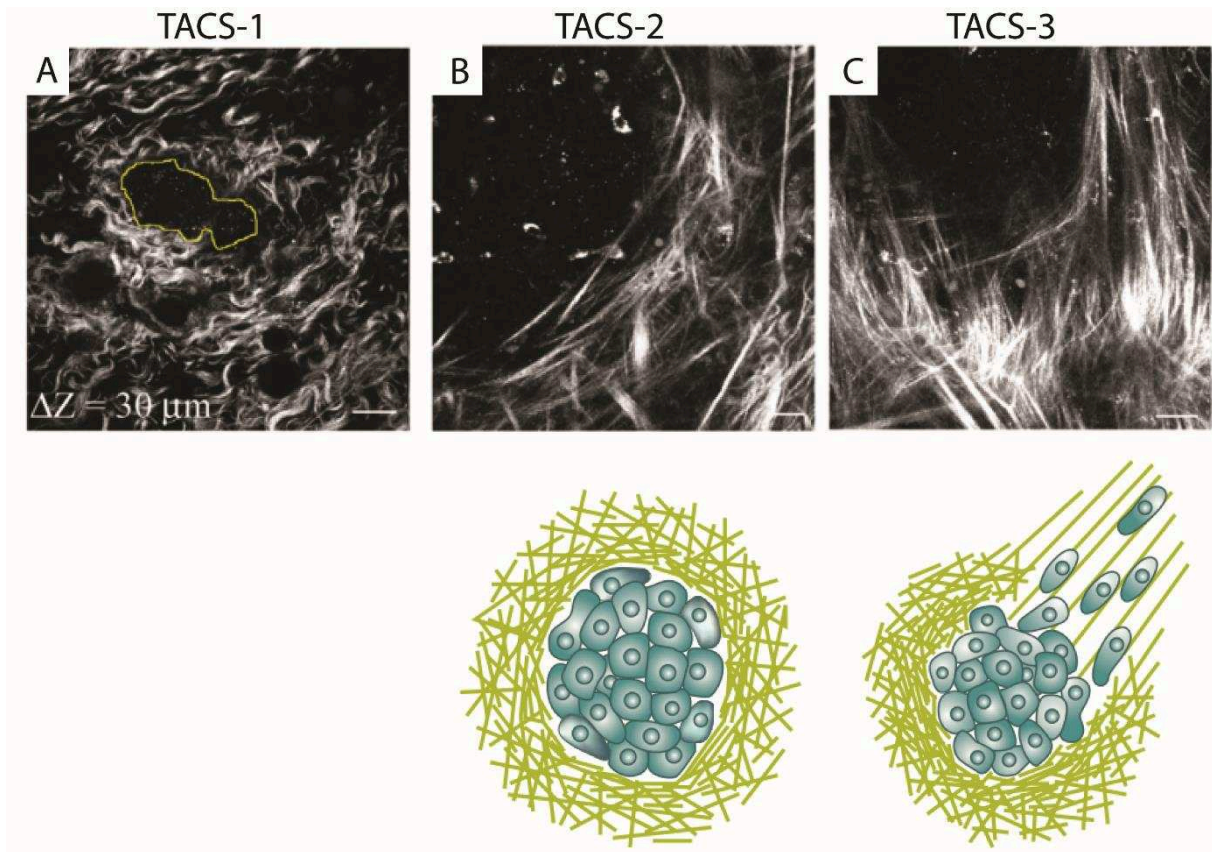


Figure 22. Tumor-associated collagen signatures (TACS). (A) Curly and anisotropic collagen fibers around a small mammary tumor. (B), up: parallel alignment of collagen fibers around a non-invasive tumor, imaged in a live mammary tumor ex vivo by multiphoton laser scanning microscopy and second harmonic generation (SHG). (B), down: scheme of collagen organization in TACS-2. (C), up: Perpendicular alignment of collagen fibers with respect to the tumor boundary. (C), down: scheme of TACS-3, with cells invading out from the tumor along aligned collagen fiber. Modified from Provenzano *et al.*, 2006 and Schedin and Keely, 2011

PART 4 - PHYSICS OF CANCER

The physical properties of the ECM refer to its stiffness, porosity, spatial arrangement and orientation. Cells that interact with the ECM have to sense and to respond to tissue mechanics, inducing transient or permanent modifications on the cellular level and on the tissue level. These modifications include tuning of cellular signaling pathways and migration, as well as ECM modifications such as stiffening and rearrangement. The mechanical relationships between the cells and their ECM are inherently bi-directional, and can be described by the term “mechanoreciprocity” (Paszek and Weaver, 2004).

I. The ECM can resist different forms of physical challenges

The proteins and polysaccharides composing the ECM give her resistance to different forms of physical challenges (Alberts *et al.*, 2014; Vogel, 2018). The collagen fibers strengthen and help organize the matrix, while other fibrous proteins, such as the rubber-like elastin, give its resilience after stretch. The polysaccharide gel, for its part, resists compressive forces on the matrix while permitting the rapid diffusion of nutrients, metabolites, and growth factors. Because of its resistance to tensile and compressive forces, and of its elasticity, the ECM exerts a buffering action that protects cells and maintains extracellular homeostasis and water retention.

a. Type I collagen resists tensile forces/ stretch

Collagen I fibrils display enormous tensile strength, exemplified by that fact that collagen can be highly stretched without being broken. Gram for gram, collagen I is stronger than steel (Alberts *et al.*, 2014). Collagen resistance to tensile forces is in part explained by the very peculiar organization of collagen fibers. Indeed, the packing side-by-side of collagen fibrils, into parallel bundles, called collagen fibers, renders the whole structure resistant to stretch (Malandrino *et al.*, 2018). The best example of such a structure is tendon, where collagen fibers connect muscles with bones and must withstand large traction forces (Malandrino *et al.*, 2018). Interestingly, in tendons there is an intrinsic anisotropy in large collagen assemblies, where bundles are all oriented in the same direction, which corresponds to the direction on which stress is normally applied on the tendon. This

anisotropy in collagen organization manifests itself in a corresponding anisotropy in collagen physical properties (Wenger *et al.*, 2007; Polacheck and Chen, 2016). Indeed, a collagen fiber is much more resistant to traction in the direction of collagen fibers, than in the orthogonal direction of its fibers (Polacheck and Chen, 2016). This anisotropy is not only found in large collagen bundles such as the tendons, but also in the smaller collagen fibers that are present in connective tissues (Polacheck and Chen, 2016).

Box 5. Physical properties of collagen fibers

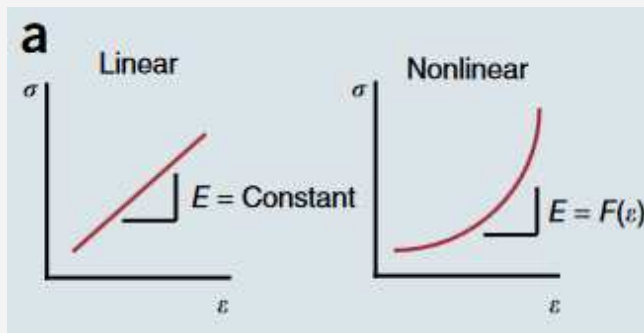
The mechanical behavior of a solid material is defined by the manner in which it deforms under applied force (Chen).

Stress is defined as a normalized load, where the force is applied to an area of tissue, therefore the units of stress are pascals (σ , in Pa) or newtons per square meter (N/m^2).

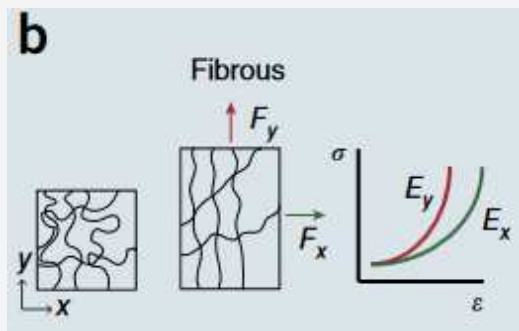
Strain is a normalized deformation, in which the change in length of the material is divided by the original length of the specimen, and is a unitless quantity (ϵ).

For **linear elastic materials**, stress increases linearly with increasing strain, and thus the relationship between stress and strain is characterized by a single parameter, E , known as the stiffness or elasticity of the material.

For **nonlinear elastic materials**, such as **collagen**, the relationship between stress and strain is a function of the magnitude of the strain. In other words, collagen, such as other biological materials, becomes stiffer when deformed. This behavior is referred to as **strain-stiffening**. The strain stiffening response gives biological materials resistance to forces exerted on them. Interestingly, collagen stiffening has been observed in fibers adjacent to the cell leading edge during migration, indicating that cell-generated forces are able to induce collagen strain stiffening (Van Helvert, Storm and Friedl, 2018). It has been proposed that stiffening of collagen allows for a more efficient cell migration and invasion.



Stiffness, given here as the Young's modulus (E), determines the relationship between stress (σ) and strain (ϵ). In linear materials (left), stiffness of the material is constant. In nonlinear materials, stiffness is a function of strain, and it increases with applied strain (right). In other words, the more you deform collagen (*ie* the more strain increases, ϵ) the more force (*ie* stress, σ) you need to apply to deform it.



Fibrous materials are nonlinear: as fibrous materials are strained, the fibers align, increasing the resistance to further strain.

Fibrous materials are often **anisotropic:** they are stiffer in the direction of aligned fibers.

From Polacheck and Chen, 2016

b. The polysaccharide hydrogel resists compressive forces

The fibrous part of the ECM is embedded in a hydrogel made of glycosaminoglycans and proteoglycans. The highly negatively charged sugars attract large quantities of water, that create a swelling pressure, or turgor, which then enables the matrix to withstand compressive forces, in contrast to collagen fibrils, which resist stretching forces. For example, the cartilage that lines the knee joint can act as a shock absorber and support pressures of hundreds of atmospheres (Alberts *et al.*, 2014).

c. Elastic fibers have the ability to stretch and recoil

A network of elastic fibers in the ECM gives tissues the resilience to recoil after transient stretch. When the fiber is stretched, elastin molecules uncoil into a more extended conformation and recoils spontaneously as soon as the stretching force is relaxed. Elastic fibers are at least five times more extensible than a rubber band of the same cross-sectional area (Rosenbloom, Abrams and Mecham, 2016). Long, inelastic collagen fibrils are interwoven with the elastic fibers to limit the extent of stretching and prevent the tissue from tearing.

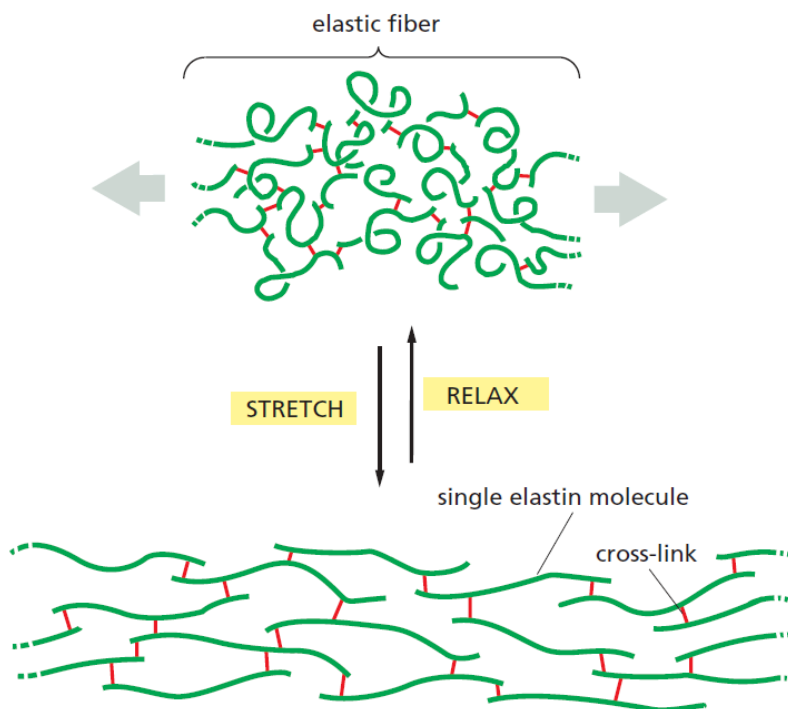
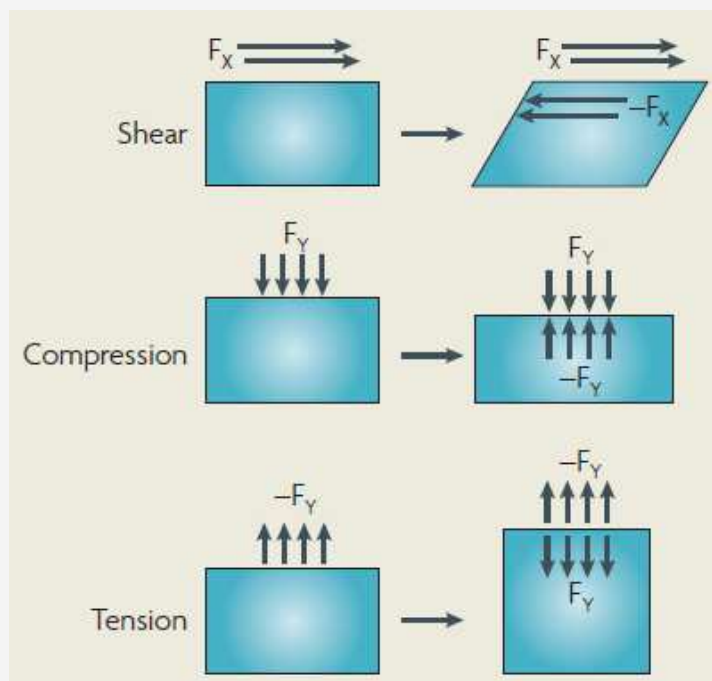


Figure 23. Elastic fibers can withstand stretches. The elastin molecules (green) are joined together by covalent bonds (red) to generate a crosslinked network. Each elastin molecule in the network can extend and relax in a manner resembling a random coil, so that the entire assembly can stretch and recoil like a rubber band. From Alberts *et al.*, 2014.

Box 6. Types of forces experienced by a cell

Normal physiological processes expose cells to a variety of mechanical stimuli including hydrostatic pressure, shear stress, compression and tensile force. Biological tissues follow laws of physics, among which Newton's third law, that states that for every action there is an equal and opposite reaction. Following this law, cells in vivo will respond to alterations in the mechanical properties of their surrounding matrix by adjusting their intracellular tension through the cytoskeletal network. Conversely, changes in cell tension will result in alterations in extracellular matrix organization, thereby changing the mechanical properties of the ECM.

The different types of forces experienced by a cell are shear stress, compression and tension.



Shear stress is stress applied parallel to the surface of the tissue (for example blood flow exerts shear stress on endothelial cells).

Compressive stress is stress applied perpendicular and towards the tissue, resulting in compaction.

Tensile stress or tension is stress applied perpendicular and away from the tissue, resulting in expansion.

Adapted from Butcher, Alliston and Weaver, 2009

II. The physical properties of the ECM are altered in cancer

During cancer progression, the biochemical and biomechanical properties of the ECM are deregulated (Bonnans, Chou and Werb, 2014). Some ECM proteins like collagens and fibronectin get enriched and others which are normally absent in the stroma, like laminin and certain tenascin isoforms, appear (Bonnans, Chou and Werb, 2014). Collagen fibers become more crosslinked, stiffened and aligned, concomitantly with the aberrant expression of ECM remodeling enzymes such as Lysyl oxidase (LOX) and MMPs (Bonnans, Chou and Werb, 2014). These alterations enhance the formation of abnormal cell-matrix adhesions such as reinforced focal adhesions and invadopodia, and therefore boost the motility, contractility, and invasive phenotype of cancer cells (Paszek and Weaver, 2004; Levental *et al.*, 2009).

a. Cancer tissues are stiffer than their normal counterparts

Stiffness is the extent to which a material resists deformation when a force is applied to it. Tissue stiffness is measured as Young's modulus (also called elastic modulus). For example, high stress is required to deform materials with high Young's modulus. Stiffness depends on the molecular composition, architecture and momentary forces acting on the tissue. Tissue stiffness varies from soft and deformable, such as brain, to very stiff and non-deformable, such as bone. The stiffness of normal soft organs usually ranges between 2 – 15 kPa. Using elastography, it was shown that the human intestine has a Young's modulus of 3 kPa (Johnson *et al.*, 2013).

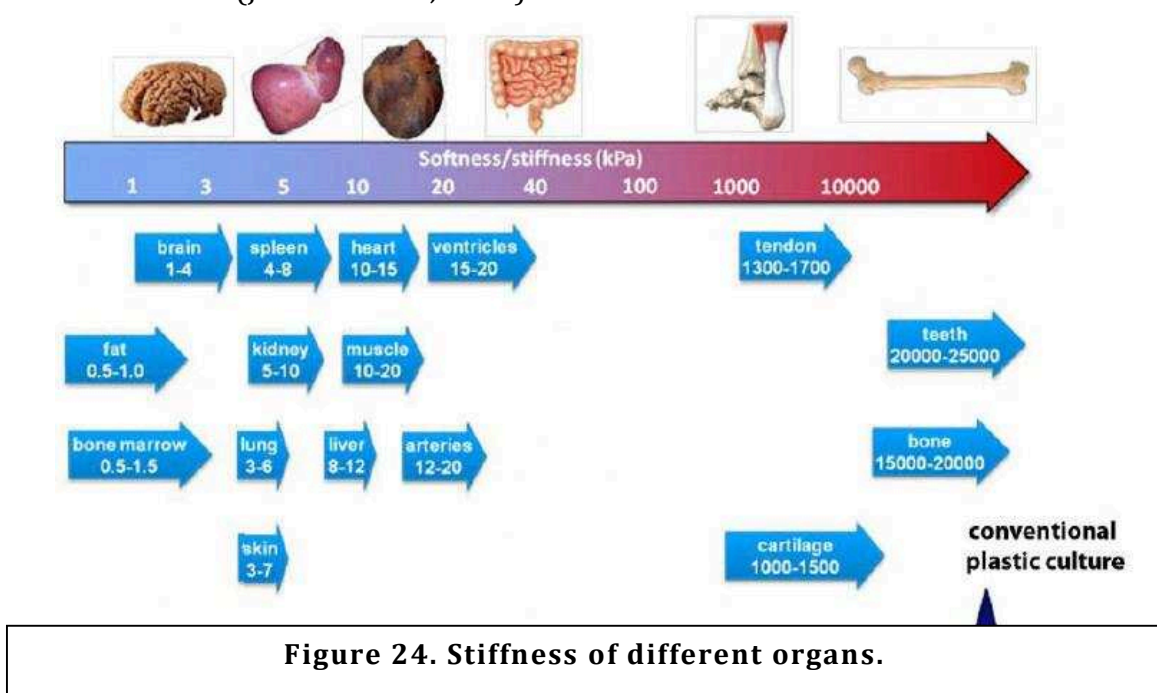


Figure 24. Stiffness of different organs.

In homeostatic conditions, it appears that each tissue has a characteristic stiffness that can change over the course of development or in pathological situations, such as tumor progression or fibrosis. Indeed, tumors are often detected as a palpable stiff mass, and approaches such as magnetic resonance imaging elastography and sono-elastography have been developed to exploit this observation to enhance cancer detection (Butcher, Alliston and Weaver, 2009). These techniques measure the average macroscopic tumor stiffness; however they cannot indicate which tumor components account for the overall increase in stiffness. Atomic force microscopy (AFM) provides the spatial resolution to probe the local stiffness at a micrometer scale (Lopez *et al.*, 2011). Using an AFM, Lopez *et al.* showed that progression of MMTV-PyMT mouse breast carcinoma is accompanied by a stiffening of the tissue (Lopez, Weaver). Using optical stretching of single cells and magnetic tweezing, it has been shown that more aggressive and metastatic breast and ovarian cancer cells tend to be softer than their normal counterparts (Guck *et al.*, 2005; Swaminathan *et al.*, 2011). Intuitively, softer cells are more deformable and thus could squeeze more easily through a dense ECM, which would allow them to disseminate more efficiently (Harada *et al.*, 2014).

Stiffness is not only a passive marker of cancer progression, but also an important regulator of cell fate and differentiation. This has elegantly been shown by plating mesenchymal stem cells on substrates with either low (0.1-1 kPa), medium (8-17 kPa) or high stiffness (25-40 kPa). In contact with these different stiffness profiles, mesenchymal stem cells differentiated respectively in neurons, muscle or bone (Engler *et al.*, 2006).

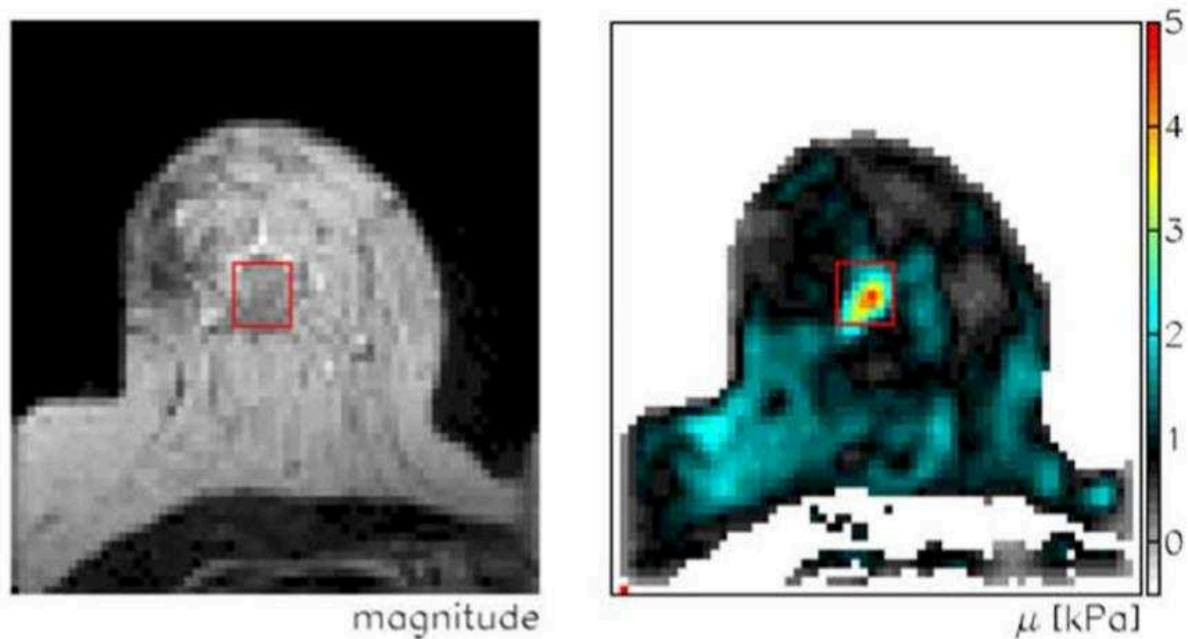


Figure 25. Cancer tissues are stiffer than normal tissues. Magnetic resonance imaging (left) and elastography (right) of a breast tumor. The tumor (red rectangle) is stiffer than its surroundings. Adapted from Sinkus *et al.*, 2005

b. The ECM is in large part responsible for the stiffening of cancer tissues

The stiffness observed in tumor tissues is mostly a result of an abnormal ECM. Collagen is the most abundant ECM scaffolding protein in the stroma and contributes significantly to the tensile strength of a tissue (Kadler *et al.*, 1996; Brinckmann, 2005). In cancer, collagen production and deposition are increased, and its organization is altered. Indeed, in tumor progression there is enhanced collagen crosslinking (Jodele *et al.*, 2006) and enhanced matrix metalloproteinase (MMP) activity. Collagen in cancerous tissues is typically abundant, highly bundled and crosslinked, therefore stiff. In cancerous tissues, collagen stiffness promotes malignant behavior as it has been shown in 3D *in vitro* models of mammary gland embedded in collagen I gels of increased stiffness (Paszek and Weaver, 2004). ECM stiffness enhances cancer cell growth and survival and promotes migration (Lo *et al.*, 2000).

Importantly, collagen crosslinking accompanies tissue fibrosis (Moriguchi and Fujimoto, 1979; Van Der Slot *et al.*, 2005), and fibrosis increases risk of malignancy (Colpaert *et al.*,

2003). Cancer cells and cancer-associated fibroblasts can secrete Lysyl oxidase (LOX), a copper-dependent amine oxidase (Kagan and Li, 2003), that initiates the process of covalent intra- and intermolecular crosslinking of collagen by oxidative deamination of specific lysine and hydroxylysine residues located in the telopeptide domains (Mouw, Ou and Weaver, 2014). Active LOX is frequently elevated in tumors (Erler *et al.*, 2006) and stiffens tissues, thus compromising their function (Pfeiffer *et al.*, 2005). Reducing LOX activity tempers tissue stiffness and prevents fibrosis (Georges *et al.*, 2007).

Integrins transduce cues from the ECM by assembling adhesion complexes that initiate biochemical signaling and stimulate cytoskeletal remodeling to regulate cell behavior (Miranti and Brugge, 2002). Any change in ECM stiffness is sensed by cells through focal adhesions (Discher, 2005). Mechanotransduction refers to the processes through which cells sense and respond to mechanical stimuli by converting them to biochemical signals that elicit specific cellular responses. Force increases integrin expression, activity, and reinforces focal adhesions (Paszek and Weaver, 2004; Sawada *et al.*, 2006). Components of focal adhesions then undergo conformational changes that eventually modify the cell's functionality. Changes in mechanical forces can be converted into deregulation of signaling pathways and growth factors secretion (Paszek and Weaver, 2004; Levental *et al.*, 2009), indicating that the physical properties of the ECM influence cell behaviors.

For example, human breast tumors are often fibrotic and stiff, and breast cancer cells that exhibit high tension have elevated integrins and focal adhesions and increased integrin signaling (Madan *et al.*, 2006; Mitra and Schlaepfer, 2006). Thus, ECM stiffness could regulate malignancy by enhancing integrin-dependent mechanotransduction. Not only is the integrin signaling enhanced in tumors, but there is an increase in expression of pro-tumorigenic integrin subunits (Hamidi and Ivaska, 2018). Consistently, breast cancer aggressiveness can be inhibited by genetically ablating integrin expression (White *et al.*, 2004). In a similar way, knockdown of the expression or inhibition of the function of focal adhesion kinase (FAK) or p130Cas, two integrin adhesion plaque proteins, impedes breast tumor progression (Cabodi *et al.*, 2006; Lahlou *et al.*, 2007).

Stiff matrices don't only affect cancer cells, they can also stimulate fibroblasts to generate mechanical forces (Barker *et al.*, 2013). A stiffer matrix maintains CAF in an activated

status through YAP translocation in the nucleus (Calvo *et al.*, 2013). Thus activated CAFs can in turn deposit and stiffen the ECM to a greater extent, establishing a positive feedback loop between CAFs and the pro-tumorigenic ECM through mechanoreciprocity.

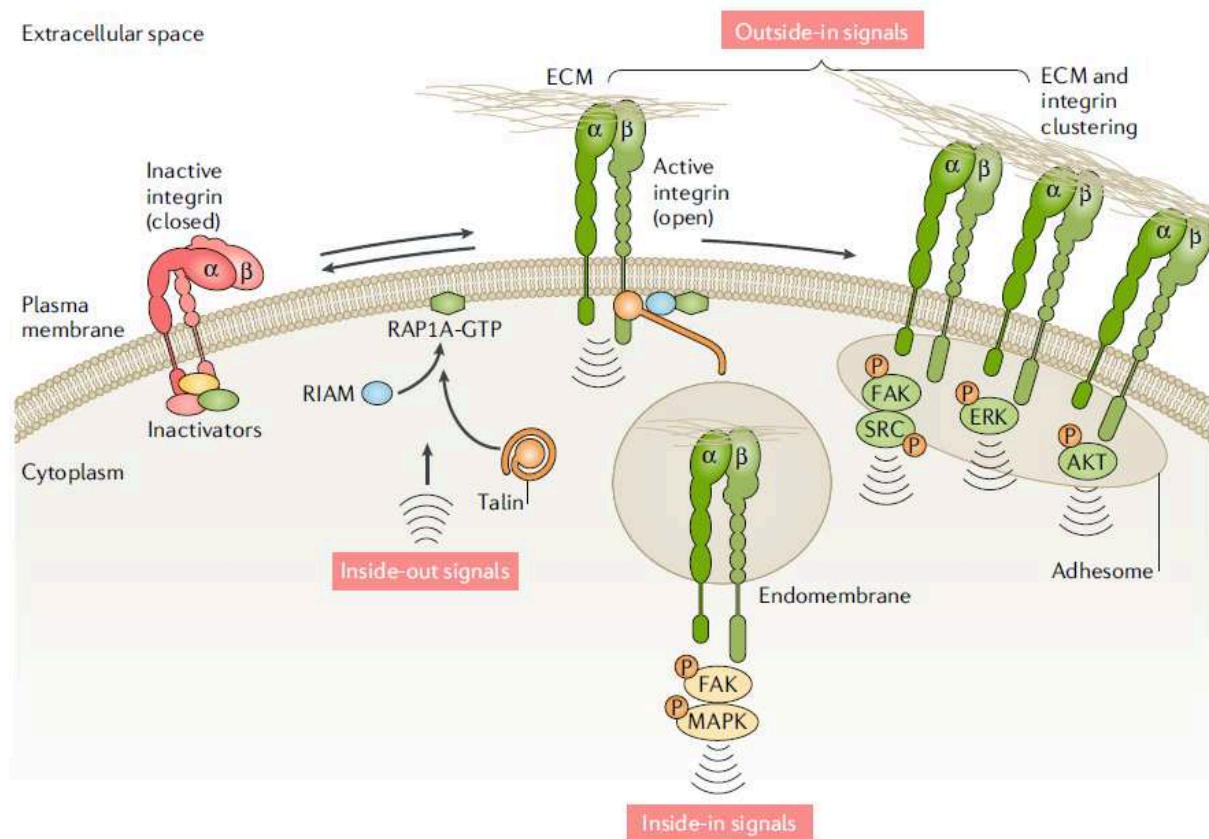


Figure 26. Integrin signaling upon activation by ECM. Integrins are bidirectional signaling molecules that exist in different conformational states: a bent (closed) and inactive conformation, with low affinity for ECM ligands, and a fully extended (open) and active conformation, capable of eliciting downstream signaling and cellular responses. Integrin–ligand engagement (adhesion) and clustering on the plasma membrane provides a platform for the assembly of multimeric complexes that provoke downstream signaling (outside-in signaling). The outside-in signal is heterodimer- and context-dependent, but typically involves recruitment and autophosphorylation of focal adhesion kinase (FAK), with subsequent recruitment and activation of SRC. Integrin adhesion also activates other pathways, such as the RAS–MAPK and PI3K–AKT pathways.

Integrins also respond to inside-out signals, where talin binding to the β -integrin subunit tail triggers an open receptor conformation and recruitment of additional integrin-activating proteins such as kindlins. Integrin activation can be tuned down by inactivating proteins such as integrin cytoplasmic domain-associated protein 1 (ICAP-1), filamin A, SHARPIN, and proteins of the SHANK family, which restrict the ability of talin to bind and activate integrins. From Hamidi and Ivaska, 2018

c. Tumor tissues experience compressive stresses

Tumor tissues are under compression, as suggested by the observation of collapsed blood vessels in tumors (Padera *et al.*, 2004). The mechanical microenvironment of solid tumors is characterized by both fluid- and solid-phase stresses. Fluid-phase stresses include the vascular and interstitial fluid pressures, as well as the shear stresses exerted by the blood flow on the vessel walls (Stylianopoulos *et al.*, 2013). The interstitial tumor pressure increases in tumors due to leaking of fluids through abnormal blood and lymphatic vessels (Stylianopoulos *et al.*, 2013). Interestingly, high interstitial fluid pressure renders cancer drug penetration more difficult in tumors.

Solid-phase stresses include the compressive and tensile stresses exerted by the non-fluid tumor components. Solid stresses can be further divided into two categories: the externally applied stress, which is developed through mechanical interactions between the solid components of the growing tumor and the surrounding normal tissue, and the growth-induced stress, which is stored within the tumor as the proliferating cancer and stromal cells push on structural components (e.g., collagen, hyaluronic acid) of the tumor microenvironment. Indeed, by depleting cancer cells, compressive stress in tumors was greatly relieved (Stylianopoulos *et al.*, 2012). In tumors, the increased amounts of ECM synthesis, deposition, and crosslinking contributes to stiffer and thickened ECM (Acerbi *et al.*, 2015). Proliferation of cancer and stromal cells generates compressive stress that accumulates due to the stiffening of the stroma, thus increasing tumor pressure (Ariffin *et al.*, 2014).

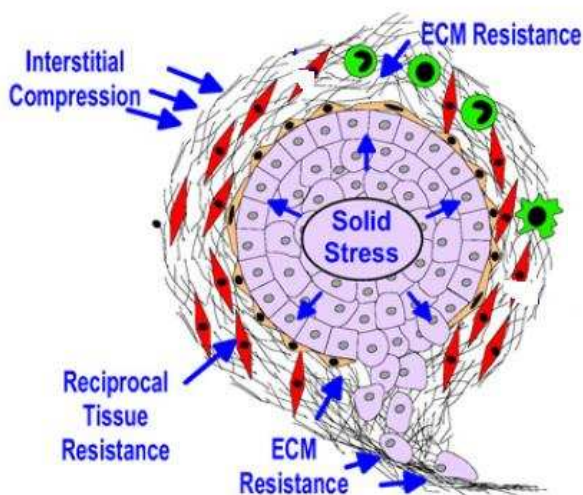
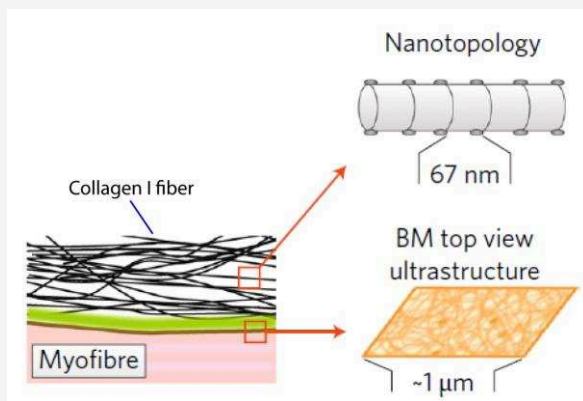


Figure 27. Tumors are under compression. Upon cancer cell proliferation, the tumor exerts pressure on the surrounding ECM, which in turn exerts compressive resistance.

Box 7. Emerging properties of cell and tissue mechanics

Porosity. The porosity of the ECM varies from $>100\mu\text{m}^2$ between collagen fibrils in loose connective tissue to $<1\mu\text{m}^2$ between dense collagen bundles (Van Helvert, Storm and Friedl, 2018). Nearly impenetrable, dense ECM impedes cell migration and requires the capacity to strongly deform the nucleus and/or to proteolytically degrade ECM to generate space. Examples of such high-density environments are collagen-rich stroma and the basement membrane.

Topology and curvature. The ordering and assembly of ECM macromolecules provide complex 3D nanopatterns on which cells can migrate. Interestingly, cells discriminate aligned from disordered patterns for guidance of migration (Van Helvert, Storm and Friedl, 2018). Tissue curvature induces spatial patterning of mechanical stresses and can pattern proliferation of cell sheets, suggesting a role in enhancing proliferation and, probably, guiding migration (Van Helvert, Storm and Friedl, 2018).



The surface of collagen fibrils provides nanotexture by D-periodic bands, and globular patterns from adhering macromolecules. The 2D structure of basement membranes is a meshwork of nanoscale pores and fibrils, that is most likely interpreted as a 2D nanotopology by cells. Adapted from Van Helvert, Storm and Friedl, 2018

Tissue hydration. Tissue hydration is maintained by interstitial fluids, which flow between ECM macromolecules. Water, both freely flowing and glycosaminoglycan-bound, fills the ECM space. When vascular permeability increases during tissue inflammation or cancer, interstitial water influx increases hydrostatic pressure, followed by tissue swelling with increased ECM network porosity and tension by hydrostatic pushing. Beyond mechanical effects, tissue swelling accelerates interstitial fluid flow, which redistributes chemotactic proteins and contributes to cell guidance (Van Helvert, Storm and Friedl, 2018).

Cell stiffness. Cell stiffness is predominantly determined by the nucleus, cytoskeleton and cortical actin (Van Helvert, Storm and Friedl, 2018). Bundled actin creates higher local stiffness compared to diffuse actin structures. Cell stiffness thus scales with the traction force generated by cells and lowering stiffness facilitates shape adaptation of moving cells (Van Helvert, Storm and Friedl, 2018). Invasive cancer cells are less rigid than benign or less invasive cells indicating distinct cytoskeletal organization.

III. Jamming transition in cancer

Physicists that are interested into biological tissues might ask themselves the following questions: do tissues behave like liquids, with properties such as viscosity and surface tension, or do they more closely resemble solids?

The idea that tissues are liquids stems from the observation that sorting and fusion of cells can be described in terms of surface tension, that is often a proxy for adhesion strength between cells (Steinberg and Takeichi, 1994; Mombach *et al.*, 2005). The collective cell motion in a free space has been described as “similar to the flow of a viscous liquid” (Beaune *et al.*, 2014). The situation changes drastically as soon as monolayers become confluent and cells do not have enough room to easily bypass each other. Upon confluency, features more complex than pure fluidity emerge, such as glass transitions, jamming and collective motion in swirls and vortexes (Oswald *et al.*, 2017).

Glasses are amorphous solids that lack the long-range order of crystalline solids. The transition from liquid to glass is reversible and temperature-induced (Oswald *et al.*, 2017). Such as glassy structure is formed when temperature is lowered, an increased particle density will dramatically slow down the dynamics of the system to the point that it can no longer relax and becomes rigid, in a phenomenon known as the jamming transition (Biroli, 2007). In 2011, Angelini and colleagues have shown that a kinetic slowing down, accompanied by collective motility patterns, appears in confluent monolayers of Madin-Darby Canine Kidney epithelial cells (MDCK) as their density increases. As clusters of collectively moving cells become larger, mean velocities decrease and seem to approach a state of arrest (Angelini *et al.*, 2011).

Jamming transition has been proposed to depend on several cell autonomous and non-cell autonomous factors. These factors include cell intrinsic motility, adhesions between cells, cell density, and possibly cell shape and applied stress (Oswald *et al.*, 2017). For example, as cellular density in a proliferating monolayer increases, cells become increasingly crowded. At some point, the crowding approaches a critical threshold in which relative motion of neighboring cells slows dramatically. Interestingly, these changes in dynamics are not accompanied by discernable alteration in cellular structure.

With more crowding each cell becomes increasingly caged by its neighbors (Angelini *et al.*, 2011; Tambe *et al.*, 2011). As the effects of caging become progressively stronger, it becomes increasingly difficult for rearrangements between neighboring cells to occur without the necessity for many cells to rearrange in some mutually cooperative fashion that causes fluctuations across the monolayer (Serra-Picamal *et al.*, 2012). Because there are increasingly large regions over which cells have to move in a cooperative manner, rearrangements within cell packs must become increasingly cooperative, bigger and slower, as well as more intermittent (Sadati *et al.*, 2013). Such a remarkable growth in time scale and length scale manifests as a transition of the monolayer from a fluid-like to a solid-like state (Sadati *et al.*, 2013).

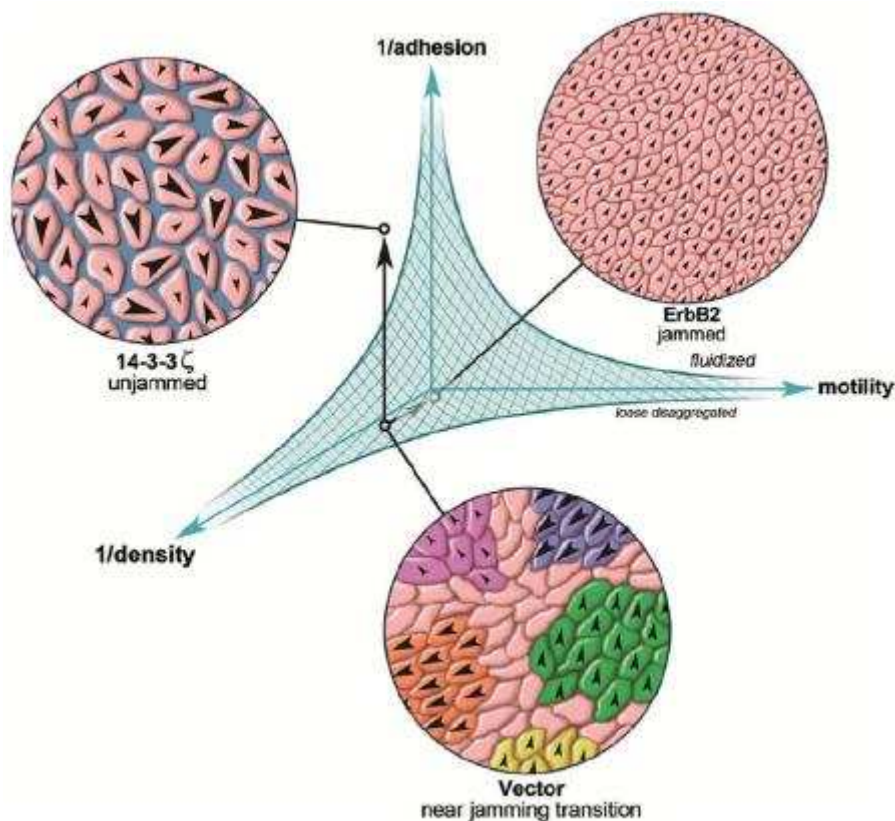


Figure 28. Hypothetical phase diagram for jamming transition in cell monolayers. Jamming has been proposed to be induced by an increase in cell adhesion, an increase in cell density, or a decrease in cell motility. As cells become more crowded, adhere more with one another or display less myosin-dependent motile force, the coordinates in phase space move progressively closer to the origin and the monolayer state becomes increasingly jammed. From Sadati *et al.*, 2013

The first study with primary cells from human patients where jamming is shown to play a role in a clinical context was concentrating on human bronchial epithelial cells from asthmatic and non-asthmatic donors (Park *et al.*, 2015, 2016). In asthma, the airway epithelium is thought to develop mechanical instabilities leading to possible stress and buckling, therefore obstructing the airways (Park *et al.*, 2015, 2016). Using primary human bronchial epithelial cells from asthmatic and non-asthmatic donors, Park *et al.* observed that the non-asthmatic tissues undergo a jamming transition during maturation, while asthmatic tissues do not. The hypothesis is thus that the lack of cell jamming in asthma contributes to the development of the mechanical instability in the disease.

Furthermore, jamming is likely also of central importance in the growth and malignant progression of tumors. Tumor migration has been associated with a fluidization, or unjamming, of cancer tissues (Oswald *et al.*, 2017). Mechanisms that lead to the unjamming of kinetically arrested monolayers have begun to be discovered. Recently, it has for example been shown that the endocytic protein RAB5A mediates monolayer unjamming by promoting the formation of polarized lamellipodia that generate traction forces, which can be transmitted at long ranges through enhanced cell-cell junctions (Malinverno *et al.*, 2017). This type of mechanism could be exploited by cancer cells to escape from a jammed epithelial tissue.

Dynamic heterogeneities in cell behaviors near jamming transition

Interestingly, on approach to jamming the dynamics of the system become increasingly heterogeneous (Abate and Durian, 2007). Such spatially heterogeneous dynamics may take the form of intermittent strings, swirls or vortexes of coordinated neighboring cells that follow one another in correlated fashion from one packing configuration to another (Abate and Durian, 2007). In the case of cell migration, characteristic dynamic heterogeneities might result in collective cell migration in local swirls and flows. Surprisingly, dynamic heterogeneities appear even in a homogeneous cell monolayer. Within the monolayer, intercellular forces fluctuate severely in space and in time, but they are tied neither to any particular position within the monolayer nor to any particular cell (Angelini *et al.*, 2011; Tambe *et al.*, 2011). The heterogeneity is dynamic, therefore not structural (Angelini *et al.*, 2011; Garrahan, 2011; Sadati *et al.*, 2013).

Objectives of my study

Cell migration is an essential process in the development and homeostasis of multicellular organisms. In pathological conditions such as metastatic cancer, cells acquire an upregulated capacity for migration (Lambert, Pattabiraman and Weinberg, 2017). Most solid tumors, including colorectal cancer, are composed of a central differentiated core region and an invasive front forming the interface between tumor and stromal tissue (Vignjevic *et al.*, 2007; Clark and Vignjevic, 2015). The invasive front is widely characterized in terms of cell morphology and molecular composition (Prall, 2007). Intravital imaging has uncovered a large diversity of cancer cell migration modes at the invasive front, ranging from collective behaviors to single cell migration (Friedl and Wolf, 2010; Clark and Vignjevic, 2015). In contrast, the dynamics of the tumor core is far less understood, and we still lack precise details of single cell dynamics and migration patterns within the tumor core. Interestingly, it has recently been shown that vascular escape can also occur in deep regions of tumors and not only in the invasive front (Deryugina *et al.*, 2017), prompting us to examine in details the behaviors of cancer cell in the tumor core.

The questions that I asked are the following:

Are cancer cells in the tumor core stationary, or do they migrate? If yes, what are the properties of this migration, and what factors determine it?

To address this, one of the aims of my PhD is to study the behavior of cancer cells in densely packed regions at the tumor core using a mouse model of genetically-induced aggressive intestinal carcinoma.

Another striking feature on cancer progression is the stiffening of the cancer tissue that accompanies and favors tumor progression (Levental *et al.*, 2009). *In vivo*, massive deposition of collagen and enzymatic collagen crosslinking by lysyl oxidase are responsible for tumor matrix stiffening (Levental *et al.*, 2009; Barker *et al.*, 2013). However, it is still unknown if this increase in matrix rigidity promotes invasion and whether this effect is constant along the course of invasion.

The questions that I asked are the following:

Does matrix stiffening induce cancer cell invasion? Is the effect of matrix stiffness on cancer cell invasion constant in time or do cells respond differently to mechanical changes in their environment depending on whether these happen during early or advanced stages of invasion?

To address this, one of the aims of my PhD was to address the temporal role of matrix stiffening on cancer cell invasion using an *in vitro* model in which the timing of the extracellular matrix stiffening can be precisely controlled.

CHAPTER 2

RESULTS

PART 1. MIGRATION OF CANCER CELLS IN TUMORS

Cancer cells in the tumor core exhibit spatially coordinated migration patterns

Ralitza Staneva^{1, 2,*}, Fatima El Marjou¹, Jorge Barbazan¹, Denis Krndija¹, Andrew Clark^{1, #}
and Danijela Matic Vignjevic^{1, #}.

¹ Institut Curie, PSL Research University, CNRS, UMR 144, F-75005 Paris, France

² University Paris Descartes, 12 rue de l'Ecole de Médecine, 75006 Paris

Authors contributed equally to this work

* Corresponding author

Foreword

In this study, we were interested in determining whether cancer cells in deep regions of the tumor core were motile, and if yes, what were the important characteristics of their migration.

To this end, we developed a methodology to culture and image tumor tissue explants over long periods of time using two-photon microscopy. This methodology will be described in details in the results section.

Abstract

In early stages of metastasis, cancer cells exit the primary tumor and enter the vasculature. Although most studies have focused on the tumor invasive front, cancer cells from the tumor core can also potentially metastasize. To address cell motility in the tumor core, we imaged tumor explants from spontaneously-forming tumors in real time using long-term two-photon microscopy. Cancer cells in the tumor core are remarkably dynamic and exhibit correlated migration patterns, giving rise to local "currents" and large-scale tissue dynamics. Collagen structures in the tumor core appear to influence the direction of these local currents. Although cells exhibit stop-and-start migration with intermittent pauses, pausing does not appear to be required during division. Our study system provides new insight into the dynamics of cancer cells in the tumor core, opening new avenues of research in understanding the migratory properties of cancer cells and later metastasis.

Introduction

Cell migration is an essential process in the development and homeostasis of multicellular organisms. In pathological conditions such as metastatic cancer, cells acquire an upregulated capacity for migration (Lambert, Pattabiraman and Weinberg, 2017). During the progression of carcinoma metastasis, cancer cells breach the surrounding basement membrane and invade into the stroma, which is composed of extracellular matrix and stromal cells (Chambers, Groom and MacDonald, 2002). In the stroma, features of the microenvironment that modulate the modes of cancer cell migration, such as collagen density and alignment, have been described (Provenzano *et al.*, 2006, 2008; Gligorijevic *et al.*, 2014). Invading cells migrate through the stroma to reach blood or lymph vessels, which are also embedded in the stromal network. Interestingly, it has recently been shown that vascular escape can also occur in deep regions of tumors and not only in the invasive front (Deryugina *et al.*, 2017).

Most solid tumors, including colorectal cancer, are composed of a central differentiated core region – or tumor bulk – and an invasive front forming the interface between tumor and stromal tissue (Vignjevic *et al.*, 2007; Clark and Vignjevic, 2015). The invasive front is widely characterized in terms of cell morphology and molecular composition (Prall,

2007). Intravital imaging has uncovered a large diversity of cancer cell migration modes at the invasive front, ranging from collective behaviors to single cell migration (Friedl and Wolf, 2010; Clark and Vignjevic, 2015). In contrast, the dynamics of the tumor core is far less understood, and we still lack precise details of single cell dynamics and migration patterns within the tumor core. To address this, we studied the behavior of cancer cells in densely packed regions at the tumor core using a mouse model of genetically-induced aggressive intestinal carcinoma.

In this model, tumors spontaneously arise in the intestine and metastasize to the lymph nodes, peritoneum and liver (Chanrion *et al.*, 2014), reflecting the heterogeneity and growth timescales of naturally-occurring tumors. Due to the inaccessibility of deep regions of intestinal tumors for intravital imaging, we imaged tumor explant slices using two-photon excitation microscopy (Staneva *et al.*, 2018). Using this model, we investigated the migratory behavior of cancer cells in the tumor core of spontaneously developing intestinal tumors and found that cancer cells in the tumor core are not stationary. On the contrary, cells in the tumor core exhibit coordinated migratory patterns that give rise to large-scale tissue dynamics.

Figure 1

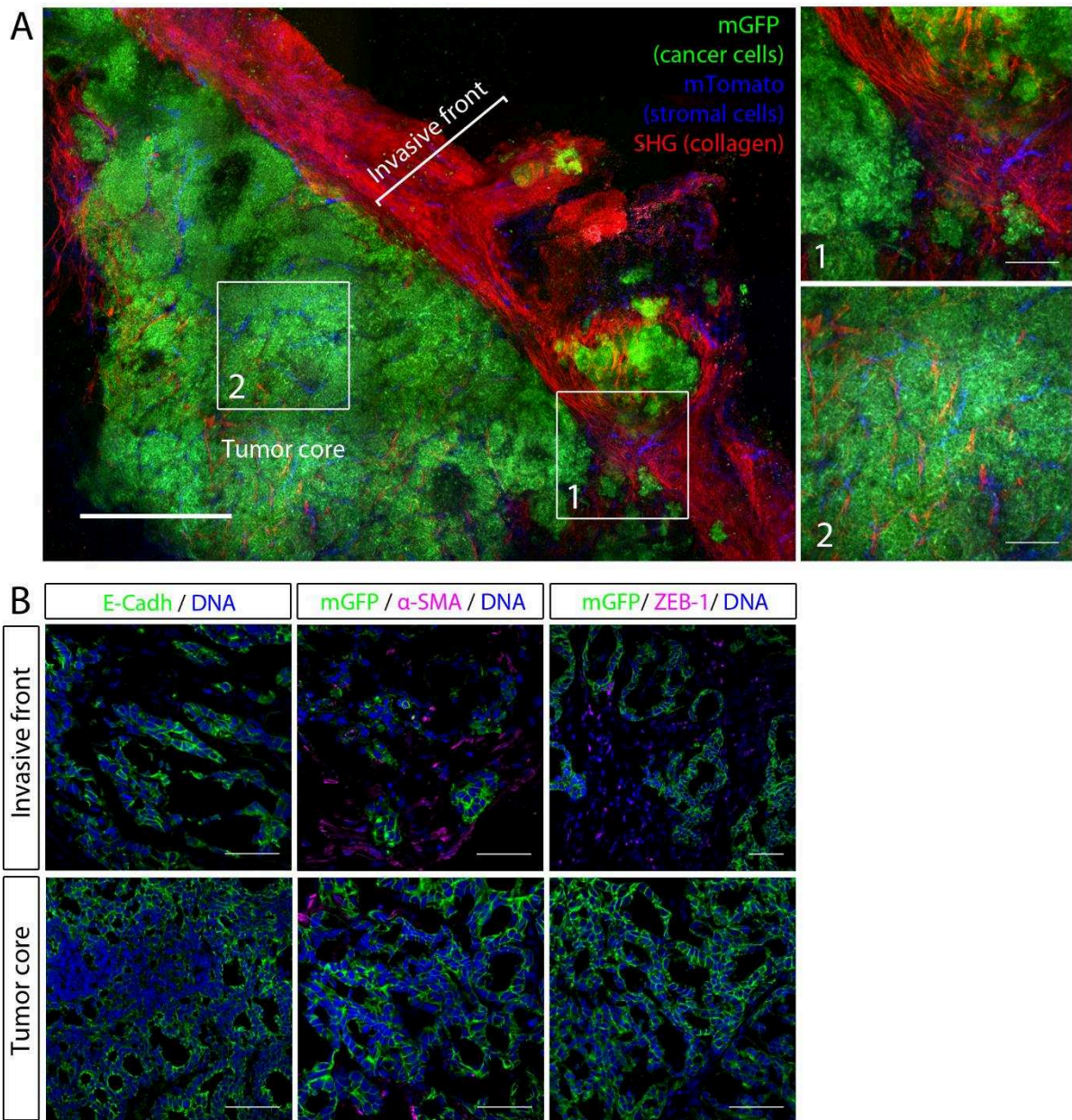


Figure 1. Architecture of the tumor core in NICD/p53^{-/-} carcinoma

A. Stitched image of a large tumor area showing the tumor core and the invasive front in a NICD/Tom/p53^{-/-} mouse, with cancer cells expressing membrane-targeted GFP (mGFP, green) and stromal cells expressing membrane-targeted Tomato (mTomato, blue). Collagen is visualized by SHG (red). Boxed region 1 (invasive front) and 2 (tumor core) from are magnified. Scale bar, 500 μ m.

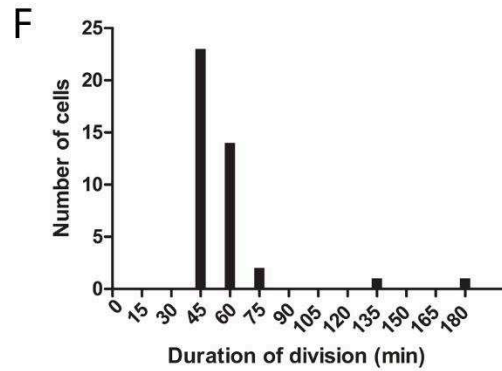
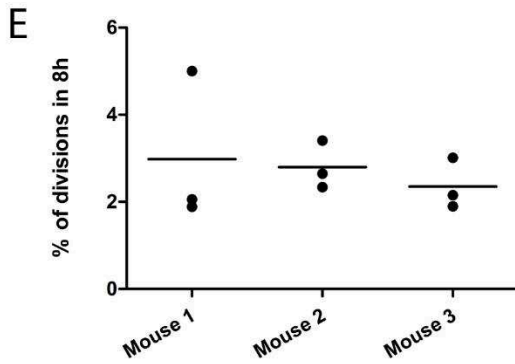
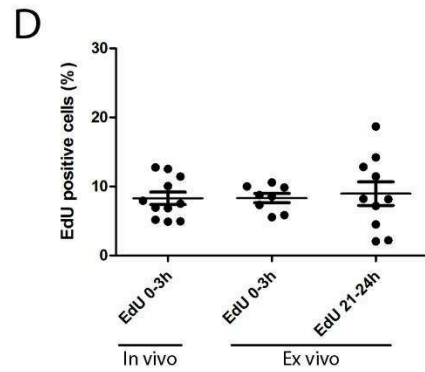
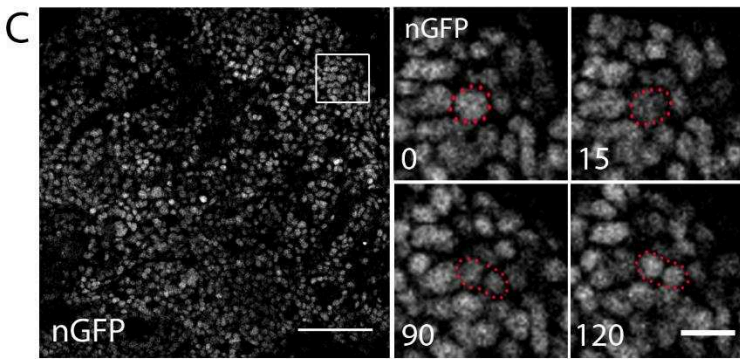
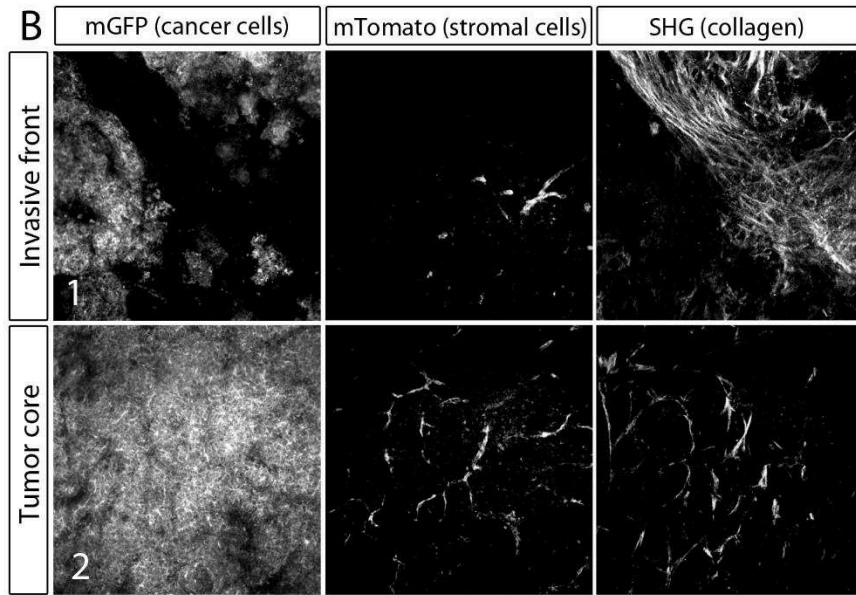
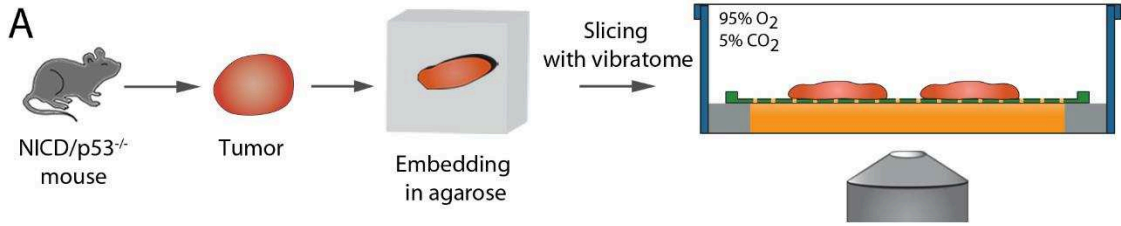
B. Staining for E-Cadherin, α -Smooth Muscle Actin (α -SMA), and ZEB-1 in the invasive front and tumor core. Scale bars, 50 μ m

Tumor explants recapitulate tissue properties found *in vivo*.

To study the growth and migratory behaviors of cancer cells in spontaneously developing tumors, we used the NICD/p53^{-/-} tumor model (Chanrion *et al.*, 2014). In this mouse model, the formation of invasive carcinoma is driven by the expression of a conditionally-activated Notch1 receptor (NICD) and the deletion of the p53 tumor suppressor in the intestinal epithelium following tamoxifen injection. Expression of nucleus-targeted GFP allows visualization and tracking of cancer cell nuclei. In addition, crossing these mice with mT/mG reporter mice (Muzumdar *et al.*, 2007) allows visualization of cell membranes.

In order to analyze cancer cell migration in deep tumor core areas, we performed live imaging on thick tumor explant slices (Staneva *et al.*, 2018) (Fig. S1A). Using this method, we were able to culture and image tumor explants for up to 40h (Supplementary movie 1). Explant culture and two-photon imaging allows for analysis of cell growth and migration in deep tumor areas that are inaccessible to intravital imaging techniques. In NICD/p53^{-/-} tumors, the invasive front comprises the collagen-rich tumor capsule, cancer cells colonizing this capsule and regions just beneath the capsule (Fig. 1A, inset 1 and Fig. S1B, upper panels). The tumor capsule is composed of fibrillar collagen bundles aligned parallel to the tumor edge and interpenetrated by blood vessels. Present at the invasive front are single cells that have undergone Epithelial-to-mesenchymal transition (EMT), as well as clusters of invasive epithelial cells, surrounded by stromal cells (Fig. 1B, upper panels). Deeper in the interior of the tumor is the tumor core, which is composed of densely packed epithelial tumor cells (Fig. 1A, inset 2, and Fig. 1B, lower panels). The tumor core also contains blood vessels, stromal cells and smaller collagen bundles that are less densely packed than in invasive regions (Fig. S1B, lower panels, and Fig. 1B, lower panels). The presence of these structures in the tumor core reflects the physiological nature of this model, where tumors and ECM co-evolve on more physiological timescales.

Supplementary Figure 1



To ensure that tumor explants remained viable, we quantified division rates (Fig. S1C-E). In order to compare the proliferation rates of NICD/p53^{-/-} tumors *in vivo* and *ex vivo*, we quantified uptake of the Thymidine analog EdU (5-ethynyl-2'-deoxyuridine), which is incorporated during S-phase. We found no significant difference in proliferation rates *in vivo* and *ex vivo*, at early or later time-points (Fig. S1D), suggesting that culturing tumors *ex vivo* does not alter their growth rate over the imaging duration. We also quantified the rate of cell division in explants using the expression of the genetically encoded nuclear GFP to observe mitotic cells undergoing mitosis (Fig. S1C). In the first 8h of imaging, on average 2.7% of cells divided (Fig. S1E) with divisions lasting 45min – 1h (Fig. S1F).

Suppl Fig1. Cell division rates in NICD/p53^{-/-} tumor slices are similar to *in vivo*

A. Spontaneously-developing intestinal tumor (red) is harvested from the NICD/p53^{-/-} mouse, embedded in a block of agarose (gray) and cut into 250-360µm-thick slices using a vibratome. Slices are deposited on top of a cell culture filter (green) and cultured at the air-liquid interface. Culture medium is added in the lower chamber (orange).

B. Single color panels from boxed region 1 (invasive front) and 2 (tumor core) from Fig. 1A are shown. mGFP (cancer cells), mTomato (stromal cells, including endothelial cells lining the blood vessels) and SHG. Scale bars, 100µm.

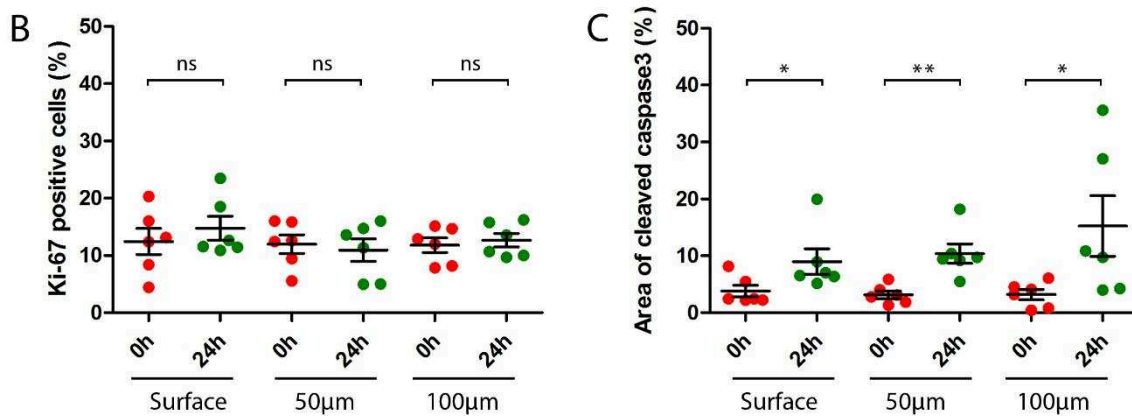
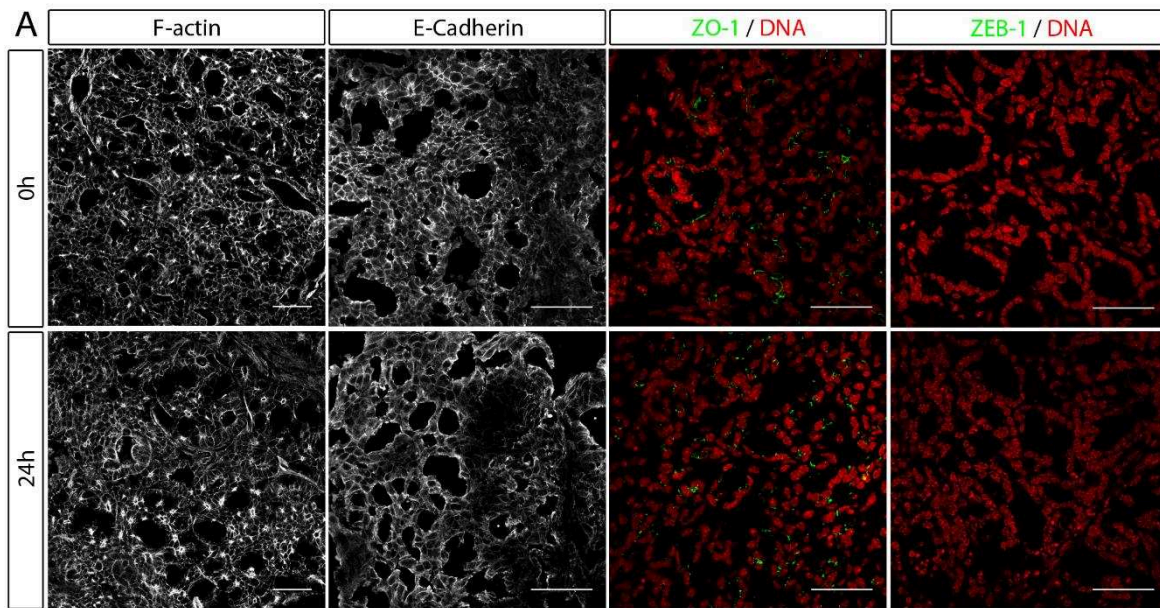
C. Cultured tumor slices retain capacity for cell division. Left panel: z-slice of NICD/p53^{-/-} tumor expressing nuclear GFP (nGFP, green). Boxed region is magnified in right panel. Scale bar, 100µm. Right panels: cancer cell undergoes rupture of the nuclear envelope and nGFP is segregated into two daughter nuclei. Scale bar, 20µm. Time in minutes. See also Supplementary movies 1, 2.

D. Percentage of EdU positive cells after a 3h pulse. Three mice were injected with EdU and sacrificed after 3 hours (*in vivo*). Tumors of six other mice were sliced and tissue explants were cultured in EdU-containing medium for 3h, either at the onset of culture (hours 0-3h, 3 mice), or at the end of culture (hours 21-24h, 3 mice). Each dot represents the mean of 1 to 5 regions of interest per slice. For each region of interest, between 163 and 750 cells were quantified (mean±SEM). Analysis of variance (Kruskal-Wallis test), p-value=0.92.

E. Percentage of cell divisions in the first 8h of three movies from three different NICD/p53^{-/-} mice. Three independent z-planes, separated by 20µm, are quantified per movie. Mean is shown. A total of 67 divisions are observed in 2657 cells. Analysis of variance (Kruskal-Wallis test), p-value=0.586.

F. Histogram of cell division duration from two movies from two different NICD/p53^{-/-} mice. n=28 and n=13 cells quantified for each mouse.

Supplementary figure 2



Suppl Fig2. Comparison of tumor explants properties before and after 24h culture

A. Comparison of tissue architecture (F-Actin, phalloidin, left), cell-cell junctions (E-cadherin and ZO-1, middle panels), and ZEB-1 (right) at 0h and after 24h of tissue explants culture. Scale bars, 50µm.

B. Percentage of Ki-67 positive cells in tumor tissue explants, at three different depths in the tissue slices (surface, 50µm deep, 100µm deep) with 3 mice per condition. Each dot represents the mean of 3-6 regions of interest for a given tissue slice. For each region, 210-829 cells were quantified. Bars, mean±SEM. Pairwise Mann-Whitney tests (0h vs. 24h), $p = 0.82, 0.82, 0.59$.

C. Percentage of tissue slice area occupied by Cleaved Caspase3 signal, at three different depths in the tissue slices (surface, 50µm deep, 100µm deep) with 3 mice per condition. Each dot represents one tissue slice. Bars, mean±SEM. Pairwise Mann-Whitney tests (0h vs. 24h), $p = 0.04, 0.004, 0.04$.

We observed that tissue architecture was conserved after long-term *ex vivo* culture, as revealed by the maintenance of actin organization and cell-cell junctions and the absence of EMT in the tumor core (Fig. S2A). Although cell death was slightly increased after 24h of incubation, cell proliferation was constant throughout the duration of tissue explant culture and in different depths of the tissue (Fig. S2B, C), indicating adequate diffusion of nutrients and gas to deep regions of the tissue explant. Together, those data show that tumor explant recapitulates tissue properties found *in vivo* and thus can be used as a model system to investigate cell behaviors in the tumor core.

Figure 2

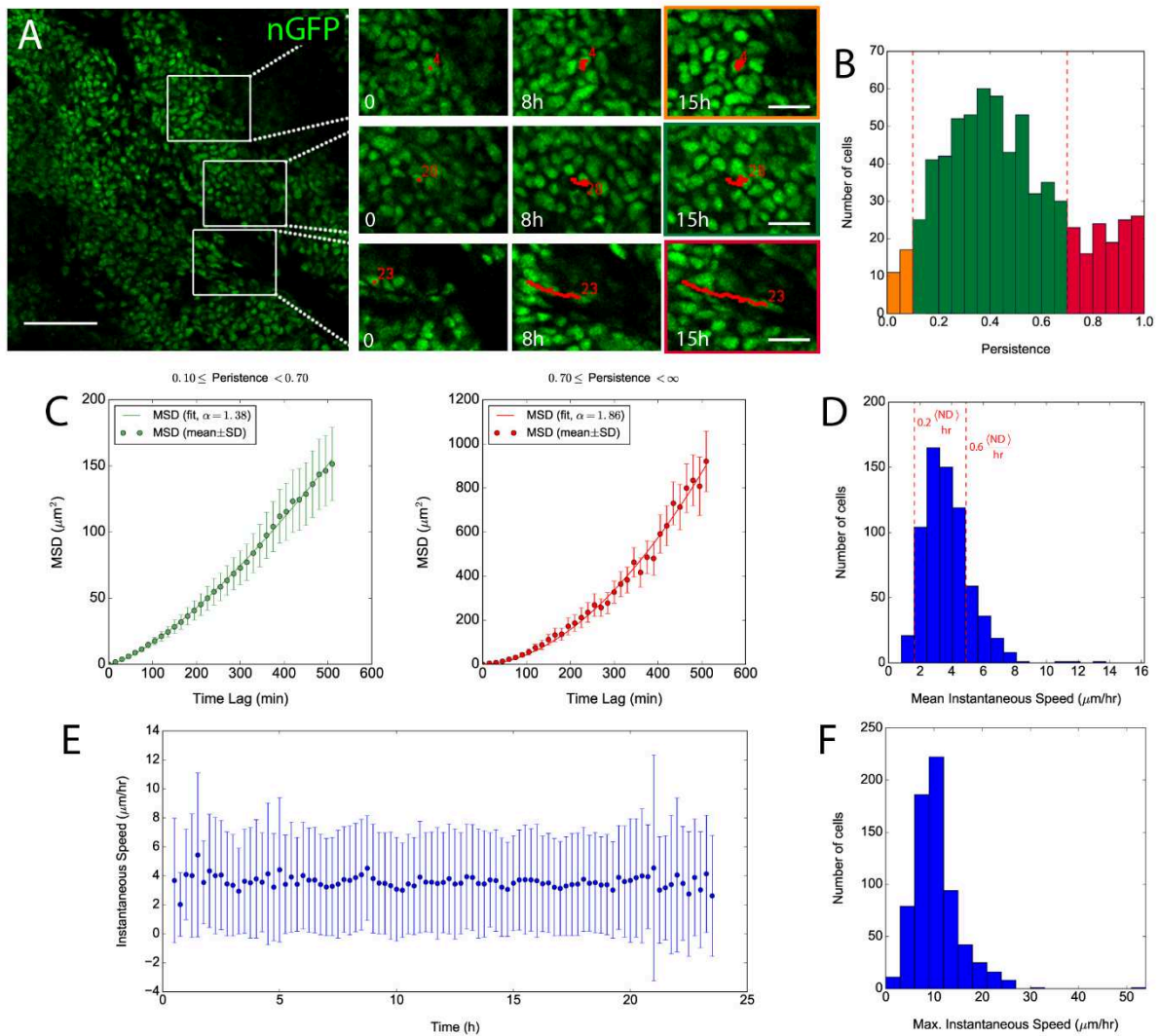


Figure 2. Cells in NICD/p53^{-/-} carcinoma are motile and display a range of speeds and persistence

A. Migration patterns of NICD/p53^{-/-} cells. Left panel: z-slice of NICD/p53^{-/-} tumor. Boxed regions are magnified in right panels. Scale bar, 100 μm . Right panels: nuclei were tracked for 15h. Color frames indicate low persistence (0.04; orange), medium persistence (0.39; green) and high persistence (0.87; red). Time in hours. Scale bars, 30 μm .

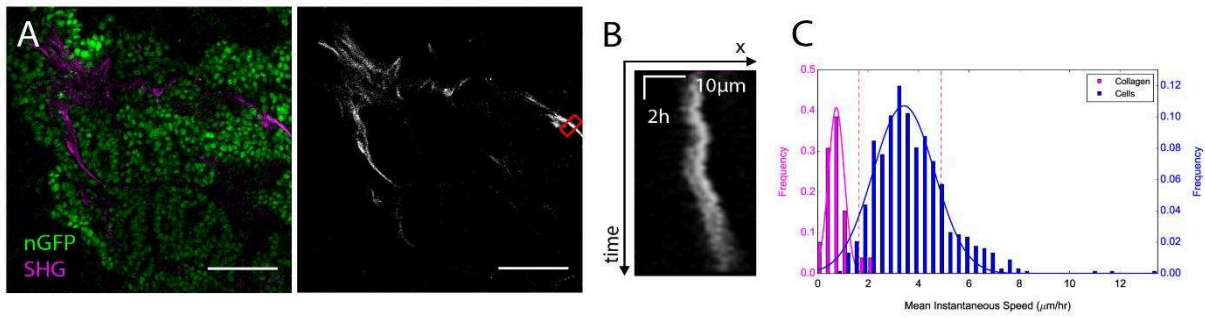
B. Histogram of persistence values from tracked cells. The red dotted lines indicate borders between cells with low (<0.1; orange), medium (0.1-0.7; green) or high (>0.7; red) persistence. 685 tracked cells from 5 mice were analyzed.

C. Average Mean Squared Displacement (MSD) plots for cells with medium (green) or high (red) persistence (from B).

Cells in tumor core display heterogeneous speeds and persistence

To analyze migration dynamics in the tumor core, we manually tracked a random selection of tumor cells (Fig. 2A; Supplementary movie 2). We observed a wide range of migration persistence, a measure of the straightness of trajectories (Fig. 2B). Approximately 75% of cells migrated with moderate persistence, between 0.10 and 0.70; ~20% of cells displayed highly persistent migration, with persistence > 0.70 (Fig. 2B). To further investigate directional migration, we calculated the average Mean Squared Displacement (MSD). For moderately-persistent cells, the MSD increased with respect to time with an exponent of ~ 1.38 (Fig. 2C, left), while highly-persistent cells had an MSD vs. time exponent of ~ 1.86 (Fig. 2C, right), suggesting that this subset of cells migrate in a highly directional manner. We found that mean instantaneous speed was normally distributed around a mean of $\sim 3.7 \mu\text{m/hr}$ and constant over more than 20 hours of imaging (Fig. 2D, E). These speeds were within the range of speeds found using intravital imaging in several mouse models (Weigelin, Bakker and Friedl, 2012; Patsialou *et al.*, 2013; Gligorijevic *et al.*, 2014; Clark and Vignjevic, 2015). Most cells (80%) migrated between 1.6 and $4.8 \mu\text{m/hr}$, corresponding to 0.2-0.6 nuclear diameters per hour (ND/hr), with 3% slower than 0.2 ND/hr and 17% faster than 0.6 ND/hr (Fig. 2D). Most cells reached a maximum instantaneous speed of $\sim 10 \mu\text{m/hr}$ (Fig. 2F). In order to estimate the noise in cell trajectories, due primarily to tissue deformations, we measured the displacement of collagen fibers in the tumor core (Fig. S3A, B). Collagen fibers exhibited mean displacements of $0.85 \mu\text{m/hr}$, with speeds substantially below that of migrating cells (Fig. S3C). This suggests that the observed cell migration is not simply a consequence of large-scale tissue deformation. Together, these data suggest that tumor cells in the core display a wide range of migration dynamics.

Supplementary figure 3



Suppl Fig3. Displacement of collagen structures during timelapse imaging

A. Left: z-slice of NICD/p53^{-/-} tumor expressing nGFP (green), with collagen bundles (SHG, magenta). Right: collagen bundles (SHG) alone. Red box indicates the region used for the kymograph in B. Scale bars, 100 μ m.

B. Kymograph of collagen displacement over time from the red box in A.

C. Histogram of instantaneous speeds measured for cells and collagen fibers. Bars: binned values from the speed measurements. Solid lines: Gaussian fits of the bin values. The red dashed lines indicate speeds of 0.2 and 0.6 nuclear diameters per hour (ND/hr), corresponding to 1.6 and 4.8 μ m/hr, respectively. Cell migration data reflects the same measurements presented in Fig. 2D. For collagen measurements, 26 collagen regions were measured from 3 different mice.

It has been long known that during cell migration, cells exhibit pausing behaviors (Abercrombie, Heaysman and Pegrum, 1970). To determine whether cells in the tumor core pause during migration, we straightened the trajectories to make kymographs. Individual kymographs revealed the cells paused intermittently, resulting in various stop-start migration patterns (Fig. 3A). On average, migrating cells were paused 20% of the time (Fig. 3B), pausing once every three hours, and with most pauses 30-40 minutes long (Fig. S4A, B). These data suggest that tumor cells in this model exhibit stop-and-start behavior, and that pausing dynamics are consistent over the whole population of tumor cells.

In many single-cell systems, migrating cells must stop in order to divide (Abercrombie, Heaysman and Pegrum, 1970), and daughter cells begin migrating only when cell division is complete. To investigate this idea in our model, we tracked mother and daughter cells and produced kymographs of their trajectories (Fig. 3C, D). In only 16.6% of cases (6/36) did the mother cell completely pause during division (Fig. 3D, dashed circle), consistent with the pause rates of non-dividing cells. In 83.4% of cases, mothers continued migrating during division (Fig. 3D, full circle). We found no significant difference in instantaneous cell speeds of cells before, during or after division (Fig. 3E). Together, these data suggest that pauses that happen to occur during division are not more frequent than outside division. Thus, cells can still be displaced during division, and there is no strict requirement for pausing during division in this system.

Figure 3

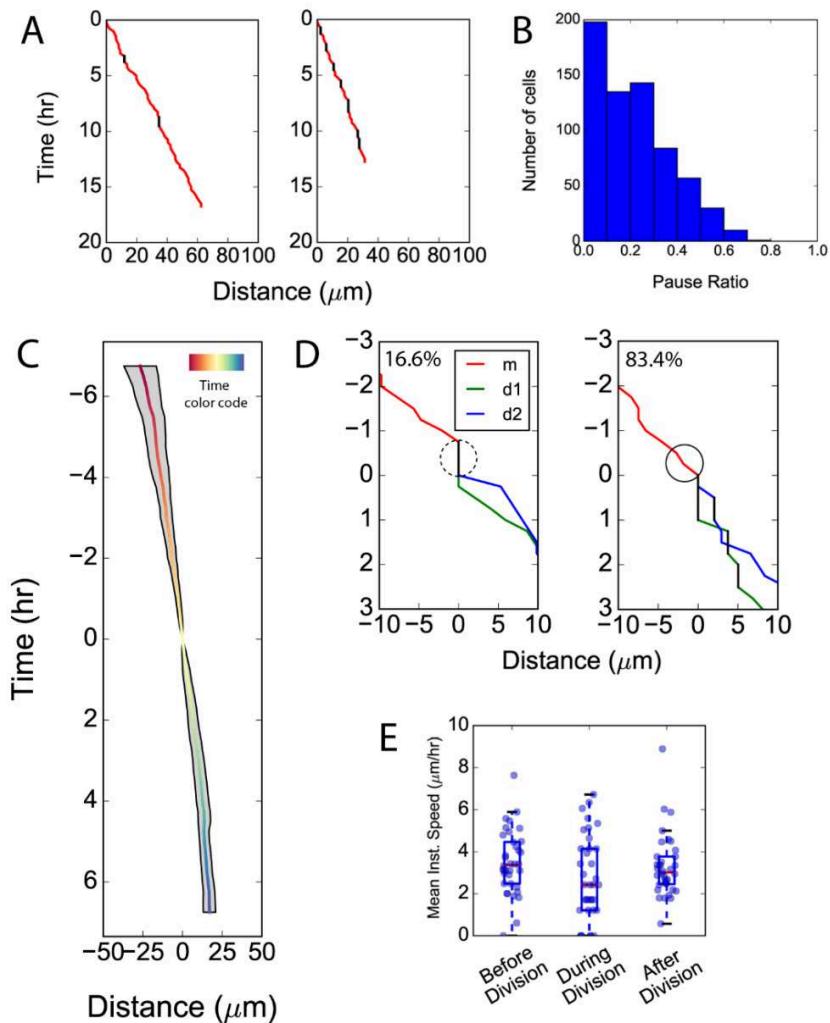


Figure 3. Pausing during cell division is not required in migrating tumor tissue

A. Individual kymographs showing different pausing behaviors, indicating periods of migration (red) interrupted by pauses (black). Pauses are defined as consecutive periods of ≥ 30 min with no detectable migration.

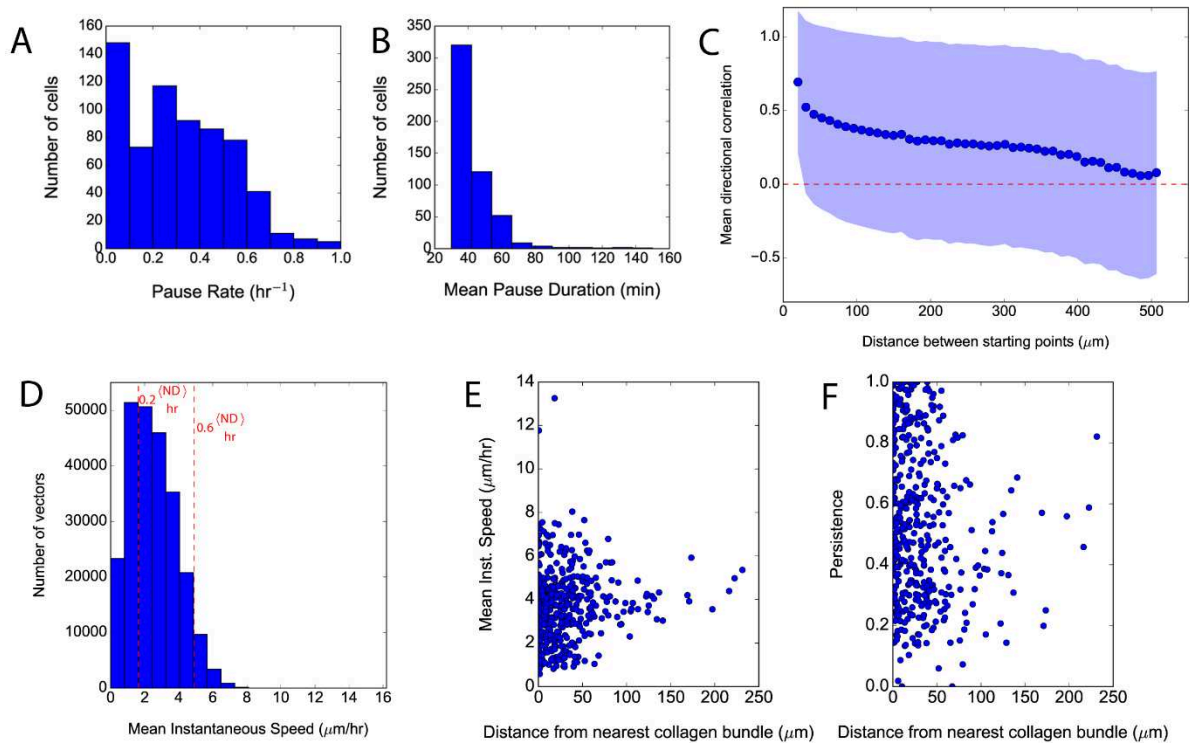
B. Histogram of pause ratios for all cell trajectories. Pause ratio is defined as the fraction of the trajectory spent paused.

C. Combined kymograph from dividing mother (red to yellow) and daughter (yellow to blue) cell trajectories ($n = 36$ individual division events from 3 mice, time color code, mean \pm SD). Kymographs were aligned such that division occurred at time=0, distance=0.

D. Kymographs from trajectories of two dividing mother cells (m, red) and their daughter cells (d1, green, d2, blue), demonstrating that some dividing cells pause their migration during division (dashed circle), while some cells continue migrating (solid circle).

E. Mean instantaneous speeds of cells before, during and after division. Analysis of variance (Kruskal-Wallis test), p -value=0.091.

Supplementary Figure 4



Suppl Fig4. Dynamics of migration of cells in NICD/p53^{-/-} tumors

A. Histogram of pause rates for all cell trajectories. Pause rate is defined as the average frequency of pauses (pauses/hr).

B. Histogram of mean pause duration for all pauses from all cell trajectories.

C. Plot of the directional correlation between displacement vectors from PIV analysis. All combinations of vectors at all analyzed time points were used for the analysis. The distance indicates the distance between the vector positions. The correlation vs. distance relationship was similar to that from manually tracked cells (Fig. 4C).

D. Histogram of vector magnitudes (speeds) from PIV analysis. The speed distribution was similar to that from manually tracked cells (Fig. 2D). The red dotted lines indicate speeds of 0.2 and 0.6 nuclear diameters per hour (ND/hr), corresponding to 1.6 and 4.8 μm/hr, respectively.

E. Scatter plot of the mean instantaneous speed as a function of the distance to the closest collagen bundle. Each dot represents one cell trajectory (n=423 cells from 3 mice).

F. Scatter plot of persistence as a function of the distance to the closest collagen bundle. Each dot represents one cell trajectory (n=423 cells from 3 mice).

Tumor cells exhibit coordinated migration patterns related to collagen bundle positions

The tumor core is dense but migratory. In *in vitro* monolayers, dense tissues exhibit collective migration and spatial inhomogeneities (Angelini *et al.*, 2011; Tambe *et al.*, 2011). In order to investigate whether such collective behavior also exists in dense and migratory tissues *in vivo*, we investigated directional correlation in tumor core cell migration (Fig. 4A). For each overlapping time point for two cell trajectories, we determined the directional correlation at that time interval, equal to 1 for perfectly parallel migration and -1 for anti-parallel migration (Fig. 4B). We then determined the mean correlation for the trajectories and compared this to the distance between the cells at the start of the trajectory (Fig. 4C). We found that cells close together (<100 μm apart) indeed displayed a directional correlation (~ 0.25), and this correlation was lost for cells $> \sim 250 \mu\text{m}$ apart (Fig. 4C).

Figure 4

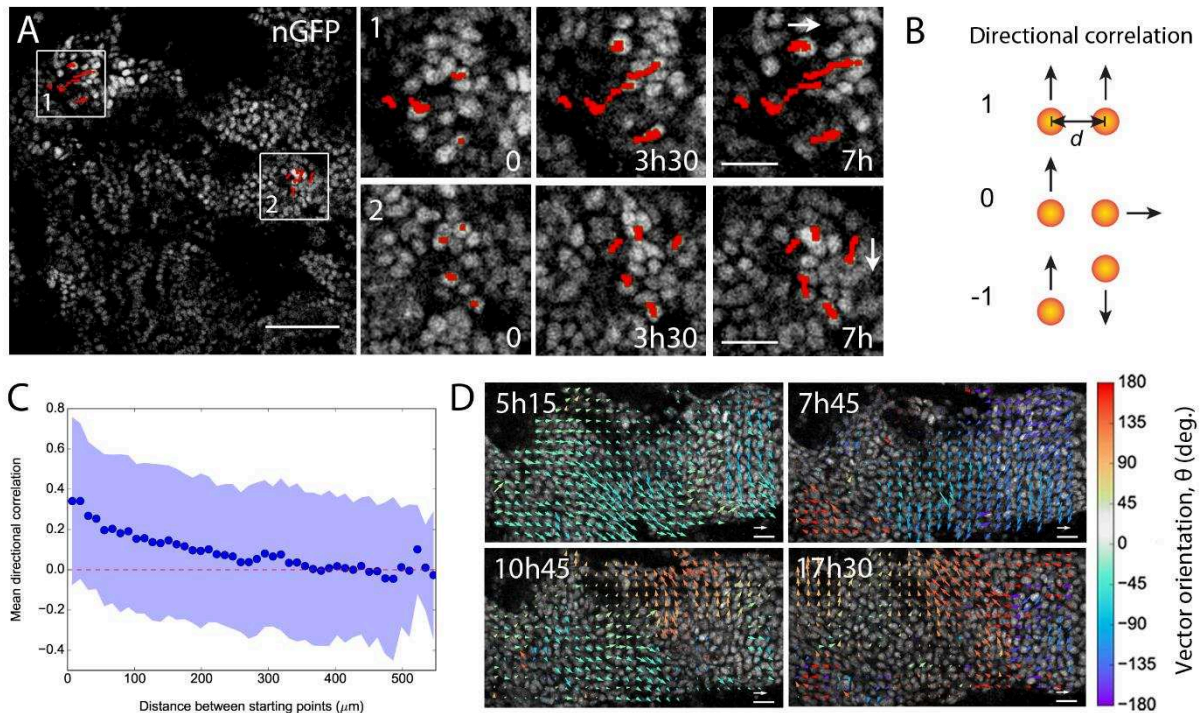


Figure 4. Tumor core cells exhibit correlated migration patterns

A. Spatial distribution of migration directions. Left panel: z-slice of NICD/p53^{-/-} tumor. Boxed regions are magnified in right panels and show similar migration directions for cells in close proximity. White arrows show the main direction of migration for the cells in proximity. Scale bars, 100μm (left), 30μm (right). Time in hours.

B. Mean directional correlation is calculated by comparing migration direction for each overlapping time step between different trajectories. Correlation is defined as $co(\theta_{i,t} - \theta_{j,t})$ for cells i and j at overlapping time point t . The mean correlation is determined by averaging the correlation at all overlapping time points and compared to the distance between the cells at the start of their trajectories, d .

C. Plot of the average directional correlation vs. distance between trajectory starting positions for 857 tracked cells from 5 mice, resulting in 19552 overlapping trajectories.

D. Examples of displacement vectors determined by particle image velocimetry (PIV) overlaid on images of tissue slices. Local currents in cell migration result in larger-scale vortex and swirl patterns. Vector colors indicate direction and lengths indicate magnitude (speeds). Scale vector (white), 6μm/hr. Scale bars, 30μm. See also Supplementary movie 3.

To further investigate the correlation in migration directions, we performed particle image velocimetry (PIV) analysis on the 2D time-lapse images (Fig. 4D and Supplementary movie 3). Surprisingly, we found numerous examples of groups of cells exhibiting local migration "currents" and vortices (Fig. 4D, Supplementary movie 3), highlighting the collective nature of cell migration in this system. To corroborate our findings on directional correlation vs. distance, we analyzed the correlation between the extracted PIV vectors and found a high directional correlation (~ 0.5) for cells $< 100 \mu\text{m}$ apart; this correlation was lost for cells $> \sim 500 \mu\text{m}$ apart (Fig. S4C). In addition, the distribution of vector magnitudes (indicating cell migration speed) was similar to speeds from manually tracked cells, suggesting that the noise in manual tracking is minimal (compare Fig. S4D and 2D). Taken together, these complementary analyses demonstrate that cells in the tumor core exhibit correlated migration direction.

In order to assess how microenvironment features contribute to the coordinated migration of cancer cells, we analyzed cell migration with respect to collagen fibers. We found no correlation between the distance from collagen fibers and cell migration speed or persistence (Fig. S4E, F). We then sought to determine whether the directionality of cell migration was correlated with collagen structures. To this end, we simultaneously imaged tumor cells and collagen bundles (Fig. 5A). After tracking tumor cells, we extracted collagen contours and curvature maps (not shown) and compared the alignment between cells direction of migration and the map of collagen contours at the cell's position. We found a striking directional bias in cell migration, with most cancer cells migrating parallel to collagen structures (Fig. 5B), even when not being in direct contact with collagen. All cells were within $\sim 100 \mu\text{m}$ (~ 10 cell diameters) of the nearest collagen structure, suggesting that collagen structures in the tumor core can effect long-range directional cues, up to at least tens of micrometers away.

Figure 5

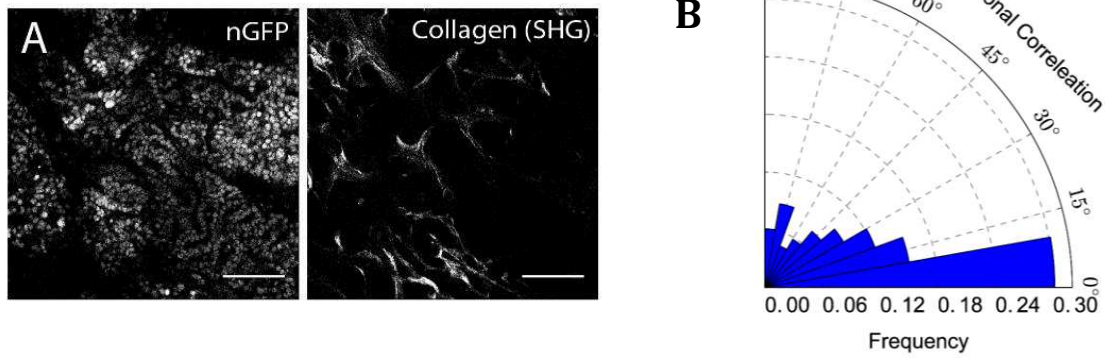


Figure 5. Cancer cells in the tumor core migrate parallel to collagen fibers

A. Representative image slice of the tumor core showing tumor cells (nGFP) and collagen bundles (SHG). Scale bars, 100 μ m.

B. Polar histogram of directional migration bias with respect to collagen structures. Angles close to 0° denote a migrate parallel to collagen structures.

Discussion

Our work aimed to decipher cancer cell migration in the tumor core with single cell resolution, using a physiological spontaneous cancer model. To address this, we used a pipeline to image tumor explants from spontaneously forming tumors in real time using long-term two-photon microscopy. We found that cells in the tumor core are remarkably dynamic. Cancer cells exhibited collective behaviors, such as coordinated migration, streaming and vortex-like movements. Coordinated migration was interspaced by brief pauses. Interestingly, there was no requirement for pausing during division, suggesting that dividing cells continue to flow with their neighbors. In addition, we found that collagen fibers within the tumor core may act as long-range directional cues, as tumor cells migrate parallel to collagen structures, even up to several cell diameters away.

Tumor explant imaging provides a bridge between 3D *in vitro* invasion assays and intravital studies in living mice. On one hand, embedding cancer cells in various 3D extracellular matrices allows for deciphering interactions with specific matrix components and molecular pathways involved in 3D migration. On the other hand, intravital imaging reveals cell dynamics in intact tissue, but xenografted tumors are not surrounded by a native stroma that co-evolves with the tumor, thus they lack a truly disease-relevant microenvironment. The core of spontaneously developing tumors contains extracellular matrix that has co-evolved with the tumor, and therefore the influence of the structure of collagen on tumor cell migration can be addressed. Imaging of spontaneous cancer models allows for a better understanding of the co-adaptation of cancer cells to their native microenvironment and how tumor cells behave in a native microenvironment.

Collective coordinated behaviors exhibited by our intestinal cancer model were reminiscent of phenotypes observed in confluent cell monolayers *in vitro* that are close to a jamming transition, with characteristic dynamic heterogeneities resulting in collective cell migration in local swirls and flows. Indeed, we observed a 2D density of 4240 ± 889 cells/mm in the tumor core, on the same order of magnitude as densities measured in monolayers near jamming transitions (~ 2000 - 3000 cells/mm (Angelini *et al.*, 2011;

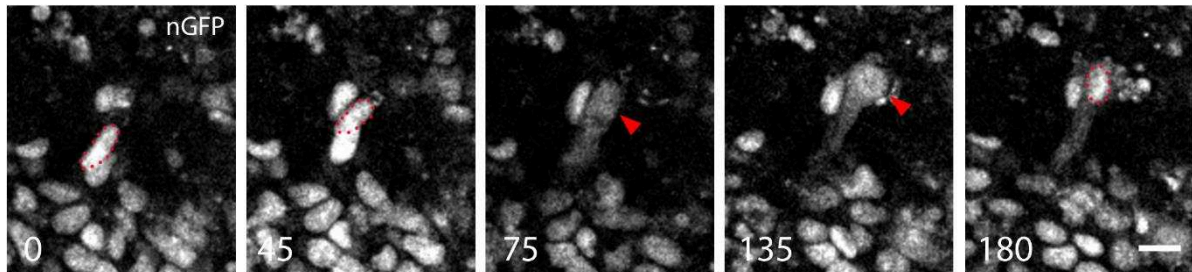
Tambe *et al.*, 2011)). The difference in densities likely reflects the fact that we image 2D slices of a 3D tissue and thus overestimate 2D cell density. These results reflect the first, to our knowledge, observation of a dynamic tumor tissue near a jamming transition and represents a new, more physiological model for studying these collective phenomena. The presence of ECM (i.e. collagen fibers) in the tumor core presents an additional layer of complexity. Guidance of tumor cell migration by collagen fibers has been observed at the invasive front of tumors, where collagen bundles perpendicular to the tumor edge direct cell invasion in the stroma (Provenzano *et al.*, 2006). We observe that cells in the tumor core migrate parallel to collagen fibers even without direct contact with collagen. This suggests that collagen may act as a long-range directional cue for cancer cell migration in highly-confined environments like the tumor core. It will be interesting in the future to explore, both *in vitro* and in explants, the effects of structural barriers like collagen fibers in densely packed tissues that exhibit spontaneous collective behaviors.

We speculate that the coordinated nature of tumor cell migration in our model is also responsible for the migratory behavior we observed during cell division. Previous work in single migrating cells *in vitro* has led to the belief that in order to divide, cells must first stop migrating (Abercrombie, Heaysman and Pegrum, 1970). However, in a densely-packed tissue, as we observe in the tumor core, dividing cells can continue to migrate during division likely because they are dragged by neighboring cells in the tissue, as previously suggested by intravital imaging of invading fibrosarcoma xenografts (Alexander *et al.*, 2013). Our data suggest that this can also occur in the core of epithelial tumors.

As cells migrate through complex microenvironments such as the tumor core, cells must adapt their shape in order to squeeze between other cells and through pores of the extracellular matrix. Recently, it has been described that such cell shape change is often accompanied by nuclear envelope rupture during migration of dendritic cells confined *in vitro* (Raab *et al.*, 2016) and cancer cell lines migrating *in vivo* (Denais *et al.*, 2016). We also observed nuclear envelope rupture in cancer cells migrating in the tumor core followed by fast repair (Fig. S5). Frequent nuclear envelope rupture could result in the

accumulation of DNA damage and increased genetic instability, which could in turn affect cancer progression.

Supplementary Figure 5



Suppl Fig5. Cancer cells in NICD/p53^{-/-} tumors can undergo nuclear envelope rupture during migration

Montage of a cell undergoing nuclear envelope rupture during migration. The nucleus of interest (circled, left panel) is initially well defined at t=0 and t=45min. nGFP signal becomes dispersed in the cytoplasm indicating nuclear envelope rupture (arrowhead, t=75min). GFP signal is then recruited back to the nucleus, which was displaced during migration (arrowhead, t=180min). The reformed nucleus is detected 20 μ m away from the site where it was ruptured. Time in minutes. Scale bar, 20 μ m.

Our tumor explant model opens new avenues for studying the behavior and dynamics of cells in the tumor core. Because vascular escape of cancer cells can also occur in deep regions of tumors, and not only at the invasive front (Deryugina *et al.*, 2017), our work provides new insight into the nature of cells in the tumor core prior to escape, which can lead to later metastasis. More broadly, our model will be an important tool to better understand collective cell behavior in tumors as well as cancer progression.

PART 2. ROLE OF MATRIX STIFFENING IN INVASION

A new biomimetic assay reveals the temporal role of matrix stiffening in cancer cell invasion

Ralitza Staneva^{1,5*}, Federica Burla^{2*}, Gijsje H. Koenderink², Stéphanie Descroix³, Danijela Matic Vignjevic¹, Youmna Attieh^{1,4†}, Marine Verhulsel^{3,4†}

¹Institut Curie, PSL Research University, CNRS, UMR 144, F-75005 Paris, France

²Department of Living Matter, AMOLF, Science Park 104, 1098 XG Amsterdam, The Netherlands

³Physicochimie Curie (Institut Curie, CNRS-UMR 168, UPMC), Institut Curie, Centre de Recherche, 26 rue d'Ulm, 75248 Paris Cedex 05, France

⁴Sorbonne Universités, UPMC Univ Paris06, IFD, 4 Place Jussieu, 75252 PARIS cedex05

⁵University Paris Descartes, 12 rue de l'Ecole de Médecine, 75006 Paris

* Authors contributed equally to this study

† Corresponding authors

Foreword

This paper was initiated by Youmna Attieh and Marine Verhulsel. The study was interested in understanding the temporal effect of collagen stiffening on cancer cell invasion. In order to efficiently crosslink and stiffen collagen, the sugar threose was used in 3D invasion assays in collagen. In this study, Youmna performed the spheroids assays and Federica Burla and Gijsje Koenderink, specialists in rheology from the Netherlands, performed the rheology part of the study. I participated in the work at the moment of the revision of the paper, and I tested the effect of threose on cell migration, adhesion and force generation. For clarity purposes, I present here the whole project.

Abstract

Tumor initiation and growth is associated with significant changes in the surrounding tissue. During carcinoma progression, a global stiffening of the extracellular matrix is observed and is interpreted as a signature of aggressive invasive tumors. However, it is still unknown if this increase in matrix rigidity promotes invasion and whether this effect is constant along the course of invasion. Here, we have developed a biomimetic *in vitro* assay that enabled us to address the question of the importance of tissue rigidity in the chronology of tumor invasion. Using low concentrations of the sugar threose, we can effectively stiffen reconstituted collagen I matrices and control the stiffening in time with no direct effect on residing cells. Our findings demonstrate that, depending on the timing of its stiffening, the extracellular matrix could either inhibit or promote cancer cell invasion and subsequent metastasis: while matrix stiffening after the onset of invasion promotes cancer cell migration and tumor spreading, stiff matrices encapsulate the tumor at an early stage and prevent cancer cell invasion. Our study suggests that adding a temporal dimension in *in vitro* models to analyze biological processes in 4D is necessary to fully capture their complexity.

Introduction

The tumor microenvironment is characterized by an abnormal synthesis of extracellular matrix (ECM) components and an overall increase of matrix stiffness (Paszek and Weaver, 2004; Levental *et al.*, 2009; Attieh and Vignjevic, 2016). Such severe changes in the microenvironment are integrated at the cellular level. As a result, the transition from a benign to a malignant tumor is not induced by tumor internal signaling alone, but results from a dynamic cross-talk between the tumor and its microenvironment (Attieh and Vignjevic, 2016).

In vivo, massive deposition of collagen and enzymatic collagen crosslinking by lysyl oxidase (LOX) are responsible for tumor matrix stiffening (Levental *et al.*, 2009; Barker *et al.*, 2013). However, their impact on tumor progression is not restricted to a mechanical effect. The increase in collagen density also correlates with a higher number of binding sites available and therefore modifies tumor cell adhesion and migration, while LOX also

acts as an intracellular factor regulating genes responsible for epithelial-mesenchymal transition (Levental *et al.*, 2009; Barker *et al.*, 2013; Attieh and Vignjevic, 2016).

Although stiff matrices are a signature of aggressive tumors, the causal connection between matrix stiffness and tumor aggressiveness has never been tested. Does matrix stiffening induce cancer cell invasion or is it a consequence of tumor spreading? And is the effect of matrix stiffness on cancer cell invasion constant in time or do cells respond differently to mechanical changes in their environment depending on whether these happen during early or advanced stages of invasion?

To address these questions, *in vitro* models are valuable tools as they are less complex than the *in vivo* microenvironment and offer the ability to decouple the different parameters at play in cancer invasion. Here, we show a new approach by which we can modify matrix stiffness alone at different time points during tumor invasion. We use threose, a sugar and natural collagen crosslinker (Kinnunen *et al.*, 2012) that is more effective than the traditional crosslinking agent ribose. As threose does not affect cell autonomous adhesion, migration and force generation, we can modulate the stiffness of collagen gels without affecting cancer cells embedded in the gel. Our results expose the importance of the temporal dimensions of biological processes and reveal that matrix stiffening inhibits invasion at an early stage but enhances it at later stage.

Results and discussion

Threose stiffens collagen more efficiently than ribose

In vitro models of tumor-matrix interactions ideally need to recapitulate the fibrillar structure, rheological properties, and the nature and spatial distribution of ligands of the *in vivo* ECM in order to provide biologically relevant insights (Verhulsel *et al.*, 2014). We therefore chose collagen I for our artificial matrix as it supports the growth of cells in 3D while closely mimicking *in vivo* fibrillar ECMs and reproducing cell-matrix interactions specific to tumors (Wolf *et al.*, 2009, 2013; Geraldo *et al.*, 2012). Amongst the different options published in the literature to stiffen collagen (Tanaka *et al.*, 1988; Paszek and Weaver, 2004; Levental *et al.*, 2009), glycation and LOX crosslinking are the only ones also occurring spontaneously *in vivo*. As LOX activity is known to modulate gene expression, glycation occurring between glucose and collagen better meets our needs for a

physiological environment (Tanaka *et al.*, 1988). Ribose is mostly used as a glucose substitute *in vitro* but the high concentrations and long incubation time required to significantly stiffen the collagen matrix are presumed to induce a diabetic phenotype in cells (Han *et al.*, 2011).

To overcome this limitation, we tested an alternative collagen crosslinker, threose, which efficiently forms crosslinks in bovine articular cartilage (Kinnunen *et al.*, 2012). We incubated collagen gels with threose after polymerization to avoid any interference with fibrillogenesis and minimize potential changes in network architecture. To test if threose is a more effective crosslinker than ribose, we compared the rheological properties of 2mg/mL collagen gels alone or supplemented for 48 hours either with 1mM of threose or with 1mM or 10mM of ribose. At concentrations of 1mM, the elastic modulus of collagen treated with ribose was similar to control whereas threose treatment induced a 1.8 fold increase in stiffness (Fig 1A). At a concentration of 10mM, ribose stiffened collagen to the same extent as 1mM threose (Fig 1A).

These results suggest that threose is effective at lower concentrations than ribose, which is advantageous as lower sugar concentrations diminish the likelihood to induce a diabetic phenotype or cause a hypertonic stress to cells.

In addition, monitoring the development of the elastic modulus of collagen gels in time revealed that ribose treatment had a delayed impact on collagen crosslinking compared to threose (Fig. 1B).

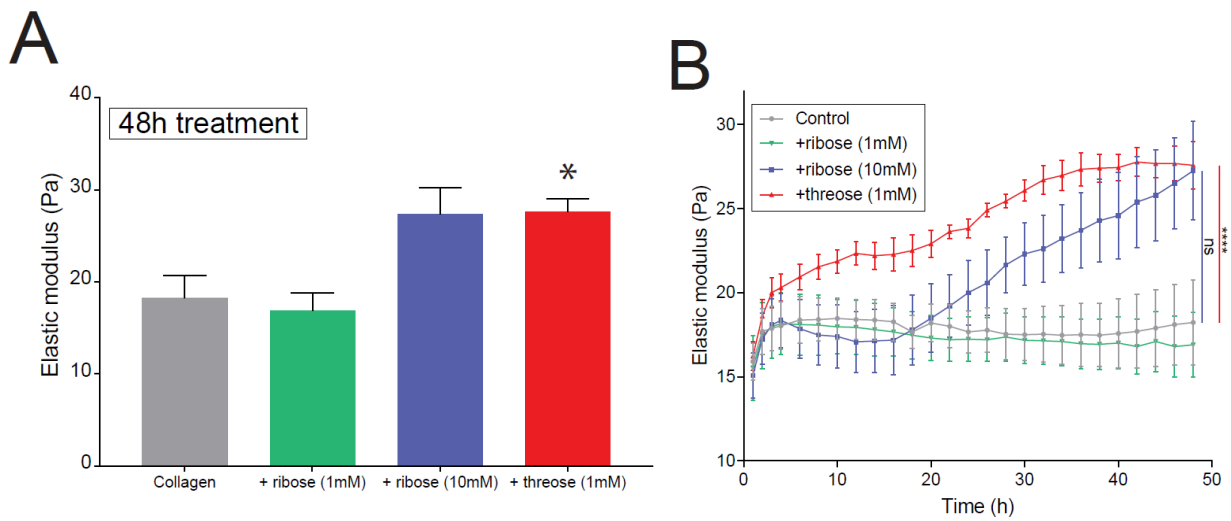


Figure 1 (part 1): Threose stiffens collagen more efficiently than ribose

(A) Elastic moduli obtained with small amplitude oscillatory rheology for untreated collagen gels, gels treated with 1 mM or 10 mM of ribose or with 1 mM threose, 48 hours after polymerization. Data represents an average over at least three independent measurements. p values are compared to control condition using Dunnett's multiple comparison test (*p<0.05, **p<0.01, ***p<0.001).

(B) Measurements of elastic moduli as a function of time over a period of 48h obtained with small amplitude oscillatory rheology on untreated collagen gels, gels treated with 1mM or 10mM of ribose, or with 1mM threose. Results are expressed as mean +/- SEM obtained as an average over at least three independent measurements. p values are compared to control condition using Dunnett's multiple comparison test (*p<0.05, **p<0.01, ***p<0.001).

Measurements of the mesh size of the networks by reflectance microscopy validated that the architecture of collagen networks was not affected by threose (Fig. 1C). This was confirmed by fluorescence microscopy imaging, although this yielded overall smaller mesh sizes than reflectance imaging because fluorescence microscopy, unlike reflectance imaging, visualizes also fibers orthogonal to the plane of imaging (Fig. 1C). Whether in control or threose-treated gels, mesh sizes similarly varied between 2 and 5 μ m, indicating that threose did not induce heterogeneous changes in ECM architecture (Fig.1D). Furthermore, we confirmed that the addition of threose did not affect fiber structure by using turbidimetry to compare fiber radii in the absence and presence of threose, which were respectively, 90 \pm 7 nm and 88 \pm 7 nm. Altogether, this characterization shows that a low concentration of threose is effective in changing the stiffness of collagen gels without altering network architecture.

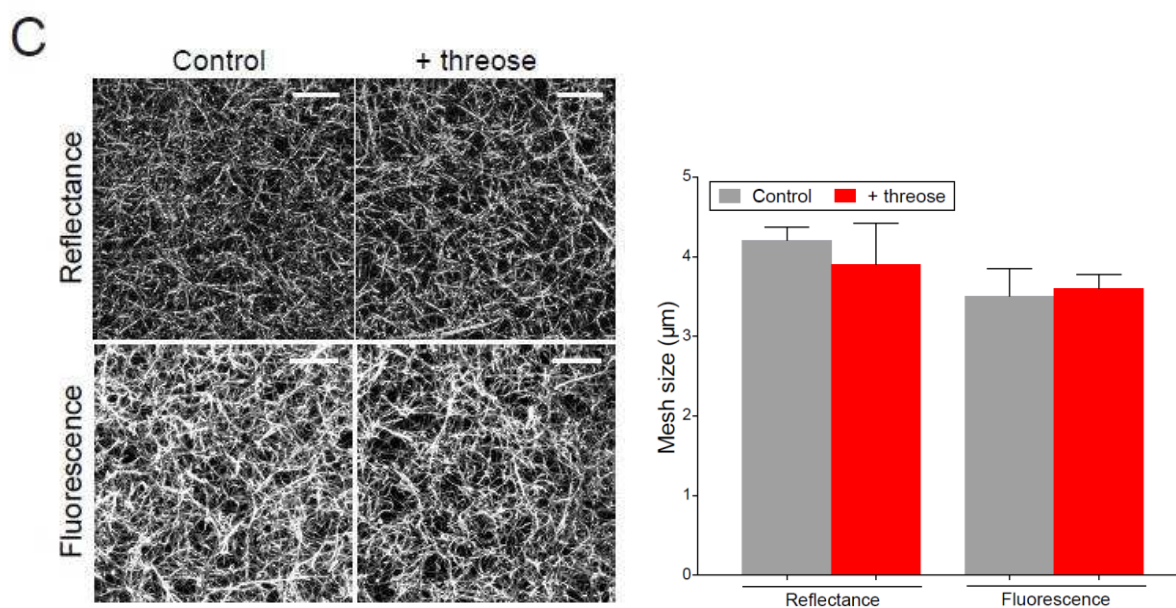


Figure 1 (part 2): Threose stiffens collagen more efficiently than ribose

(C) Left: Maximum intensity projections of reflectance and fluorescence images of collagen networks with or without 1mM of threose added during 48h. Scale bar = 10 μ m. Right: Mesh size measurements of collagen networks. Results are represented as a histogram with mean + SEM for n=8 positions over n=3 independent samples. p values were calculated using an unpaired t-test for each separate condition and showed no statistical difference. The mesh size measured with fluorescence microscopy is smaller because confocal reflectance does not allow for visualization of fibers perpendicular to the imaging plane.

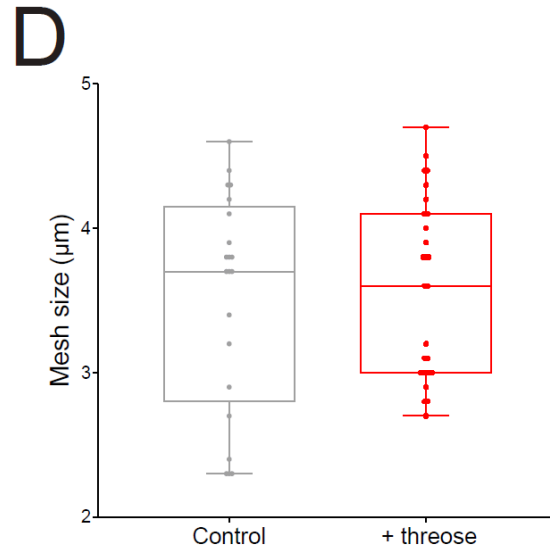


Figure 1 (part 3): Threose stiffens collagen more efficiently than ribose

(D) Mesh size distribution within collagen networks acquired by fluorescence. Results are represented as box and whiskers (minimum to maximum), where each point represents a different region within the matrix, with $n > 20$ positions over $n=3$ independent samples. p values were calculated using an unpaired t -test for each separate condition and showed no statistical difference.

Collagen stiffening before the onset of invasion inhibits cancer cell invasion

We first considered the influence of matrix stiffening at an early stage, when cancer cell invasion has not yet started. To model tumor invasion *in vitro*, we mixed spheroids of CT26 intestinal adenocarcinoma invasive cells with 2mg/mL collagen solutions. Once collagen polymerized, gels containing spheroids were incubated in 1mM of threose for a 24h or 48h treatment (Fig 2A – Thr_24h; Thr_48h). Invasion was quantified 3 days after embedding. The number of cells that invaded out of the spheroid was counted using a 3D automated software. This quantification method generates an invasion index which represents the number of invading cancer cells normalized to the surface area of the spheroid contour. Therefore, we only scored active cell migration and did not discriminate spheroids based on their size (Attieh et al., 2017).

Matrix stiffening before the onset of invasion dramatically inhibited cell invasion when collagen was treated with threose compared to control (Fig. 2B, C). Treating collagen with threose for an additional day did not further impede the invasion capacity of cancer cells, as it was already almost completely blocked upon a 24h treatment (Fig. 2B, C).

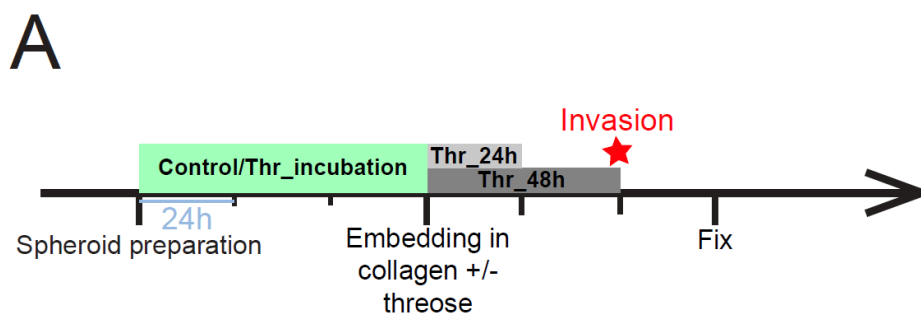


Figure 2 (part 1): Collagen stiffening before the onset of invasion inhibits cancer cell invasion

(A) Timeline representing the chronology of the experiment. Cancer cells were plated in agarose-coated wells for 3 days to form spheroids, in the absence (Control) or presence of threose (Thr_incubation). Spheroids were then embedded in collagen droplets with or without threose. Threose was washed out 24h (Thr_24h) and 48h (Thr_48h) later. All spheroids were fixed at day 3 post-embedding.

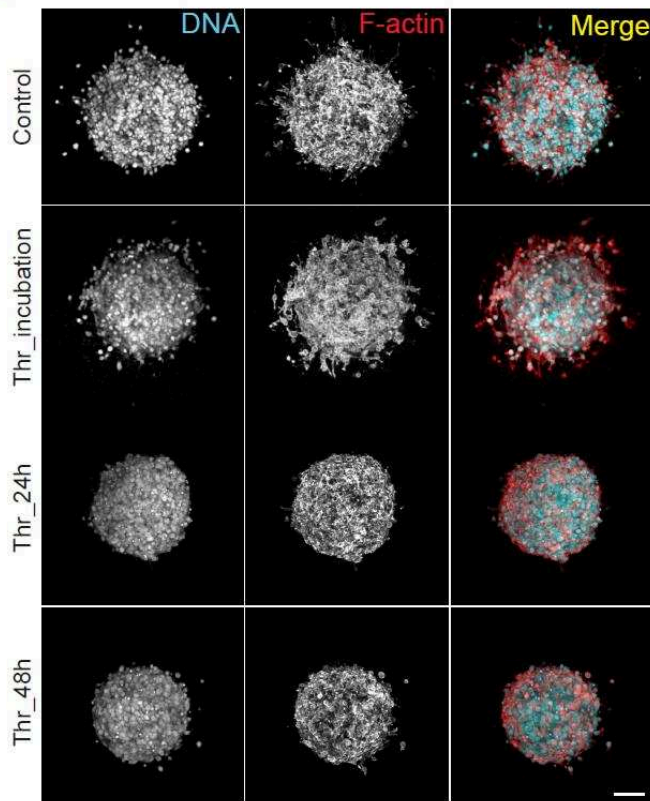
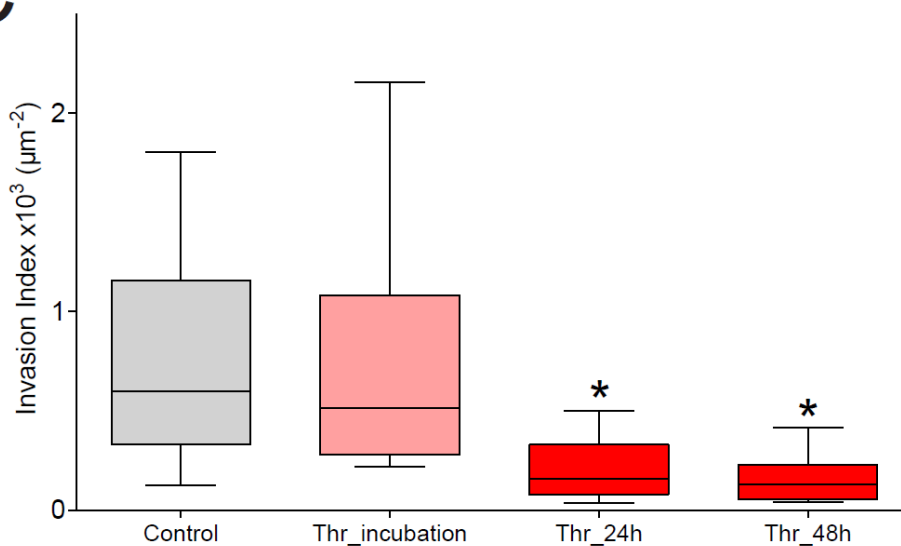
B

Figure 2 (part 2): Collagen stiffening before the onset of invasion inhibits cancer cell invasion

(B) Maximum intensity projections of cancer cell spheroids at day 3. F-actin (red) and DNA (cyan) were respectively stained with phalloidin-rhodamin and DAPI. Scale bar indicates 100 μ m.

(C) Quantification of cancer cell invasion. Invasion index is defined as the ratio between the number of invading nuclei of cancer cells and the area of the spheroid contour. Data are expressed as box and whiskers (minimum to maximum) of at least N=3 separate experiments. p values are compared to control condition using Newman-Keuls multiple comparison test (*p<0.05, **p<0.01, ***p<0.001).

C

Consistent with these findings, CT26 cancer cells invaded collagen gels with slower speed in the presence of threose when embedded as single cells (Fig. 2D). Cell persistence was similar in both conditions, indicating that it was the cells' capacity to move rather than the directional persistence of their movement that was compromised in a stiffer matrix (Fig. 2D).

D

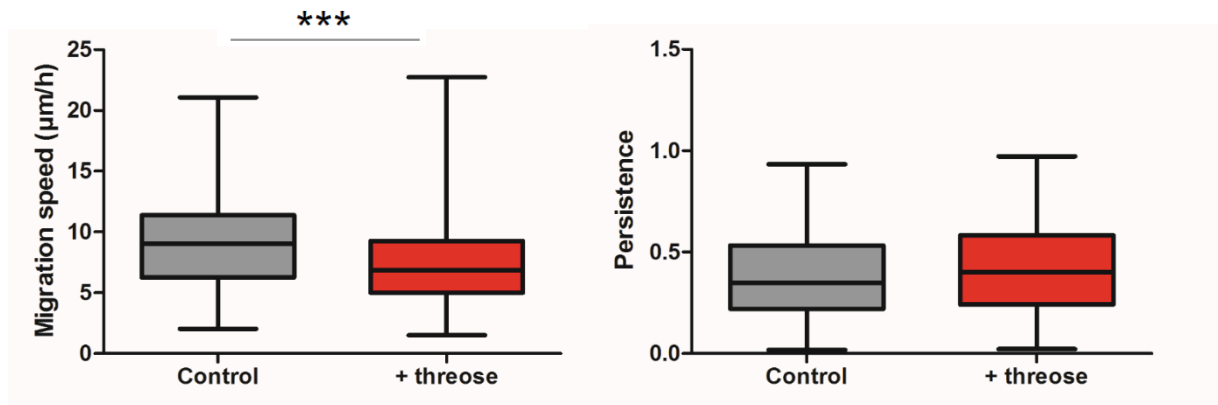


Figure 2 (part 3): Collagen stiffening before the onset of invasion inhibits cancer cell invasion

(D) Quantification of single cell invasion/migration in 3D collagen gels (up: speed; bottom: persistence) +/- 1mM of threose, after a 48h incubation in threose. Persistence was defined as the final cell displacement divided by the length of the trajectory. Results are represented as box and whiskers (minimum to maximum) where each point represents an individual cell. P-value was calculated using Mann-Whitney test for n = 107 cells for control and n = 105 cells for threose, over n = 3 separate experiments (*p<0.05, **p<0.01, ***p<0.001).

Inhibition of invasion could be due to an increase in matrix stiffness or to a direct effect of threose on cells. To check whether threose impeded the invasive phenotype of cells, CT26 were pre-incubated in 1mM threose for 3 days while spheroids were forming (Fig. 2A – Thr_incubation). Invasion was similar for pre-incubated and control spheroids, indicating that threose did not alter the invasive phenotype of cancer cells (Fig 2B, C).

We further verified whether threose could alter the molecular machinery driving cell migration by plating cancer cells on glass as an inert substrate that cannot be glycosylated, and treated with increasing concentrations of threose (Fig. 2E). Cells migrated with equivalent speed and persistence regardless of threose concentration, suggesting that threose did not affect the migratory phenotype of cancer cells.

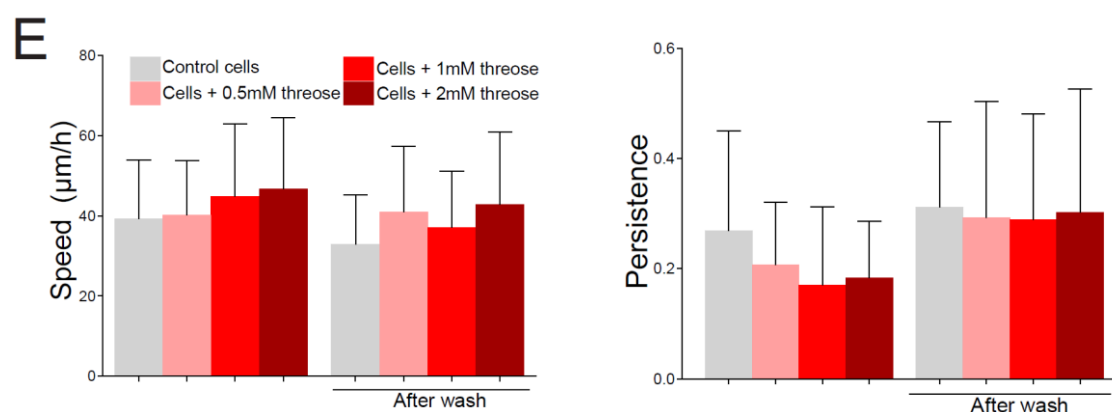


Figure 2 (part 4): Collagen stiffening before the onset of invasion inhibits cancer cell invasion

(E) Quantification of migration speed and persistence of CT26 cancer cells with increasing concentrations of threose treatment plated on glass. Measurements were performed during threose treatment and after wash. Results are represented as a histogram with mean + SD for 3 independent experiments. p values were calculated using Newman-Keuls multiple comparison test and showed no statistical difference.

Alternatively, threose could decrease adhesion of cells to collagen. We tested the latter hypothesis by plating cells on 2D collagen matrices for increment time-points and measuring the percentage of adhered cells after wash (Fig. 2F). We found that cell adhesion was unaffected whether collagen (Coll_thr), cells (Cells_Thr) or both (Cells_Thr + Coll_Thr) were treated with threose compared to control, suggesting that threose did neither modify collagen adhesion sites nor the adhesion capacity of cancer cells (Fig 2F). We thus concluded that the inhibition of invasion at an early stage was only due to matrix stiffening.

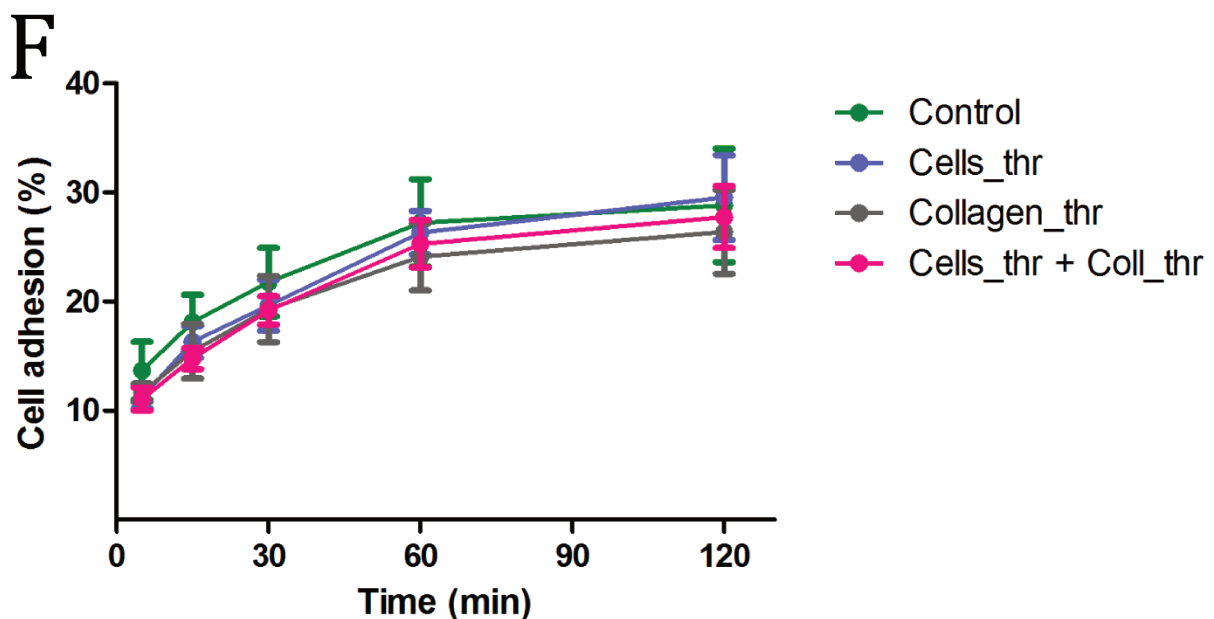


Figure 2 (part 5): Collagen stiffening before the onset of invasion inhibits cancer cell invasion

(F) Quantification of the capacity of control cells to adhere to collagen (control, green) or to threose-treated collagen (Collagen_thr, gray), and of threose-treated cells to adhere to control collagen (Cells_thr, blue) or to threose-treated collagen (Cells_thr + coll_thr, pink). Measurements were performed at 0, 15min, 30min, 1h and 2h. Results are expressed as an XY coordinate with mean +/- SD with data representing an average over three independent measurements. p values are compared to control condition using Dunnett's multiple comparison test and showed no statistical difference.

Collagen stiffening before the onset of invasion prevents fiber alignment by cancer cells

Previous reports have shown that prior to invasion, cancer cells contract and align collagen fibers in the direction of their movement (Provenzano *et al.*, 2008; Riching *et al.*, 2015; Kopanska *et al.*, 2016). Once collagen is aligned, cancer cells migrate in a fast and persistent manner promoting tumor spreading (Riching *et al.*, 2015). In *in vitro* models, collagen fibers are initially aligned parallel to the edge of the tumor (Kopanska *et al.*, 2016). To evaluate if cells remodeled the matrix, we imaged collagen I fibers surrounding spheroids 3 days post-polymerization and quantified fiber orientation of control and threose-treated gels. Imaging of collagen I revealed that non-crosslinked collagen fibers were not parallel to the edge of the tumor and were randomly organized, while fiber alignment parallel to the spheroid was maintained in threose treated samples (Fig. 3A). This observation was validated by the quantification of the orientation of collagen fibers with respect to the spheroid edge (Fig. 3B). In threose treated collagen gels, fibers were mainly parallel to the spheroid, whereas this tendency was less pronounced in control matrices as the proportion of fibers oriented between 0 and 30° was 20% lower (Fig 3B). We thus concluded that 3 days after spheroid embedding, cells started remodeling collagen fibers in control gels but not in threose-treated samples.

Impaired matrix remodeling observed in threose-treated hydrogels could be either due to a stiffer matrix or to a direct effect of threose on cell mechanisms regulating contractile forces. To test the latter hypothesis, we performed traction force microscopy on cells plated on polyacrylamide gels containing fluorescent beads. Both control and threose-treated cells exerted comparable traction forces, indicating that threose does not affect traction force generation and that matrix stiffening alone prevented matrix remodeling (Fig. 3C). Altogether these results suggest that matrix remodeling is necessary for cancer cells to migrate out of the spheroid and that a stiffer matrix inhibits this process.

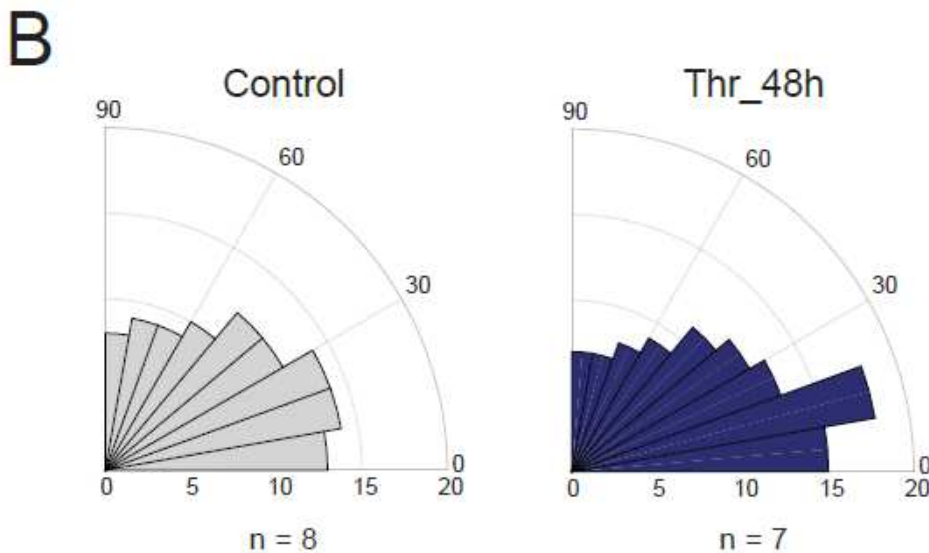
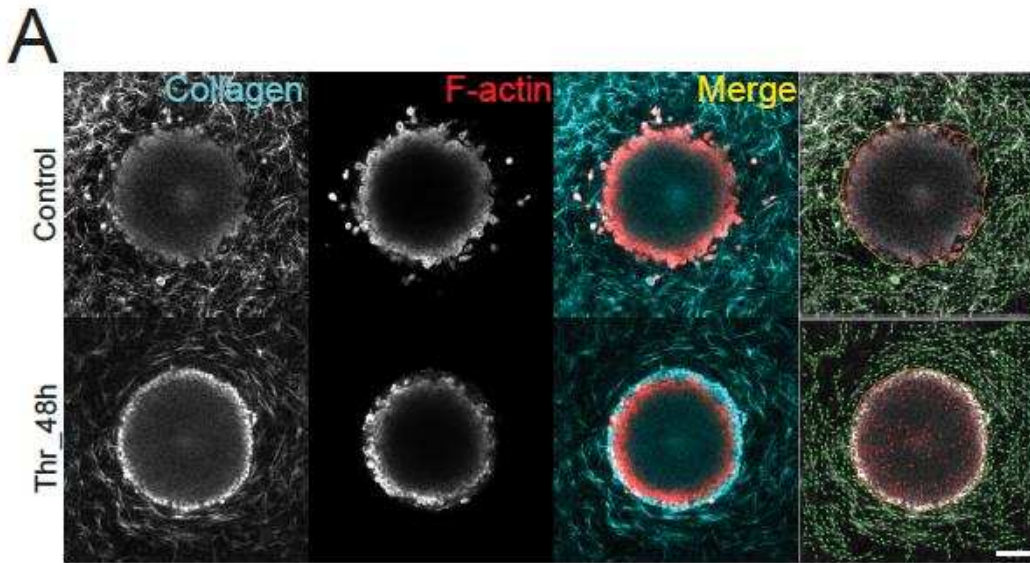


Figure 3 (part 1): Collagen stiffening before the onset of invasion prevents fiber alignment by cancer cells

(A) 2D slices of cancer cell spheroids in collagen I at day 3. F-actin (red) was stained with phalloidin-rhodamine and collagen was imaged using reflectance (cyan). Right panel: overlaid images of collagen I matrices containing cancer cell spheroids generated using the software CurveAlign (UW-Madison; <http://loci.wisc.edu/software/curvealign>). Yellow line indicates the edge of the spheroid and green lines indicate fibers orientation with respect to the closest point on the spheroid edge. Scale bar = 100 μ m.

(B) Rose plots representing the frequency of distribution of the absolute angles of collagen fibers within the range of 0 to 90° with respect to the closest point on the spheroid edge. Data represent the average of 7 < n < 8 spheroids. Fibers parallel to the tumor edge lie in the 0-30° angles.

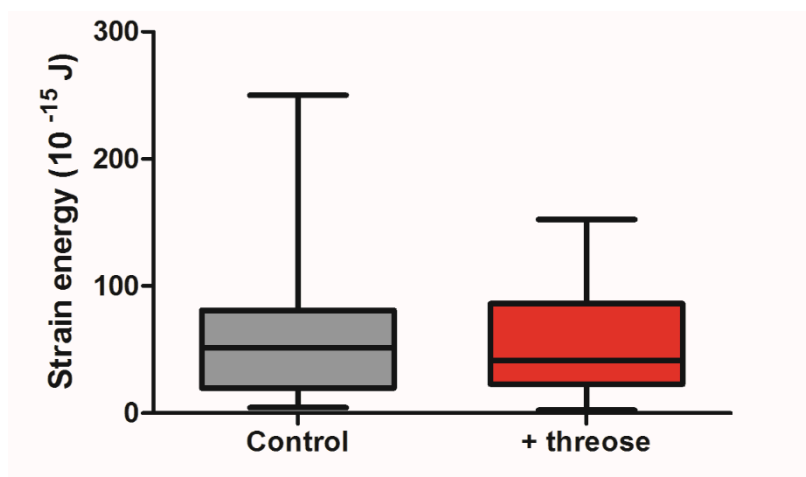
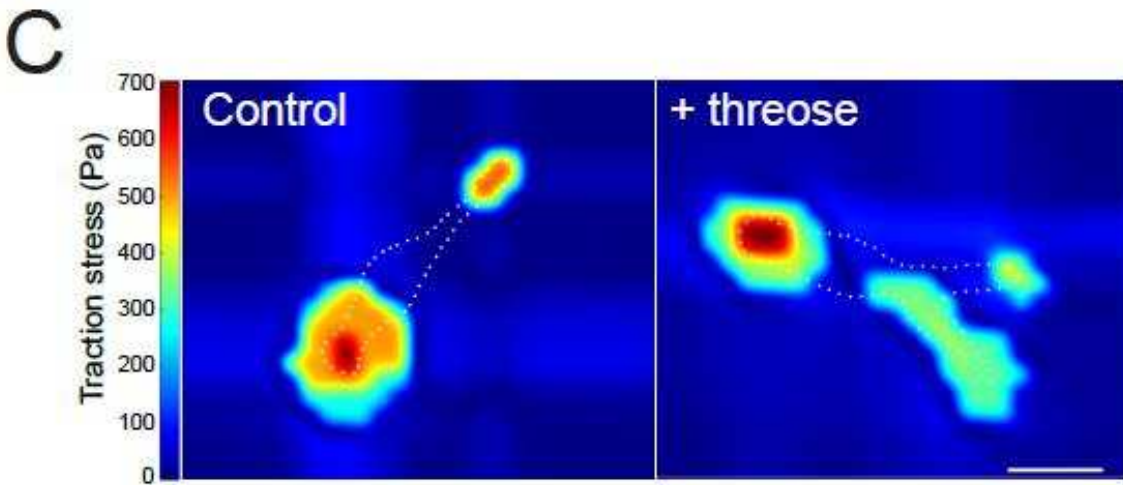


Figure 3 (part 2): Collagen stiffening before the onset of invasion prevents fiber alignment by cancer cells

(C) Up: Representative traction force map of a control and a threose-treated cell on collagen-coated polyacrylamide gels with Young's modulus of 5 kPa. White dotted line represents the cell's edge. Color code gives the magnitude of traction stress in Pa, which corresponds to forces of ($\text{pN}/\mu\text{m}^2$). Scale bar = $20\mu\text{m}$. Down: Corresponding mean force (strain energy) exerted by CT26 cancer cells. Results are represented as box and whiskers (minimum to maximum) where each point represents an individual cell. P-value was calculated using Mann-Whitney test for $n = 27$ cells for control and $n = 25$ cells for threose, over 3 independent experiments and showed no statistical difference.

Collagen stiffening after the onset of invasion favors cancer cell invasion

The reduced invasion we observed in a stiffer environment is surprising, as aggressive tumors are typically characterized by high tissue rigidity. However, it is still not known whether the matrix gets stiffer before or after cancer cell invasion (Attieh and Vignjevic, 2016). Matrix stiffening after the onset of invasion might favor cell invasion, as the critical step of matrix remodeling and fiber alignment is then already complete. To test this hypothesis, we embedded spheroids in collagen and monitored how the invasion rate would change when threose was added after invasion started (i.e. from day 3 to day 5 after embedding spheroids in collagen) (Fig. 4A – Thr_d3d5). Stiffening after the onset of invasion was compared to early stiffening (Thr_d0d2) and control. Experiments were extended to 7 days after embedding spheroids in collagen in order to allow for cells to properly invade out of the spheroid. Similarly to the shorter-term experiments, pre-incubating cancer cells in threose (Fig. 4A - Thr_incubation) did not affect their invasion index compared to control, confirming that threose at a concentration of 1mM does not alter cancer cells' invasive phenotype even at longer times (Fig. 4B, C).

Surprisingly, cancer cell invasion was increased 2-fold when the matrix was stiffened after the onset of invasion compared to control (Fig.4B, C – Thr_d3d5). Moreover, we observed that the decrease of cell invasion observed at day 3 upon threose treatment, before the onset of invasion (Fig. 2B, C), vanished when cancer cells were examined at day 7 (Fig.4B, C – Thr_d0d2): cells showed the same final invasion state as cells invading control gels after 7 days of culture in collagen droplets. This observation indicates that, although matrix stiffening slows down the initiation stage, it enhances cell migration once cells invade the matrix. Given that threose does not interfere with the autonomous migratory phenotype of cancer cells (Fig. 2E), we concluded that matrix stiffening enhances cell migration, resulting in extensive invasion at later stages of tumor development.

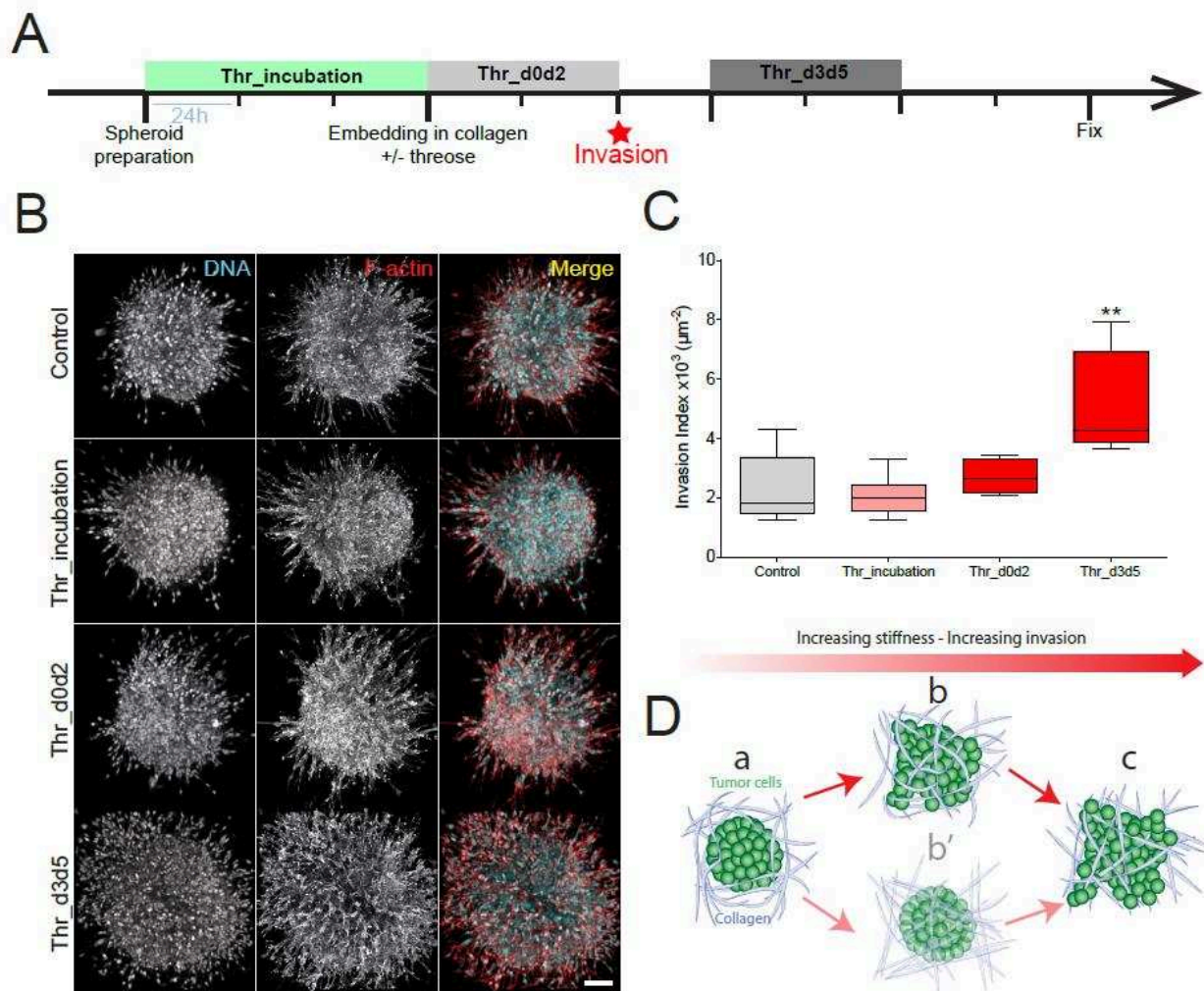


Figure 4: Collagen stiffening after the onset of invasion favors cancer cell invasion

(A) Timeline representing the chronology of the experiment. Cancer cell spheroids were left to form in agarose-coated wells for 3 days, with (Thr_incubation) or without threose (Control). Spheroids were then embedded in collagen droplets with (Thr_d0d2) or without (Control) threose for 48hours. 3 days post-embedding, threose was added in the media for 48h (Thr_d3d5). All spheroids were fixed at day 7 post-embedding.

(B) Maximum intensity projections of cancer cell spheroids at day 7. F-actin (red) and DNA (cyan) were respectively stained with phalloidin-rhodamin and DAPI. Scale bar indicates 100 μm.

(C) Quantification of cancer cell invasion. Invasion index is defined as the ratio between the number of invading nuclei of cancer cells and the area of the spheroid contour. Quantification results are expressed as box and whiskers (minimum to maximum) of N=3 separate experiments. p values are compared to control condition using Newman-Keuls multiple comparison test (*p<0.05, **p<0.01, ***p<0.001).

(D) Model: tumor cells are surrounded by the ECM (a). Cancer cells start invading the ECM before the matrix gets remodeled (b) rather than the matrix being remodeled beforehand (b'). As cancer cells invade the matrix, collagen fibers get aligned, which sets up positive feedback to enhance invasion.

Altogether, these experiments highlight the importance of the chronology of events in cancer cell invasion. Depending on the stage of the tumor, the changes in the mechanical properties of its microenvironment could differentially influence its aggressiveness. Matrix stiffening before invasion is initiated could slow down the transition from non-invasive to invasive tumor stage. On the contrary, stiffening of the matrix after the onset of tumor invasion could intensify tumor invasion. We propose here a model where, within the chronology of cancer development, cancer cells first migrate out of the tumor site, then stiffening of the matrix occurs (Fig. 4D).

We have thus uncovered a novel model of tumor invasion by effectively modulating matrix stiffness in time without altering cancer cells' autonomous phenotype. We have developed a physiological tumor model composed of spheroids embedded in 3D collagen matrices and selected a natural crosslinker to stiffen collagen. This *in vitro* model allowed us to directly test the correlation between matrix stiffness and tumor aggressiveness observed in patients (Cox and Epler, 2011; Pickup, Mouw and Weaver, 2014; Acerbi *et al.*, 2015).

As opposed to other crosslinkers commonly used in the field, threose presents the advantage of effectively stiffening collagen at low concentrations. As proven by our experiments, a strong advantage of using threose is that it does not induce changes in the collagen network architecture in terms of mesh size and fibril diameter, while being effective in changing the stiffness of the matrix. This increase in stiffness is most likely due to a stabilization and an increase in crosslinking of already existing contact points.

Using threose at low concentrations allowed us to modify matrix stiffness while tumor cells were embedded in their physiological 3D matrix, as opposed to studies exposing cancer cells to previously treated and already stiff gels, or collagen gels of varying densities that cannot be modulated in time (Paszek and Weaver, 2004; Provenzano *et al.*, 2008; Levental *et al.*, 2009; Krndija *et al.*, 2010). We were thus able to control the temporal onset of matrix stiffening. Although we worked at lower collagen concentration and thereby at lower stiffness than analogous studies using ribose, cells were highly responsive suggesting that cells could be more sensitive to relative changes in matrix rigidity than to its intrinsic value (Bordeleau *et al.*, 2017; Carey, Martin and Reinhart-King, 2017). At an early stage of invasion, cells first remodel the matrix to effectively migrate out of the tumor niche. Contractile forces of cancer cells are required to deform the ECM

and lead to tensile radial forces on the matrix that orient the collagen fibers perpendicular to the surface of the tumor (Provenzano *et al.*, 2008; Riching *et al.*, 2015; Kopanska *et al.*, 2016). As there is a mechanical relation between the tensile state of the ECM and invasion, collagen organization at the onset of invasion could play a critical role towards the outcome of tumor development. Our results support this hypothesis as threose-treated matrices are stiffer and therefore more difficult to remodel than control matrices. This is evidenced by the high proportion of collagen fibers oriented parallel to the edge of the tumor 3 days after embedding and the consequent inhibition of cancer cell invasion. Stiffer matrices are also known to favor a migratory phenotype in cancer cells (Paszek and Weaver, 2004; Levental *et al.*, 2009). This biomechanical process is consistent with the cell response observed when we added threose after the onset of invasion, which led to a two-fold increase in invasion. This antagonistic influence of matrix stiffening in the early and late stages of invasion is clearly illustrated by the behavior of cancer cells when collagen is exposed to threose in the early stage: although the transition from non-invasive to invasive phenotype is delayed compared to control, once invasion is initiated, migration is enhanced as cancer cells catch up with control conditions within 4 days of invasion. As CT26 are invasive cancer cells with a mesenchymal-like phenotype, this result is consistent with new findings suggesting that only malignant cancer cells have the ability to adjust to collagen matrices of different densities (Wullkopf *et al.*, 2018).

In conclusion, our *in vitro* 3D culture model provides a physiologically relevant microenvironment to study the effect of matrix stiffness per se on the transition from benign to malignant tumor. We report here the first data on *in vitro* collagen crosslinking using threose, which allows to significantly stiffen collagen matrices without interfering with the phenotype of cancer cells. Furthermore, this study highlights the need to introduce a fourth dimension into cell biological models. Indeed, a static assay where all factors are initially set and remain unchanged could fail to capture the complexity of cancer invasion. The flexibility of our system allowed us to tackle the question of the dynamics of matrix stiffening during tumorigenesis. Our study illustrates that within the chronology of tumor development, neither matrix stiffening nor softening are the most favorable, but rather an interchanging state that is used by cancer cells to efficiently invade.

PART 3. INVASION OF THE BASEMENT MEMBRANE BY CANCER TUMOROIDS

Tumoroids invade the Basement membrane either as single cells or collective clusters

Foreword

The use of physiological 3D models to model disease progression has been increasingly developed in the last decade. Tumor cell behaviors can be modeled by the use of tumor organoids, or tumoroids, that represent primary cultures of 3D mini-tumors in a dish. Tumoroids can be isolated from mouse tumors and grown *in vitro* in Matrigel. I used tumoroids isolated of NICD/p53/Tom tumors in order to study the first steps of carcinoma invasion, that is the breaching of the basement membrane.

The mouse mesentery as a model for native basement membrane

Mouse mesentery has been previously used by my PhD lab and others as a model system to study basement membrane invasion by cancer cells (Hotary *et al.*, 2006; Rowe and Weiss, 2008; Schoumacher *et al.*, 2010, 2013; Schoumacher, Louvard and Vignjevic, 2011). The mesentery is a peritoneal folding that connects the intestine to the posterior abdominal wall, maintaining the intestines in place. It also serves as a conduit for blood and lymphatic vessels that irrigate the intestine and colon (www.embryology.ch). The mesentery consists of two layers of peritoneum with a fibrillar collagen matrix in between, where fibroblasts, immune cells, nerves, blood vessels and lymphatics are located (Figure 1). The mesentery is covered on its both sides by a monolayer of flat squamous epithelial cells called mesothelial cells (Mutsaers, 2002), which sit on a basement membrane, as shown in Figure 1B). The mesentery is therefore composed of two BMs, one on top of the other (Witz *et al.*, 2001). The BMs are mainly composed of networks of laminin, collagen IV, perlecan (Figure 1C) and nidogen.

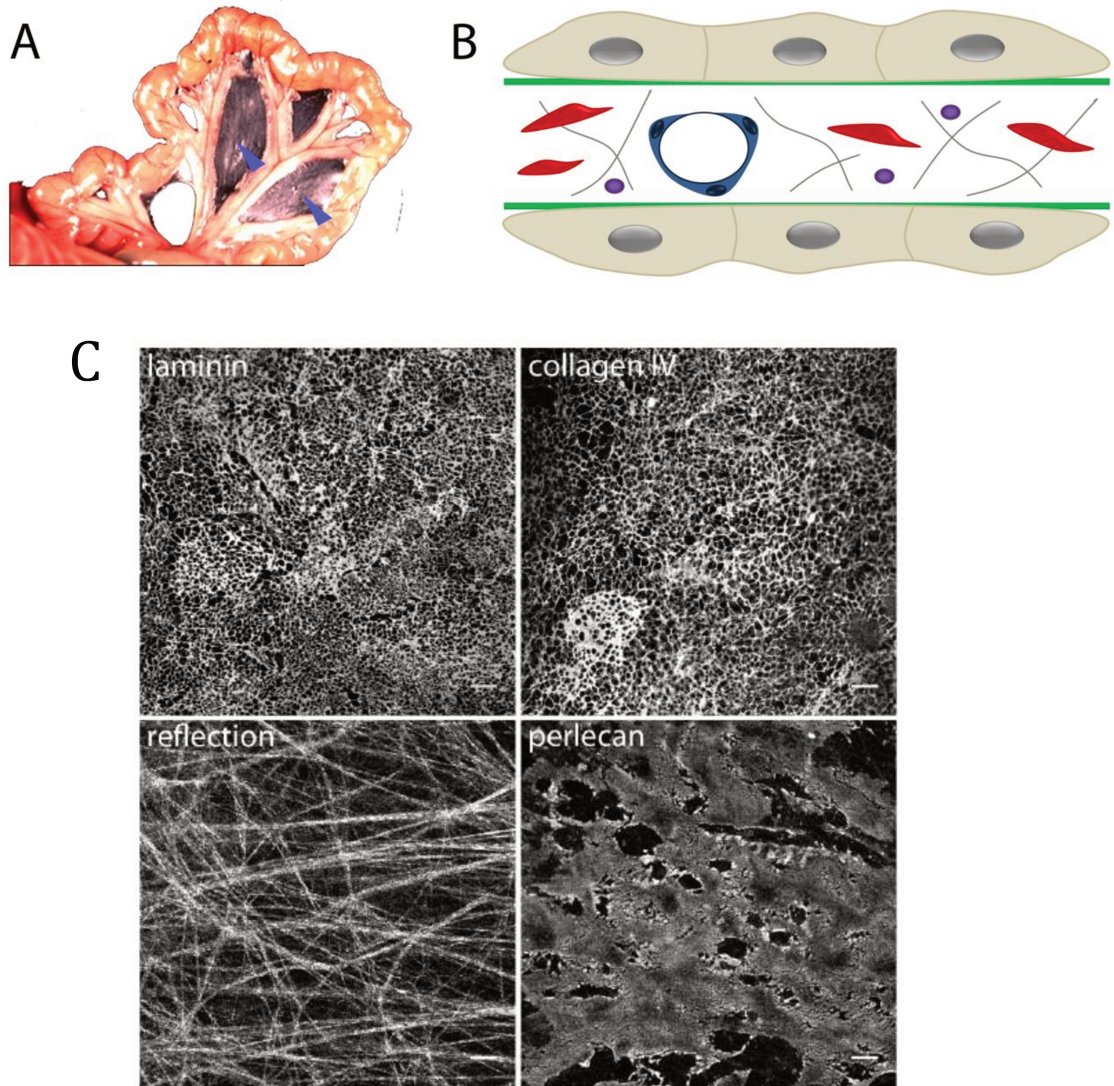


Figure 1. Mesentery localization and structure.

A. Mouse intestine with its mesentery (blue arrowheads), a thin gelatinous membrane.

B. Scheme of the mesentery, viewed from the side. The mesentery is composed of two mesothelial cell layers (gray), sitting on a basement membrane each (green). Between the basement membranes, there is extracellular matrix (gray fibers) containing fibroblasts (red), immune cells (violet) and vessels (blue).

C. ECM components of the mouse mesentery BM revealed by immunofluorescence. The fibrillar network of the different collagens is revealed by reflection microscopy. Scale bar, 20 μ m. From Glentis et al, 2017

The ultrastructure of the mesenteric BM, as revealed by scanning electron microscopy, consists of a complex network of interconnected fibers of different thicknesses. Bundles are also present, whose size varies from few to hundreds of filaments, forming a network composed of big “cables” interconnected by single filaments. Interestingly, the structure of ECM can vary from mouse to mouse and even from area to area within the same mesentery. In some areas, the fibers have approximately the same size (Figure 3, top), while in others they were organized into big bundles forming “highways” within the membrane (Figure 3, bottom). A general feature of the mesenteric BM is that it is organized in a tight network with a very small pore size that doesn’t exceed 1 μ m in diameter. This suggests that cancer cells need to degrade or drastically remodel the ECM in order to invade, as the pores are too small for the cell to squeeze through. Based on its organization and molecular composition, we decided to use mouse mesentery as a model system to study invasion of cancer cells.

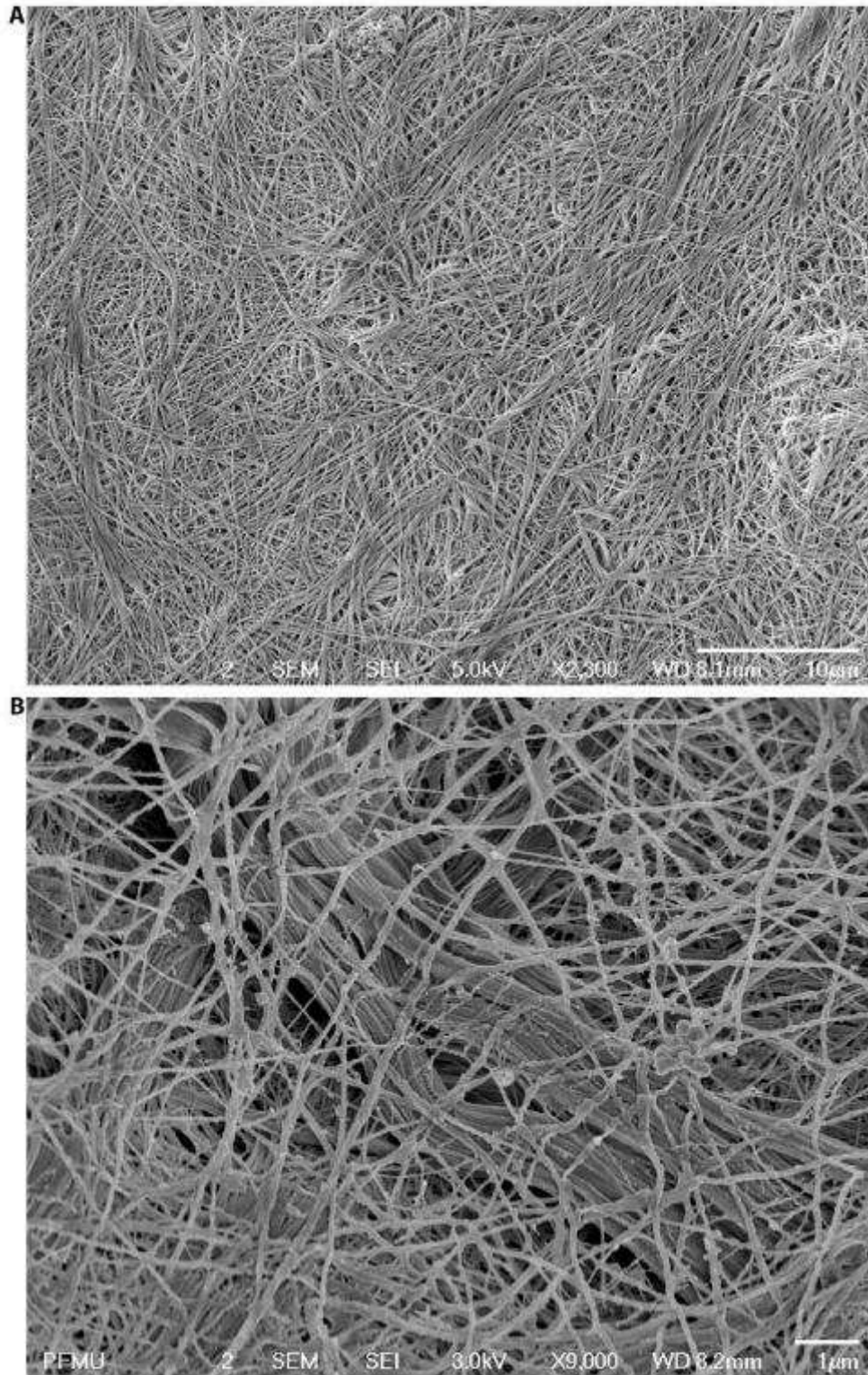


Figure 2. Ultrastructural organization of the ECM of mouse mesentery

Two examples of the ECM of mouse mesentery revealed by scanning electron microscopy after chemical removal of resident cells. Courtesy of Alexandre Glentis

In order to study the first steps of basement membrane invasion, I developed a 3D invasion assay of tumoroids seeded on a native mesentery. In order to study the interactions between cancer cells and the ECM, I decellularised the mesentery using a chemical treatment which removed mesothelial cells, fibroblasts and immune cells, leaving the ECM structure intact. I isolated tumoroids from spontaneously developed intestinal tumors due to expression of a constitutively active Notch oncogene and deletion of p53. These mice also expressed a membrane Tomato. In NICD/p53/Tom tumoroids, cancer cells display a green nucleus and red cell membrane. For the invasion assay, tumoroids are deposited on top of the mesentery isolated from a wild-type mouse.

Using two-photon live cell microscopy, I observed that tumoroids invade the mesentery using two distinct invasion modes, either collective or, more frequently, as single cells.

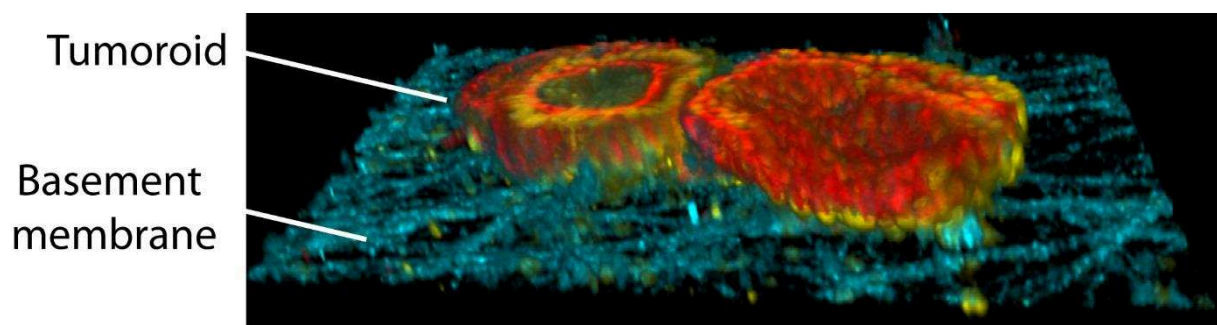


Figure 3. Tumoroids deposited on the mesenteric basement membrane.

F-actin (phalloidin, red), DNA (DAPI, yellow), ECM (reflection, cyan).

Single cell invasion of the mesentery

The single cell invasion mode is accompanied by the formation of a hole in the mesentery (Figure 5, A, arrowhead). The diameter of the hole is approximatively the size of the cell, 20 μ m in the shown example. Interestingly, the formation of the hole and cell invasion can happen relatively fast, in two to three hours. Three time points of the widening of the hole are shown in Figure 5, B. In the depicted kymograph, we first detect signal coming from the cell membrane (red), probably due to membrane protrusions, concomitant to the

mesentery breaching (Figure 5, C). Then the hole enlarges relatively rapidly in 2.5 hours, followed by passing of the nucleus (green).

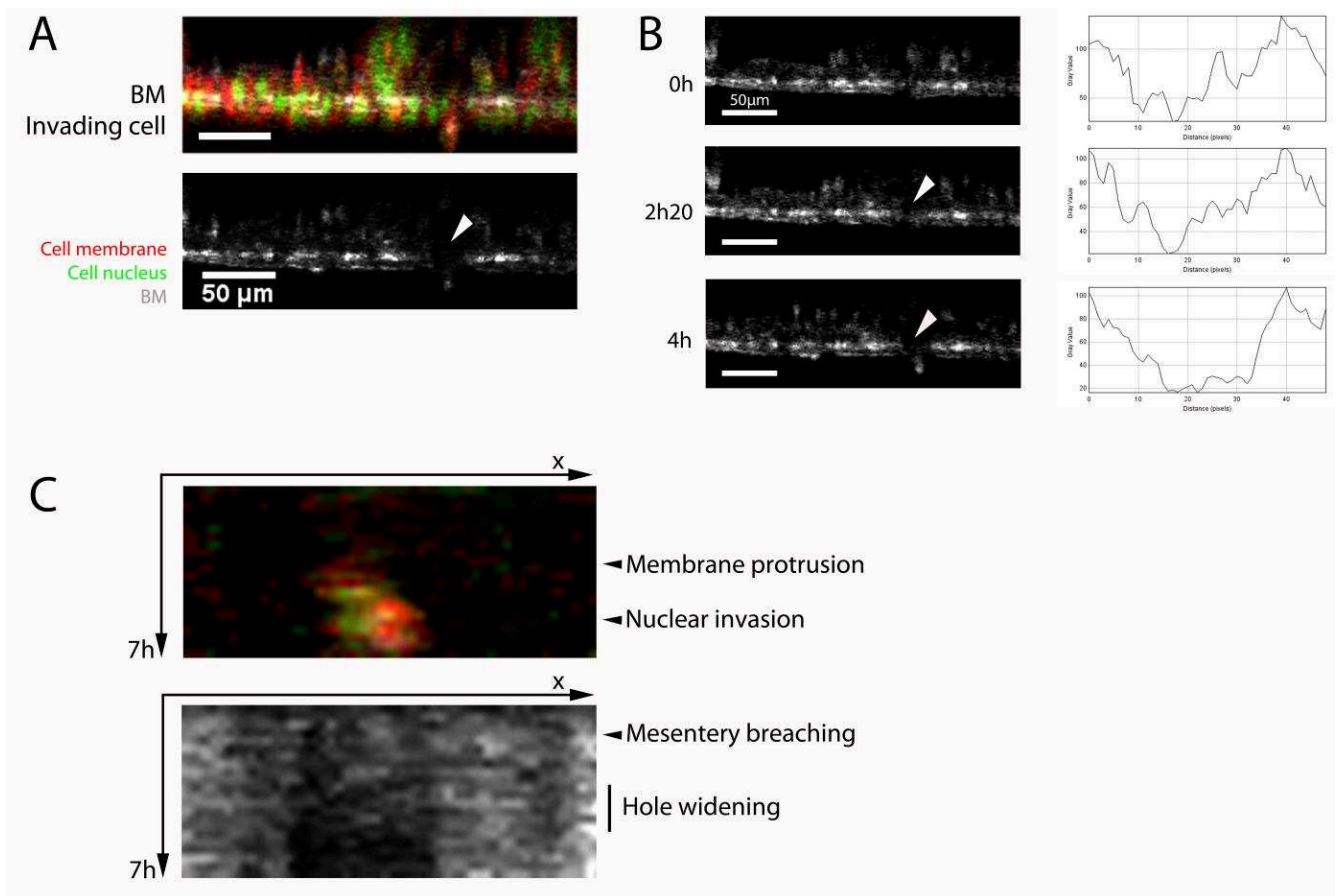


Figure 4. Single cell invasion of the mesentery *in vitro*.

A. XZ view of the invasion assay showing the mesentery separating an upper side where the tumoroids are seeded, and a lower region where invasion occurs. The arrowhead points to a hole created upon invasion. Cell membranes (Tomato, red), cell nuclei (green), mesentery (reflection, white). Scale bars, 50 μm .

B. Left: time-course of the hole widening. Right: Intensity profiles over a linescan encompassing the hole and adjacent regions. Scale bars, 50 μm .

C. Kymographs of cell invasion and hole widening, showing first membrane protrusions, concomitant to breaching of the mesentery. Nuclear invasion is simultaneous to the widening of the hole.

Collective invasion of the mesentery

When invading collectively, cancer cells get accumulated between the two BM layers (Figure 6, A, upper panel). One or several holes, with an average size of $17\mu\text{m}$, can be seen on the upper BM layer (Figure 6, B, arrowheads), whereas the lower layer appears bended (Figure 6, A, lower panel). Thus, we speculate that cells breach the first BM, get in the space between the two BMs, and exert a pressure on the second BM layer, making it bend.

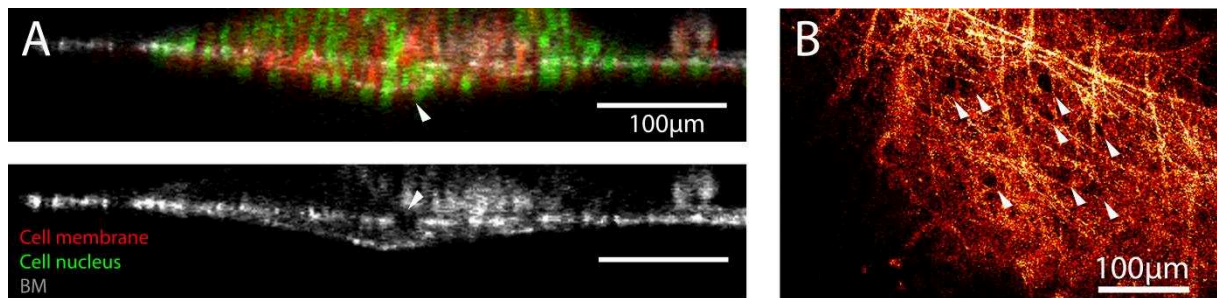


Figure 5. Collective invasion of the mesentery *in vitro*.

A. XZ view of the *in vitro* assay showing collective invasion of the mesentery. Arrowheads point to the bending of the mesentery (upper panel), and to a hole in the first basement membrane layer (lower panel). Cell membranes (Tomato, red), cell nuclei (green), mesentery (reflection, white). Scale bars, $100\mu\text{m}$.

B. Single slice of a z-stack showing several holes on the first basement membrane layer of the mesentery. Arrowheads point to the larger holes. Scale bar, $100\mu\text{m}$.

Conclusion and discussion on the 3D invasion assay of the mesentery

The study of invasion of cancer tumoroids on the native mesentery shows that NICD/p53/Tom tumoroids have the intrinsic capacity to breach the basement membrane, confirming the invasive nature of these cells. The capacity to invade BM *in vitro* lines up with the high aggressiveness and invasiveness of the NICD/p53 tumor model. Interestingly, all cancer cell lines do not have the capacity to breach the mesenteric BM. For example, human colon carcinoma HT29 cells are not able to invade native BM, even stimulated by 20% serum and by the presence of CAFs (Schoumacher *et al.*, 2010; Glentis *et al.*, 2017). On the contrary, the human colon cancer cell line HCT116 is able to invade the native BM when stimulated by serum, and to a greater extent upon CAFs presence. Therefore, BM invasion assay could serve as a test for the invasiveness of cancer cell lines. Another application of this assay, could be to study the interaction of cancer cells with other cell types that could stimulate the invasion of cancer cells, such as CAFs (Glentis *et al.*, 2017) or immune cells.

The observed modifications of the BM upon cancer cell invasion, namely formation of holes in the BM and physical displacement of the BM in the case of collective invasion suggests that the BM could be breached either in a proteolysis-dependent manner, or in a force dependent manner. Indeed, collective clusters of tumoroids cells seem to exert a pushing force on the BM that might favor its breaching.

The mouse mesentery tissue is native and harbors all the complexity of *in vivo* basement membranes, in terms of composition, network architecture, and pore size. Therefore, mesentery invasion assays are physiological *in vitro* assays for mimicking the transition between the carcinoma *in situ* and invasive carcinoma stages. Interestingly, the architecture, composition and pore size of stromal ECM differ from those of the basement membranes, therefore cells could possibly use different strategies when invading one or the other of these matrices.

The mesenteric BM is a versatile tool to study the interaction of cells with a complex and physiological ECM environment. The possibility to extract the BM from the mouse and to use it in an *in vitro* setting allows for easy tuning of the parameters of the experiment, such as the presence of different cell types and growth factors, or even chemical modifications of the BM structure or stiffness.

The versatility of the mouse mesenteric BM has allowed my collaborators to use it as a model for interaction between endothelial cells and a physiological ECM. Indeed, Arthur-Charles Orszag et al have shown that the endothelial cell membrane is able to form nanoscale protrusions that align on nanoscale fibers of the BM through a mechanism of 1D membrane wetting (Figure 7). The manuscript is provided in the Annexes.

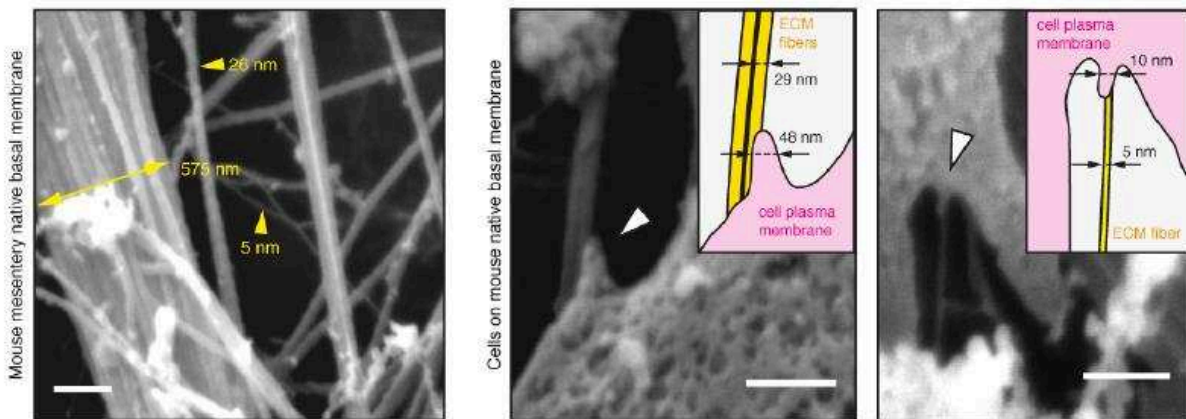


Figure 6. Mesenteric BM is a versatile tool for the study of cell-ECM interactions

Left: Scanning electron microscopy shows that native basal membranes from mouse mesentery feature fibers with diameters down to 5 nm. Scale bar, 250 nm.

Middle and right: Endothelial cells cultured on such extracellular matrices show nanoscale plasma membrane protrusions aligning on nanoscale fibers. Scale bars, 250 and 200 nm.

PART 4. INTRAVITAL IMAGING OF CANCER CELLS IN INTESTINAL TUMORS

Intravital imaging of cancer cells in intestinal tumors in mice

Imaging of tumor explants allowed us to describe properties of cancer migration in deep regions of the tumors inaccessible to intravital imaging. However, explanted tissues lack some features of the native cancer microenvironment, such as perfused blood vessels, that have been proposed as a source of chemoattractants for cancer cells. We have therefore decided to use intravital imaging in order to observe intestinal tumors in their native setting, the living mouse.

Intravital imaging in the mouse intestine requires the use of an abdominal optical window that allows imaging of cancer cells in the living mouse with cellular resolution using two-photon microscopy. The major advantage of this approach is the possibility to image cells in the living animal with intact vasculature and to have a broader time frame for imaging (several days versus several hours *ex vivo*). I visited Jacco van Rheenen's lab to learn how to install a ventral optical window for intravital imaging of the mouse intestine. I succeeded in surgically installing the imaging window and in monitoring the health of the mouse over the time of imaging (pulse, T° , anesthesia levels and perfusion). Figure 1 shows three optical slices at three different depths in the intestinal tissue of a WT mouse expressing (p villin-Cre mTom/mGFP Flox). In this mouse, all cells express membrane Tomato, and some intestinal epithelial cells express a membrane GFP in a mosaic way. Using intravital imaging of intact small intestine, I first accessed the muscle layer surrounding the intestine, then the stromal tissue, followed by the intestinal crypts and the intestinal villi. Because the villi are located deep when accessing the tissue from the muscle layer, we can only access approximately the first third of the villi (Figure 1)

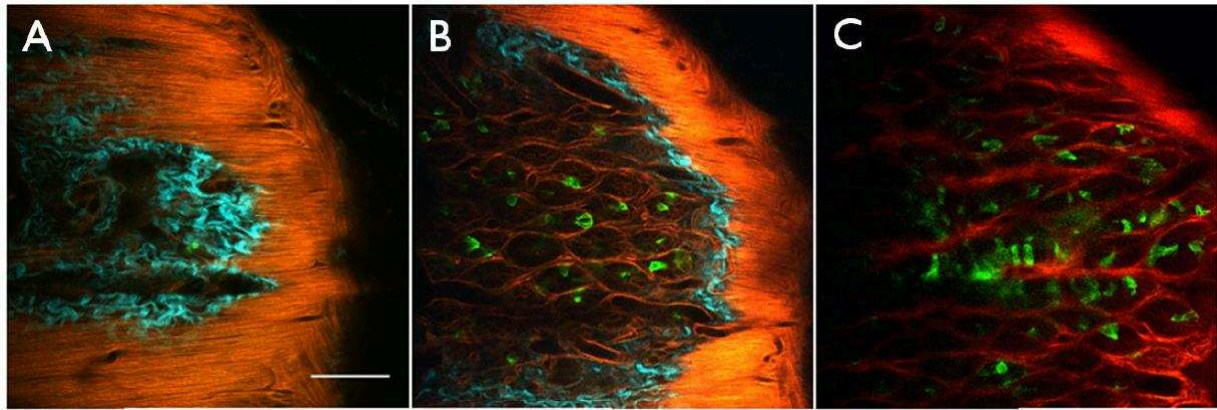


Figure 1. Three slices at different depths along the crypt-villus axis in the healthy intestine of a villinCre pCAG-LSL-mTom/mGFP mouse.

A. $z=0\mu\text{m}$, muscle layer, stromal collagen and bottom of the crypts.

B. $z=28\mu\text{m}$, crypts.

C. $z=92\mu\text{m}$, crypts and bottom of villi. All cell membranes (Tomato, red), mosaic labeling of intestinal cells (GFP, green), ECM (SHG, cyan). Scale bar, $100\mu\text{m}$.

Switching to NICD/p53 mice with tumors, I adapted the positioning of the window in order to fit the tumor inside. I found that using this technique, the tumor is sufficiently close to the objective to be properly imaged. I imaged cancer cells (nuclear GFP) and collagen fibers (visualized using their intrinsic properties by Second Harmonic Generation) using two-photon microscopy. I found that diverse collagen structures are present in different fields of the same tumor. For example, collagen was organized into a thick shell encapsulating a large tumor mass (Figure 2, A, left panel), or it formed thinner fibers surrounding smaller clusters (Figure 2, A, middle and right panels). There were also regions of curly and thin collagen fibers, resembling the organization of collagen found in the normal gut, and reminiscent of the Tumor-Associated Collagen Signature 1, defined by P. Keely's lab (Conklin and Keely 2012), as seen in Figure 2, B, left panel. I also observed regions of very thick and dense fibers, running parallel to the tumor edge, encapsulating large tumor clusters (TACS-2, Figure 2, B, middle panel), as well as fibers aligned perpendicularly to the tumor edge, shown to be pro-invasive (TACS-3, (Provenzano *et al.*, 2006), and Figure 2, B, right panel).

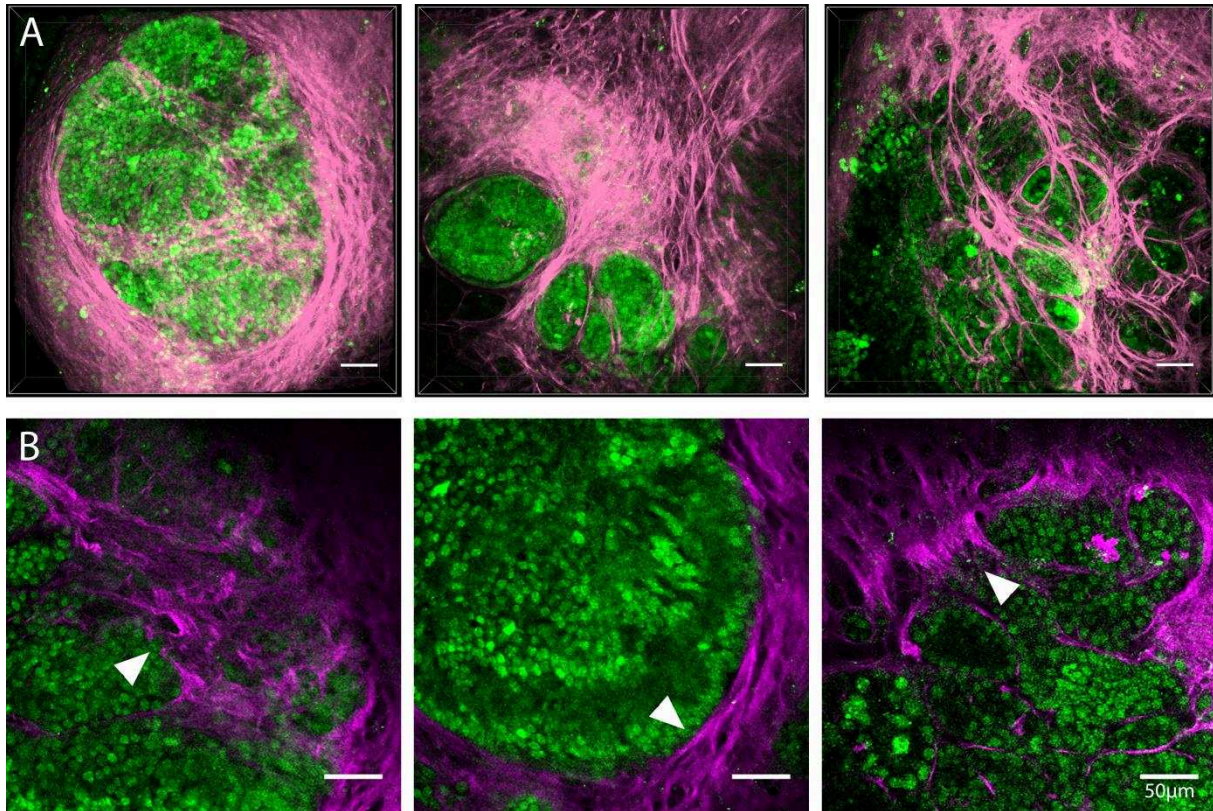


Figure 2. Intravital imaging reveals various collagen patterns in NICD/p53 tumors.

A. Various collagen structures found in a single NICD/p53 tumor. Cancer cells (nuclear GFP, green), collagen fibers (SHG, magenta). 3D rendering is done using the Nikon NIS-Elements software. Scale bars, 50µm.

B. Left panel, TACS-1, curly collagen structure; middle panel, TACS-2, strait and aligned collagen, parallel to the tumor edge; right panel, TACS-3, collagen aligned perpendicularly to the tumor edge. Cancer cells (nuclear GFP, green), collagen (SHG, pink). Arrowheads point to distinct collagen organization modes. Scale bars, 50µm.

Interestingly, the collagen structures with fibers aligned perpendicularly to the tumor edge have been recreated *in vitro* by our collaborators using cancer cell spheroids invading collagen gels (Kopanska *et al.*, 2016). Indeed, Kopanska *et al* has shown that cancer cell spheroids exert pulling forces on the 3D collagen matrix *in vitro*, that deform the collagen radially. This inherently creates a preferential alignment of the fibers perpendicular to the spheroid surface, that is very similar to the fiber alignment observed *in vivo* (Figure 2). This collaboration has led to the publication of the study “Tensile forces originating from cancer spheroids facilitate tumor Invasion” that is enclosed in the Annexes part of my thesis.

CHAPTER 3

CONCLUSION AND DISCUSSION

My PhD was aimed at better understanding cancer cell migration and the role of the microenvironment in invasion. In order to determine the dynamics of cancer cells in a poorly studied cancer region, the tumor core, I developed a methodology to image tumor explants for long periods *ex vivo*. I found that cancer cells in the tumor core were remarkably dynamic and that they exhibited coordinated migration patterns, giving rise to swirls and vortexes. In a complementary approach we addressed the importance of collagen stiffening in cancer cell invasion using 3D collagen matrices *in vitro*. This approach allowed us to unravel the importance of the timing of collagen stiffening in invasion: when matrices are stiffened before the onset on invasion, invasion is delayed, whereas stiffening after the onset on invasion renders it even faster.

Tumor explant imaging as a bridge between 3D *in vitro* assays and intravital imaging

The main aim of my PhD was to decipher cancer cell migration in the tumor core with single cell resolution, using a physiological spontaneous cancer model. Previously, orthotopic mouse models have suggested that cells in the tumor core are motile (Kedrin *et al.*, 2008a; Canel *et al.*, 2010; Fumagalli *et al.*, 2017), but details on the dynamics of migration were lacking. To address this, we developed a pipeline to image tumor explants from spontaneously forming tumors in real time using long-term two-photon microscopy. We found that cells in the tumor core are remarkably dynamic. Cancer cells exhibited collective behaviors, such as coordinated migration, streaming and vortex-like movements. In addition, we found that collagen fibers within the tumor core may act as long-range directional cues, as tumor cells migrate parallel to collagen structures, even up to several cell diameters away. Coordinated migration was interspaced by brief pauses. Interestingly, there was no requirement for pausing during division, suggesting that dividing cells continue to flow with their neighbors.

Tumor explant imaging provides a bridge between 3D *in vitro* invasion assays and intravital studies in living mice. On one hand, embedding cancer cells in various 3D extracellular matrices allows for deciphering interactions with specific matrix components and molecular pathways involved in 3D migration. 3D models are versatile

and tunable, thus they allow for manipulation of the different parameters in play in cell migration, such as the properties of the extracellular matrix, or cell-intrinsic properties. It is for example possible to vary the molecular composition of the matrices. The most commonly used matrices are made of polymerized networks of collagen I (Wolf *et al.*, 2009; Friedl and Alexander, 2011), that can be complemented with other matrix types, such as Matrigel, or fibronectin. Physical properties of collagen I matrices, such as pore size, can be further tuned by varying the collagen polymerization temperature (Wolf *et al.*, 2013). The topology of the matrix can also be engineered, to allow for either aligned or random bundle organization. We took advantage of the versatility of 3D collagen networks in order to study the temporal role of collagen stiffening in invasion. I will come back to this point in section “Importance of the timing of collagen stiffening in invasion”. As tunable as they can be, 3D assays do not recapitulate the full complexity of the extracellular matrix organization, of tissue heterogeneity and cell-cell interactions. Therefore, a complementary more physiological approach might prove of great value to better understand the interactions between cancer cells and their native microenvironment. Intravital imaging allows for direct observation of cell behaviors in the living animal in an almost unperturbed setting. However, intravital imaging has technical drawbacks that prevent its use for studying some organs. Intravital imaging is most often used for easily accessible organs, such as skin or breast (Alexander *et al.*, 2008; Kedrin *et al.*, 2008a; Ewald, Werb and Egeblad, 2011). To follow the migration of cells in densely packed tumor areas, until now only orthotopic xenograft models have been used (Kedrin *et al.*, 2008b; Canel *et al.*, 2010; Gligorijevic *et al.*, 2012; Fumagalli *et al.*, 2017). Xenograft models have the advantages of relatively rapid tumor growth and straightforward genetic manipulation of the tumor cells prior to injection. However, because these tumors are not surrounded by a native stroma that co-evolves with the tumor, they still lack a truly disease-relevant microenvironment. Imaging of spontaneous cancer models allows for a better understanding of the co-adaptation of cancer cells to their native microenvironment and how tumor cells behave in a native microenvironment.

We attempted to use an intravital approach to study cancer cell migration in NICD/p53 tumor core regions. We adapted the intravital methodology that is used in the normal

mouse intestine, to our mouse intestinal tumors. In this process, we faced several difficulties that we had to overcome. Because cell migration in tumors is a slow process, one would need acquisitions of at least 6h in order to visualize cell displacements. Because deep anesthesia is a heavy procedure for the mouse, long-term intravital imaging was not feasible in NICD/p53 mice with intestinal tumors. An option to circumvent the difficulty brought by slow cell migration was to do short imaging sessions of the same tumor region several days in a row. When trying this approach, we noticed that laser penetration depth was greatly diminished when tumors were imaged several days after installation of the optical window. This was due to the fact that the windows get opacified within few days, possibly due to immune reaction of the tissue to surgery. This could be overcome by using optical windows with replaceable glass coverslips so they can be regularly cleaned prior to imaging. In conclusion, we found that the time-frame of imaging needed for cell migration in NICD/p53 tumors was not compatible with intravital imaging.

The time-frame put aside, the two-photon laser used in intravital imaging was unable to penetrate deep enough in the tissue in order to reach the core region of NICD/p53 tumors. Indeed, we could only visualize with a satisfactory resolution the collagenous capsule surrounding the tumor, and the first patches of cells beyond that capsule. In order to have access to deep regions of the tumor core, we believe that these regions need to be physically excavated and put closer to the microscope objective. This is made possible by the method that we developed and that consists to image explant taken out from the mouse.

Limits of tumor explant imaging

We validated the robustness of our explant imaging model by comparing characteristic features of the explants to tumors *in vivo*. Because tumors are resected from mice, some physiological features found *in vivo* were not recapitulated in our model. For example, we found a decrease in the hypoxic factor HIF1 α upon culture of tumor slices out of the mouse in 95% O₂ (data not shown). This suggests that the tumor core undergoes reoxygenation, and therefore our tumor explant culturing pipeline is likely not suitable for analysis of hypoxia-dependent cell behaviors. Interestingly, tumors are often hypoxic, with oxygen tension ranging 1-30mmHg, which corresponds to 0.2-4% of oxygen. Oxygen tension in

the arteries is 75-100mmHg (10-13% oxygen). Thus, the surface layer of the tissue slices is exposed to hyperoxic conditions (95% oxygen, surface oxygen tension 712mmHg). However, besides the amount of the external oxygen amount, the distance to which oxygen penetrates through the tissue depends also on the respiratory rate of the given tissue. Consequently, the diffusion penetration depth varies in different tissues. For example, diffusion penetration depth of oxygen at 100mmHg is 220 μ m for skeletal muscle, 120 μ m for brain and only 74 μ m or 59 μ m for liver and kidney, respectively (Ivanova et al, 2012). Data regarding diffusion penetration depth or respiratory rate of tumors is lacking in the literature. However, if the respiratory rate of tumors is similar to kidney or liver, then to penetrate 250 μ m (thickness of the slice), the surface oxygen needs to be increased to 95%. This could explain why the survival of tumor slices is favored at 95% oxygen. To study tumor tissue behavior in hypoxic conditions, one could use a so-called hypoxic chamber, that represents a hermetic chamber that can be filled with the desired mixture of gases (let's say low oxygen), and then put in a cell culture incubator for a proper temperature control.

Intravital studies have suggested an enhanced migratory phenotype in proximity to blood vessels (Kedrin *et al.*, 2008a). In our system blood perfusion was abolished, so the contribution of the vasculature to tumor cell migration cannot be addressed. However, these factors did not appear to affect tumor cell morphology, proliferation rates and migration speeds, which were stable over long imaging periods and fell within the range of migration speeds observed in intravital studies. For example, collective strands of B16F10 melanoma cells migrate at a speed of 15 μ m/h (Weigelin, Bakker and Friedl, 2012), while multicellular streams of MDA-MB-231 breast cancer cells exhibit a speed of 1.8-72 μ m/h (Patsialou *et al.*, 2013; Gligorijevic, Bergman and Condeelis, 2014).

Collective behaviors of cancer cells in the tumor core

Using explant imaging, we have observed coordinated collective behaviors of cancer cells that were reminiscent of phenotypes observed in confluent cell monolayers *in vitro* that are close to a jamming transition. Recently, jamming was for the first time described *in vivo* in development, during zebrafish body axis elongation (Mongera *et al.*, 2018). We

plan to characterize in more details the jamming phenotypes in NICD/p53 tumors. To do so, we will quantify the tissue properties that hint to a transition from a fluid to a solid state (Garcia *et al.*, 2015; Oswald *et al.*, 2017; Atia *et al.*, 2018). Cells in a jammed state tend to have more hexagonal and regular shapes, while unjammed cells display more elongated and irregular shapes (Atia *et al.*, 2018). This implies that there is a connection between static cell shapes and the dynamic behavior of the whole cell sheet, and that the dynamic state of a tissue can be inferred by static cell shape (Oswald *et al.*, 2017; Atia *et al.*, 2018). In order to determine whether the tumor core is behaving more as a fluid or as a solid, we will calculate the cell shape index (Oswald *et al.*, 2017). We will correlate cell shape in different regions with the observed dynamic behavior in order to determine if there is a correlation between cell shape and cell dynamics. In order to test if the fluidity of the tissue evolves in time, we will describe the evolution of velocity correlation lengths in time (Garrahan, 2011; Garcia *et al.*, 2015). Velocity correlation lengths measure whether cells that moved fast (or slow) are clustered together in space with equally fast (or slow)-moving cells. When a system approaches jamming transition, these spatial correlations in the dynamics become more pronounced with increasing density and consequent decreasing mobility (Garrahan, 2011). We will describe the evolution of correlation lengths in our system to determine if the tumor core tissue evolves to a jamming state (Garrahan, 2011; Garcia *et al.*, 2015; Oswald *et al.*, 2017).

In NICD/p53 tumor tissues, the presence of collagen fibers presents an additional layer of complexity. We observed that tumor cells migrate parallel to collagen bundles even without directly contacting them. This suggests that collagen may act as a long-range directional guide for cancer cell migration. It will be interesting in the future to explore the effects of structural barriers like collagen fibers on jamming transitions in tumor tissues.

Finally, the mechanism of cancer cell migration in the tumor core remains open. Are cells passively migrating because they get pushed by their neighbors that divide? Or do cells migrate in an active way, using the actomyosin machinery? To do so, we will quantify cell velocity in the presence of proliferation inhibitors (hydroxyurea and mitomycin C), blebbistatin, a myosin II inhibitor, and cytochalasin D, an inhibitor of actin polymerization. If migration in the tumor core is a passive mechanism driven by cell

proliferation, we expect to find a decrease in migration speed upon hydroxyurea and mitomycin C treatment. If the migration is active, we expect a drop in velocity upon blebbistatin or cytochalasin D treatments.

Importance of the timing of collagen stiffening in invasion

Intravital imaging reveals cell dynamics in intact tissues, but these dynamics are much more difficult to perturb. The amount of collagen crosslinking could be modulated in the living mouse by L-ribose and β -aminopropionitrile (BAPN) injections (Levental *et al.*, 2009; Gligorijevic, Bergman and Condeelis, 2014). L-ribose is a collagen cross-linking agent (Levental *et al.*, 2009), whereas BAPN is an inhibitor of lysyl oxidase. These treatments resulted in a different behavior of cancer cells, with increased number of invadopodia (Gligorijevic, Bergman and Condeelis, 2014) and focal adhesions (Levental *et al.*, 2009) forming upon L-ribose treatment, and a decrease in invadopodia number upon BAPN treatment. However, as these treatments also affect collagen density (Gligorijevic, Bergman and Condeelis, 2014), it is difficult to disentangle the respective roles of collagen stiffening versus density on cancer cell behaviors in these mouse models. To study the temporal role of collagen stiffening on cancer cell migration, we used a 3D model of reconstituted collagen I matrices. We followed and quantified in time the stiffening of the gels using rheology, which is very difficult in the living organism because of a limited access to the tissue.

Collagen glycation spontaneously occurs *in vivo* and it results in non-enzymatic collagen crosslinking (Francis-Sedlak *et al.*, 2009). *In vitro* the reaction can be accelerated by replacing glucose by ribose which is more reactive. Ribose concentrations of up to 100mM resulted in 3-fold increase of collagen stiffness, up to 515 Pa (Mason and Reinhart-King, 2013). Increasing the concentration of ribose to 150mM or greater also resulted in increased matrix stiffness but the fibrous properties of the matrices change as well (Mason and Reinhart-King, 2013). However, the high concentrations and long incubation time required to significantly stiffen the collagen matrix are presumed to induce a diabetic phenotype in cells (Han *et al.*, 2011). To overcome this limitation, we used an alternative collagen crosslinker, threose, which efficiently stiffens and forms crosslinks in human and

bovine articular cartilage (Verzijl *et al.*, 2002; Kinnunen *et al.*, 2012). We found that threose is effective at lower concentrations than the traditional crosslinking agent ribose, which is advantageous as lower sugar concentrations diminish the likelihood to induce a diabetic phenotype or cause a hypertonic stress to cells. Indeed, with as little as 1mM concentration, threose induced a 1.8 fold increase in stiffness, whereas 10mM of ribose were needed for the same effect. Interestingly, this almost 2-fold increase in collagen stiffness was sufficient to induce a drastic effect on CT26 cells behavior, indicating that these cells are relatively sensitive to variations of microenvironmental stiffness. It would be interesting to test the sensitivity of other cell types to matrix stiffness variations. It is indeed possible that the sensitivity to stiffness is related with the aggressive potential of cells.

In the study of Kopanska et al to which we collaborated, it has been shown that cancer cells exert contractile forces on 3D collagen gels, which builds up tension in the 3D collagen I matrix (Kopanska *et al.*, 2016). This tension helps cancer cells migrate out of the tumor spheroid and efficiently invade the matrix. Interestingly, contractile forces appear before cells start to invade the matrix, which lead us to hypothesize that cells first need to build up some tension on the collagen matrix before efficiently invading. Because exerting traction on collagen fibers makes them stiffer (Polacheck and Chen, 2016), it is possible that before cells exert tension on the ECM, the ECM is too soft to provide the mechanical resistance to sustain the forces required to detach a cell from the spheroid. As Timo Betz used to say, unstiffened collagen is like loose ropes, or a spaghetti dish. When starting to pull on those loose ropes or spaghetti, they do not offer sufficient resistance, and get displaced perpendiculars the pulling force, not allowing for a displacement of the cell that is pulling them. Because the other end of the loose ropes is attached to a substrate (the bottom of the dish or other collagen ropes), the ropes get stiffer when being sufficiently pulled. We believe that this is the moment when cells start to efficiently migrate out of the spheroid. This would indicate that there is a threshold of stiffness of the collagen gels that would allow for the onset of cell migration, as well as a succession of events that need to be efficiently accomplished before cells can invade collagen.

In order to study in more details the timing of collagen stiffening and its role in cell invasion, we developed a biomimetic assay that allowed us to control the timing of collagen stiffening. We used the sugar threose, a natural collagen crosslinker (Verzijl *et*

al., 2002; Kinnunen *et al.*, 2012) that is more effective than the traditional crosslinking agent ribose. Threose was added either before, or after the onset of cell invasion. We showed that early collagen stiffening inhibited cell invasion, whereas stiffening of collagen after the onset of invasion favored and accelerated cell invasion. This result can be interpreted in the light of Kopanska *et al.* Indeed, before invasion occurs, cells need to exert traction on the collagen, in order to realign its fibers radially to the cancer mass. If collagen is already made stiff at this stage (as in the case of an early threose addition), it is more difficult for cells to reorganize it, thus delaying invasion. However, once cells have locally reorganized collagen, a stiffening of collagen possibly favors cell migration by enhancing cell tractions exerted on collagen fibers. Therefore it appears that realignment of fibers prior to their stiffening is crucial for cell invasion. Interestingly, we can draw parallel between the realignment of fibers perpendicular to the cancer cells mass in 3D invasion assays and the observed perpendicular fibers (TACS-3) observed in tumors in mice. In mice, cancer cells have been shown to use these perpendicular fibers to migrate out of the tumor (Provenzano *et al.*, 2006). Therefore *in vitro* models are valuable tools to understand the crucial mechanisms involved in this step. The two studies, ours and the one of Kopanska, highlight the effect of matrix remodeling by cells and of exogenous matrix stiffening, on the invasive properties of cancer cells.

It is well established that cancerous tissues are stiffer than their normal counterparts (Guck *et al.*, 2005; Lopez *et al.*, 2011; Swaminathan *et al.*, 2011). However, an important point is that the stiffness in cancer tissues is heterogeneously distributed (Acerbi *et al.*, 2015; Glentis *et al.*, 2017). Indeed, invasive luminal ductal carcinoma (a type of breast cancer), has been shown to display a heterogeneous distribution of stiffness with a dramatic increase in stromal stiffness in the invasive region of the tissue (Acerbi *et al.*, 2015). Indeed, Acerbi and colleagues have found up to a 4-fold increase in the average elastic modulus in the tumor invasive front relative to the non-invasive regions and the normal adjacent stroma, using atomic force microscopy (Acerbi *et al.*, 2015). Interestingly, they found that the two more aggressive breast tumor subtypes, Her2+ and triple negative breast carcinoma, had a much wider distribution of stiffness, and a greater skew towards high stiffness (Acerbi *et al.*, 2015). This indicates that the more aggressive a breast tumor is, the more heterogeneous its stroma is in terms of stiffness. This heterogeneity could be

exploited by cancer cells, that could possibly be able to adapt to a range of tissue physical properties. Cancer cells might be more sensitive to local changes in ECM stiffness, than to the increase in the mean ECM stiffness upon tumor progression. Indeed, a migrating cell presumably senses the local stiffness of particular collagen fibers through integrins locally engaged with these particular fibers. Therefore, a local change in collagen physical properties, as it is the case in heterogeneous ECM stiffening, might be crucial to explain cancer cell invasion phenotypes.

A previous study in our lab has addressed the mechanisms of CAF-mediated cancer cell invasion of the basement membrane and the associated change of tissue stiffness (Glentis *et al.*, 2017). Using AFM, they showed a global softening in BMs remodeled by CAFs, with a heterogeneous stiffness profile. Interestingly, cancer cell invasion is increased upon alteration of the basement membrane by CAFs. So how is it possible that a softer BM is favorable to invasion, whereas several studies, such as the one of Acerbi and colleagues, have found invasion to correlate with an increased stiffness? It is possible that the necessity for ECM stiffening, that has been observed for the 3D invasion of cancer cells out a tumor mass (Acerbi *et al.*, 2015), does not hold true for the invasion of a topologically different 2D environment such as the BM. On the BM, Glentis and colleagues observed a heterogeneous distribution of stiffness upon remodeling by CAFs. Indeed, there was a reduction in fibers of intermediate stiffness, and an increase of patches of soft, inhomogeneous material sparsely interspersed with thick and stiff fibers. This indicates that the decrease in BM stiffness is most likely the result of rearrangement of ECM network, as CAFs alter the organization and physical properties of the BM by enlarging holes, making it permissive to cancer cell invasion. The disrupted organization of the ECM results in a decreased BM stiffness and integrity, thereby reducing its barrier functions and making it more permissive to cancer cell invasion.

General conclusion

In my PhD, I studied cancer cell migration dynamics using different settings. Using a mouse model of intestinal carcinogenesis, I showed that cancer cells in deep regions of the tumor core are motile and exhibit coordinated migration patterns. Using 3D models, I addressed the temporal role of matrix stiffening in cancer cell migration. More broadly,

better understanding collective cell behavior in tumors and the effect of extracellular matrix modification on cancer cell migration will allow for an improved grasp of the complexity of metastasis.

CHAPTER 4

MATERIALS AND METHODS

Imaging Cancer Cell Migration in Intestinal Tumors

Before starting tissue isolation, prepare the following solutions:

- Working solution: Leibovitz's L-15 medium supplemented with 1% anti-anti. Keep at 4 °C.
- Imaging medium: DMEM-GlutaMAX (Gibco) supplemented with 2.5% FBS, 0.25 U/mL insulin (Sigma-Aldrich), 100 µg/mL transferrin (Holo, Human Plasma, Calbiochem), 10 ng/mL murine EGF (Peprotech) and 1% Antibiotic-Antimycotic (Life Technologies).

1. Prepare 4% (w/v) low melting point agarose (Life Technologies) in the working solution. Let it cool down at 37 °C in a water bath (see Note 1).
2. Sacrifice the tumor-bearing mouse.
3. Open the abdomen and keep it humidified throughout the procedure with cold PBS supplemented with 1% Antibiotic-Antimycotic (Life Technologies).
4. Cut out the intestinal tumor with 1 cm of healthy intestine on both sides and put it in a petri dish filled with cold PBS/1% anti-anti (see Note 2).
5. Flush the intestinal tumor with cold PBS/1% anti-anti by inserting a syringe fitted with a cannula in the intestine.
6. Cut the intestine and tumor longitudinally using scissors in order to have the luminal side of intestine and tumor facing you.
7. Remove the healthy intestine from the tumor using a sterile scalpel.
8. Cut 3–6 mm tumor pieces and make sure to have at least one flat side to allow for an easier cutting later on.
9. Embed the tumor pieces in the melted agarose solution using a tissue cassette. Make sure that a side with a flat cut surface is facing the bottom of the cassette (Fig. 2, middle panel).
10. Place cassettes at 4 °C for 5 min to allow gelation of the agarose.

Tissue Sectioning

1. Clean a single-use razor blade using papers soaked with the following solutions in this order: acetone, water, ethanol 70%.
2. Insert the blade into the knife holder on the vibratome (Leica VT1000S).
3. Put ice into the cooling bath of the vibratome.
4. Take the agarose block with embedded explant out of the cassette. Trim the agarose block if necessary, but leave at least 2 mm agarose around the tissue. Be careful not to remove the tissue from the agarose block.
5. Fix the agarose block onto the cutting surface using instant glue. Make sure the flat side of the explant that was previously facing the bottom of the cassette is now facing you.
6. Fill the buffer tray with cold working solution. Make sure that the agarose block is entirely covered.
7. We recommend the following vibratome settings for tumor slices: speed 3 (0.125 mm/s), frequency 7 (70 Hz). Vibratome speed can be adjusted according to the stiffness of your tissue (see Note 5).
8. Section at 250–360 μm thickness.
9. Collect the agarose-embedded sections from the working solution gently, using a perforated spoon or a spatula (see Note 7). Transfer the sections to a petri dish with working solution, on ice.
10. Gently remove the agarose around the slices using tweezers.

Mounting the Explants, Live-Cell Imaging and Image Analysis

1. Put 1 mL of imaging medium into the glass-bottom cell culture dish.
2. Place the cell culture insert filter (Millicell, 30mm diameter, pore size 0,4 μm , Merck Millipore) carefully into the Fluorodish, to avoid bubble formation. The cell culture insert should sit on the inner ring of the Fluorodish and be in contact with the medium.

3. Position up to five tissue slices on the cell culture insert (see Note 7). Slices are at the air-liquid interface, exposed to air, but in contact with cell culture medium through the perforated membrane insert.

4. For cell migration analysis, time-lapse movies are acquired with a two-photon confocal microscope (see Note 10). We use an inverted Leica SP8 microscope coupled to a femtosecond Chameleon Vision II laser (680–1350 nm; Coherent, Inc.), using a Leica 25×/0.95NA water immersion objective (see Note 11). Imaging of the explant mounted as described requires use of a long working distance objective. For live imaging, the microscope should be equipped with a stage top incubator (e.g., Okolab) to allow gas, temperature and humidity control. Tissue is maintained at 37 °C, in 95% O₂/5% CO₂ atmosphere, with 95% humidification. Image acquisition and microscope control are performed using the Leica LAS X software.

5. Detectors with suitable filters for the fluorophores in use are required. We use three non-descanned Leica Hybrid detectors, that have the following filters: 525/25 nm (GFP), 575/25 nm (Tomato) and <492 nm (Second harmonic Generation, SHG). The excitation wavelength used is 960 nm for GFP and Tomato, 910 nm for SHG.

6. Stacks are recorded at intervals suitable for the dynamics of the cell behavior you wish to observe. For cell migration analysis, we record stacks every 15–30 min, up to 48 h. The step size can be adapted according to the desired resolution in the z plane. We obtained 3D stacks at a step size of 1–2 μm intervals, using 25× objective.

7. Time-lapse processing and analysis are done using LAS X (Leica), ImageJ (NIH) or Imaris (Bitplane). All images are corrected for brightness and contrast using the ImageJ software. 3D registration can be done using the “Correct 3D drift” plugin. Cells can be tracked either manually, or automatically, provided that image segmentation can be implemented. In primary tumors, we manually track cell nuclei in 2D using the MTrackJ plugin and in 3D using Imaris (Bitplane).

Notes

1. Work fast with liquid agarose, as it will rapidly polymerize at room temperature.

2. For better viability, make sure to keep the tissue on ice at all steps prior to incubation and imaging.
3. In case of tissue with higher stiffness, vibratome speed can be increased and frequency can be decreased. You will need to find optimal settings for your tissue of interest.
4. Always manipulate the tissue slices gently, preferably with blunt-edge tweezers and/or a perforated spoon.
5. Tissue viability and dynamics vary in different tissues of interest. For example, intestinal tumor tissue has a viability of 48 h in imaging conditions, liver 30 h and normal gut mucosa <10 h.
6. For purposes other than live imaging, gut and tumor slices can be cultured in a tissue incubator at 37 °C in 95% O₂/5% CO₂ atmosphere. This allows a variety of applications, such as labeling (e.g., BrdU/EdU for cell proliferation), transfection, or drug treatments.
7. Two-photon microscopy is used for long-term deep tissue imaging with reduced phototoxicity. Confocal imaging with visible lasers is also possible, but will yield more photobleaching and shorter imaging depth.
8. Imaging of the explant mounted as described requires the use of an inverted microscope.

Cell lines

Mouse intestinal cancer cells CT26 were obtained from American Type Culture Collection (ATCC). Cells were cultured in Dulbecco's Modified Eagle Medium (DMEM) (Life Technologies) supplemented with 10% FBS (Invitrogen) and 5% CO₂. Mycoplasma testing was performed every 2 weeks in order to verify that cells were clear of infections.

Mice

All experiments were conducted in accordance with the guidelines of European Directive 2010/63/EU and national regulation for the protection of vertebrate animals used for experimental purposes (Decree 2013-118). All mice were kept in the Institut Curie Specific Pathogen Free (SPF) animal house for breeding.

In order to obtain the NICD/p53^{-/-} mice (pVillin-CreER^{T2}; LSL-NICD-nGFP; p53^{F/F}) and NICD/Tom/p53^{-/-} mice (pVillin-CreER^{T2}; LSL-NICD-nGFP; mT/mG; p53^{F/F}), previously described mice were crossed: the pVillin-CreER^{T2} mice (El Marjou *et al.*, 2004), p53^{F/F} mice (Jonkers *et al.*, 2001), Rosa26-mT/mG mice (Muzumdar *et al.*, 2007) and Rosa26-N1ic mice, referred to as NICD (Murtaugh *et al.*, 2003). Rosa26-mT/mG mice express a membrane-targeted tandem dimer Tomato (mT) prior to Cre-mediated excision and a membrane-targeted EGFP (mG) following excision (Muzumdar *et al.*, 2007). Membrane targeting was achieved by the MARCKS membrane tag (Muzumdar *et al.*, 2007). Four-week-old mice were injected intraperitoneally with tamoxifen (1mg/day) for 5 consecutive days. Eight months after tamoxifen injection, mice spontaneously develop invasive intestinal carcinoma as described in (Chanrion *et al.*, 2014).

Isolation and culture of tumoroids from mouse intestinal tumors

First, a 10X collagenase III (Worthington) solution was prepared by dissolving collagenase powder to 15 000 units in 5mL of H₂O. 50mL of dissociating medium with 1X Collagenase III, 2% antibiotic/Antimycotic, in DMEM (Gibco) was prepared. The tumor was finely cut with a sterile scalpel in a Petri dish with a little of dissociating medium. The tumor pieces were incubated 2h at 37°C at 180rpm agitation in a small sterile Erlenmeyer. After filtration at 100µm then at 40µm, the mix was centrifuged at 1000rpm for 6min. The

pellet was resuspended to a final concentration of 50% cells and 50% Matrigel. 50 μ L drops were deposited in a small Petri dish and covered with 2mL of culture medium after Matrigel gelation, 40min later. Culture medium was composed of DMEM-GlutaMAX (Gibco) supplemented with 2.5% FBS, 0.25 U/mL insulin (Sigma-Aldrich), 100 μ g/mL transferrin (Holo, Human Plasma, Calbiochem), 10 ng/mL murine EGF (Peprotech) and 1% Antibiotic-Antimycotic (Life Technologies). Tumoroids were passaged twice a week, by breaking the Matrigel and dissociation by serial pipetting. After 5min centrifugation in 600rpm, the pellet was resuspended in the adequate amount of Matrigel to have 50% Matrigel and 50% tumoroids. The mix was deposited in 50 μ L drops and covered with culture medium after gelation of Matrigel.

3D collagen invasion assay of CT26 cells

Agarose (Invitrogen) was dissolved in water to a concentration of 0.01g/mL and boiled. 150 μ L of the solution were added to wells of a 48 well-plate and agarose was left to polymerize for at least 10min at RT. A solution of 10⁴ cells/mL of CT26 cancer cells was made, and 75 to 100 μ L of the solution was added to the wells. The wells were subsequently filled with DMEM supplemented with 10% FBS +/- threose (1mM, T7642, Sigma) and spheroids were left to form for 3 to 4 days.

30mm² tissue culture plates were specifically fashioned for the invasion assay: 3 holes of approximately 3-4mm in diameter were drilled in a plate and widened around the edges using a scalpel.

2mg/mL rat tail collagen I (Corning) was prepared in DMEM, 10X PBS and 1M NaOH, to a pH=7 as described in sample preparation. The solution was kept on ice in order to avoid collagen polymerization. Spheroids were embedded in 15 μ L collagen drops, positioned in the hole of the culture plate. After filling all 3 holes, the plate was flipped every 30s for 5min, in order for the cells to stay in the middle of the collagen drop (preventing sedimentation of spheroids to the glass or to collagen/air interface). Collagen was left to polymerize for an additional 15min at room temperature before 3mL of DMEM supplemented with 5% FBS, 1% AA were added, +/- 1mM of threose.

2D migration of CT26 cells

CT26 cells were incubated for two days with the following concentrations of threose: 0mM, 0.5mM, 1mM and 2mM in DMEM supplemented with 10% FBS and 1% AA. After two days, CT26 were resuspended and 2500 cells were seeded on uncoated glass-bottom wells of a 96-well plate. After overnight imaging, all the wells were washed and DMEM 10% FBS 1% AA was added, and cell migration was imaged for 8 more hours.

3D migration of single CT26 cells

2mg/mL rat tail collagen I (Corning) was prepared in DMEM, 10X PBS and 1M NaOH, to a pH=7 as described in sample preparation. The solution was kept on ice in order to avoid collagen polymerization. Glass-bottom cell culture dishes (FluoroDish, World Precision Instruments) were coated with poly-L-Lysine (Sigma-Aldrich) for 5min, and washed 3 times with PBS. CT26 cells were resuspended and 5000 cells were embedded in 40 μ L collagen drops that were deposited on the bottom of the culture dishes. Dishes were flipped for 1.5min, in order for the cells to stay in the center of the collagen drop. Collagen was left to polymerize for an additional 30min at room temperature before 2mL of DMEM supplemented with 10% FBS, 1% AA were added, +/- 1mM of threose. Dishes were maintained for two days at 37°C, 5% CO₂.

Basement membrane isolation and preparation

BMs were prepared as previously described (Hotary *et al.*, 2006; Rowe and Weiss, 2008) and ourselves (Schoumacher *et al.*, 2010). Mesentery was isolated from female C57B/6 mice. First, the membrane of a 24 well-plate 6.5-mm diameter transwell (BD Bioscience) was cut out using a razor blade. Mice were euthanized after isoflurane anesthesia and the abdomen was opened and regularly humidified with PBS 1% Antibiotic-Antimycotic. The intestine was pulled out without being cut and without damaging the mesentery part, using blunt tweezers. Surgical glue (3M Vetbond) was is applied on the sides of the insert, and the mesentery was stretched around the insert using tweezers and pressed to ensure attachment. The non-used mesentery was cut and the intestine removed. The insert was placed in a 24-well plate filled with PBS 1% Anti/Anti on ice for washing. To decellularize the membranes, the inserts were placed in wells with ammonium hydroxide (NH₄OH) at

1M for 1 hour at room temperature. Then the inserts were transferred to clean wells and washed 3 times in PBS and stored at 4°C for up to 24 hours.

Basement membrane invasion assay

Inserts were placed in wells filled with DMEM-GlutaMAX (Gibco) supplemented with 2.5% FBS, 0.25 U/mL insulin (Sigma-Aldrich), 100 µg/mL transferrin (Holo, Human Plasma, Calbiochem), 10 ng/mL murine EGF (Peprotech) and 1% Antibiotic-Antimycotic (Life Technologies). Tumoroids were resuspended, gently dissociated by pipetting and deposited in the inserts, on the mesentery. Inserts were incubated for several days at 37°C and 5% CO₂. Samples were either subjected to live two-photon imaging or fixed for immunofluorescence.

Imaging

- Time-lapse image acquisition of tissue slices

Tissue explant was maintained at 37°C in the microscope stage top incubator (Okolab), in 95% O₂, 5% CO₂, 95% humidification. The explant was imaged using two-photon excitation microscopy on an inverted Leica SP8 microscope coupled to a femtosecond Chameleon Vision II laser (680-1350 nm; Coherent, Inc.), using a Leica 25x/0.95NA water immersion objective.

Three non-descanned Leica Hybrid detectors were used, with the following filters: 525/25nm (GFP), 575/25 (Tomato) and <492nm (Second harmonic Generation, SHG). The excitation wavelength was 960nm for GFP and Tomato, and SHG was obtained at a wavelength of 910nm.

Images were recorded every 15 to 30min up to 40h. 3D stacks were obtained at a step size of 0,5-2µm intervals.

For the analysis of tumor cell migration, we used a total of 5 NICD/p53^{-/-} mice, with one tumor explant being used for imaging per mouse. Several positions were acquired per tumor explant, among which 7 positions where retained for our study. From these 7 positions, 14 z-slices were selected for manual tracking in 2D. A total of 685 cell trajectories were analyzed for the dynamics studies in Fig. 2 and 5, 857 cells for the

directional correlation in Figure 4C, 423 cells (3 mice) were used for the study of cell migration with respect to collagen (Fig. 5C) and 36 division events (3 mice) were used in Fig. 3C-E.

- **Imaging 3D collagen networks**

The pure and threose supplemented collagen networks were imaged in confocal reflectance and confocal fluorescence mode using an inverted Eclipse Ti microscope (Nikon, Tokyo, Japan), a 488 nm Argon laser (Melles Griot, Albuquerque, NM) for illumination and a 100× objective (Nikon, N.A. 1.49). Z-stacks were acquired 10 μm above the coverslip to avoid surface effects, over a depth of 10 μm, with a step of 0.2 μm and shown as a maximum projection. The networks were allowed to polymerize for 48 hours at 37°C with controlled humidity. To visualize fluorescent collagen, we added the collagen binding protein CNA35 (Aper et al., 2014) tagged with eGFP (pET28a-EGFP-CNA35, AddGene) to collagen prior to polymerization in a molar ratio of 20:1.

- **Imaging 3D spheroids**

Images were acquired with an inverted AOBs two-photon laser scanning confocal microscope SP8 (Leica) coupled to femtosecond laser Chameleon Vision II (Coherent Inc) using 25x/1.0NA water-immersion objective. The microscope is equipped with two non-descanned HyD detectors: NDD1 (500–550 nm) and NDD2 (≥590nm). Fluorescence channels were recorded simultaneously using the excitation wavelength 980nm. Collagen was visualized by confocal reflectance microscopy, using light at a wavelength of 488 nm and a standard photomultiplier tube (PMT) detector, at a low gain (500V). 3D stacks were obtained at a step size of 2 μm intervals. The images were processed with Leica Application Suite (LAS), ImageJ (NIH) and Imaris (Bitplane).

- **Imaging CT26 migration and image analysis**

2D and 3D culture were imaged using an Inverted Nikon Ti-E microscope equipped with a sCMOS 2048 ORCA Flash4.0 V2 camera (Hamamatsu) using the following objectives:

Plan Fluor 10x Ph1 DL and Plan Apo VC 20x DIC N2. Images were acquired every 10 to 20min for 8 to 12h.

A random population of cells was selected and manually tracked in 2D using the MTrackJ plugin (Meijering et al., 2012) in ImageJ (Bitplane). Following tracking of cells, the trajectories were analyzed using custom software written in Python. Migration persistence was defined as the final cell displacement divided by the length of the trajectory.

- **Imaging of fixed basement membrane invasion assay**

Cells were imaged with 25x/0.8 oil objective on an inverted Laser Scanning Confocal microscope (LSM880NLO Zeiss) equipped with the following lasers: 405/457/488/514/561/633nm. Collagen fibers were visualized by reflection as previously described (Friedl et al., 1997). The images were processed with ImageJ.

- **Live imaging of basement membrane invasion**

The invaded basement membranes were maintained at 37°C in the microscope stage top incubator (Okolab), in 5% CO₂ and 95% humidification. The samples were imaged using two-photon excitation microscopy on an inverted Leica SP8 microscope coupled to a femtosecond Chameleon Vision II laser (680-1350 nm; Coherent, Inc.), using a Leica 25x/0.95NA water immersion objective. Two non-descanned Leica Hybrid detectors were used, with the following filters: 525/25nm (green) and 575/25 (red). Fibers of the basement membrane were imaged using reflection.

- **Intravital imaging of tumor tissue**

Intravital imaging of intestinal tumors was performed on an upright A1R NLO confocal laser scanning microscope (Nikon) equipped with InSight DeepSee laser (680-1300 nm; Spectra-Physics) and with a 25x/1.1 Apo LWD water immersion objective (Nikon). Nuclear GFP was imaged with 940nm laser on a NDD GaAsP detector equipped with

525/50nm detector and second harmonic generation was imaged at 940nm on a NDD GaAsP detector equipped with <492nm filter.

- **Scanning electron microscopy**

In order to reveal the ultrastructure of the mesenteric basement membrane, we used scanning electron microscopy. Basement membranes were fixed in 2,5% glutaraldehyde in a 0.1M cacodylate buffer overnight, at 4°C. Samples put in a 0.2M cacodylate buffer and washed 3 times 5min in 0.1M cacodylate buffer. Samples were incubated for contrasting in 1% osmium tetroxide in 0,2M cacodylate buffer for 1h at room temperature away from light. After 3 washes of 5min in water, samples were dehydrated in a series of ethanol baths (25%, 50%, 75%, 95% and 100%) and then treated for critical point drying by CO₂, using Baltec CPD030 technology and gold-palladium metallization, using an Ion Beam Coater GATAN. The observations were made with a Jeol 6700F microscope in Pasteur Institute (Paris).

Image analysis

- **Image analysis of tissue slices**

Z stacks were processed using ImageJ (NIH). All images were corrected for brightness and contrast using the ImageJ software. 3D registration was performed using the “Correct 3D drift” plugin (Parslow, Cardona and Bryson-Richardson, 2014). Rigid body registration (“correct 3D drift”) did not differ in terms of population-level cell dynamics when affine registration was added using collagen structures as a reference channel. For tracking, a random population of cells was selected without prior knowledge of the migration. These nuclei were then manually tracked in 2D using the MTrackJ plugin (Meijering, Dzyubachyk and Smal, 2012). Tracking of large numbers of cells in 3D was not feasible as the high crowding of cancer cells in the tumor core does not allow for accurate segmentation. To obtain large field of view (Fig. 1A), z-projected 3D stacks were stitched using the Grid/Stitching plugin (Preibisch, Saalfeld and Tomancak, 2009) following flat-field correction after determining intensity inhomogeneity by imaging a uniform fluorescent field.

- Analysis of migration trajectories in tissue slices

Following manual tracking of cell nuclei, cell trajectories were analyzed using custom analysis software written in Python (www.python.org) using the following packages: numpy, scipy and matplotlib. Migration persistence is defined as the final displacement of a cell divided by the total trajectory length. MSD was determined using a Fast Fourier Transform based on the algorithm in (Calandrini *et al.*, 2011). To determine directional correlation, for a given time-lapse image, all possible combinations of cells were determined for a given time-lapse movie. Directional correlation, defined as $\cos(\theta_{i,t} - \theta_{j,t})$ for cells i and j , was calculated for overlapping time frames t to determine the mean correlation. PIV analysis was performed using the OpenPIV (www.openpiv.net) package in Python, with a window size of 32×32 px² ($\sim 29 \times 29$ μm^2) and window overlap of 16×16 px² ($\sim 15 \times 15$ μm^2). To avoid tracking noisy pixels, a mask was generated based on a thresholded image of the tissue. Only pixels within this mask were considered in the PIV analysis. Spurious vectors were identified by cross-correlation signal-to-noise analysis. For Fig. 4D and Supplementary movie 3, noisy vectors within the mask region were replaced by a local mean interpolation. For the directional correlation analysis, noisy vectors were eliminated. Directional correlation vs. distance was determined from vectors resulting from the PIV analysis by comparing the correlation and distance between vectors for all given time frames.

For the PIV analysis of directional axes with respect to collagen, a brightest point projection of the collagen (SHG) signal over time was first generated. This projection was used to generate a binary mask of the collagen regions. PIV analysis was performed for regions outside of the mask for successive time points as described above. For each frame pair, the vectors at each position were converted to axes by projection onto 180° . These axes were then averaged by taking the mean at each position over time. For visualization purposes, the axes lines were normalized to a uniform length.

For the analysis of cell migration dynamics and collagen structures, a binary mask was generated from 2D collagen images by Gaussian filtering, thresholding and removal of small objects. The mean position of each cell trajectory was compared with the collagen mask to determine the minimum distance and direction vector from the cell trajectory to the collagen mask. The directional bias was defined as $\cos(\theta_i - \Phi_i)$, where θ_i is the overall trajectory vector (from the position of the first to last time point) and Φ_i is the direction

vector from the mean trajectory position to the closest point of the nearest collagen bundle. For the Rayleigh test of uniformity, the directional bias was rescaled to angular directions.

To generate kymographs, cell trajectories were projected onto one dimension and plotted against time. Pauses were defined as consecutive time periods of ≥ 30 min without detectable movement of the nucleus. For comparison of speeds in dividing cells, the period "during division" was defined as the 45mins prior to the appearance of the daughter cell nuclei. For quantification of collagen displacement, kymographs were generated in ImageJ. For each kymograph, the mean displacement speed was determined from the time points where the displacement was maximal.

- **Mesh size analysis of 3D collagen gels**

The mesh size of the networks was determined using an algorithm described in (Kaufman et al., 2005). Images were background-subtracted and binarized with an Otsu threshold using ImageJ. The resulting image was then analyzed in a custom-written Python routine, which counted the distance between on and off pixels along the rows and columns. The distances obtained were then fitted with an exponential probability distribution and the mean value (converted from pixels to μm) was taken as the average mesh size. For each condition, we analyzed at least 8 randomly sampled images.

- **Fiber diameter analysis in 3D collagen gels**

To analyze the average diameters of the collagen fibers, we performed turbidity measurements with a Lambda 35 dual-beam spectrophotometer (PerkinElmer, Waltham, MA). Samples were polymerized inside a plastic cuvette (UV-Cuvette micro, Plastibrand, Germany) or a quartz cuvette for 48h before measuring. Subsequently, the optical density of the sample was measured in the wavelength range 650-900 nm. The measured optical density I_0 was converted into turbidity τ using the formula: $\tau = I_0 \ln \left(\frac{I_0}{I} \right) / L$

where L represents the optical path length. To extract fiber radii and mass-length ratios, we employed the following relation (Yeromonahos et al., 2010): $\tau \lambda^5 = A(\lambda^2 - B a^2)$

Where A and B are constants corresponding respectively to $(88/15)c_p\pi^3n_s(dn/dc_p)^2/NA$ and $(184/154)\pi^2n_s^2$. Here, c_p represent the collagen concentration, n_s the refractive index of the solvent, dn/dc_p is the refractive index increment, NA is the Avogadro constant, μ the mass per length ratio and a the fiber radius.

- **Invasion counter software**

Quantification of cell invasion from spheroids was performed as already described using a custom semi-automated image analysis program written in Python (Attieh et al., 2017).

Immunofluorescence staining and image acquisition

- **Immunofluorescence of tissue slices**

In order to minimize tissue heterogeneity, staining at 0h and at 24h was performed on matched samples, where two 250 μ m-thick adjacent tissue slices were used, one for the 0h time point and the other for the 24h time-point after incubation. 250 μ m-thick tissue explant slices were embedded in OCT and sliced to 5 μ m-thin cryosections. Immunofluorescence was performed using the following antibodies: anti-E-Cadherin (20 μ g/mL, Life Technologies, 13-1900), anti-ZO-1 (5 μ g/mL, EMD Millipore, MABT11), anti-ZEB-1 (1:100, Bethyl laboratories IHC-00419), anti- α -SMA (1:200, Dako, M0851), anti-Ki-67 (2.5 μ g/mL, Abcam, ab15580) and anti-Cleaved-Caspase3 (1:100, Cell signaling technologies, 9661). F-actin was labeled using Phalloidin (1:150, Alexa Fluo 633, Invitrogen, A22284) and DNA was detected using Dapi (1:500).

Immunofluorescence images were acquired using an Inverted Laser Scanning Confocal LSM880NLO Zeiss microscope equipped with spectral detection confocal head. We used laser lines 405, 488, 561 and 633nm and the following objectives: 25x/0,8 OIL, W, Gly LD LCI PL APO (UV) VIS-IR, 40x/1,3 OIL DICII PL APO (UV) VIS-IR and 63x/1,4 OIL DICII PL APO. Images were processed using ImageJ (NIH).

- **Immunofluorescence of 3D collagen assay**

Spheroids embedded in collagen were fixed using 4% paraformaldehyde (PFA) in PBS for 30min at RT. Spheroids were then washed with PBS and permeabilized with 0.1% Triton X-100 in PBS for 30min at RT. DNA and F-actin were stained using DAPI and Phalloidin respectively (Life Technologies). Collagen was imaged using confocal reflection microscopy.

- **Immunofluorescence of tumoroids invasion**

Basement membranes with invading tumoroids were washed with PBS for 5 min and fixed in 4% paraformaldehyde for 40 min. They were permeabilized in PBS 1% Triton for 30min and washed in PBS for 5 min. Primary antibody was incubated overnight at 4°C and then washed 3 times for 15min at RT. Secondary antibody was incubated for 4h at RT. DAPI 1/1000 and Phalloidin (rhodamine, 1/200) were added to the secondary antibody mix. After 3 washes of 15min, the samples were mounted on a Fluorodish with Polymount medium (Polysciences). We used one Polymount drop on the bottom of the glass dish and one drop on the top of the basement membrane. Samples were kept in the dark at 4°C.

EdU incorporation study

For this study, NICD/p53^{-/-} or NICD/Tom/p53^{-/-} tumor bearing mice were used. Three mice were intraperitoneally injected with 100μm of EdU at 10mM and sacrificed 3 hours later (*in vivo* EdU condition). Tumors were sliced and EdU incorporation was revealed using a standard procedure (Click-iT EdU Alexa Fluor 647 kit, Invitrogen). Six other mice were sacrificed and tumors were sliced to 250μm-thick slices using a vibratome (Leica VT1000S). Slices were incubated as described above and 10μM EdU was added to the medium for hours 0-3h or 21-24h, with 3 mice per condition. Following incubation, EdU was revealed using a standard protocol.

Quantification of the percentage of cleaved-caspase3 areas

Stitched images of entire thin tissue slices (approximately 3mm x 2mm) were acquired using an Inverted Laser Scanning Confocal LSM880NLO Zeiss microscope (25x/0,8 OIL, W, Gly LD LCI PL APO (UV) VIS-IR objective) for DAPI and Cleaved-caspase3 (CC3) channels. Stitching was performed using the ZEN software (Carl Zeiss). Following z-projection, channels were filtered (Gaussian) and thresholded. The ratio of CC3 area to DAPI area was calculated for two separate slices from three different mice, at three different depths from the surface (0, 50 and 100 μ m), at 0h and after 24h of culturing.

Installation of the imaging window for intravital imaging

Surgery and installation of the intestinal imaging window was done as previously described (Ritsma, Ellenbrook). Mouse with a tumor was anesthetized with isoflurane during the surgery and imaging. Prior to surgery, analgesic buprenorphine was injected IP (Buprecare). Gel (Civigel) was applied to the eyes of the mouse to avoid dehydration. The mouse was lying on her right flank. The left side of the abdomen was shaved and cleaned with antiseptic (Betadine). A small incision was done on the skin and muscle on the right side of the abdomen. Using a needle holder, a purse-string suture was made that surrounded the incision through the abdominal wall and skin with non-absorbable threads. We used the same intestinal optical windows as the ones described by Ritsma et al. The intestinal tumor was put close to the imaging window. The mesentery close to the tumor was immobilized on a small portion of the glass coverslip using glue (Superglue). The tumor was then put inside the imaging window and pressed close to the coverslip. A little bit of surgical glue was applied on the inner ring of the imaging window and the intestine surrounding the tumor was glued on it. The intestine and mesentery that were in the imaging window were covered with a thermoresversible transparent gel (CyGel) in order to allow for a more thorough immobilization of the tissue. The imaging window was placed in the incision on the abdomen of the mouse and the skin and muscle were put in the inner groove of the ring of the window. Threads were gently pulled, allowing for the suture of the skin and muscle around the window. Mice were directly imaged and kept in a conventional animal facility with daily check-up and regular analgesia.

Rheological measurements of collagen gels

The samples were prepared on ice to prevent early polymerization of collagen. First, collagen was pipetted into an Eppendorf tube and weighed to determine the volume of the final solution. Samples were prepared to have a final collagen concentration of 2 mg/ml, in phosphate buffer saline (PBS) and pH set to 7 with addition of NaOH and topped up to the final volume with DMEM.

Rheology tests were performed on an Anton Paar Physica MCR 501 rheometer, with a stainless steel 30 mm diameter and 1° truncation angle cone-plate geometry (CP30-1). The plates were heated to 37° before loading the sample. Water was added to the solvent trap to maintain a moist environment. 20 minutes after loading the sample, a solution of either pure DMEM, or DMEM supplemented with 1-10mM ribose or 1mM threose was placed around the geometry and allowed to diffuse in the sample for 48 hours. To prevent evaporation during the measurement, a layer of mineral oil was further added around the measuring geometry. During the whole 48h, the elastic and viscous moduli of the network were probed by applying an oscillatory deformation with 0.5% strain amplitude and a frequency of 0.5 Hz. Results show the values of elastic and viscous moduli after 48 hours, averaged over at least three different independent repeats, while the error reported is the standard error of the mean.

Cell adhesion assay

CT26 cells were pre-treated for two days with 1mM of threose or no threose in DMEM supplemented with 10% FBS and 1% AA. 50µL of collagen (2m/mL) was polymerized in 96-well plates and was pre-treated for two days with 1mM of threose or no threose in DMEM and 1% AA. After two days, CT26 cells were stained with CellTracker™ Red CMTPX Dye (ThermoFisher) and 2.105 cells were seeded per well in the 96-well plate. Cells were then incubated at 37°C for 5min, 15min, 30min, 1h or 2h and washed three times to remove non-adherent cells. Fluorescence intensity was measured using a FluoStar fluorescence plate reader (BMG Labtech). Adhesion was represented as the percentage of adherent cells per condition. Collagen topography measurements Fibers alignment and their angles with respect to the spheroid edge were measured on images acquired using reflection microscopy with the available software CurveAlign (UW-Madison;

<http://loci.wisc.edu/software/curvealign>) in MatLab. The angles of collagen fibers compared to the spheroid edge were determined for 7-8 slices per condition.

Traction force microscopy

Traction force microscopy was conducted as previously described (Elkhatib et al., 2014). 35mm glass-bottom cell culture dishes (FluoroDish, World Precision Instruments) were silanized with (3-aminopropyl)trimethoxysilane (Sigma-Aldrich) for 15min and extensively washed with water. The glass surface of the dishes was treated with 0.5% glutaraldehyde (Electron Microscopy sciences) for 30min and extensively washed with water. Acrylamide 40% (93.3 μ L) and 2% bisacrylamide (11 μ L) were mixed in PBS solution to a final volume of 500 μ L to achieve a Young's modulus of 5 kPa. For traction force measurements, FluoSphere bead solution (0.2 μ m, 580/605 nm; Invitrogen) was added at 2% volume. Polymerization was initiated by addition of 2.5 μ L ammonium persulfate (10% w/v solution) and 0,25 μ L of N,N,N',N'-tetramethylethane-1,2-diamine (TEMED). 12 μ L of the polyacrylamide solution was rapidly deposited onto the glass-bottom dish and covered with a 18mm coverslip. After one hour PBS was added to the dishes for 10min and the coverslips were gently removed under PBS. To allow for collagen coating, the gel surface was activated using Sulfo-SANPAH (1mg/mL, ThermoFisher) that was photoactivated by UV (365nm) for 10min. After 3 washes with HEPES and PBS, the gels were coated with monomeric collagen (100 μ g/mL) overnight at 4°C. The next day gels were washed 3 times with PBS. CT26 cells were pre-treated for 1 day with +/- 1mM threose prior to seeding on the gels. 1.104 CT26 cells were plated per gel in DMEM supplemented with 10% FBS, 2% AA, +/- 1mM threose and cultured on the gels one additional day, thus allowing for a total two-day incubation with +/- threose.

To image traction force experiments, we used an Inverted Nikon Ti-E microscope equipped with a sCMOS 2048 ORCA Flash4.0 V2 camera (Hamamatsu) and a 40x Plan Fluor dry objective (0.75 NA; Nikon). A fluorescent image of the FluoSphere beads and a phase contrast image of the cells were acquired. At the end of the acquisition cells were detached from the gels using 0.5% Trypsin-EDTA (Gibco) and a reference image without cells was recorded. We used a previously described correlation algorithm to extract the bead displacement fields. Traction force was determined using the Fourier transform

traction force algorithm, as introduced by (Butler et al., 2002). To quantify the force applied by a cell, we measured the strain energy that corresponds to the energy the cell exerts to deform the substrate, which is proportional to the average force applied by a cell.

Statistical analysis

Statistical analysis was performed using Python, using the scipy and astropy packages, and GraphPad (Prism).

CHAPTER 5

BIBLIOGRAPHY

- Abate, A. R. and Durian, D. J. (2007) 'Topological persistence and dynamical heterogeneities near jamming', *Physical Review E - Statistical, Nonlinear, and Soft Matter Physics*, 76(2), pp. 1–9. doi: 10.1103/PhysRevE.76.021306.
- Abercrombie, M. (1961) 'The bases of the locomotory behaviour of fibroblasts', *Experimental Cell Research*, 8(SUPPL.), pp. 188–198. doi: 10.1016/0014-4827(61)90348-2.
- Abercrombie, M., Heaysman, J. E. M. and Pegrum, S. M. (1970) 'The locomotion of fibroblasts in culture II. "Ruffling"', *Experimental Cell Research*, 60, pp. 437–444. Available at: <https://api-istex-fr.insb.bib.cnrs.fr/document/16F992E701AB8723024310B960A4137C11426FD1/fulltext/pdf?auth=ip,fede&sid=ebSCO> (Accessed: 1 June 2017).
- Acerbi, I. *et al.* (2015) 'Human breast cancer invasion and aggression correlates with ECM stiffening and immune cell infiltration', *Integrative Biology (United Kingdom)*, 7(10), pp. 1120–1134. doi: 10.1039/c5ib00040h.
- Alberts, B. *et al.* (2014) *Molecular Biology of the Cell 6e*, Garland Science. doi: 10.1002/1521-3773(20010316)40:6<9823::AID-ANIE9823>3.3.CO;2-C.
- Alexander, S. *et al.* (2008) 'Dynamic imaging of cancer growth and invasion: a modified skin-fold chamber model', *Histochemistry and Cell Biology*, 130(6), pp. 1147–1154. doi: 10.1007/s00418-008-0529-1.
- Alexander, S. *et al.* (2013) 'Preclinical intravital microscopy of the tumour-stroma interface : invasion , metastasis , and therapy response Intrinsic contrast', *Current Opinion in Cell Biology*. Elsevier Ltd, 25(5), pp. 659–671. doi: 10.1016/j.ceb.2013.07.001.
- Angelini, T. E. *et al.* (2011) 'Glass-like dynamics of collective cell migration.', *Proceedings of the National Academy of Sciences of the United States of America*. National Academy of Sciences, 108(12), pp. 4714–9. doi: 10.1073/pnas.1010059108.
- Aoki, K. *et al.* (2003) 'Colonic polyposis caused by mTOR-mediated chromosomal instability in Apc+/ Δ 716Cdx2+/-compound mutant mice', *Nature Genetics*, 35(4), pp. 323–330. doi: 10.1038/ng1265.
- Argraves, W. S. *et al.* (2003) 'Fibulins: Physiological and disease perspectives', *EMBO Reports*, 4(12), pp. 1127–1131. doi: 10.1038/sj.embor.7400033.
- Ariffin, A. B. *et al.* (2014) 'Releasing pressure in tumors: What do we know so far and where do we go from here a review', *Cancer Research*, 74(10), pp. 2655–2662. doi: 10.1158/0008-5472.CAN-13-3696.
- Artavanis-Tsakonas, S., Rand, M. D. and Lake, R. J. (1999) 'Notch signaling: cell fate control and signal integration in development.', *Science (New York, N.Y.)*, 284(1999), pp. 770–776. doi: 10.1126/science.284.5415.770.
- Astbury, W. T. and Woods, H. J. (1934) 'X-Ray Studies of the Structure of Hair, Wool, and Related Fibres. II. The Molecular Structure and Elastic Properties of Hair Keratin', *Philosophical Transactions of the Royal Society A: Mathematical, Physical and Engineering Sciences*, 232(707–720), pp. 333–394. doi: 10.1098/rsta.1934.0010.
- Atia, L. *et al.* (2018) 'Geometric constraints during epithelial jamming', *Nature Physics*. Springer US, 14(6), pp. 613–620. doi: 10.1038/s41567-018-0089-9.

- Attieh, Y. *et al.* (2017) 'Cancer-associated fibroblasts lead tumor invasion through integrin-beta3-dependent fibronectin assembly', *The Journal of cell biology*, 216(11), pp. 1–12. doi: 10.1083/jcb.201702033.
- Attieh, Y. and Vignjevic, D. M. (2016) 'The hallmarks of CAFs in cancer invasion', *European Journal of Cell Biology*. Elsevier GmbH., 95(11), pp. 493–502. doi: 10.1016/j.ejcb.2016.07.004.
- Baeriswyl, V. and Christofori, G. (2008) 'The angiogenic switch in tumorigenesis', *Tumor Angiogenesis: Basic Mechanisms and Cancer Therapy*, 19, pp. 67–88. doi: 10.1007/978-3-540-33177-3_4.
- Baker, S. J. *et al.* (1990) 'p53 Gene Mutations Occur in Combination with 17p Allelic Deletions as Late Events in Colorectal Tumorigenesis', *Cancer Research*, 50(23), pp. 7717–7722. doi: 10.1158/0008-5472.can-10-4563.
- Baluk, P. *et al.* (2003) 'Abnormalities of Basement Membrane on Blood Vessels and Endothelial Sprouts in Tumors', *American Journal of Pathology*. American Society for Investigative Pathology, 163(5), pp. 1801–1815. doi: 10.1016/S0002-9440(10)63540-7.
- Barker, H. E. *et al.* (2013) 'Tumor-Secreted LOXL2 Activates Fibroblasts through FAK Signaling', *Molecular Cancer Research*, 11(11), pp. 1425–1436. doi: 10.1158/1541-7786.MCR-13-0033-T.
- Barker, N. (2014) 'Adult intestinal stem cells: Critical drivers of epithelial homeostasis and regeneration', *Nature Reviews Molecular Cell Biology*. Nature Publishing Group, 15(1), pp. 19–33. doi: 10.1038/nrm3721.
- Beaune, G. *et al.* (2014) 'How cells flow in the spreading of cellular aggregates', *Proceedings of the National Academy of Sciences*, 111(22), pp. 8055–8060. doi: 10.1073/pnas.1323788111.
- Becker, C., Fantini, M. C. and Neurath, M. F. (2007) 'High resolution colonoscopy in live mice', *Nature Protocols*, 1(6), pp. 2900–2904. doi: 10.1038/nprot.2006.446.
- Bert Vogelstein, *et al.* (1981) 'Genetic alterations during colorectal-tumor development'.
- Bettenworth, D. *et al.* (2016) 'Endoscopy-guided orthotopic implantation of colorectal cancer cells results in metastatic colorectal cancer in mice', *Clinical & Experimental Metastasis*, 33(6), pp. 551–562. doi: 10.1007/s10585-016-9797-7.
- Biroli, G. (2007) 'A new kind of phase transition?', *Nature Physics*, 3(April), pp. 222–223.
- Bissell, M. J. and Hines, W. C. (2011) 'Why don't we get more cancer? A proposed role of the microenvironment in restraining cancer progression', *Nature Medicine*. Nature Publishing Group, 17(3), pp. 320–329. doi: 10.1038/nm.2328.
- Bonnans, C., Chou, J. and Werb, Z. (2014) 'Remodelling the extracellular matrix in development and disease', *Nature Reviews Molecular Cell Biology*. Nature Publishing Group, 15(12), pp. 786–801. doi: 10.1038/nrm3904.
- Bordeleau, F. *et al.* (2017) 'Matrix stiffening promotes a tumor vasculature phenotype', *Proceedings of the National Academy of Sciences*, 114(3), pp. 492–497. doi: 10.1073/pnas.1613855114.
- Brabletz, T. *et al.* (2001) 'Variable b-catenin expression in colorectal cancers indicates

- tumor progression driven by the tumor environment', *Proceedings of the National Academy of Sciences*, 98(18), pp. 10356–10361. doi: 10.1073/pnas.171610498.
- Bray, S. J. (2006) 'Notch signalling: A simple pathway becomes complex', *Nature Reviews Molecular Cell Biology*, 7(9), pp. 678–689. doi: 10.1038/nrm2009.
- Brinckmann, J. (2005) 'Collagens at a glance', *Topics in Current Chemistry*, 247, pp. 1–6. doi: 10.1007/b103817.
- Bruckner, P. (2010) 'Suprastructures of extracellular matrices: Paradigms of functions controlled by aggregates rather than molecules', *Cell and Tissue Research*, 339(1), pp. 7–18. doi: 10.1007/s00441-009-0864-0.
- Butcher, D. T., Alliston, T. and Weaver, V. M. (2009) 'A tense situation: Forcing tumour progression', *Nature Reviews Cancer*, 9(2), pp. 108–122. doi: 10.1038/nrc2544.
- Cabodi, S. *et al.* (2006) 'p130Cas as a new regulator of mammary epithelial cell proliferation, survival, and HER2-Neu oncogene- dependent breast tumorigenesis', *Cancer Research*, 66(9), pp. 4672–4680. doi: 10.1158/0008-5472.CAN-05-2909.
- Calandrini, V. *et al.* (2011) 'nMoldyn - Interfacing spectroscopic experiments, molecular dynamics simulations and models for time correlation functions', *École thématique de la Société Française de la Neutronique*. EDP Sciences, 12, pp. 201–232. doi: 10.1051/sfn/201112010.
- Calvo, F. *et al.* (2013) 'Mechanotransduction and YAP-dependent matrix remodelling is required for the generation and maintenance of cancer-associated fibroblasts', *Nat Cell Biol.* Nature Publishing Group, 15(6), pp. 637–646. doi: ncb2756 [pii]\n10.1038/ncb2756.
- Canel, M. *et al.* (2010) 'Quantitative In vivo Imaging of the Effects of Inhibiting Integrin Signaling via Src and FAK on Cancer Cell Movement : Effects on E-cadherin Dynamics', pp. 9413–9423. doi: 10.1158/0008-5472.CAN-10-1454.
- Carey, S. P., Martin, K. E. and Reinhart-King, C. A. (2017) 'Three-dimensional collagen matrix induces a mechanosensitive invasive epithelial phenotype', *Scientific Reports*. Nature Publishing Group, 7(February), pp. 1–14. doi: 10.1038/srep42088.
- Carmeliet, P. (2005) 'Angiogenesis in life, disease and medicine', *Nature*, 438(7070), pp. 932–936. doi: 10.1038/nature04478.
- Carrel, A. and Burrows, M. T. (1911) 'Cultivation of Tissues in Vitro and Its Technique', *The Journal of experimental medicine*, XIII(4), pp. 387–406. doi: 10.1084/jem.13.3.387.
- Chambers, A. F., Groom, A. C. and MacDonald, I. C. (2002) 'Dissemination and growth of cancer cells in metastatic sites.', *Nature reviews. Cancer*, 2(8), pp. 563–72. doi: 10.1038/nrc865.
- Chanrion, M. *et al.* (2014) 'Concomitant Notch activation and p53 deletion trigger epithelial-to-mesenchymal transition and metastasis in mouse gut', *Nature Communications*, 5, p. 5005. doi: 10.1038/ncomms6005.
- Chiquet-Ehrismann, R. *et al.* (1986) 'Tenascin: an extracellular matrix protein involved in tissue interactions during fetal development and oncogenesis.', *Cell*, 47(1), pp. 131–9. doi: 10.1016/0092-8674(86)90374-0.

- Chiquet-Ehrismann, R. *et al.* (2014) 'Tenascins in stem cell niches', *Matrix Biology. International Society of Matrix Biology*, 37, pp. 112–123. doi: 10.1016/j.matbio.2014.01.007.
- Christiansen, J. J. and Rajasekaran, A. K. (2006) 'Reassessing epithelial to mesenchymal transition as a prerequisite for carcinoma invasion and metastasis', *Cancer Research*, 66(17), pp. 8319–8326. doi: 10.1158/0008-5472.CAN-06-0410.
- Clark, A. G. and Vignjevic, D. M. (2015) 'Modes of cancer cell invasion and the role of the microenvironment', *Current Opinion in Cell Biology*. Elsevier Ltd, 36, pp. 13–22. doi: 10.1016/j.ceb.2015.06.004.
- Clevers, H. (2013) 'The intestinal crypt, a prototype stem cell compartment', *Cell*. Elsevier Inc., 154(2), pp. 274–284. doi: 10.1016/j.cell.2013.07.004.
- Colnot, S. *et al.* (1998) 'Intestinal Expression of the Calbindin-D9K Gene in Transgenic Mice', 273(48), pp. 31939–31946.
- Colpaert, C. G. *et al.* (2003) 'The presence of a fibrotic focus in invasive breast carcinoma correlates with the expression of carbonic anhydrase IX and is a marker of hypoxia and poor prognosis', *Breast Cancer Research and Treatment*, 81(2), pp. 137–147. doi: 10.1023/A:1025702330207.
- Conklin, M. W. and Keely, P. J. (2012) 'Why the stroma matters in breast cancer', (June), pp. 249–260.
- Costell, M. *et al.* (1999) 'Perlecan maintains the integrity of cartilage and some basement membranes', *Journal of Cell Biology*, 147(5), pp. 1109–1122. doi: 10.1083/jcb.147.5.1109.
- Cox, T. R. and Ertler, J. T. (2011) 'Remodeling and homeostasis of the extracellular matrix: implications for fibrotic diseases and cancer', *Disease Models & Mechanisms*, 4(2), pp. 165–178. doi: 10.1242/dmm.004077.
- Cunningham, D. *et al.* (2010) 'Colorectal cancer', *The Lancet*. Elsevier Ltd, 375(9719), pp. 1030–1047. doi: 10.1016/S0140-6736(10)60353-4.
- Van Cutsem, E. *et al.* (2006) 'Towards a pan-European consensus on the treatment of patients with colorectal liver metastases.', *European journal of cancer*, 42(14), pp. 2212–2221. doi: 10.1016/j.ejca.2006.04.012.
- Denais, C. M. *et al.* (2016) 'Nuclear envelope rupture and repair during cancer cell migration', *Science*, 352(6283), pp. 353–358. doi: 10.1126/science.aad7297.
- DeNardo, D. G., Andreu, P. and Coussens, L. M. (2010) 'Interactions between lymphocytes and myeloid cells regulate pro-versus anti-tumor immunity', *Cancer and Metastasis Reviews*, 29(2), pp. 309–316. doi: 10.1007/s10555-010-9223-6.
- Deryugina, E. I. *et al.* (2017) 'Intratumoral Cancer Cell Intravasation Can Occur Independent of Invasion into the Adjacent Stroma Article Intratumoral Cancer Cell Intravasation Can Occur Independent of Invasion into the Adjacent Stroma', *CellReports*. ElsevierCompany., 19(3), pp. 601–616. doi: 10.1016/j.celrep.2017.03.064.
- Dickinson, R. B., Guido, S. and Tranquillo, R. T. (1994) 'Biased cell migration of fibroblasts exhibiting contact guidance in oriented collagen gels', *Annals of Biomedical Engineering*, 22(4), pp. 342–356. doi: 10.1007/BF02368241.

- Discher, D. E. (2005) 'Tissue Cells Feel and Respon to the Stiffness of Their Substrate', *Science*, 310(5751), pp. 1139–1143. doi: 10.1126/science.1116995.
- Edelmann, W. *et al.* (1999) 'Tumorigenesis in Mlh1 and Mlh1 / Apc1638N Mutant Mice', *Cancer Research*, 59, pp. 1301–1307.
- Egeblad, M., Rasch, M. G. and Weaver, V. M. (2010) 'Dynamic interplay between the collagen scaffold and tumor evolution', *Current Opinion in Cell Biology*. Elsevier Ltd, 22(5), pp. 697–706. doi: 10.1016/j.ceb.2010.08.015.
- Ellisen, L. W. *et al.* (1991) 'TAN-1, the human homolog of the Drosophila Notch gene, is broken by chromosomal translocations in T lymphoblastic neoplasms', *Cell*, 66(4), pp. 649–661. doi: 10.1016/0092-8674(91)90111-B.
- Engler, A. J. *et al.* (2006) 'Matrix Elasticity Directs Stem Cell Lineage Specification', *Cell*, 126(4), pp. 677–689. doi: 10.1016/j.cell.2006.06.044.
- Erickson, H. P. (2017) 'Protein unfolding under isometric tension — what force can integrins generate, and can it unfold FNIII domains?', *Current Opinion in Structural Biology*. Elsevier Ltd, 42, pp. 98–105. doi: 10.1016/j.sbi.2016.12.002.
- Erler, J. T. *et al.* (2006) 'Lysyl oxidase is essential for hypoxia-induced metastasis', *Nature*, 440(7088), pp. 1222–1226. doi: 10.1038/nature04695.
- Van Es, J. H. *et al.* (2005) 'Notch/ γ -secretase inhibition turns proliferative cells in intestinal crypts and adenomas into goblet cells', *Nature*, 435(7044), pp. 959–963. doi: 10.1038/nature03659.
- Ewald, A. J., Werb, Z. and Egeblad, M. (2011) 'Preparation of mice for long-term intravital imaging of the mammary gland', *Cold Spring Harbor Protocols*, 6(2). doi: 10.1101/pdb.prot5562.
- Fackler, O. T. and Grosse, R. (2008) 'Cell motility through plasma membrane blebbing', *Journal of Cell Biology*, 181(6), pp. 879–884. doi: 10.1083/jcb.200802081.
- Faix, J. and Rottner, K. (2006) 'The making of filopodia', *Current Opinion in Cell Biology*, 18(1), pp. 18–25. doi: 10.1016/j.ceb.2005.11.002.
- Feil, S., Valtcheva, N. and Feil, R. (2009) 'Inducible Cre Mice', 530(March 2015). doi: 10.1007/978-1-59745-471-1.
- Ferlay, J. *et al.* (2015) 'Cancer incidence and mortality worldwide: Sources, methods and major patterns in GLOBOCAN 2012', *International Journal of Cancer*, 136(5), pp. E359–E386. doi: 10.1002/ijc.29210.
- Fidler, A. L. *et al.* (2017) 'Collagen iv and basement membrane at the evolutionary dawn of metazoan tissues', *eLife*, 6, pp. 1–24. doi: 10.7554/eLife.24176.001.
- Fodde, R. *et al.* (1994) 'A targeted chain-termination mutation in the mouse Apc gene results in multiple intestinal tumors.', *Proceedings of the National Academy of Sciences of the United States of America*, 91(19), pp. 8969–73. doi: 10.1073/pnas.91.19.8969.
- Francis-Sedlak, M. E. *et al.* (2009) 'Characterization of type I collagen gels modified by glycation', *Biomaterials*. Elsevier Ltd, 30(9), pp. 1851–1856. doi: 10.1016/j.biomaterials.2008.12.014.

- Frantz, C., Stewart, K. M. and Weaver, V. M. (2010) 'The extracellular matrix at a glance', *Journal of Cell Science*, 123(24), pp. 4195–4200. doi: 10.1242/jcs.023820.
- Fre, S. *et al.* (2005) 'Notch signals control the fate of immature progenitor cells in the intestine.', *Nature*, 435(7044), pp. 964–8. doi: 10.1038/nature03589.
- Friedl, P. *et al.* (2012) 'Classifying collective cancer cell invasion', *Nature Cell Biology*. Nature Publishing Group, 14(8), pp. 777–783. doi: 10.1038/ncb2548.
- Friedl, P. and Alexander, S. (2011) 'Cancer invasion and the microenvironment: Plasticity and reciprocity', *Cell*. Elsevier Inc., 147(5), pp. 992–1009. doi: 10.1016/j.cell.2011.11.016.
- Friedl, P. and Gilmour, D. (2009) 'Collective cell migration in morphogenesis, regeneration and cancer', *Nature Reviews Molecular Cell Biology*. Nature Publishing Group, 10(7), pp. 445–457. doi: 10.1038/nrm2720.
- Friedl, P. and Wolf, K. (2003) 'Tumour-cell invasion and migration: diversity and escape mechanisms', *Nature Reviews Cancer*. Nature Publishing Group, 3(5), pp. 362–374. doi: 10.1038/nrc1075.
- Friedl, P. and Wolf, K. (2010) 'Plasticity of cell migration: A multiscale tuning model', *Journal of Cell Biology*, 188(1), pp. 11–19. doi: 10.1083/jcb.200909003.
- Fumagalli, A. *et al.* (2017) 'Genetic dissection of colorectal cancer progression by orthotopic transplantation of engineered cancer organoids'. doi: 10.1073/pnas.1701219114.
- Gaggioli, C. *et al.* (2007) 'Fibroblast-led collective invasion of carcinoma cells with differing roles for RhoGTPases in leading and following cells.', *Nature cell biology*, 9(12), pp. 1392–1400. doi: 10.1038/ncb1658.
- Garber, K. (2007) 'Notch emerges as new cancer drug target.', *Journal of the National Cancer Institute*, 99(17), pp. 1284–1285. doi: 10.1093/jnci/djm148.
- Garcia, S. *et al.* (2015) 'Physics of active jamming during collective cellular motion in a monolayer', *Proceedings of the National Academy of Sciences*, 112(50), pp. 15314–15319. doi: 10.1073/pnas.1510973112.
- Gardel, M. L. *et al.* (2010) 'Mechanical Integration of Actin and Adhesion Dynamics in Cell Migration', *Annual Review of Cell and Developmental Biology*, 26(1), pp. 315–333. doi: 10.1146/annurev.cellbio.011209.122036.
- Garrahan, J. P. (2011) 'Dynamic heterogeneity comes to life', *Proceedings of the National Academy of Sciences*, 108(12), pp. 4701–4702. doi: 10.1073/pnas.1101436108.
- Gaudet, C. *et al.* (2003) 'Influence of Type I Collagen Surface Density on Fibroblast Spreading, Motility, and Contractility', *Biophysical Journal*. Elsevier, 85(5), pp. 3329–3335. doi: 10.1016/S0006-3495(03)74752-3.
- Geiger, B., Spatz, J. P. and Bershadsky, A. D. (2009) 'Environmental sensing through focal adhesions', *Nature Reviews Molecular Cell Biology*, 10(1), pp. 21–33. doi: 10.1038/nrm2593.
- Geiger, B. and Yamada, K. M. (2011) '10. Molecular Architecture and Function of', pp. 1–22. doi: 10.1101/cshperspect.a005033.

- Georges, P. C. *et al.* (2007) 'Increased stiffness of the rat liver precedes matrix deposition: implications for fibrosis', *AJP: Gastrointestinal and Liver Physiology*, 293(6), pp. G1147–G1154. doi: 10.1152/ajpgi.00032.2007.
- Geraldo, S. *et al.* (2012) 'Do cancer cells have distinct adhesions in 3D collagen matrices and in vivo?', *European Journal of Cell Biology*. Elsevier GmbH, 91(11–12), pp. 930–937. doi: 10.1016/j.ejcb.2012.07.005.
- Giannone, G. and Sheetz, M. P. (2006) 'Substrate rigidity and force define form through tyrosine phosphatase and kinase pathways', *Trends in Cell Biology*, 16(4), pp. 213–223. doi: 10.1016/j.tcb.2006.02.005.
- Giblin, S. P. and Midwood, K. S. (2015) 'Tenascin-C: Form versus function', *Cell Adhesion and Migration*, 9(1–2), pp. 48–82. doi: 10.4161/19336918.2014.987587.
- Gibson, M. A. *et al.* (1986) 'The major antigen of elastin-associated microfibrils is a 31-kDa glycoprotein', *Journal of Biological Chemistry*, 261(24), pp. 11429–11436.
- Glentis, A. *et al.* (2017) 'Cancer-associated fibroblasts induce metalloprotease-independent cancer cell invasion of the basement membrane', *Nature Communications*. Nature Publishing Group, 8(1), p. 924. doi: 10.1038/s41467-017-00985-8.
- Glentis, A., Gurchenkov, V. and Vignjevic, D. M. (2014) 'Assembly, heterogeneity, and breaching of the basement membranes', *Cell Adhesion and Migration*, 8(3), pp. 236–245. doi: 10.4161/cam.28733.
- Gligorijevic, B. *et al.* (2012) 'N-WASP-mediated invadopodium formation is involved in intravasation and lung metastasis of mammary tumors', pp. 724–734. doi: 10.1242/jcs.092726.
- Gligorijevic, B. *et al.* (2014) 'Multiparametric Classification Links Tumor Microenvironments with Tumor Cell Phenotype', *PLoS Biology*. Edited by L. Machesky. Public Library of Science, 12(11), p. e1001995. doi: 10.1371/journal.pbio.1001995.
- Gligorijevic, B., Bergman, A. and Condeelis, J. (2014) 'Multiparametric Classification Links Tumor Microenvironments with Tumor Cell Phenotype', *PLoS Biology*, 12(11). doi: 10.1371/journal.pbio.1001995.
- Goetz, J. G. *et al.* (2011) 'Biomechanical remodeling of the microenvironment by stromal caveolin-1 favors tumor invasion and metastasis', *Cell*, 146(1), pp. 148–163. doi: 10.1016/j.cell.2011.05.040.
- Gracz, A. D. and Magness, S. T. (2014) 'Defining hierarchies of stemness in the intestine: evidence from biomarkers and regulatory pathways', *AJP: Gastrointestinal and Liver Physiology*, 307(3), pp. G260–G273. doi: 10.1152/ajpgi.00066.2014.
- Grivennikov, S. I., Greten, F. R. and Karin, M. (2010) 'Immunity, Inflammation, and Cancer', *Cell*. Elsevier Inc., 140(6), pp. 883–899. doi: 10.1016/j.cell.2010.01.025.
- Guck, J. *et al.* (2005) 'Optical deformability as an inherent cell marker for testing malignant transformation and metastatic competence', *Biophysical Journal*, 88(5), pp. 3689–3698. doi: 10.1529/biophysj.104.045476.
- Haggar, F. a, Boushey, R. P. and Ph, D. (2009) 'Colorectal Cancer Epidemiology : Incidence , Mortality , Survival , and Risk Factors', *Clinics in colon and rectal surgery*, 6(212), pp. 191–

197. doi: 10.1055/s-0029-1242458.

Halfter, W. *et al.* (2013) 'Protein composition and biomechanical properties of in vivo-derived basement membranes', *Cell Adhesion and Migration*, 7(1), pp. 64–71. doi: 10.4161/cam.22479.

Hamidi, H. and Ivaska, J. (2018) 'Every step of the way: integrins in cancer progression and metastasis', *Nature Reviews Cancer*. Springer US, pp. 1–16. doi: 10.1038/s41568-018-0038-z.

Han, C. *et al.* (2011) 'D-ribose induces cellular protein glycation and impairs mouse spatial cognition', *PLoS ONE*, 6(9). doi: 10.1371/journal.pone.0024623.

Hanahan, D. and Folkman, J. (1996) 'Patterns and emerging mechanisms of the angiogenic switch during tumorigenesis', *Cell*, 86(3), pp. 353–364. doi: 10.1016/S0092-8674(00)80108-7.

Hanahan, D. and Weinberg, R. A. (2011) 'Hallmarks of cancer: The next generation', *Cell*. Elsevier Inc., 144(5), pp. 646–674. doi: 10.1016/j.cell.2011.02.013.

Harada, N. *et al.* (1999) 'Intestinal polyposis in mice with a dominant stable mutation of the β -catenin gene', *EMBO Journal*, 18(21), pp. 5931–5942. doi: 10.1093/emboj/18.21.5931.

Harada, T. *et al.* (2014) 'Nuclear lamin stiffness is a barrier to 3D migration, but softness can limit survival', *Journal of Cell Biology*, 204(5), pp. 669–682. doi: 10.1083/jcb.201308029.

Harley, B. A. C. *et al.* (2008) 'Microarchitecture of three-dimensional scaffolds influences cell migration behavior via junction interactions', *Biophysical Journal*. The Biophysical Society, 95(8), pp. 4013–4024. doi: 10.1529/biophysj.107.122598.

Harrison, R. G. (1910) 'The outgrowth of the nerve fiber as a mode of protoplasmic movement', *Journal of Experimental Zoology*, 9(4), pp. 787–846. doi: 10.1002/jez.1400090405.

Haston, W. S., Shields, J. M. and Wilkinson, P. C. (1982) 'Lymphocyte locomotion and attachment on two-dimensional surfaces and in three-dimensional matrices', *Journal of Cell Biology*, 92(3), pp. 747–752. doi: 10.1083/jcb.92.3.747.

He, X. C. *et al.* (2007) 'PTEN-deficient intestinal stem cells initiate intestinal polyposis', *Nature Genetics*, 39(2), pp. 189–198. doi: 10.1038/ng1928.

Van Helvert, S., Storm, C. and Friedl, P. (2018) 'Mechanoreciprocity in cell migration', *Nature Cell Biology*. Springer US, 20(1), pp. 8–20. doi: 10.1038/s41556-017-0012-0.

Hinz, B. *et al.* (2001) 'Alpha-Smooth Muscle Actin Expression Upregulates Fibroblast Contractile Activity', *Molecular Biology of the Cell*, 12(9), pp. 2730–2741. doi: 10.1091/mbc.12.9.2730.

Hotary, K. *et al.* (2006) 'A cancer cell metalloprotease triad regulates the basement membrane transmigration program', *Genes and Development*, 20(19), pp. 2673–2686. doi: 10.1101/gad.1451806.

Hynes, R. O. (2009) 'Extracellular matrix: not just pretty fibrils', 326(November), pp. 1216–1220.

- Hynes, R. O. (2012) 'The evolution of metazoan extracellular matrix', *Journal of Cell Biology*, 196(6), pp. 671–679. doi: 10.1083/jcb.201109041.
- Hynes, R. O. and Naba, A. (2012) 'Overview of the matrisome-An inventory of extracellular matrix constituents and functions', *Cold Spring Harbor Perspectives in Biology*, 4(1). doi: 10.1101/cshperspect.a004903.
- Iozzo, R. V., Zoeller, J. J. and Nyström, A. (2009) 'Basement membrane proteoglycans: Modulators Par Excellence of cancer growth and angiogenesis', *Molecules and Cells*, 27(5), pp. 503–513. doi: 10.1007/s10059-009-0069-0.
- Isenberg, B. C. *et al.* (2009) 'Vascular smooth muscle cell durotaxis depends on substrate stiffness gradient strength', *Biophysical Journal*. Biophysical Society, 97(5), pp. 1313–1322. doi: 10.1016/j.bpj.2009.06.021.
- Janssen, K. P. *et al.* (2002) 'Targeted expression of oncogenic K-ras in intestinal epithelium causes spontaneous tumorigenesis in mice', *Gastroenterology*, 123(2), pp. 492–504. doi: 10.1053/gast.2002.34786.
- Janssen, L. M. E. *et al.* (2017) 'The immune system in cancer metastasis: Friend or foe?', *Journal for ImmunoTherapy of Cancer*. Journal for ImmunoTherapy of Cancer, 5(1), pp. 1–14. doi: 10.1186/s40425-017-0283-9.
- Järveläinen, H. *et al.* (2009) 'Extracellular matrix molecules: potential targets in pharmacotherapy', *Pharmacol Rev.*, 61(2), pp. 198–223. doi: 10.1124/pr.109.001289.provided.
- Jodele, S. *et al.* (2006) 'Modifying the soil to affect the seed: Role of stromal-derived matrix metalloproteinases in cancer progression', *Cancer and Metastasis Reviews*, 25(1), pp. 35–43. doi: 10.1007/s10555-006-7887-8.
- Johnson, L. A. *et al.* (2013) 'Matrix stiffness corresponding to strictured bowel induces a fibrogenic response in human colonic fibroblasts', *Inflammatory Bowel Diseases*, 19(5), pp. 891–903. doi: 10.1097/MIB.0b013e3182813297.
- Jonkers, J. *et al.* (2001) 'Synergistic tumor suppressor activity of BRCA2 and p53 in a conditional mouse model for breast cancer', *Nature Genetics*. Nature Publishing Group, 29(4), pp. 418–425. doi: 10.1038/ng747.
- Joyce, J. a and Pollard, J. W. (2009) 'Microenvironmental regulation of metastasis.', *Nature reviews. Cancer*, 9(4), pp. 239–252. doi: 10.1038/nrc2618.
- Kadler, K. E. *et al.* (1996) 'Collagen fibril formation', *Journal of Biochemistry*, 316(Pt 1), pp. 1–11. doi: 10.1042/bj3160001.
- Kagan, H. M. and Li, W. (2003) 'Lysyl oxidase: Properties, specificity, and biological roles inside and outside of the cell', *Journal of Cellular Biochemistry*, 88(4), pp. 660–672. doi: 10.1002/jcb.10413.
- Kalluri, R. and Zeisberg, M. (2006) 'Fibroblasts in cancer', *Nature reviews. Cancer*, 6(5), pp. 392–401. doi: 10.1038/nrc1877.
- Kedrin, D. *et al.* (2008a) 'Intravital imaging of metastatic behavior through a mammary imaging window', *Nature Methods*, 5(12), pp. 1019–1021. doi: 10.1038/nmeth.1269.
- Kedrin, D. *et al.* (2008b) 'Intravital imaging of metastatic behavior through a mammary

- imaging window.', *Nature methods*. NIH Public Access, 5(12), pp. 1019–21. doi: 10.1038/nmeth.1269.
- Kelley, L. C. *et al.* (2014) 'Traversing the basement membrane in vivo: A diversity of strategies', *Journal of Cell Biology*, 204(3), pp. 291–302. doi: 10.1083/jcb.201311112.
- Khoshnoodi, J., Pedchenko, V. and Hudson, B. G. (2008) 'Mammalian collagen IV', *Microscopy Research and Technique*, 71(5), pp. 357–370. doi: 10.1002/jemt.20564.
- King, S. J. and Parsons, M. (2011) 'Imaging Cells Within 3D Cell-Derived Matrix', 769(1), pp. 53–64. doi: 10.1007/978-1-61779-207-6.
- Kinnunen, J. *et al.* (2012) 'Nondestructive fluorescence-based quantification of threose-induced collagen cross-linking in bovine articular cartilage', *Journal of Biomedical Optics*, 17(9), p. 970031. doi: 10.1117/1.JBO.17.9.097003.
- Kinzler, K. W. *et al.* (1991) 'Identification of FAP locus genes from chromosome 5q21', *Science*, 253(5020), pp. 661–665. doi: 10.1126/science.1651562.
- Kinzler, K. W. and Vogelstein, B. (1998) 'Landscaping the cancer terrain', *Science*, 280(5366), pp. 1036–1037. doi: 10.1126/science.280.5366.1036.
- Knouf, E. C. *et al.* (2012) 'An integrative genomic approach identifies p73 and p63 as activators of miR-200 microRNA family transcription', *Nucleic Acids Research*, 40(2), pp. 499–510. doi: 10.1093/nar/gkr731.
- Kopanska, K. S. *et al.* (2016) 'Tensile forces originating from cancer spheroids facilitate tumor invasion', *PLoS ONE*, 11(6), pp. 1–23. doi: 10.1371/journal.pone.0156442.
- Korinek, V. *et al.* (1998) 'Depletion of epithelial stem - cell compartments in the small intestine of mice lacking Tcf - 4', 19(august), pp. 379–383. doi: 10.1038/1270.
- Krndija, D. *et al.* (2010) 'Substrate stiffness and the receptor-type tyrosine-protein phosphatase alpha regulate spreading of colon cancer cells through cytoskeletal contractility', *Oncogene*, 29(18), pp. 2724–2738. doi: 10.1038/onc.2010.25.
- Labernadie, A. *et al.* (2017) 'A mechanically active heterotypic E-cadherin/N-cadherin adhesion enables fibroblasts to drive cancer cell invasion', *Nature Cell Biology*, 19(3), pp. 224–237. doi: 10.1038/ncb3478.
- Lahlou, H. *et al.* (2007) 'Mammary epithelial-specific disruption of the focal adhesion kinase blocks mammary tumor progression.', *Proceedings of the National Academy of Sciences of the United States of America*, 104(51), pp. 20302–7. doi: 10.1073/pnas.0710091104.
- Lambert, A. W., Pattabiraman, D. R. and Weinberg, R. A. (2017) 'Emerging Biological Principles of Metastasis', *Cell*. Elsevier Inc., 168(4), pp. 670–691. doi: 10.1016/j.cell.2016.11.037.
- Lämmermann, T. and Sixt, M. (2009) 'Mechanical modes of "amoeboid" cell migration', *Current Opinion in Cell Biology*, 21(5), pp. 636–644. doi: 10.1016/j.ceb.2009.05.003.
- Lemmon, C. A., Chen, C. S. and Romer, L. H. (2009) 'Cell traction forces direct fibronectin matrix assembly', *Biophysical Journal*. The American Society of Human Genetics, 96(2), pp. 729–738. doi: 10.1016/j.bpj.2008.10.009.

- Levental, K. R. *et al.* (2009) 'Matrix Crosslinking Forces Tumor Progression by Enhancing Integrin Signaling', *Cell*. Elsevier Ltd, 139(5), pp. 891–906. doi: 10.1016/j.cell.2009.10.027.
- Li, A. C. Y. and Thompson, R. P. H. (2003) 'Basement membrane components', *Journal of Clinical Pathology*, 56(12), pp. 885–887. doi: 10.1136/jcp.56.12.885.
- Li, S., Guan, J.-L. and Chien, S. (2005) 'Biochemistry and Biomechanics of Cell Motility', *Annual Review of Biomedical Engineering*, 7(1), pp. 105–150. doi: 10.1146/annurev.bioeng.7.060804.100340.
- Lo, C. M. *et al.* (2000) 'Cell movement is guided by the rigidity of the substrate', *Biophysical Journal*. Elsevier, 79(1), pp. 144–152. doi: 10.1016/S0006-3495(00)76279-5.
- Lopez, J. I. *et al.* (2011) 'In situ force mapping of mammary gland transformation', *Integrative Biology*, 3(9), pp. 910–921. doi: 10.1039/c1ib00043h.
- Lorentzen, A. *et al.* (2011) 'An ezrin-rich, rigid uropod-like structure directs movement of amoeboid blebbing cells', *Journal of Cell Science*, 124(8), pp. 1256–1267. doi: 10.1242/jcs.074849.
- Lu, J. *et al.* (2013) 'Endothelial Cells Promote the Colorectal Cancer Stem Cell Phenotype through a Soluble Form of Jagged-1', *Cancer Cell*. Elsevier Inc., 23(2), pp. 171–185. doi: 10.1016/j.ccr.2012.12.021.
- Lu, P., Weaver, V. M. and Werb, Z. (2012) 'The extracellular matrix: A dynamic niche in cancer progression', *Journal of Cell Biology*, 196(4), pp. 395–406. doi: 10.1083/jcb.201102147.
- Madan, R. *et al.* (2006) 'Focal adhesion proteins as markers of malignant transformation and prognostic indicators in breast carcinoma', *Human Pathology*, 37(1), pp. 9–15. doi: 10.1016/j.humpath.2005.09.024.
- Madsen, C. D. and Sahai, E. (2010) 'Cancer Dissemination-Lessons from Leukocytes', *Developmental Cell*. Elsevier Inc., 19(1), pp. 13–26. doi: 10.1016/j.devcel.2010.06.013.
- Maier, H. J. *et al.* (2010) 'NF- κ B promotes epithelial-mesenchymal transition, migration and invasion of pancreatic carcinoma cells', *Cancer Letters*. Elsevier Ireland Ltd, 295(2), pp. 214–228. doi: 10.1016/j.canlet.2010.03.003.
- Malandrino, A. *et al.* (2018) 'Complex mechanics of the heterogeneous extracellular matrix in cancer', *Extreme Mechanics Letters*. Elsevier Ltd, 21, pp. 25–34. doi: 10.1016/j.eml.2018.02.003.
- Malinverno, C. *et al.* (2017) 'Endocytic reawakening of motility in jammed epithelia'. doi: 10.1038/NMAT4848.
- El Marjou, F. *et al.* (2004) 'Tissue-specific and inducible Cre-mediated recombination in the gut epithelium', *Genesis*, 39(3), pp. 186–193. doi: 10.1002/gene.20042.
- Markowitz, S. D. and Bertagnoli, M. M. (2010) 'Molecular basis of colorectal cancer.', *N Engl J Med*, 362(13), pp. 1245–1247. doi: 362/13/1245 [pii] 10.1056/NEJMc1000949.
- Marshman, E., Booth, C. and Potten, C. S. (2002) 'The intestinal epithelial stem cell', *BioEssays*, 24(1), pp. 91–98. doi: 10.1002/bies.10028.

- Mason, B. N. and Reinhart-King, C. A. (2013) 'Controlling the mechanical properties of three-dimensional matrices via non-enzymatic collagen glycation', *Organogenesis*, 9(2), pp. 70–75. doi: 10.4161/org.24942.
- McKee, K. K. *et al.* (2007) 'Role of laminin terminal globular domains in basement membrane assembly', *Journal of Biological Chemistry*, 282(29), pp. 21437–21447. doi: 10.1074/jbc.M702963200.
- Mecham, R. P. (2012) 'Overview of extracellular matrix', *Current Protocols in Cell Biology*, (SUPPL.57), pp. 1–16. doi: 10.1002/0471143030.cb1001s57.
- Meijering, E., Dzyubachyk, O. and Smal, I. (2012) 'Methods for cell and particle tracking', *Methods in enzymology*, 504, pp. 183–200. doi: 10.1016/B978-0-12-391857-4.00009-4.
- Midwood, K. *et al.* (2005) 'Coregulation of Fibronectin Signaling and Matrix Contraction by Tenascin-C and Syndecan-4', *Molecular biology of the cell*, 16(1), pp. 1–13. doi: 10.1091/mbc.E04.
- Midwood, K. S. *et al.* (2016) 'Tenascin-C at a glance', *Journal of Cell Science*, 129(23), pp. 4321–4327. doi: 10.1242/jcs.190546.
- Midwood, K. S. and Schwarzbauer, J. E. (2002) 'Elastic Fibers : Building Bridges Between Cells and Their Matrix Extracellular elastic fibers confer resilience and', 12(2), pp. 279–281.
- Miller, E. J. and Matukas, V. J. (1969) 'Chick cartilage collagen: a new type of alpha 1 chain not present in bone or skin of the species.', *Proceedings of the National Academy of Sciences of the United States of America*, 64(4), pp. 1264–8. doi: 10.1073/pnas.64.4.1264.
- Miranti, C. K. and Brugge, J. S. (2002) 'Sensing the environment: A historical perspective on integrin signal transduction', *Nature Cell Biology*, 4(4). doi: 10.1038/ncb0402-e83.
- Mishra, P. J. *et al.* (2008) 'Carcinoma-associated fibroblast-like differentiation of human mesenchymal stem cells', *Cancer Research*, 68(11), pp. 4331–4339. doi: 10.1158/0008-5472.CAN-08-0943.
- Mitchell, B. S., Horny, H. P. and Schumacher, U. (1997) 'Immunophenotyping of human HT29 colon cancer cell primary tumours and their metastases in severe combined immunodeficient mice.', *The Histochemical journal*, 29(5), pp. 393–9. Available at: <http://www.ncbi.nlm.nih.gov/pubmed/9184853>.
- Mitra, S. K. and Schlaepfer, D. D. (2006) 'Integrin-regulated FAK-Src signaling in normal and cancer cells', *Current Opinion in Cell Biology*, 18(5), pp. 516–523. doi: 10.1016/j.ceb.2006.08.011.
- Mohammadi, M., Olsen, S. K. and Goetz, R. (2005) 'A protein canyon in the FGF-FGF receptor dimer selects from an à la carte menu of heparan sulfate motifs', *Current Opinion in Structural Biology*, 15(5), pp. 506–516. doi: 10.1016/j.sbi.2005.09.002.
- Mombach, J. C. M. *et al.* (2005) 'Rounding of aggregates of biological cells: Experiments and simulations', *Physica A: Statistical Mechanics and its Applications*, 352(2–4), pp. 525–534. doi: 10.1016/j.physa.2005.02.008.
- Mongera, A. *et al.* (2018) 'A fluid-to-solid jamming transition underlies vertebrate body axis elongation', *Nature*. doi: 10.1038/s41586-018-0479-2.

- Moriguchi, T. and Fujimoto, D. (1979) 'Crosslink of collagen in hypertrophic scar', *Journal of Investigative Dermatology*, 72(3), pp. 143–145. doi: 10.1111/1523-1747.ep12530609.
- Morin, P. J. *et al.* (1997) 'Activation of beta-catenin-Tcf signaling in colon cancer by mutations in beta-catenin or APC.', *Science (New York, N.Y.)*, 275(5307), pp. 1787–1790. doi: 10.1126/science.275.5307.1787.
- Morrissey, M. A. and Sherwood, D. R. (2015) 'An active role for basement membrane assembly and modification in tissue sculpting', *Journal of Cell Science*, 128(9), pp. 1661–1668. doi: 10.1242/jcs.168021.
- Moser, A., Pitot, H. C. and Dove, W. F. (1990) 'A Dominant Mutation That Predisposes to Multiple Intestinal Neoplasia in the Mouse', 247(4940), pp. 322–324.
- Mouw, J. K., Ou, G. and Weaver, V. M. (2014) 'Extracellular matrix assembly: A multiscale deconstruction', *Nature Reviews Molecular Cell Biology*. Nature Publishing Group, 15(12), pp. 771–785. doi: 10.1038/nrm3902.
- Murtaugh, L. C. *et al.* (2003) 'Notch signaling controls multiple steps of pancreatic differentiation.', *Proceedings of the National Academy of Sciences of the United States of America*, 100(25), pp. 14920–5. doi: 10.1073/pnas.2436557100.
- Mutsaers, S. E. (2002) 'Mesothelial cells: Their structure, function and role in serosal repair', *Respirology*, 7(3), pp. 171–191. doi: 10.1046/j.1440-1843.2002.00404.x.
- Muzumdar, M. D. *et al.* (2007) 'A global double-fluorescent Cre reporter mouse', *genesis*, 45(9), pp. 593–605. doi: 10.1002/dvg.20335.
- Naba, A. *et al.* (2012) 'The Matrisome: *In Silico* Definition and *In Vivo* Characterization by Proteomics of Normal and Tumor Extracellular Matrices', *Molecular & Cellular Proteomics*, 11(4), p. M111.014647. doi: 10.1074/mcp.M111.014647.
- Nabeshima, K., Inoue, T. and Shima, Y. (2000) 'Front-Cell-specific Expression of Membrane-Type 1 Matrix Metalloproteinase and Gelatinase A during Cohort Migration of Colon Carcinoma Cells Induced by Hepatocyte Growth Factor / Scatter Factor Front-Cell-specific Expression of Membrane-Type 1 Matrix Meta', *Cancer Research*, 60(13), pp. 3364–3369. Available at: <http://cancerres.aacrjournals.org/content/60/13/3364.full>.
- Nishisho, I. *et al.* (1991) 'Mutations of Chromosome-5q21 Genes in Fap and Colorectal-Cancer Patients', *Science*, 253(5020), pp. 665–669.
- Olsen, R. (1997) 'Collagen IX', 29(4), pp. 555–558.
- Olsson, A. K. *et al.* (2006) 'VEGF receptor signalling - In control of vascular function', *Nature Reviews Molecular Cell Biology*, 7(5), pp. 359–371. doi: 10.1038/nrm1911.
- Orimo, A. *et al.* (2005) 'Stromal fibroblasts present in invasive human breast carcinomas promote tumor growth and angiogenesis through elevated SDF-1/CXCL12 secretion', *Cell*, 121(3), pp. 335–348. doi: 10.1016/j.cell.2005.02.034.
- Oshima, H. *et al.* (1997) 'Morphological and Molecular Processes of Polyp Formation in Apc{Delta}716 Knockout Mice', *Cancer Res.*, 57(9), pp. 1644–1649. doi: 10.1158/0008-5472.can-06-2707.
- Oshima, M. *et al.* (1995) 'Loss of Apc heterozygosity and abnormal tissue building in nascent intestinal polyps in mice carrying a truncated Apc gene.', *Proceedings of the*

- National Academy of Sciences*, 92(10), pp. 4482–4486. doi: 10.1073/pnas.92.10.4482.
- Oswald, L. *et al.* (2017) 'Jamming transitions in cancer', *Journal of Physics D: Applied Physics*, 50(48). doi: 10.1088/1361-6463/aa8e83.
- Ozbek, S. *et al.* (2010) 'The Evolution of Extracellular Matrix Suat', *Molecular biology of the cell*, 21(24), pp. 4325–4337. doi: 10.1091/mbc.E10.
- Padera, T. P. *et al.* (2004) 'Cancer cells compress intratumour vessels', *Nature*, 427(6976), p. 695. doi: 10.1038/427695a.
- Paiva, A. E. *et al.* (2018) 'Pericytes in the Premetastatic Niche', *Cancer Research*, 78(11), pp. 2779–2786. doi: 10.1158/0008-5472.CAN-17-3883.
- Paluch, E. *et al.* (2006) 'Dynamic modes of the cortical actomyosin gel during cell locomotion and division', *Trends in Cell Biology*, 16(1), pp. 5–10. doi: 10.1016/j.tcb.2005.11.003.
- Pankov, R. and Yamada, K. (2002) 'Fibronectin at a glance', *Journal of Cell Science*, 115(20), pp. 3861–3863. doi: 10.1242/jcs.00059.
- Park, J.-A. *et al.* (2016) 'Collective migration and cell jamming in asthma, cancer and development', *Journal of Cell Science*, 129(18), pp. 3375–3383. doi: 10.1242/jcs.187922.
- Park, J. A. *et al.* (2015) 'Unjamming and cell shape in the asthmatic airway epithelium', *Nature Materials*, 14(10), pp. 1040–1048. doi: 10.1038/nmat4357.
- Parslow, A., Cardona, A. and Bryson-Richardson, R. J. (2014) 'Sample Drift Correction Following 4D Confocal Time-lapse Imaging', *Journal of Visualized Experiments*, (86). doi: 10.3791/51086.
- Paszek, M. J. and Weaver, V. M. (2004) 'The tension mounts: Mechanics meets morphogenesis and malignancy', *Journal of Mammary Gland Biology and Neoplasia*, 9(4), pp. 325–342. doi: 10.1007/s10911-004-1404-x.
- Patsialou, A. *et al.* (2013) 'Intravital multiphoton imaging reveals multicellular streaming as a crucial component of in vivo cell migration in human breast tumors', *IntraVital*. Taylor & Francis, 2(2), p. e25294. doi: 10.4161/intv.25294.
- Pauling, L. and Corey, R. (1951) 'The structure of fibrous proteins of the collagen-gelatin group', *Proceedings of the National Academy of Sciences*.
- Peltomäki, P. (2003) 'Role of DNA mismatch repair defects in the pathogenesis of human cancer', *Journal of Clinical Oncology*, 21(6), pp. 1174–1179. doi: 10.1200/JCO.2003.04.060.
- Petrie, R. J., Doyle, A. D. and Yamada, K. M. (2009) 'Random versus directionally persistent cell migration', *Nature Reviews Molecular Cell Biology*. Nature Publishing Group, 10(8), pp. 538–549. doi: 10.1038/nrm2729.
- Peyton, S. R. *et al.* (2008) 'The effects of matrix stiffness and RhoA on the phenotypic plasticity of smooth muscle cells in a 3-D biosynthetic hydrogel system', *Biomaterials*, 29(17), pp. 2597–2607. doi: 10.1016/j.biomaterials.2008.02.005.
- Pfeiffer, B. J. *et al.* (2005) 'Alpha 2(I) collagen deficient oim mice have altered biomechanical integrity, collagen content, and collagen crosslinking of their thoracic

- aorta', *Matrix Biology*, 24(7), pp. 451–458. doi: 10.1016/j.matbio.2005.07.001.
- Pickup, M. W., Mouw, J. K. and Weaver, V. M. (2014) 'The extracellular matrix modulates the hallmarks of cancer', *EMBO reports*, 15(12), pp. 1243–1253. doi: 10.15252/embr.201439246.
- Poincloux, R. *et al.* (2011) 'Contractility of the cell rear drives invasion of breast tumor cells in 3D Matrigel', *Proceedings of the National Academy of Sciences*, 108(5), pp. 1943–1948. doi: 10.1073/pnas.1010396108.
- Polacheck, W. J. and Chen, C. S. (2016) 'Measuring cell-generated forces: A guide to the available tools', *Nature Methods*, 13(5), pp. 415–423. doi: 10.1038/nmeth.3834.
- Pollard, J. W. (2004) 'Tumour-educated macrophages promote tumour progression and metastasis', *Nature Reviews Cancer*, 4(1), pp. 71–78. doi: 10.1038/nrc1256.
- Pollard, T. D. and Borisy, G. G. (2003) 'Cellular motility driven by assembly and disassembly of actin filaments', *Cell*, 112(4), pp. 453–465. doi: 10.1016/S0092-8674(03)00120-X.
- Poschl, E. *et al.* (2004) 'Collagen IV is essential for basement membrane stability but dispensable for initiation of its assembly during early development', *Development*, 131(7), pp. 1619–1628. doi: 10.1242/dev.01037.
- Poulson, D. F. (1937) 'Chromosomal Deficiencies and the Embryonic Development of *Drosophila Melanogaster*', *Proceedings of the National Academy of Sciences of the United States of America*, 23(3), pp. 133–137. doi: 10.1073/pnas.23.3.133.
- Prall, F. (2007) 'Tumour budding in colorectal carcinoma', *Histopathology*. Blackwell Publishing Ltd, 50(1), pp. 151–162. doi: 10.1111/j.1365-2559.2006.02551.x.
- Preibisch, S., Saalfeld, S. and Tomancak, P. (2009) 'Globally optimal stitching of tiled 3D microscopic image acquisitions', 25(11), pp. 1463–1465. doi: 10.1093/bioinformatics/btp184.
- Provenzano, P. P. *et al.* (2006) 'Collagen reorganization at the tumor-stromal interface facilitates local invasion.', *BMC medicine*, 4(1), p. 38. doi: 10.1186/1741-7015-4-38.
- Provenzano, P. P. *et al.* (2008) 'Collagen density promotes mammary tumor initiation and progression.', *BMC medicine*, 6, p. 11. doi: 10.1186/1741-7015-6-11.
- Qian, B. Z. and Pollard, J. W. (2010) 'Macrophage Diversity Enhances Tumor Progression and Metastasis', *Cell*, 141(1), pp. 39–51. doi: 10.1016/j.cell.2010.03.014.
- Qiao, L. and Wong, B. C. Y. (2009) 'Role of notch signaling in colorectal cancer', *Carcinogenesis*, 30(12), pp. 1979–1986. doi: 10.1093/carcin/bgp236.
- Raab, M. *et al.* (2016) 'ESCRT III repairs nuclear envelope ruptures during cell migration to limit DNA damage and cell death', *Science*, 352(6283), pp. 359–362. doi: 10.1126/science.aad7611.
- Radtke, F., Clevers, H. and Riccio, O. (2006) 'From Gut Homeostasis to Cancer', *Current Molecular Medicine*, 6(3), pp. 275–289. doi: 10.2174/156652406776894527.
- Rahman, S. *et al.* (2005) 'Novel hepatocyte growth factor (HGF) binding domains on fibronectin and vitronectin coordinate a distinct and amplified Met-integrin induced

signalling pathway in endothelial cells', *BMC Cell Biology*, 6, pp. 1–17. doi: 10.1186/1471-2121-6-8.

Ricard-Blum, S. (2011) 'The Collagen Family', *Cold Spring Harbor Perspectives in Biology*, 3(1), pp. 1–19. doi: 10.1101/cshperspect.a004978.

Riching, K. M. *et al.* (2015) '3D collagen alignment limits protrusions to enhance breast cancer cell persistence', *Biophysical Journal*. Biophysical Society, 107(11), pp. 2546–2558. doi: 10.1016/j.bpj.2014.10.035.

Ries LAG, Melbert D, Krapcho M, Stinchcomb DG, Howlader N, Horner MJ, Mariotto A, Miller BA, Feuer EJ, Altekruse SF, Lewis DR, Clegg L, Eisner MP, Reichman M, E. B. (2007) 'SEER Cancer Statistics Review, 1975-2005, National Cancer Institute. Bethesda, MD'.

Romagnolo, B. *et al.* (1999) 'Intestinal dysplasia and adenoma in transgenic mice after overexpression of an activated β -catenin', *Cancer Research*, 59(16), pp. 3875–3879.

Rosenbloom, J., Abrams, R. and Mecham, R. (2016) 'Extracellular matrix 4: The elastic fiber', *The FASEB Journal*, 7(13), pp. 1208–1218.

Rottner, K. *et al.* (2017) 'Actin assembly mechanisms at a glance', *Journal of Cell Science*, 130(20), pp. 3427–3435. doi: 10.1242/jcs.206433.

Roussos, E. T. *et al.* (2011) 'Mena invasive (MenaINV) promotes multicellular streaming motility and transendothelial migration in a mouse model of breast cancer', *Journal of Cell Science*, 124(13), pp. 2120–2131. doi: 10.1242/jcs.086231.

Rowe, R. G. and Weiss, S. J. (2008) 'Breaching the basement membrane: who, when and how?', *Trends in Cell Biology*, 18(11), pp. 560–574. doi: 10.1016/j.tcb.2008.08.007.

Rozario, T. and DeSimone, D. W. (2010) 'The extracellular matrix in development and morphogenesis: A dynamic view', *Developmental Biology*. Elsevier Inc., 341(1), pp. 126–140. doi: 10.1016/j.ydbio.2009.10.026.

Rubinfeld, B. *et al.* (1993) 'Association of the APC gene product with beta-catenin', *Science*, 262(5140), pp. 1731–1734. doi: 10.1126/science.8259518.

Rustgi, A. K. (2007) 'The genetics of hereditary colon cancer The genetics of hereditary colon cancer', *Genes & Development*, 21, pp. 2525–2538. doi: 10.1101/gad.1593107.

Sadati, M. *et al.* (2013) 'Collective migration and cell jamming', *Differentiation*, 86(3), pp. 121–125. doi: 10.1016/j.diff.2013.02.005.

Sanz-Moreno, V. and Marshall, C. J. (2010) 'The plasticity of cytoskeletal dynamics underlying neoplastic cell migration', *Current Opinion in Cell Biology*. Elsevier Ltd, 22(5), pp. 690–696. doi: 10.1016/j.ceb.2010.08.020.

Sarrazin, S., Lamanna, W. C. and Esko, J. D. (2011) 'Heparan Sulfate Proteoglycans', *Cold Spring Harbor Perspectives in Biology*, 3(7), pp. a004952–a004952. doi: 10.1101/cshperspect.a004952.

Sawada, Y. *et al.* (2006) 'Force Sensing by Mechanical Extension of the Src Family Kinase Substrate p130Cas', *Cell*, 127(5), pp. 1015–1026. doi: 10.1016/j.cell.2006.09.044.

Schaefer, L. and Schaefer, R. M. (2010) 'Proteoglycans: From structural compounds to signaling molecules', *Cell and Tissue Research*, 339(1), pp. 237–246. doi: 10.1007/s00441-

009-0821-y.

Schedin, P. and Keely, P. J. (2011) 'Mammary gland ECM remodeling, stiffness, and mechanosignaling in normal development and tumor progression', *Cold Spring Harbor Perspectives in Biology*, 3(1), pp. 1–22. doi: 10.1101/cshperspect.a003228.

Schmeichel, K. L. and Bissel M. (2003) 'Modeling tissue-specific signaling and organ function in three dimensions', *Journal of Cell Science*, 116(12), pp. 2377–2388. doi: 10.1242/jcs.00503.

Schoumacher, M. *et al.* (2010) 'Actin, microtubules, and vimentin intermediate filaments cooperate for elongation of invadopodia', *Journal of Cell Biology*, 189(3), pp. 541–556. doi: 10.1083/jcb.200909113.

Schoumacher, M. *et al.* (2013) 'Basement Membrane Invasion Assays: Native Basement Membrane and Chemoinvasion Assay', in: Humana Press, Totowa, NJ, pp. 133–144. doi: 10.1007/978-1-62703-538-5_8.

Schoumacher, M., Louvard, D. and Vignjevic, D. (2011) 'Cytoskeleton networks in basement membrane transmigration', *European Journal of Cell Biology*. Elsevier GmbH., 90(2–3), pp. 93–99. doi: 10.1016/j.ejcb.2010.05.010.

Schwarzbauer, J. E. and DeSimone, D. W. (2011) 'Fibronectins, their fibrillogenesis, and in vivo functions', *Cold Spring Harbor Perspectives in Biology*, 3(7), pp. 1–19. doi: 10.1101/cshperspect.a005041.

Serra-Picamal, X. *et al.* (2012) 'Mechanical waves during tissue expansion', *Nature Physics*. Nature Publishing Group, 8(8), pp. 628–634. doi: 10.1038/nphys2355.

Shoulders, M. D. and Raines, R. T. (2009) 'Collagen Structure and Stability', *Annual Review of Biochemistry*, 78(1), pp. 929–958. doi: 10.1146/annurev.biochem.77.032207.120833.

Simon-Assmann, P. *et al.* (1988) 'Epithelial-mesenchymal interactions in the production of basement membrane components in the gut', *Development*, 102(2), pp. 339–347. Available at: <http://www.ncbi.nlm.nih.gov/pubmed/17061377>.

Van Der Slot, A. J. *et al.* (2005) 'Elevated formation of pyridinoline cross-links by profibrotic cytokines is associated with enhanced lysyl hydroxylase 2b levels', *Biochimica et Biophysica Acta - Molecular Basis of Disease*, 1741(1–2), pp. 95–102. doi: 10.1016/j.bbadis.2004.09.009.

Small, J. V. and Resch, G. P. (2005) 'The comings and goings of actin: Coupling protrusion and retraction in cell motility', *Current Opinion in Cell Biology*, 17(5 SPEC. ISS.), pp. 517–523. doi: 10.1016/j.ceb.2005.08.004.

Song, S. *et al.* (2005) 'PDGFR β +perivascular progenitor cells in tumours regulate pericyte differentiation and vascular survival', *Nature Cell Biology*, 7(9), pp. 870–879. doi: 10.1038/ncb1288.

Staneva, R. *et al.* (2018) 'Cell Migration in Tissues: Explant Culture and Live Imaging', in *Methods in molecular biology (Clifton, N.J.)*, pp. 163–173. doi: 10.1007/978-1-4939-7701-7_13.

Steinberg, M. S. and Takeichi, M. (1994) 'Experimental specification of cell sorting, tissue spreading, and specific spatial patterning by quantitative differences in cadherin

- expression.', *Proceedings of the National Academy of Sciences*, 91(1), pp. 206–209. doi: 10.1073/pnas.91.1.206.
- Stylianopoulos, T. *et al.* (2012) 'Causes, consequences, and remedies for growth-induced solid stress in murine and human tumors', *Proceedings of the National Academy of Sciences*, 109(38), pp. 15101–15108. doi: 10.1073/pnas.1213353109.
- Stylianopoulos, T. *et al.* (2013) 'Coevolution of solid stress and interstitial fluid pressure in tumors during progression: Implications for vascular collapse', *Cancer Research*, 73(13), pp. 3833–3841. doi: 10.1158/0008-5472.CAN-12-4521.
- Su, L.-K., Vogelstein, B. and Kinzler, K. W. (1993) 'Association of the APC Tumor-Suppressor Protein with Catenins', *Science*, 262(5140), pp. 1734–1737. Available at: <http://eutils.ncbi.nlm.nih.gov/entrez/eutils/elink.fcgi?dbfrom=pubmed&id=8259519&retmode=ref&cmd=prlinks%5Cnpapers3://publication/uuid/704D2AE7-5D2D-4B72-8FC9-3921F6623BE2>.
- Su, L. K. *et al.* (1992) 'Multiple intestinal neoplasia caused by a mutation in the murine homolog of the APC gene', *Science*, 256(5057), pp. 668–670. doi: 10.1126/science.1350108.
- Suzuki, R. *et al.* (2004) 'Sequential observations on the occurrence of preneoplastic and neoplastic lesions in mouse colon treated with azoxymethane and dextran sodium sulfate', *Cancer Science*, 95(9), pp. 721–727. doi: 10.1111/j.1349-7006.2004.tb03252.x.
- Swaminathan, V. *et al.* (2011) 'Mechanical Stiffness grades metastatic potential in patient tumor cells and in cancer cell lines', *Cancer Research*, 71(15), pp. 5075–5080. doi: 10.1158/0008-5472.CAN-11-0247.
- Takaku, K. *et al.* (1998) 'Intestinal tumorigenesis in compound mutant mice of both Dpc4 (Smad4) and Apc genes', *Cell*, 92(5), pp. 645–656. doi: 10.1016/S0092-8674(00)81132-0.
- Taketo, M. M. and Edelmann, W. (2009) 'Mouse Models of Colon Cancer', *Gastroenterology*. AGA Institute American Gastroenterological Association, 136(3), pp. 780–798. doi: 10.1053/j.gastro.2008.12.049.
- Tambe, D. T. *et al.* (2011) 'Collective cell guidance by cooperative intercellular forces.', *Nature Materials*. Nature Publishing Group, 10(6), pp. 469–475. doi: 10.1038/nmat3025.
- Tanaka, S. *et al.* (1988) 'Glycation induces expansion of the molecular packing of collagen', *Journal of Molecular Biology*, 203(2), pp. 495–505. doi: 10.1016/0022-2836(88)90015-0.
- Tanaka, T. *et al.* (2003) 'A novel inflammation-related mouse colon carcinogenesis model induced by azoxymethane and dextran sodium sulfate', *Cancer Science*, 94(11), pp. 965–973. doi: 10.1111/j.1349-7006.2003.tb01386.x.
- Ulrich, T. A., De Juan Pardo, E. M. and Kumar, S. (2009) 'The mechanical rigidity of the extracellular matrix regulates the structure, motility, and proliferation of glioma cells', *Cancer Research*, 69(10), pp. 4167–4174. doi: 10.1158/0008-5472.CAN-08-4859.
- Valastyan, S. and Weinberg, R. a. (2011) 'Tumor metastasis: Molecular insights and evolving paradigms', *Cell*. Elsevier Inc., 147(2), pp. 275–292. doi: 10.1016/j.cell.2011.09.024.

- Vasen, H. F. A. and Boland, C. R. (2005) 'Progress in genetic testing, classification, and identification of lynch syndrome', *Journal of the American Medical Association*, 293(16), pp. 2028–2030. doi: 10.1001/jama.293.16.2028.
- Verhulsel, M. *et al.* (2014) 'A review of microfabrication and hydrogel engineering for micro-organs on chips', *Biomaterials*. Elsevier Ltd, 35(6), pp. 1816–1832. doi: 10.1016/j.biomaterials.2013.11.021.
- Verzijl, N. *et al.* (2002) 'Crosslinking by Advanced Glycation End Products Increases the Stiffness of the Collagen Network in Human Articular Cartilage', *Arthritis and rheumatism*, 46(1), pp. 114–123. doi: 10.1002/art.10025.
- Vignjevic, D. *et al.* (2007) 'Fascin, a novel target of β -catenin-TCF signaling, is expressed at the invasive front of human colon cancer', *Cancer Research*, 67(14), pp. 6844–6853. doi: 10.1158/0008-5472.CAN-07-0929.
- Vogel, V. (2018) 'Unraveling the Mechanobiology of Extracellular Matrix', *Annual Review of Physiology*, 80(1), pp. 353–387. doi: 10.1146/annurev-physiol-021317-121312.
- Weaver, V. M. *et al.* (1997) 'Reversion of the Malignant Phenotype of Human Breast Cells in Three-Dimensional Culture and In Vivo by Integrin Blocking Antibodies', *The Journal of Cell Biology*, 137(1), pp. 231–245. doi: 10.1083/jcb.137.1.231.
- Weigelin, B., Bakker, G.-J. and Friedl, P. (2012) 'Intravital third harmonic generation microscopy of collective melanoma cell invasion', *IntraVital*. Taylor & Francis, 1(1), pp. 32–43. doi: 10.4161/intv.21223.
- Weng, A. P. *et al.* (2004) 'Activating mutations of NOTCH1 in human T cell acute lymphoblastic leukemia', *Science*, 306(5694), pp. 269–271. doi: 10.1126/science.1102160.
- Wenger, M. P. E. *et al.* (2007) 'Mechanical properties of collagen fibrils', *Biophysical Journal*. Elsevier, 93(4), pp. 1255–1263. doi: 10.1529/biophysj.106.103192.
- De Wever, O. *et al.* (2004) 'Tenascin-C and SF/HGF produced by myofibroblasts in vitro provide convergent pro-invasive signals to human colon cancer cells through RhoA and Rac', *The FASEB Journal*, 18(9), pp. 1016–1018. doi: 10.1096/fj.03-1110fje.
- White, D. E. *et al.* (2004) 'Targeted disruption of β 1-integrin in a transgenic mouse model of human breast cancer reveals an essential role in mammary tumor induction', *Cancer Cell*, 6(2), pp. 159–170. doi: 10.1016/j.ccr.2004.06.025.
- Wierzbicka-Patynowski, I. and Schwarzbauer, J. (2003) 'The ins and outs of fibronectin matrix assembly', *Journal of Cell Science*, 116(16), pp. 3269–3276. doi: 10.1242/jcs.00670.
- Witz, C. A. *et al.* (2001) 'Composition of the extracellular matrix of the peritoneum', *Journal of the Society for Gynecologic Investigation*, 8(5), pp. 299–304. doi: 10.1016/S1071-5576(01)00122-8.
- Wolf, K. *et al.* (2003) 'Amoeboid shape change and contact guidance: T-lymphocyte crawling through fibrillar collagen is independent of matrix remodeling by MMPs and other proteases', *Blood*, 102(9), pp. 3262–3269. doi: 10.1182/blood-2002-12-3791.
- Wolf, K. *et al.* (2007) 'Multi-step pericellular proteolysis controls the transition from individual to collective cancer cell invasion.', *Nature cell biology*, 9(8), pp. 893–904. doi:

10.1038/ncb1616.

Wolf, K. *et al.* (2009) 'Collagen-based cell migration in vitro and in vivo', *Seminars in Cell & Developmental Biology*, 20(8), pp. 931–941. doi: 10.1016/j.semcdb.2009.08.005.Collagen-based.

Wolf, K. *et al.* (2013) 'Physical limits of cell migration: Control by ECM space and nuclear deformation and tuning by proteolysis and traction force', *Journal of Cell Biology*, 201(7), pp. 1069–1084. doi: 10.1083/jcb.201210152.

Wu, J.-J. *et al.* (2010) 'Type III Collagen, a Fibril Network Modifier in Articular Cartilage', *Journal of Biological Chemistry*, 285(24), pp. 18537–18544. doi: 10.1074/jbc.M110.112904.

Wullkopf, L. *et al.* (2018) 'Cancer cell ability to mechanically adjust to extracellular matrix stiffness correlates with their invasive potential', *Molecular Biology of the Cell*, p. mbc.E18-05-0319. doi: 10.1091/mbc.E18-05-0319.

Wyckoff, R., Corey, R. and Bischoff, J. (1935) 'X-Ray reflections of long spacing from tendon', *Science*.

Yurchenco, P. D. (2011) 'Basement Membranes: Cell Scaffoldings and Signaling Platforms', pp. 1–28. doi: 10.1101/cshperspect.a004911.

Yurchenco, P. D. and Wadsworth, W. G. (2004) 'Assembly and tissue functions of early embryonic laminins and netrins', *Current Opinion in Cell Biology*, 16(5), pp. 572–579. doi: 10.1016/j.ceb.2004.07.013.

Zhu, Y. *et al.* (1998) 'Smad3 Mutant Mice Develop Metastatic Colorectal Cancer', *Cell*, 94(6), pp. 703–714. doi: 10.1016/S0092-8674(00)81730-4.

CHAPTER 6

ANNEXES

